UNIVERSITY OF LONDON

IMPERIAL COLLEGE OF SCIENCE AND TECHNOLOGY

DEPARTMENT OF ELECTRICAL ENGINEERING

CIRCUIT REPRESENTATION OF INVERTER-FED SYNCHRONOUS MOTORS

by

Michael John Carpenter

Thesis submitted for the degree of
Doctor of Philosophy and the Diploma of
Imperial College in the Faculty of Engineering.

January 1988

ABSTRACT

Natural commutation of thyristors in inverter-fed synchronous motors is used to transfer current from one phase to the next. The commutation time of inverter-fed synchronous motors is commonly expressed in terms of the commutation reactance, Xc. A precise method of calculating Xc is desirable, especially for solid salient pole motors, since the motor power factor will reduce as commutation time increases.

A magnetic circuit method, based on the work of C.J. Carpenter, models a machine cross section which is linked to the stator electrical circuit making possible a direct coupling of the magnetic circuit with the inverter. The inter-linking of magnetic and electric circuits is achieved by the use of gyrators which fully satisfy the electromagnetic linkage equations. This method also allows an exact representation of each stator phase-band distribution in the magnetic circuit. A layered structure of permeances regularly interspersed with magnetic resistors allows for skin effects associated with flux penetration in the solid rotor poles, magnetic resistances representing damping due to eddy currents in the solid iron. The circuits are solved using a numerical circuit solving routine called S.P.I.C.E.

Treating commutation as a line-to-line short circuit initial studies are performed on a two pole pitch model neglecting motion. Commutation of a micro-alternator fitted with a solid rotor is measured and results compare well with those computed from the circuit approach.

Motion is considered by rotating stator linkages relative to the stationary stator and rotor. A field circuit linked to the magnetic circuit rotor enables the generation of back e.m.f.'s within the model. A full representation of the synchro-inverter system is thus made possible with the addition of the inverter power electronics in the stator circuit.

ACKNOWLEDGEMENTS

I wish to express my sincere thanks to my Ph.D. supervisor Dr Donald C. Macdonald, for his keen interest in this project, his support and invaluable advice.

I am grateful to the Science and Engineering Research Council for the funding of this project under a research assistantship.

Thanks must go to Dr Lawrence Haydock for his encouragement and advice. Also to Mr Mike Tarkanyi (GEC Large Machines Rugby) for his help in the early stages of this project, Professor R. Spence for allowing me to use his section's computing facilities and Miss Claire Soulal for typing this thesis.

Without the support of my many friends and acquaintances at College life would have been unbearable! I wish to thank them all, including the boys of level 8 (and the "squash-ball"), the mob on level 7, level 10 (especially Jenny), the rest of the power systems group on level 4, and the "heavies" of level 1. I am grateful to my friends in Imperial Balloon Club and Imperial Dance Club who made my time at Imperial so different!

I wish to dedicate this thesis to

Mum, Dad and my sister, Lyn,

for their patience and quiet support.

TABLE OF CONTENTS

	Page
Abstract	(i)
Acknowledgements	(iii)
Table of Contents	(v)
List of Symbols and Abbreviations	(ix)
Chapter One: Introduction	1
1.1 The Converter Fed Synchronous Motor	1
1.2 Operational Considerations	5
1.3 Synchro-Inverter System Incorporating a Solid Rotor	6
1.4 Performance Prediction	7
1.5 Contribution of the Thesis	8
1.6 Outline of the Thesis	8
Chapter Two: The Laboratory System	11
2.1 Introduction	11
2.2 Design Considerations and Operation of the Synchro-Inverter System	11
2.3 Inverter Control Circuitry	13
2.3.1 Earthing and De-Coupling	15
2.3.2 Signal Processing Circuits	16
2.4 The Synchronous Motor	27
2.5 Measurement of Overlap Angle, μ	32
2.6 Measurement of Machine Operational Inductances	32
Chapter Three: An Analysis of Commutation	36
3.1 Introduction	36
3.2 Commutation as Seen by the Inverter	37

3.3 Factors Influencing Commutation Time 43

3.4 The Value of Commutation Reactance 45

3.5 Influence of Commutation on the Motor Magnetic Field 45

3.5.1 Influence of Commutation on a two Pole Motor Magnetic Field Pattern 45

3.5.2 Stator Flux Distortion 50

3.6 Estimation of Overlap Angle Using Machine Reactances 52

3.7 Conclusion 54

Chapter Four: The Magnetic Circuit Model and Linked Inverter Circuit 56

4.1 Introduction 56

4.2 A Simple Magnetic Circuit 57

4.3 The Gyrator, a Linkage Device 61

4.4 Gyrator Implementation in Discrete Element Form 62

4.5 Linkage of the Machine Stator to the Electric Circuit Using Gyrators 64

4.6 Permeance Representation 71

4.7 The Solid Rotor 73

4.7.1 Solid Iron Permeances 73

4.8 Rotor Eddy Currents 78

4.8.1 Basic Concepts and Assumptions 78

4.8.2 Solid Rotor Eddy Current Paths 80

4.9 The Inverter Power Electronics 87

4.9.1 A Thyristor Model 90

4.9.2 A Simple Switch 90

4.9.3 The Inverter 96

4.9.4 Additional Components 96

4.10 The Circuit Solver, S.P.I.C.E. 98

4.11 Conclusions 98

Chapter Five: Relative Motion Between Rotor and Stator 100

5.1 Introduction 100

5.2 Representing Motion by Varying the Air Gap Permeance 101

5.2.1 Analysis of Varying Air Gap Permeance 101

5.2.2 Other Work 104

5.2.3 Variable Air Gap Permeances of a Simple Machine 107

5.3 The Solid Rotor 107

5.3.1 A Means of Reducing the Number of Air Gap Permeances 111

5.3.2 Selection of an Air Gap Permeance Function 116

5.4 Move the Stator Conductors 128

5.4.1 Linkages Represented as a Function of Time 133

5.4.2 S.P.I.C.E. Implementation of Stator Movement 138

5.4.3 The Flux Cutting Rule and its Application 142

5.4.4 Polarity of Rotational e.m.f. 147

5.4.5 Setting Up the Initial Field Pattern 150

5.5 Conclusions 151

Chapter Six: Simulation of the Synchro-Inverter System and a Comparison with Conventional Calculations 154

6.1 Introduction 154

6.2 Static Frequency Response Analyses 154

6.3 Calculation of Commutation Time, using an Operational Inductance 155

6.4 Line-to-Line Short Circuit Static Test 163

6.5 The Full Synchro-Inverter Model 165

6.6 Comparison of Voltage and Current Waveforms and Observations 165

6.7 Conclusions 193

Chapter Seven: The Influence of Link Inductance and Machine Design of Synchro-Inverter Performance 195

7.1 Introduction 195

7.2 A Laminated Rotor 195

7.3 Reduction of Slot Leakage and Increase in Air Gap Length 198

7.4 Reduction of Link Inductance 204

7.5 Conclusions 204

Chapter Eight: Conclusions 206

8.1 General Conclusions 206

8.2 The Magnetic Circuit Method 208

8.3 The Solving Routine - S.P.I.C.E. 210

8.4 Machine Design Change and System Modifications 211

8.5 Further Work 212

References 216

Appendix

A Non-Linear Dependent Sources 222

B Variation of Capacitor Value by the Use of Dependent Sources 228

Symbols and Abbreviations

SYMBOLS

Upper Case

A Anode (thyristor)

B Magnetic Flux Density

C Constant, Capacitance (electric or magnetic)

D Direct-axis, Diameter

G Gain

H Magnetic field strength, Henries

I Current (electric or magnetic)

K Cathode (thyristor)

L Inductance

M Current meter

N Linkage

Q Quadrature-axis

R Resistance (electric or magnetic)

V Voltage (electric or magnetic)

X Reactance

Lower Case

a area, constant, phase a, armature

b phase b,

c capacitance (electric or magnetic), comparator voltage, phase c.

d direct axis, damping

e induced voltage, voltage controlled voltage source

f frequency, field, magnetomotive force, filtered voltage signal

g gap length, gate (thyristor), voltage controlled current source

h gyrator symbol, current controlled voltage source

i instantaneous current (electric or magnetic), constant, integer

j integer

l length, inductance

m magnetic, monostable voltage, magnetomotive force

n neutral, integer

o oscillator output

p (d/dt), pole

q instantaneous charge (electric or magnetic), shift register voltage

r resistance (electric or magnetic), reset (shift register), resultant

s seconds, set (shift register), snubber, stator, slot

t time, tooth

u velocity

v instantaneous voltage (electric or magnetic)

w width

x reactance, constant

Superscripts

"	subtransient value

Specific Subscripts

a	phase a
b	phase b
c	phase c, commutation
cc	logic signal supply
d	direct-axis
eff	effective
f	field
g	air gap
gt	gate (thyristor)
m	magnetic
md	magnetic dual
ph	phase
ref	reference
q	quadrature axis
s	synchronous
TH	Thyristor

Greek

α Gyration constant, rectifier firing angle

β Inverter firing angle

γ slot pitch

δ load angle, safety angle

Θ angle

Λ magnetic permeance

μ magnetic permeability, overlap or commutation angle

π 3.142

ρ resistivity

Φ magnetic flux

Ω ohms.

ω angular velocity

Abbreviations

$\int$	Integral sign
AVR	Automatic Voltage Regulator
a.c, ac	alternating current
CMOS	Complementary Metal Oxide Semiconductor
C.P.U.	Central Processing Unit
d/dt	differential coefficient (wrto time)
d.c, dc	direct current
E.M.	Electro-Magnetic
e.m.f., emf	electromotive force
G.E.C.	General Electric Co., (UK)
m.m.f., mmf	magnetomotive force
op-amp	operational amplifier
p.f., pf	power factor
rev/min	revolutions per minute
S.M.	Synchronous Motor
S.P.I.C.E.	Simulation Program for Integrated Circuit and Electronics
v.t.	voltage transformer
w.r.t.	with respect to
$\triangleq$	defined as
<	less than
nc	no connection
Re	Real part

CHAPTER ONE

INTRODUCTION

1.1 The Converter Fed Synchronous Motor

The variable speed drive system consisting of a rectifier supplying a synchronous motor through an inverter is a well established system [1], known as the converter fed synchronous motor or synchro-inverter, fig 1.1. Its high torque capability over a wide speed range makes the system suitable for a large number of high power drive applications, with supersynchoronous drives [2], capable of speeds from 2,000 to 10,000 rev/min.

Applications include fans, pumps and compressors where the benefits of high speed operation enables the unit size to be reduced and efficiency of operation increased. The system's wide controlled stepless speed range with a torque speed characteristic similar to a shunt fed or converter fed d.c. motor make it suited to situations normally requiring a mechanical gear box. Unlike the d.c. motor though, the drawbacks encountered with mechanical commutators and brushes are avoided.

Synchro-inverters are used widely, in power stations as boiler feed water pumps, as gas compressors in chemical refineries, pumps in gas and oil pipelines and for starting gas turbine sets. A special application is in run of river hydro and wind generation where the system can run as a synchronous generator supplying the mains through the two converters and an intermediate d.c. link. The variable speed

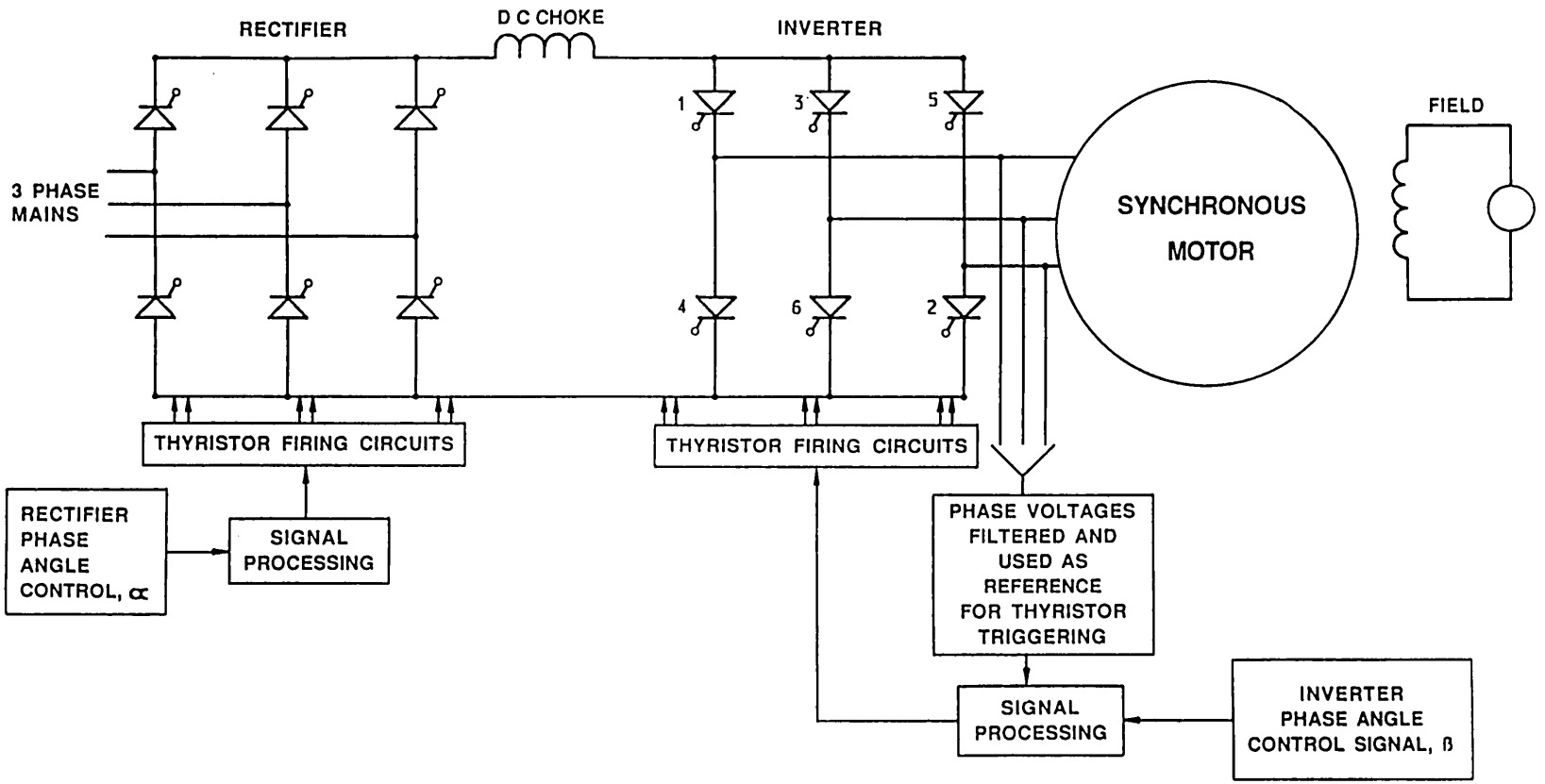


Fig.1.1. Basic Synchro-inverter System.

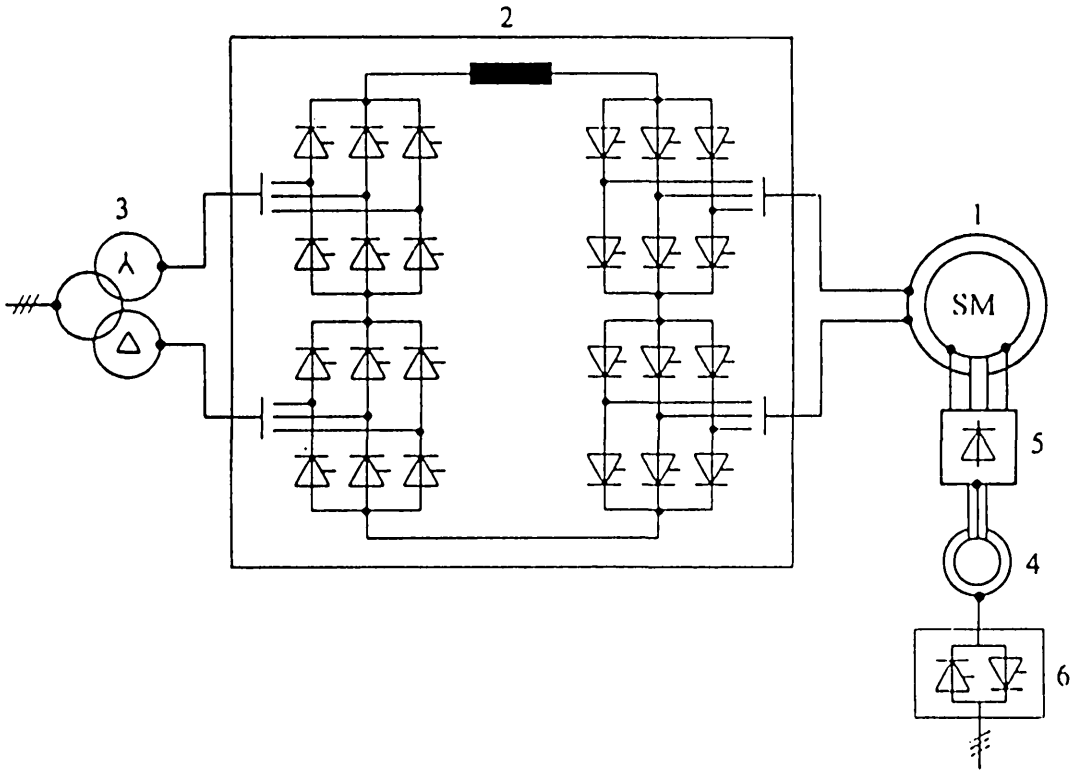
generator gives a higher efficiency than a constant speed machine.

Energy reversal is possible with additional control circuity and the system is capable of four quadrant operation. Irrespective of operation mode, the rotor is always in step with the stator field and there are therefore no slip losses. Despite remaining losses overall system efficiency is good.

A number of inverter/rectifier configurations are possible [3] with single and dual wound motors. The various schemes each have their own benefits, higher pulse number configurations, such as a twelve pulse system of fig 1.2, reduce harmonics fed back into the mains, reduce starting transients allowing a "soft start" and enable higher voltage motors to be used.

Harmonic effects are present in the stator windings due to the steep rising and falling edges of the phase current wave forms. Voltage notches are generated in the machine phases each time current is switched from one phase to the next. This causes increased stress on stator phase insulation and should be considered at the design stage.

Pulsating torques will be generated every instant the stator current sheet is suddenly switched around the windings. The rotor torque ripple will be six and twelve times the motor frequency in the case of a six pulse converter. Torque ripple can be reduced by increasing the pulse number of the converter. It is essential at the design stage to ensure that the frequencies of pulsating torque do not coincide with the natural torsional frequency of the mechanical shaft system.



1 = Synchronous motor with two stator windings
2 = Converter
3 = Three-winding transformer
4 = Exciter machine
5 = Rotating diode rectifier
6 = Three-phase control element

Fig.1.2. Converter-fed Synchronous Motor with Converter in Twelve-pulse Configuration.

Additional losses in stator conductor copper will be present and stator harmonics will generate harmonic currents in the rotor damping circuits or via eddy currents in a solid rotor construction.

1.2 Operational Considerations

The rectifier and intermediate d.c. link feeding the motor inverter can either be of the current-source or voltage-source type. The current-source type is of principal interest here although the effects of varying the d.c. choke value and therefore the uniformity of the direct current are discussed. The choke minimizes rectifier/inverter interaction, too low an inductance value resulting in high link current ripple leading to the possibility of de-stabilizing the whole system.

Both rectifier and inverter are commutated naturally, the rectifier by the mains voltage and the inverter by the e.m.f. generated by the synchronous machine. This avoids the necessity for providing relatively expensive commutation circuitry, as required for converter d.c. link systems used with induction motors.

The natural commutation of the inverter requires a finite period of time to take place, necessitating the over-excitation of the motor. The motor power factor will always be less than unity since commutation has to be completed before the commutating line-to-line voltage falls to zero. It is therefore desirable to minimize commutation time, or overlap angle.

The reliance of inverter commutation upon sufficient machine e.m.f. magnitude requires an alternative commutation technique at speeds below about 10% of full speed when the motor e.m.f. will be too low to commutate thyristors. Two techniques for starting are used. The synchronous run up technique pulses the d.c. link through the frequency range from zero to several Hz. The other method, not so common, runs the machine up to speed, as an induction motor, by supplying the machine direct from the mains via a matching transformer and allowing the inverter to take over later.

Fig 1.1 shows how the inverter thyristor firing is derived from the motor phase voltage. The frequency of the inverter is manifestly dictated by the motor speed so that the stator current pattern will automatically precede the rotor axis with a predetermined load angle at a frequency fixed by the rotor speed. Over the complete speed range the motor and inverter are in synchronism. Speed variation, by adjustment of the direct current magnitude, is achieved by controlling the rectified output voltage. Since torque is developed from the interaction between field flux and armature current, an increase in load current, for a constant applied load torque, will momentarily increase the mechanical torque, accelerating the rotor to a higher speed. The drive naturally operates at a speed that will bring the system, into balance and the synchro-inverter is by nature inherently stable.

1.3 Synchro-Inverter System Incorporating a Solid Rotor

Practical benefits can be gained by the incorporation of a motor having a solid salient rotor. The relatively high thermal capacity of such rotors make them suited to synchro-inverter drives where rotor

damping currents and harmonic rotor currents are prevelant. Synchro-inverters are often required to operate in a wide range of adverse conditions and the inherent robust mechanical structure of a solid rotor lends itself to such applications. For supersynchronous operation the use of a laminated rotor structure is generally ruled out and forged cylindrical solid rotors of the type used in turbo-generators are employed.

The complex distribution of flux and eddy currents within a solid salient rotor makes performance prediction more formidable than for a laminated rotor. Investigation of the solid salient rotor case has been undertaken and a method of performance prediction promoted.

1.4 Performance Prediction

The satisfactory operation and the success of a control strategy [4] requires a knowledge of all the problems which converter fed motors can pose. Such considerations are essential when designing the converter, the motor, and the control and protection devices. A design engineer therefore needs to predict how a motor will behave in a synchro-inverter system. Consideration of motor parameters is important since the damping effects of the solid iron eddy currents will influence the machine transient reactance during commutation. The nature of the problem requires the analyis of a loaded machine continuously experiencing unbalanced transients.

The performance of a motor may be estimated from two axis theory [5] if the machine parameters are known. The parameters for a laminated motor can be calculated from design data and verified by test. Solid rotor parameters can be expressed as impedances although the values

vary with both flux and slip frequency in a complicated manner. The d-q axis theory does not allow for the complicated distribution of flux within the solid iron of the rotor.

A more precise method of performance analysis is therefore sought which takes account of flux and eddy current disturbances, and the unbalanced nature of the problem at commutation.

1.5 Contribution of the Thesis

The thesis introduces the use of the equivalent magnetic circuit approach [6,7] to model a machine cross section linked directly to a representation of the inverter power electronics. This forms a self contained network of discrete component form. The novel use of gyrator elements to model linkage betwen magnetic and electric circuits is shown to exactly represent the interface between electric and magnetic quantities. Simulation of relative motion between rotor and stator is achieved by effectively moving stator conductors around the stator circumference by making linkages a function of time. Induced e.m.f.s due to motion are then calculated and allowed for in the model. Use of a layered permeance structure, allowing for eddy current effects, simulates the solid iron of the rotor. The calculation of model parameters is from the machine geometry requiring no machine tests to obtain further information.

1.6 Outline of the Thesis

A brief description of the contents of each chapter follows.

In Chapter two the design and construction of a laboratory converter fed synchronous motor is described. Details of inverter construction are included with a description of the inverter control circuitry. A brief description of the machine is included with cross sectional diagrams and relevant data. A complete system was constructed for tests over wide speed, load current and firing angle ranges. Methods of recording waveforms and determining commutation times are outlined. The frequency response method has been used to determine machine parameters and the technique's validity is discussed.

The commutation process is described in chapter three from an electric and magnetic field point of view. Factors influencing commutation are listed and the idea of a cummutation reactance introduced. A brief review of previous work is included with criticism of the validity of the techniques reviewed.

The formulation of a computer model is given in chapter four, the magnetic circuit approach being described. The gyrator is defined as the element which links electric and magnetic circuits and it is shown how the use of gyrators enables an exact representation of the stator phase band distribution to be achieved.

Calculation of permeances and the method of representing the solid iron as a layered strucutre of permeances is shown. Allowance for eddy current effects with the use of "magnetic dampances" completes the rotor model. The inverter power electronics are considered and a simple, but novel, method of thyristor representation put forward.

In chapter five, two techniques to simulate motion are analysed. The method of varying air gap permeances is rejected due to computational

anomalies and a method of moving the stator conductors adopted. The implementation of the moving stator method requires the definition of basic rules regarding polarity of rates of change of flux and e.m.f. These rules have been defined. The representation of motion by other authors is discussed. Setting up of initial conditions is critical and the method of initial condition determination outlined.

In chapter six computed results are presented and compared to actual voltage and current waveforms. The method of solution promoted by this thesis is compared with other methods of calculation of overlap angle and the equivalent circuit technique is shown to be more accurate. It is shown that account must be taken of the intervening period between commutations and how the solid rotor load angle and eddy currents influence commutation reactance.

In chapter seven the expansion of the electric circuit to include interaction effects when a low value of link inductor is considered. Also two hypothetical cases are studied: the machine topology is adjusted to a machine with a larger air gap and larger stator slot openings; A laminated machine is compared with results of a solid rotor machine.

The main results and conclusions are presented in chapter eight along with topics for future work.

CHAPTER TWO

THE LABORATORY SYSTEM

2.1 Introduction

To study the behaviour of current-source inverter fed synchronous motors a laboratory model was constructed according to the scheme of fig 1.1. The objectives were to study the machine performance and record current and voltage waveforms for a range of speeds, load currents and inverter firing angles. Since analysis of steady state operation only was considered an electronic start up arrangement was not incorporated. Start up was achieved by the use of Ward Leonnard control of a d.c. machine.

This chapter describes the design and construction of the inverter and associated control circuits. The stator and rotor cross-sections are included. Also, the static frequency response method used to obtain synchronous motor reactances is described.

2.2 Design Considerations and Operation of the Synchro-Inverter System

A phase controlled rectifier, fig 1.1, supplies a direct voltage, V_{dc}, to the d.c. link and inverter. If L_{dc} is chosen large enough the link current will be virtually constant and the rectifier will act as a controllable current source.

Studies on the system were begun by suppressing rectifier and inverter interaction by setting L_{dc} to a large value, 0.7H. This provided a

constant link current, I_{dc}. In practice L_{dc} is minimized as an increase in inductance entails an increase in its size, weight and cost. Guidelines used in industry for choosing L_{dc} for a current source system are given as

$$L(mH) = \frac{150}{f_s} \frac{V_{dc}}{I_{dc}}$$

or elsewhere as

L_{dc} chosen for I_{dc} ripple < 10%.

The choice of a large inductance resulted in machine waveforms unaffected by rectifier/inverter interaction. Overlap angle was then readily measurable.

The motor and inverter frequencies are locked together by the control loop of fig 1.1. With an applied load the motor takes up a speed that brings the whole system into balance. For a constant mechanical load variation of speed is achieved by adjusting the level of V_{dc}. The firing angle, β, of the inverter sets the point at which phase current transfer takes place and its influence on motor speed was a second order effect. Forcing the inverter frequency to equal the rotor frequency is, in theory, simply achieved by monitoring motor phase voltages to provide a time reference for the firing angle, β.

The motor stator is connected in star with the star point floating. Each commutation is then similar to a line-to-line short circuit [8,9] and earthing the star point of the motor would set up a detrimental earth loop.

Firing angle, β, must be of sufficient duration for commutation to take place, as well as allowing a safety angle after commutation to ensure thyristors have fully recovered, before the line-to-line voltage falls to zero. Since phase currents are leading phase voltages the motor must be over-excited. A constant field current was set for all tests although in practice an AVR may be used to compensate for armature reaction (v/f = constant field control).

The need for a complex electronic starting scheme was avoided by mechanically coupling the synchronous motor to a d.c. machine connected in a Ward Leonnard arrangement as in fig. 2.1. In this way the d.c. machine was used as a motor to run the synchronous machine up to a speed until sufficient motor back e.m.f. existed for thyristor commutation. The converter was then gradually brought in by increasing the link current. Adjustment of C_2 field, fig 2.1, subsequently provided a load control on the synchronous motor.

The rotor load angle was measured for each test with a stroboscope synchronized with the motor phase voltage. The strobe light was shone onto a disc attached to the motor shaft having a circumference marked in degrees. A pointer attached to the stator frame provided a fixed datum for measurements. This method was chosen for its simplicity and the accuracy achieved was half a degree mechanical, ie one degree electrical.

2.3 Inverter Control Circuitry

The inverter control loop was based on a design used at GEC Large Machines of Rugby. A schematic showing the signal processing sections is given in fig 2.3.

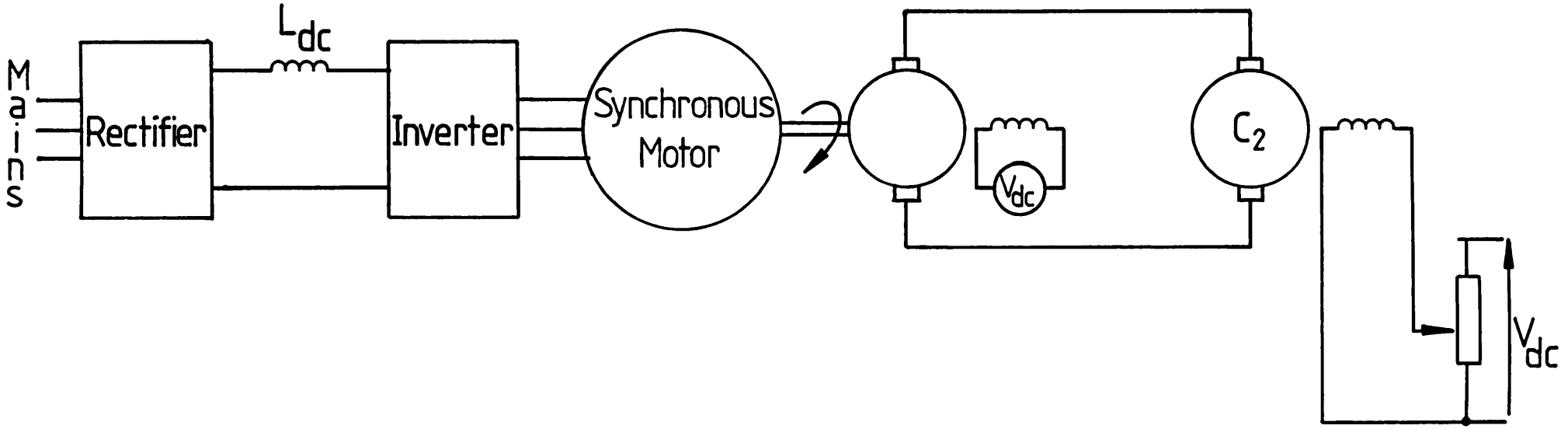


Fig.2.1. Laboratory System showing Ward-Leonnard Connection.

2.3.1 Earthing and De Coupling

Particular care was paid to grounding and eliminating noise from control circuits. The following precautions were adhered to, thereby reducing electro-magnetic pick up and coupling.

1. CMOS (B) logic circuity and op-amps were used throughout for their noise immunity.

2. Each chip was decoupled to ground with a 0.1 F capacitor situated as close as possible to the power supply pins.

3. Earth loops were avoided. Signal grounds, equipment, chassis, and power grounds were kept separate but brought to a single common point.

4. The logic circuits were enclosed in a die-cast box to further minimize E.M. pick up.

5. Electronic logic circuits and thyristor firing circuits were supplied from separate power sources.

6. Screened cables, kept as short as possible, connected the processing circuits with thyristor firing circuits. Cable loops were also avoided.

7. Switching transients were minimized by connecting snubbers directly across thyristor terminals.

8. Pulse transformers isolated the logic circuits from the inverter power circuit.

2.3.2 Signal Processing Circuits

The object of the signal processing section was to derive the correcct firing sequence for the six inverter thyristors from the motor phase voltages.

Voltage transformers, fig 2.2 (a), stepped down the phase voltage signals to a level compatible with the logic circuits. Each phase was monitored and transformer secondaries were centre tapped thereby doubling the signals available for processing. This was necessary to obtain the six pulses per cycle for thyristor triggering. Fig 2.2(b) shows how the six pulses were derived from the phase voltage waveforms.

Potentiometers were incorporated to balance the phase signals to give equal voltage amplitudes for processing. It was found that the firing angle of the thyristors was not identical between phases. These differences were attributed to the voltage-transformer load resistors not being set identically. The tuning of the resistors was very sensitive. However, the method proved to be satisfactory even if rather crude.

Fig 2.3 represents the processing circuits for three firing channels. Voltages v_a, v_b and v_c were picked up from the points denoted in fig 2.2(a). The signals in each set of three channels were therefore displaced by 60^o. This circuit was duplicated for the remaining three channels whose input signals were v_a', v_b' and v_c'. A description of

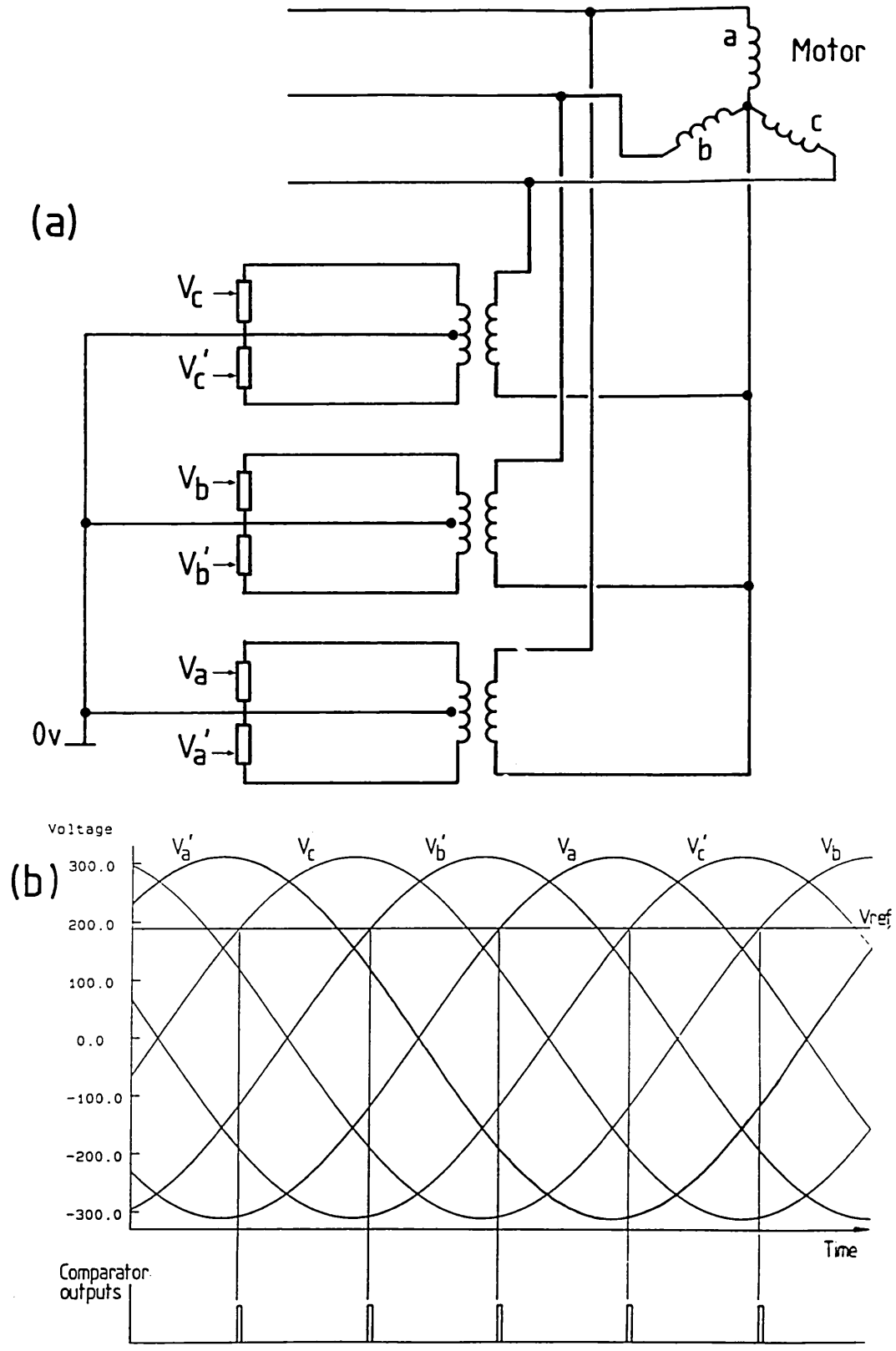


Fig.2.2 Derivation of Firing Pulses.

the processing stages follows, with specific reference to the schematic of fig 2.3 and corresponding waveforms of fig 2.4.

Low pass filters removed commutation notching and other noise present in the phase voltage waveforms. Single stage Butterworth filters [10] were used with a cut off frequency of 80Hz (fig 2.5). The filtered signals, fig 2.4(b), were compared to an adjustable reference voltage, setting the firing angle, β. The comparator (fig 2.6) produced a pulse every time the signal f_n went positive and equalled V_{ref}. The resulting narrow pulse width of the comparator signal, c_n, was not in itself of sufficient duration to provide a reliable clocking signal for the S-R latch. Comparator outputs were therefore expanded using monostables (fig 2.7) giving a 3.3ms fixed pulse length, m_n.

To ensure thyristor switching was successful the gating signal was enabled for as long as possible. To maximize the time a thyristor was enabled a set of S-R flip-flops were configured as in fig 2.8. The arrival of a pulse at a latch not only enabled that particular latch but switched the last latch off (fig 2.8). Thus at any one instant one S-R latch was on, in the top and bottom sets of channels. The pulse train of fig 2.4(e) resulted (the numbers on each waveform corresponding to relevant inverter thyristors, fig 1.1).

To give reliable operation multipulse firing was adopted where the outputs of the shift registers enabled an astable circuit, fig 2.9, in each line. The advantage with this circuit was that the first firing pulse occurred immediately upon arrival of the S-R gating signal. The operating frequency of the astable was determined by the values of discrete components and the threshold levels of the gates used, in this case a frequency of 8kHz was used. This high frequency was

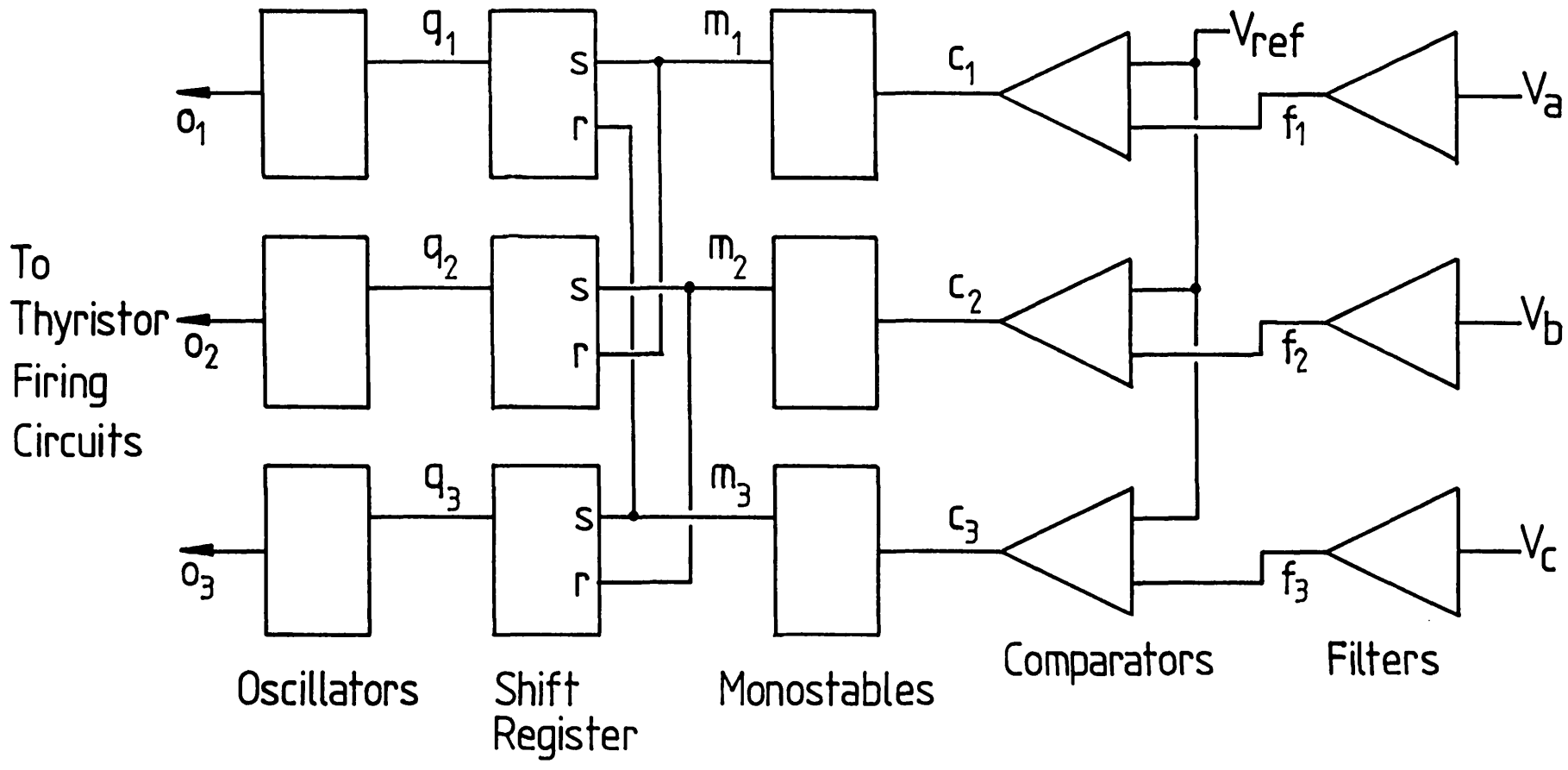


Fig.2.3. Schematic Showing Firing Channels for Three Channels.

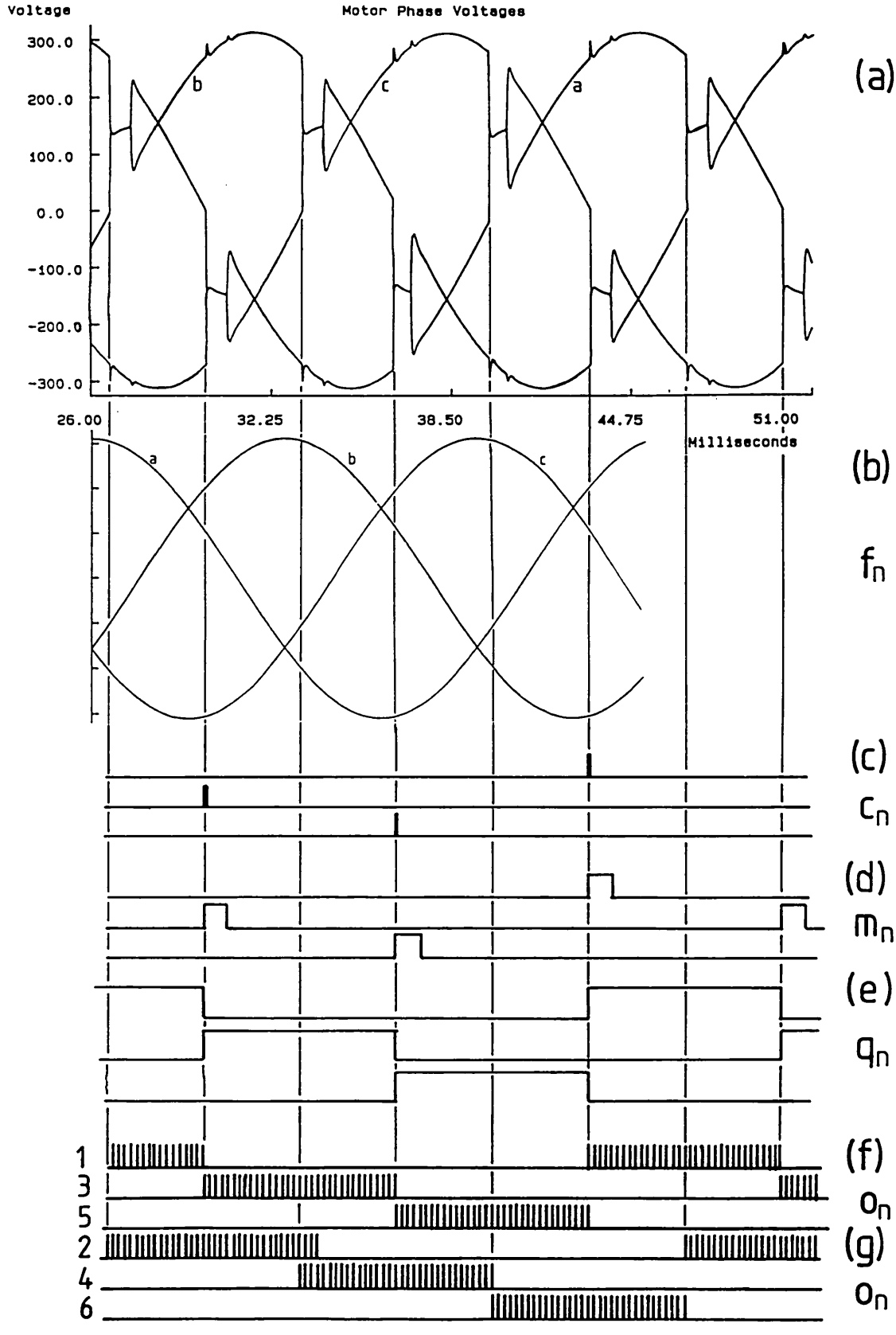
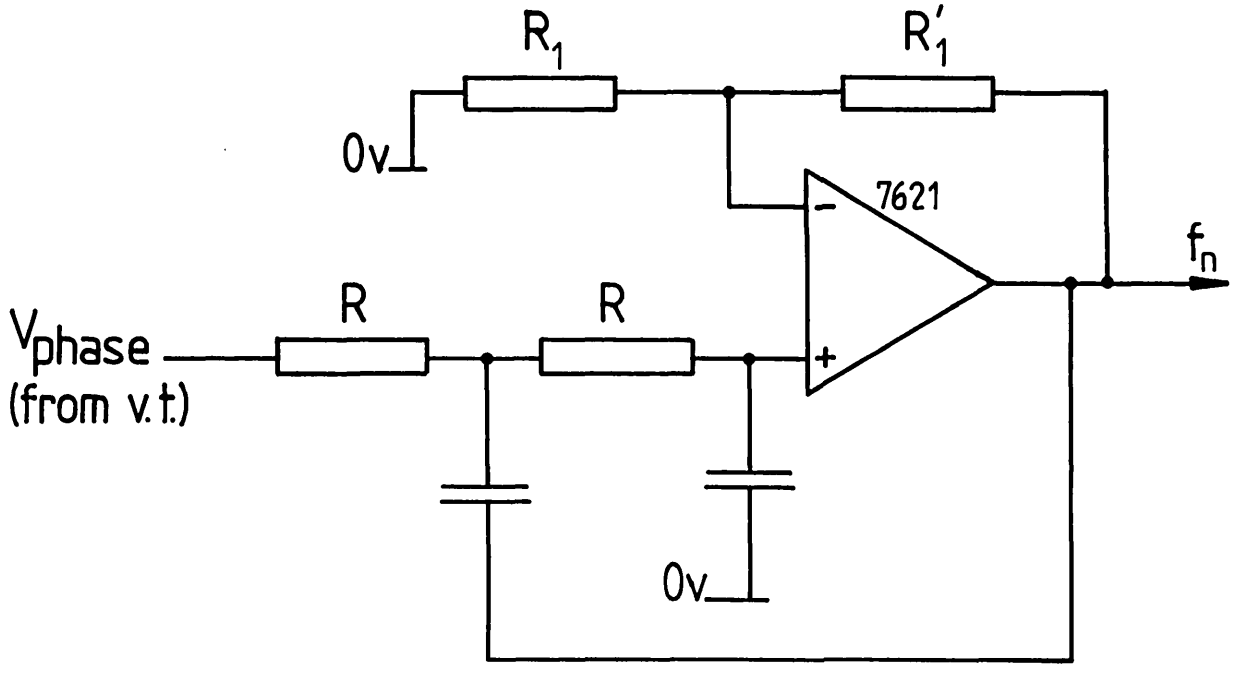


Fig.2.4. Waveforms Corresponding to Fig.2.3.



R =10k
R =12k
R =20k
C =0.1μF
Cut off frequency=80Hz

Fig.2.5. Butterworth Second Order Low Pass Filter.

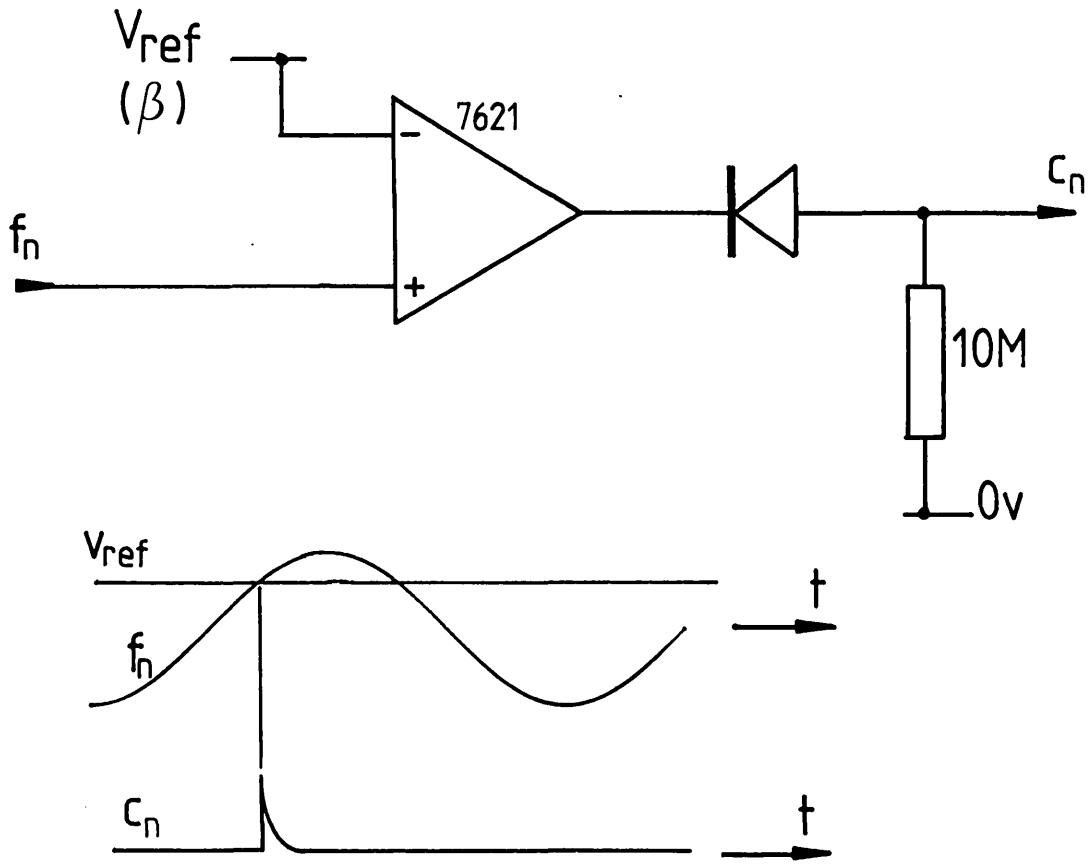
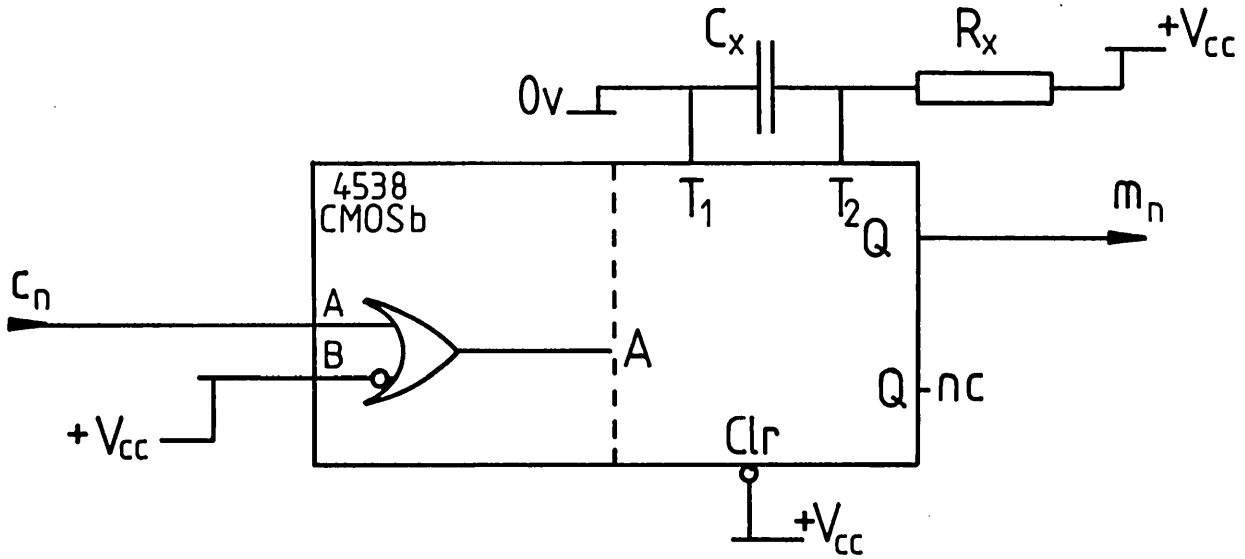


Fig. 2.6. Comparator.

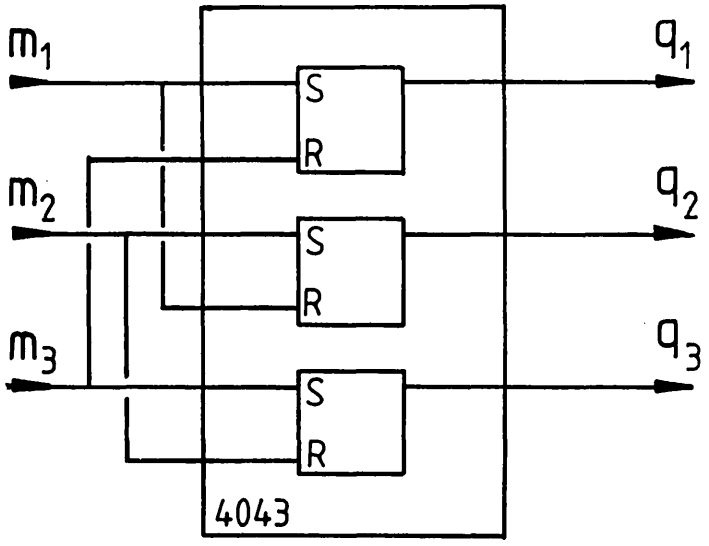


C = 0.1μF
R = 47k

Pulse width = 3.3 ms

Fig. 2.7. Monostable.

Monostable signals



Truth table for a single r/s latch

S	R	Q_{n+1}
0	0	Q_n
0	1	0
1	0	1
1	1	?

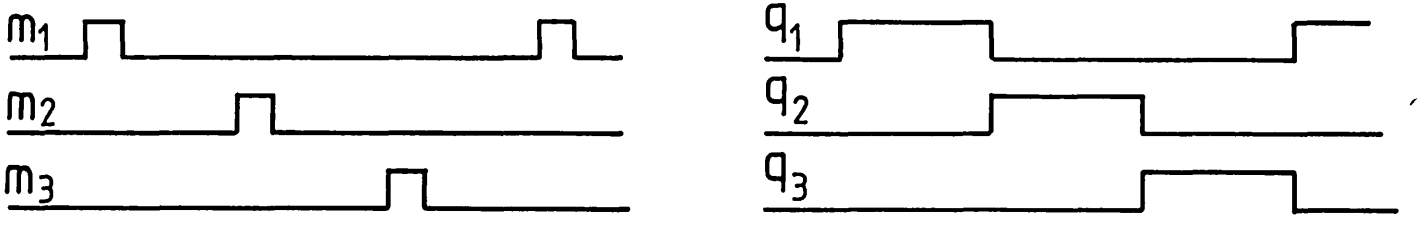
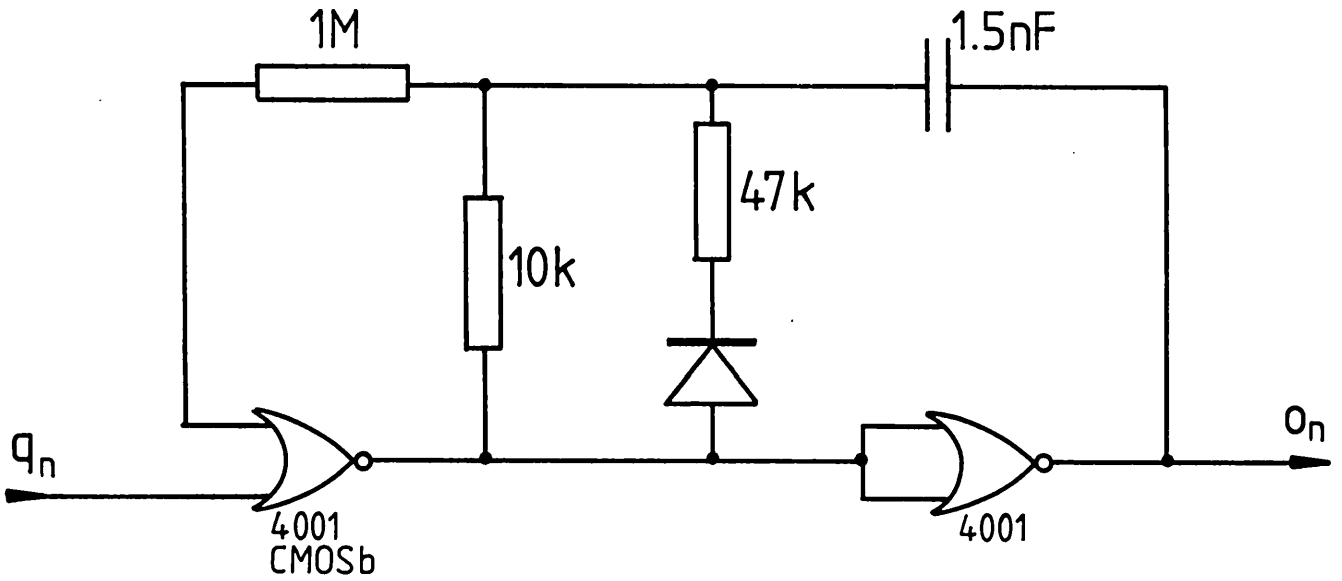


Fig.2.8. Shift Register Using a CMOS 4043(b) R/S Latch.



Frequency of oscillation = 7kHz

Fig. 2.9. Oscillator.

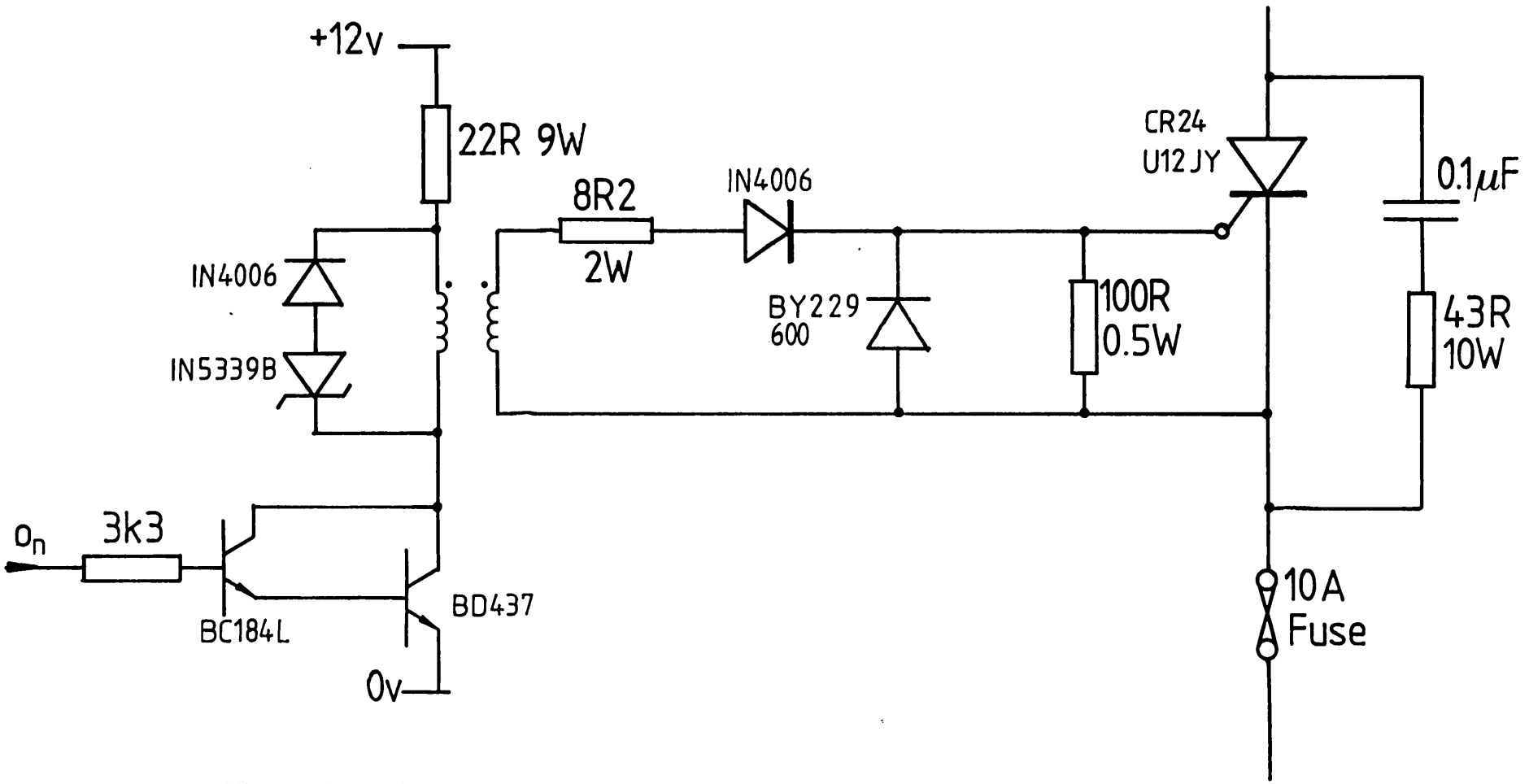


Fig. 2.10. Thyristor Trigger Circuit.

necessary to avoid saturation of the pulse transformers.

The complete set of resulting signals is shown in fig 2.4(f) and (g). Thus providing the correct thyristor firing sequence, the top set (f) firing thyristors 1, 3 and 5, and (g) the lower set firing 4, 6 and 2.

The astable pulses were amplified by the Darlington pair of fig 2.10, the transistors then driving a pulse transformer providing isolation between thyristors and logic circuits.

The thyristor side firing circuit was designed to limit gate current and protect against over-voltages and reverse gate voltages. C_S and R_S constitute a snubber circuit limiting voltage transients at switching. A separate firing circuit d.c. power supply avoided supply line noise affecting logic suplies.

2.4 The Synchronous Motor

The main experimental tests were conducted on a Mawdsleys four pole micro-alternator of stator type described by fig 2.11, fig 2.12 and table 2.1, connected in three phase star. No data was available for the solid salient rotor except for an engineering drawing giving rotor dimensions. The rotor cross section is given in fig 2.13.

Some preliminary tests were performed on a micro-alternator (No 1) having a laminated rotor (No 5) with a damper cage [11].

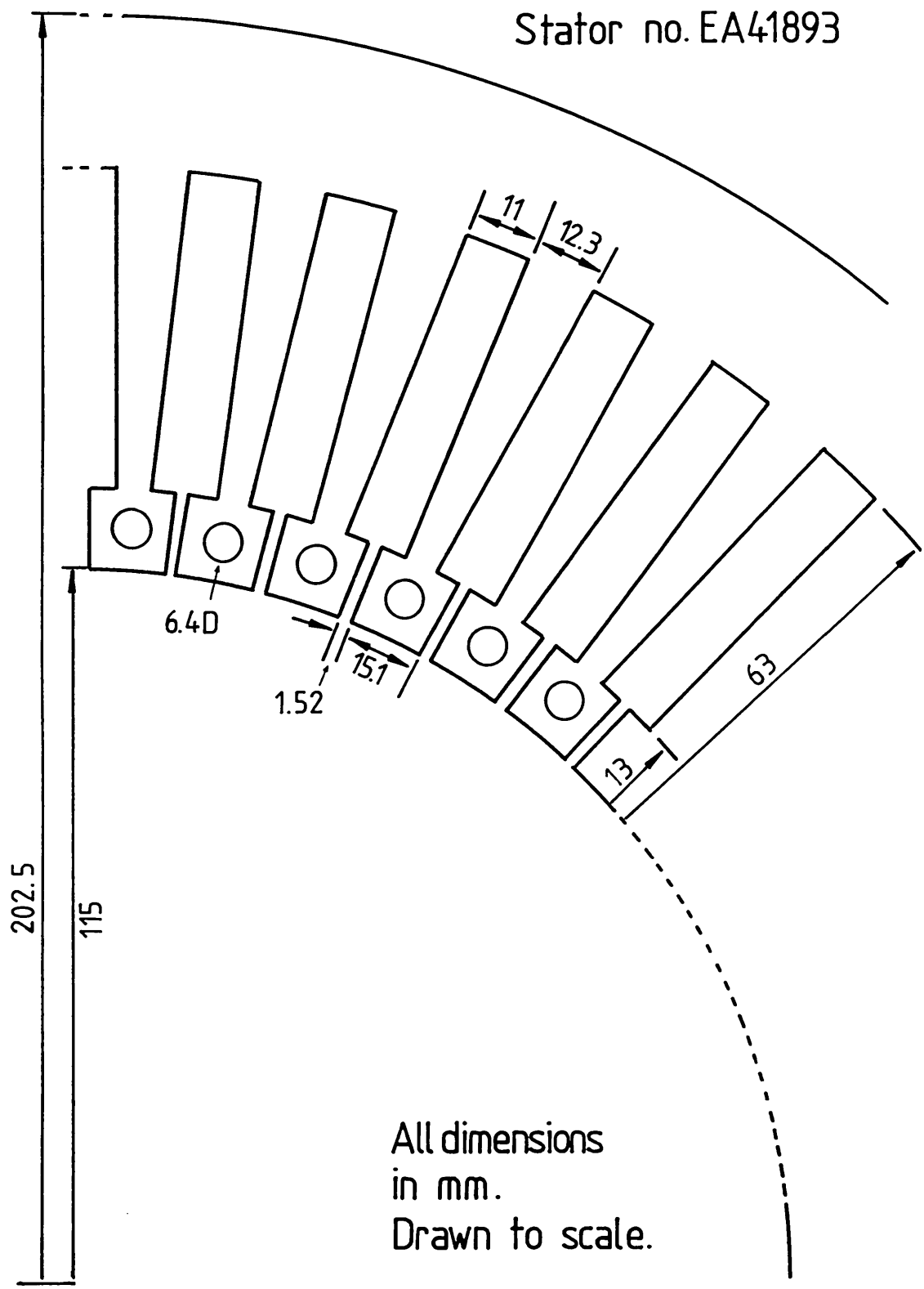


Fig.2.11. Sator Cross Section.

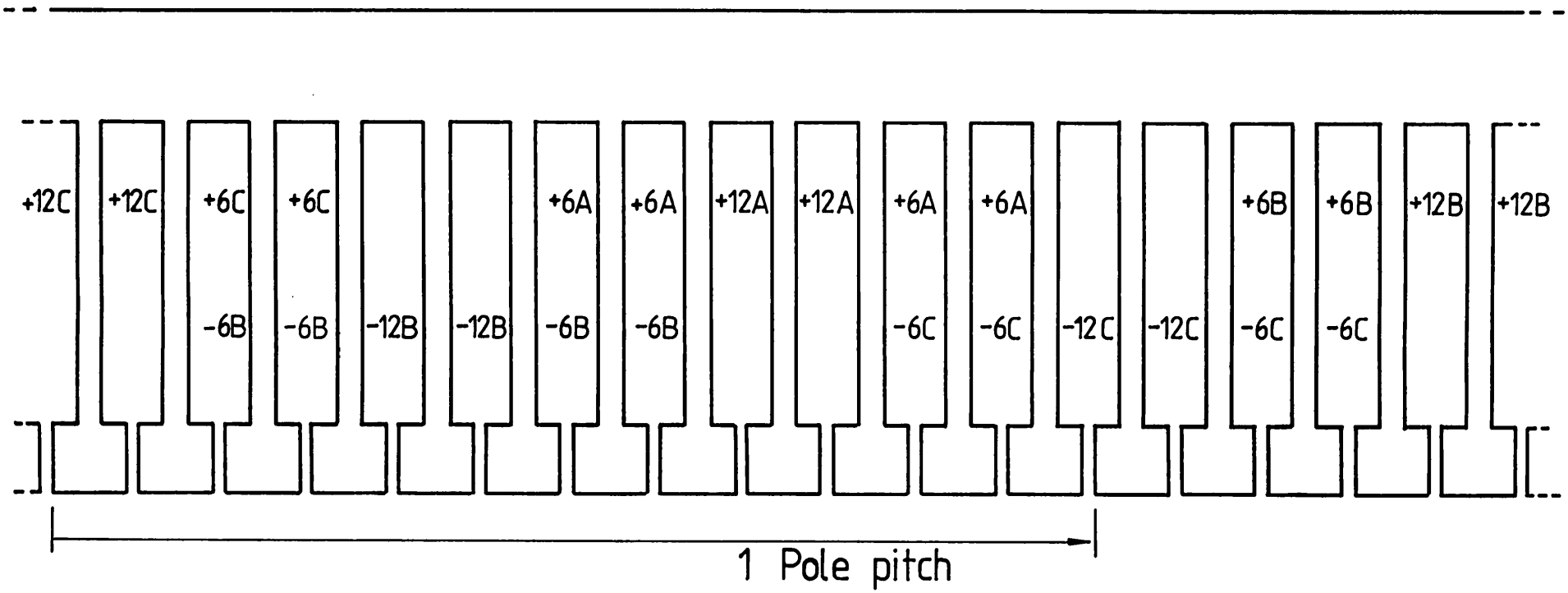


Fig.2.12. Developed Stator Cross Section Showing Phase Band Distribution.

Table 2.1

Mawdsley Microalternator stator No EA41893

3kVA 11Ø/635v, 6 phase star connected 5ØHz, or 22Ø/127v, 3 phase star connected. 5ØHz.

Phase volts	= 62v
Iph (full load)	= 8A
Poles	= 4
Frequency	= 5ØHz
Slots	= 48
Conds/slot	= 12
Turn/phase	= 48
Winding type	= 2 tier double layer
Coil pitch	= 1-11
Winding factor	= .92
Phase Resistance (15°C)	= .Ø35
Slot skew	= One slot pitch
Axial length gross	= 14cm
Axial length effective	= 13.2cm

All dimensions in mm.
Drawn to scale.

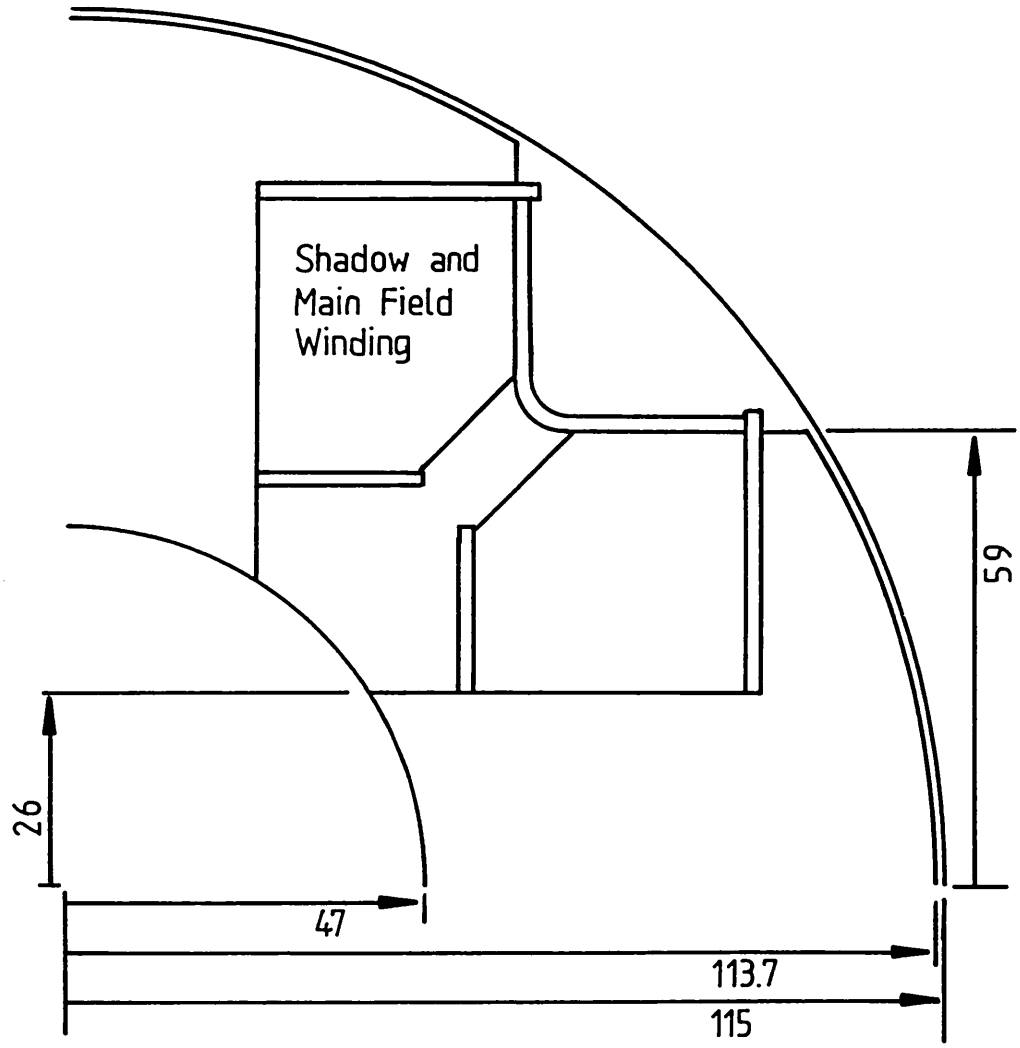


Fig.2.13. Solid Rotor Cross Section.

2.5 Measurement of Overlap Angle, μ.

The commutation time, also referred to as overlap angle, is defined as the time taken for current to transfer from one phase to the next. The aim of laboratory tests was to record the variation of commutation angle, μ, for different operating points and to use results for validation of computer simulations. The inclusion of a large d.c. choke facilitated the measurements of μ from either the phase voltage or current waveform, as shown by the waveforms of fig 2.14.

Hall effect current transducers provided a safe and accurate means of measuring alternating and direct currents around the synchro-inverter system.

2.6 Measurement of Machine Operational Inductances

The static frequency response test method [12,13] was adopted to obtain stator operational inductances for d and q axes. An attractive feature of this method was that low test currents pose no hazard to the machine windings. The experimental test set up is shown in fig 2.15.

Two phases were connected in series to limit the stator current, i_s. Thus requiring the field axis to be aligned with the appropriate combined stator phase axis for d and q axis tests. The field circuit was shorted throughout tests. A current shunt (0.05 Ω) was used to monitor i_s. Measurements of magnitudes and angles of v_s and i_s were carried out with a transfer function analyser for a range of frequencies from .01Hz to 1kHz. The flux level was kept constant by adhering to v_s/f = constant for the duration of testing.

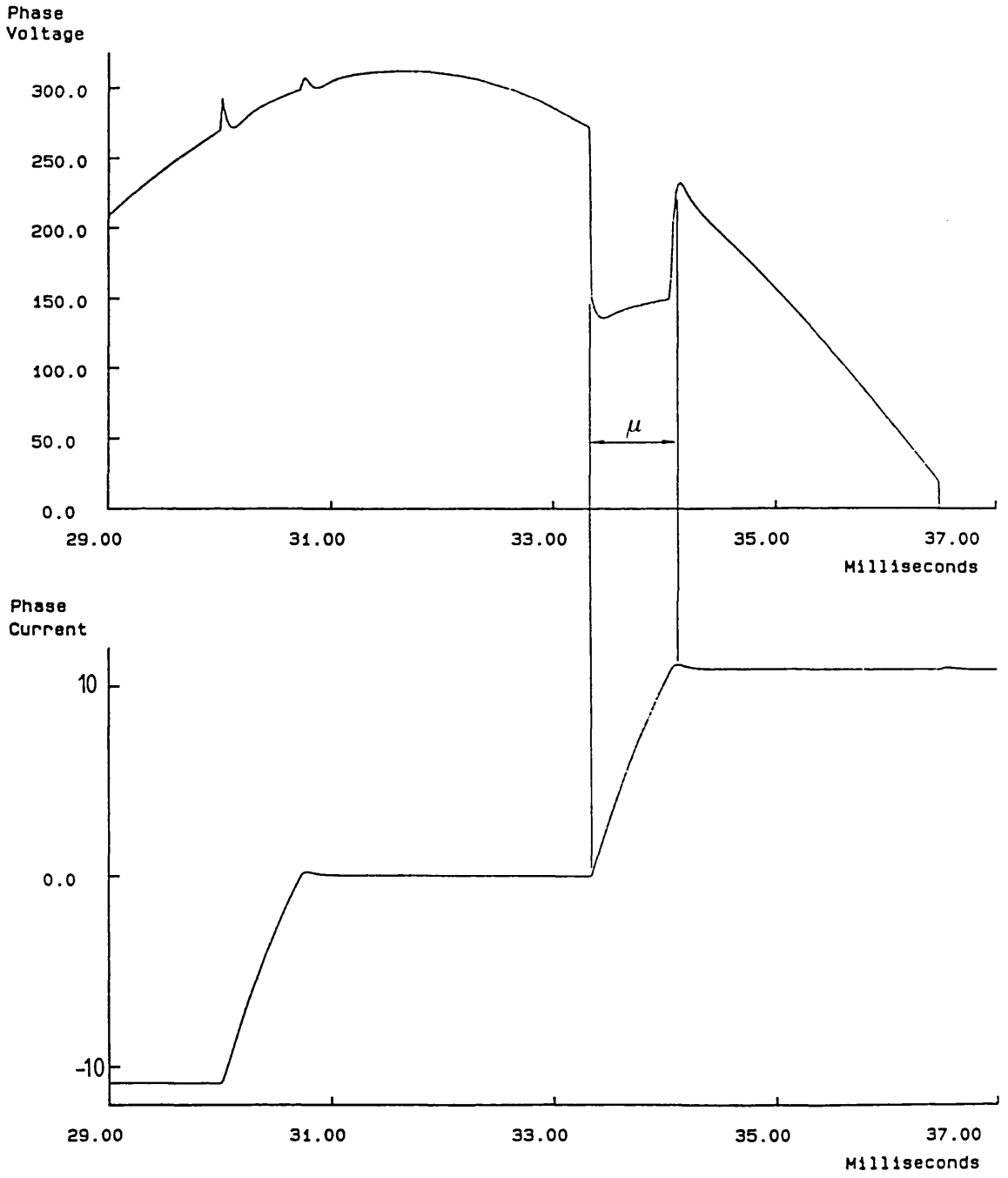


Fig. 2.14 Measurement of Overlap Angle

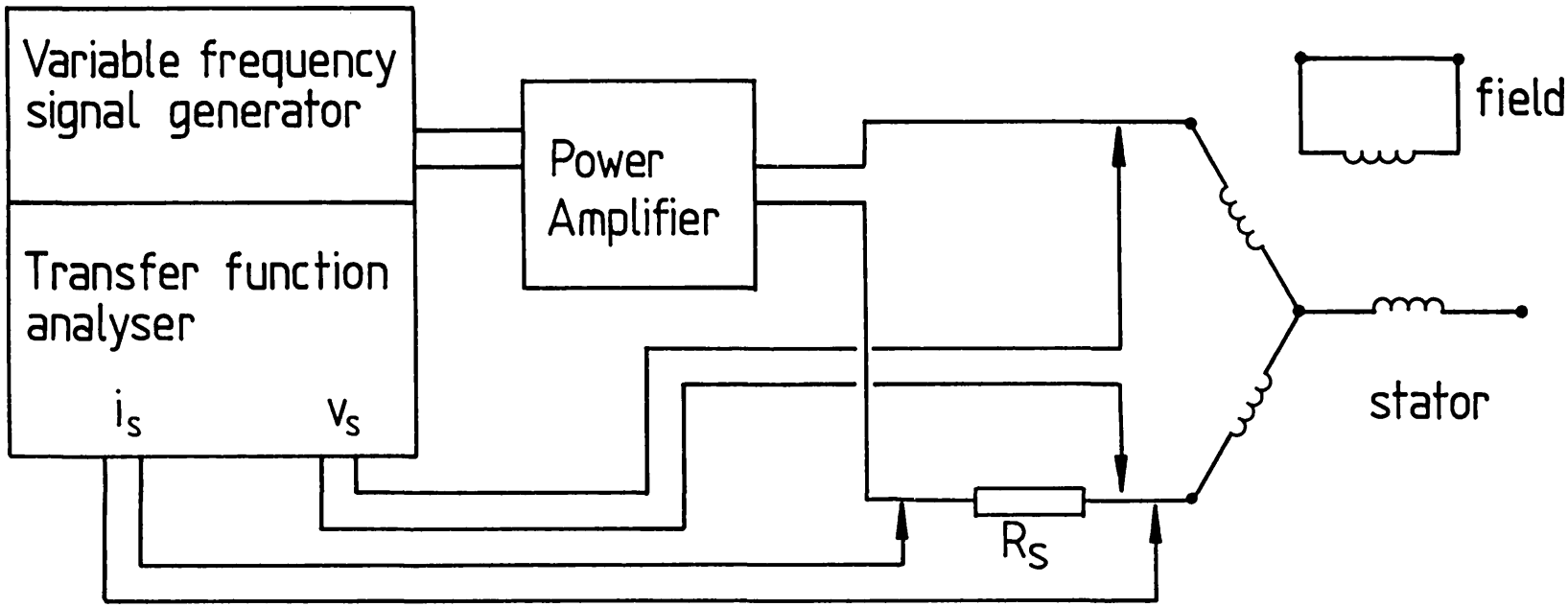


Fig. 2.15. Static Frequency Response Test Circuit.

Operational inductances were calculated from v_s and i_s by finding the phase impedance,

$$\bar{Z}_s(\omega) = \frac{v_s \angle \gamma}{2 \cdot i_s \angle \theta} \quad (\omega) \quad ,$$

for a single winding. The operational reactance was therefore,

$$\bar{X}(\omega) = \bar{Z}_s(\omega) - R_a,$$

where R_a was the d.c. armature resistance. This yielded a set of inductance magnitudes and associated angles for a range of ω.

The validity of the frequency response method is questionable [14,15]. Errors in measurement are dominant at low frequencies where very small currents must be measured and the measuring equipment sensitive enough to record phase angles of a few degrees. However, interest was at the high frequency range of operational inductance, the region representing the machine's subtransient reactance. Results are shown in chapter six.

CHAPTER THREE

AN ANALYSIS OF COMMUTATION

3.1 Introduction

The synchronous motor's power factor is determined by the inverter firing angle, β. Sufficient time must be allowed for the commutation of thyristors plus a safety angle, δ. An appraisal of the commutating duration is necessary since an increased β is required for longer commutation times. Motor performance is therefore subject to the length of commutation.

A synchro-inverter system incorporating a laminated rotor machine can be analysed successfully using two axis theory and the performance may be estimated even more simply by consideration of the electrical switching network only, with a constant value of reactance behind the machine voltage (usually the subtransient reactance). The parameters of a solid pole motor can be expressed as impedances, but the values vary as a function of duration of commutation and flux distribution in a complicated manner.

The calculation of machine parameters for a solid rotor machine requires a field solution allowing for rotor position, the distortion of flux and eddy currents with associated skin effects. The flux pattern may be distorted before commutation, previous commutations having already upset the field pattern.

3.2 Commutation as Seen by the Inverter

During steady state operation the inverter switches a direct current pattern around the stator windings producing torque by the advancement of stator m.m.f. A positive power flow into the motor is accomplished by switching positive current into a phase while phase voltage is positive. The inverter firing sequence (corresponding to fig 1.1) is shown in fig 3.1 with the three phase currents and voltages. Apart from the commutation period two phases are connected in series with the d.c. link at any one time. The stages of commutation are shown in fig 3.2 corresponding to fig 3.3.

At the instant before commutation, as shown in fig 3.2(a), direct current is flowing in phases a and c through thyristors one and two. Current must next be transferred from a to phase b, current in c remaining the same. Thyristor one must be switched off and number three switched on. Commutation is accomplished by switching thyristor three on, fig 3.2(b), connecting the line-to-line voltage v_{ab}, fig 3.3(c), across the cathode to anode of thyristor one. v_{ab}'s polarity opposes the current flow in thyristor one and if of sufficient magnitude will force i_a to zero, fig 3.2(c). The relevant current and voltage waveforms are given in fig 3.3. Commutation is not instantaneous, the current will have a certain gradient, fig 3.3(b). Also, commutation forms a line-to-line short circuit across the motor so that the phase voltages will step to the average of the two phase values resulting in "notching", fig 3.3(a).

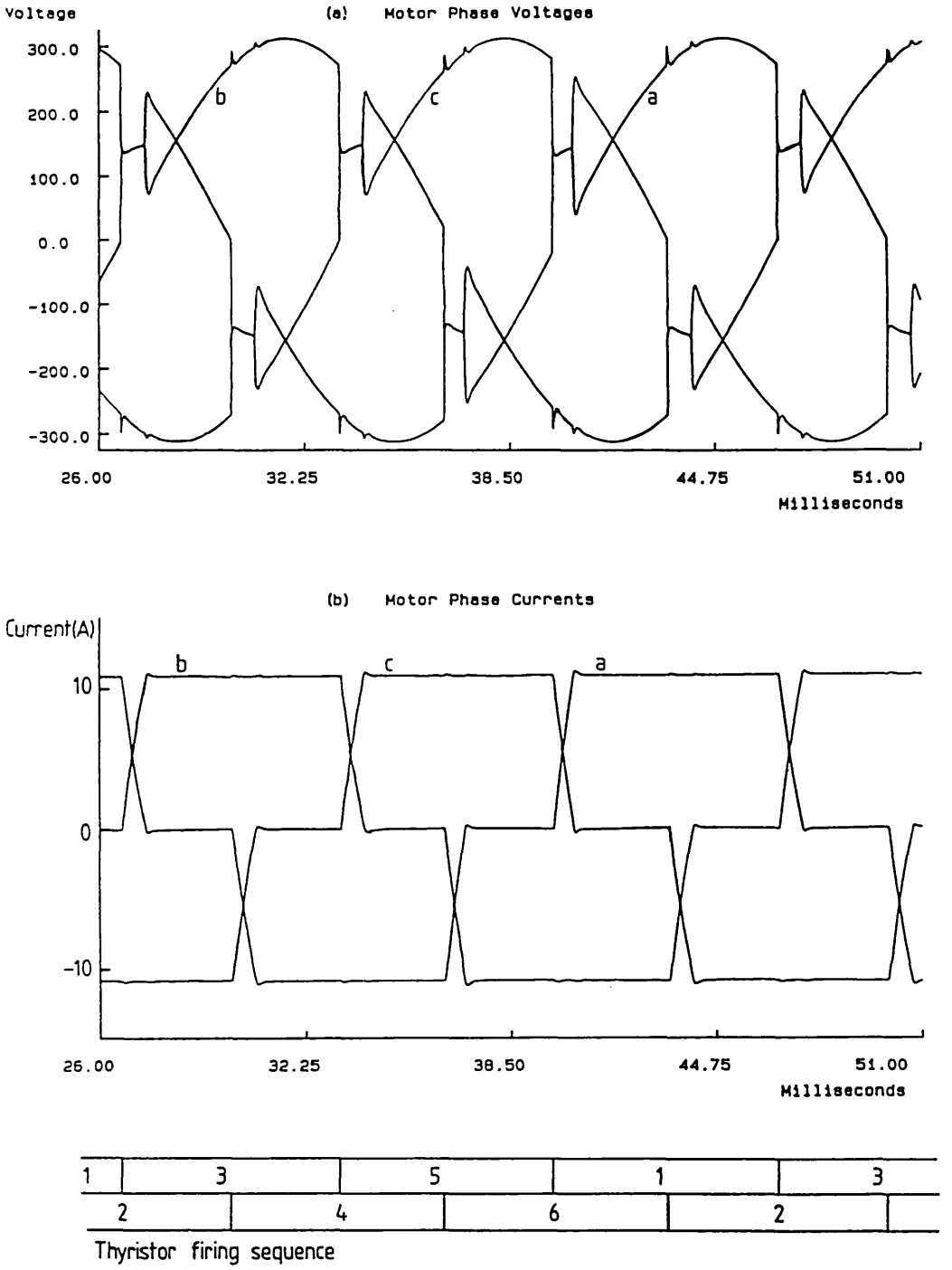


Fig.3.1. Motor Phase Voltage and Current Waveforms Corresponding to fig.1.1.

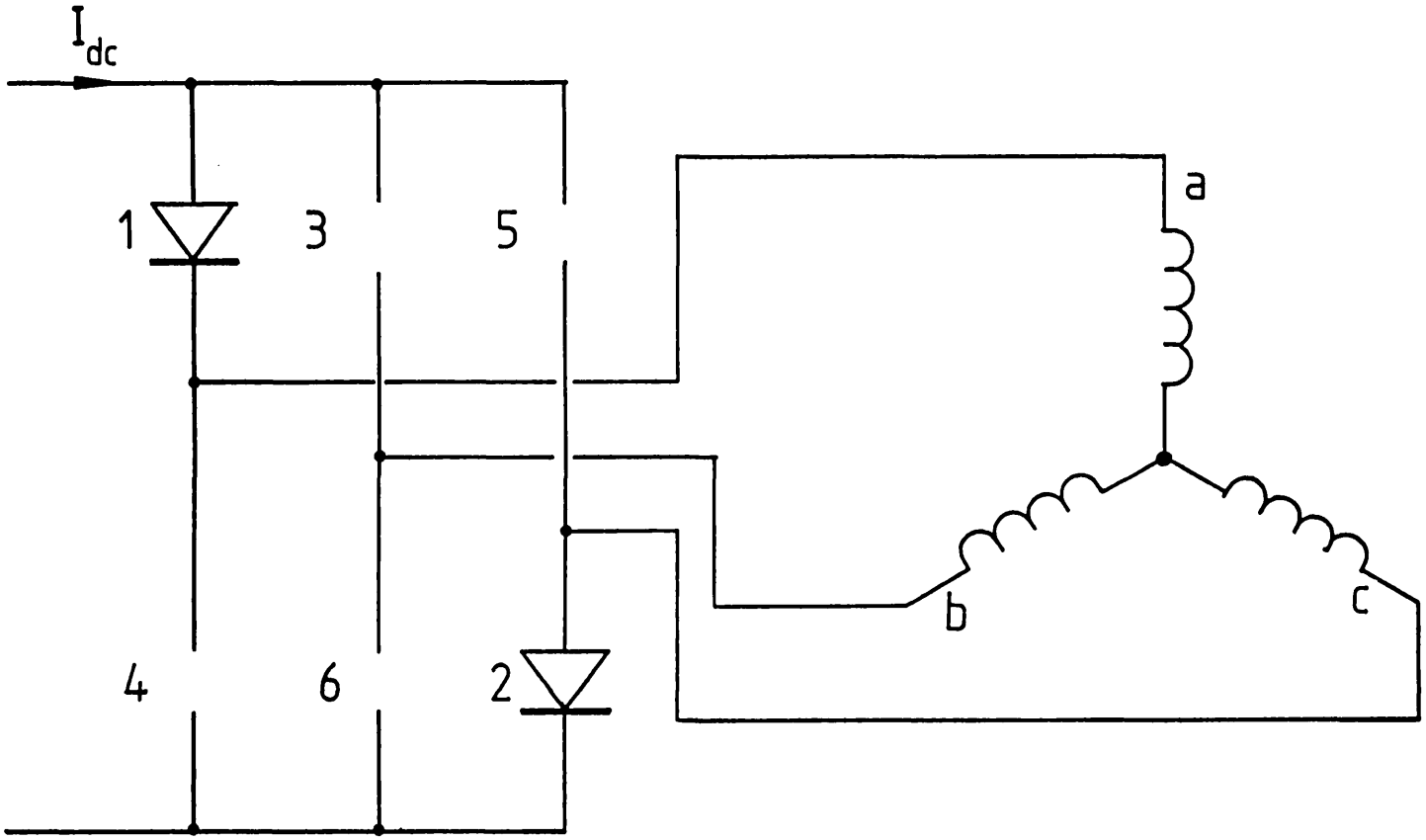


Fig.3.2(a). Phase a and c Carrying I_{dc}.

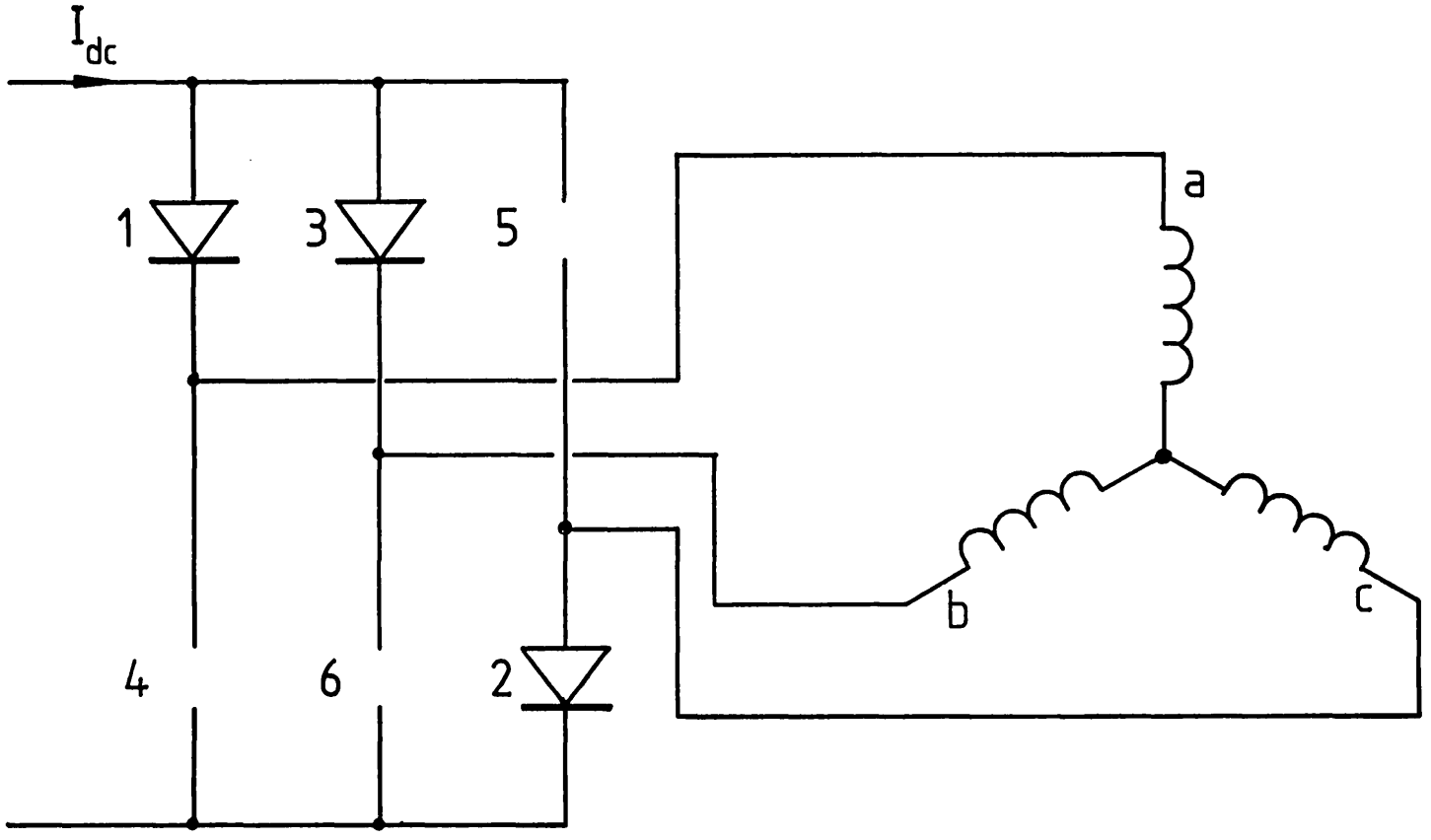


Fig.3.2(b). Commutation of Current from Phase a to b.

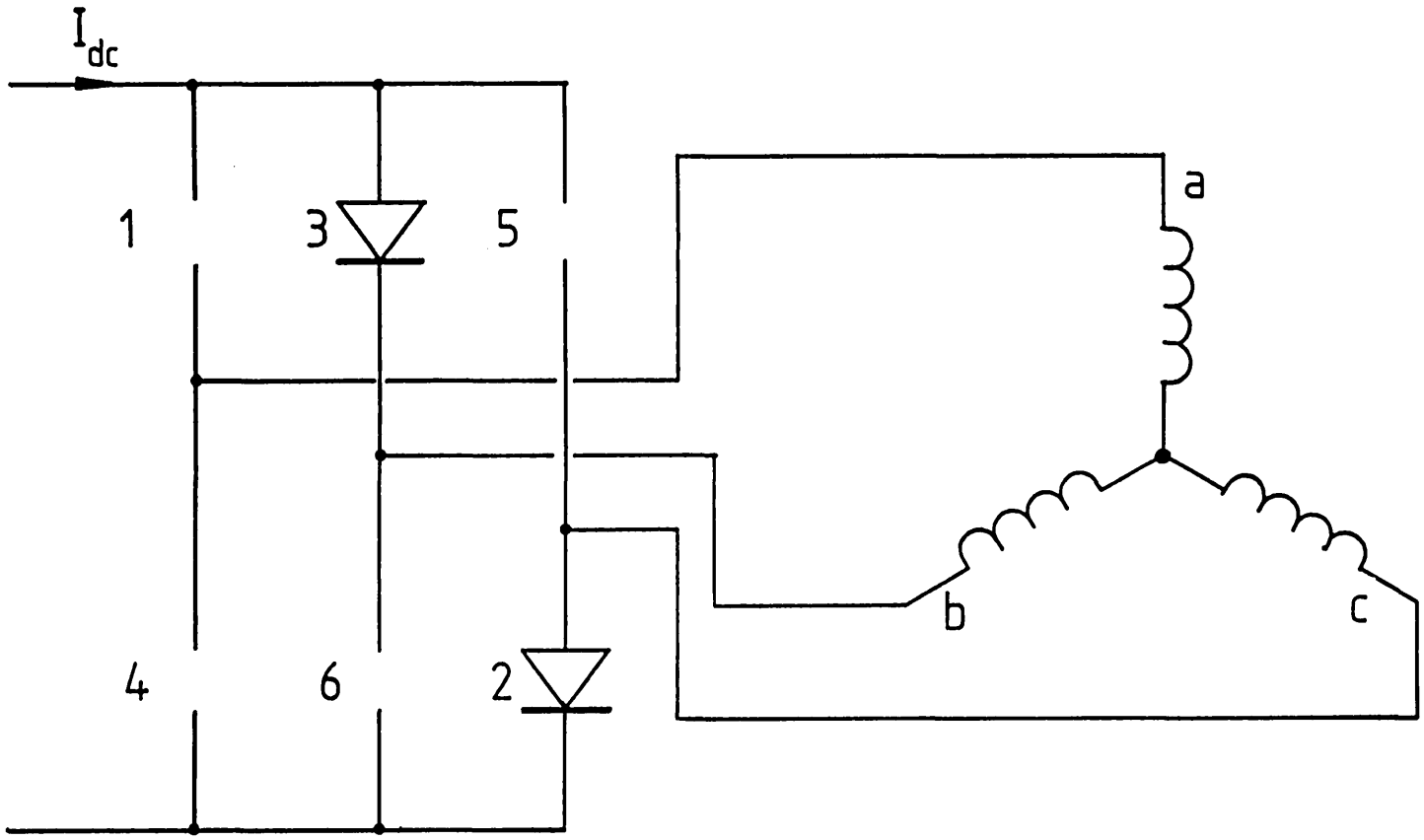
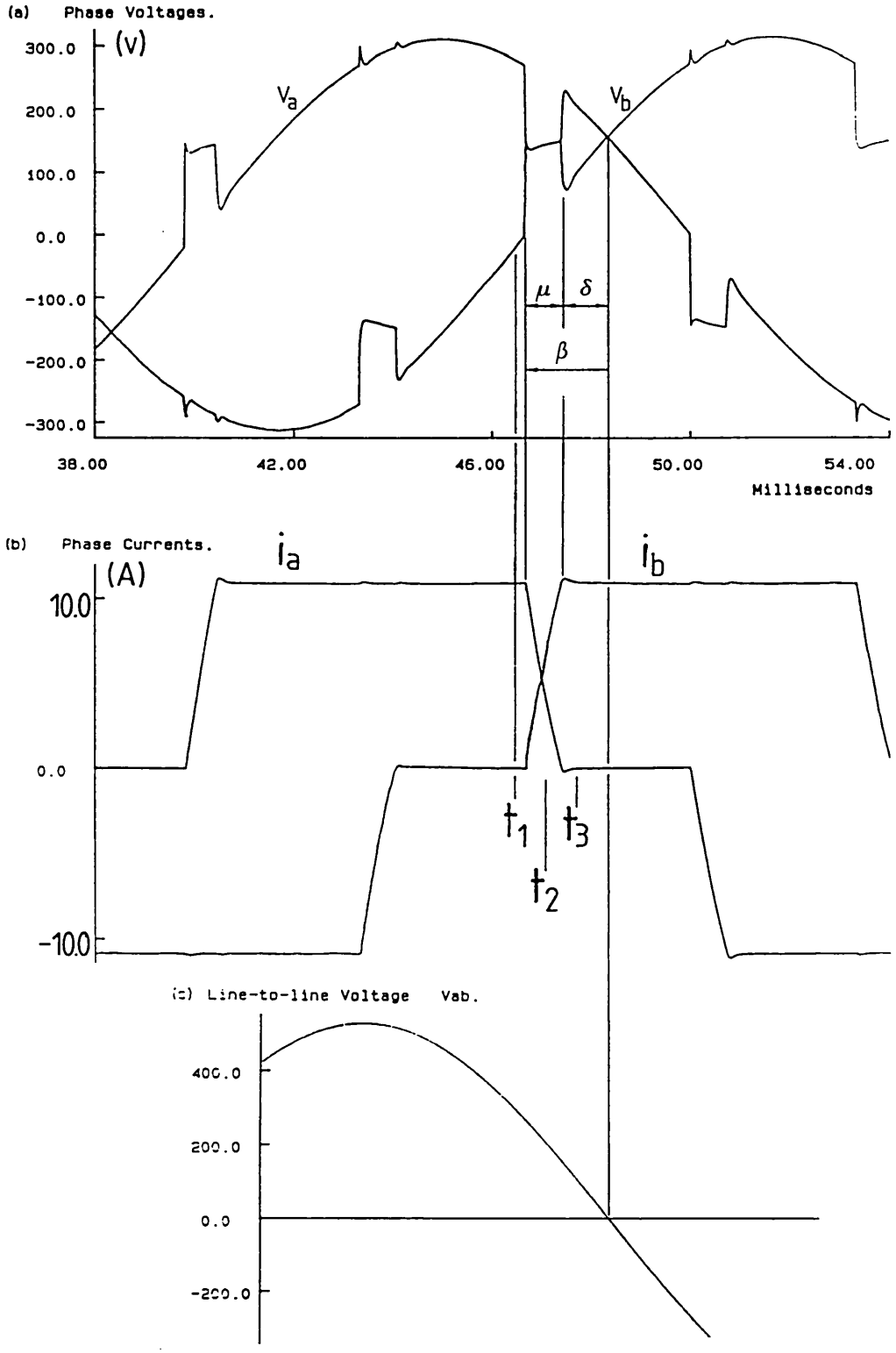


Fig. 3.2(c). Phase b and c Carrying I_{dc}.



δ = Safety angle
μ = Commutation angle
β = Firing angle

Fig.3.3. Voltage and Current Waveforms Corresponding to fig.3.2.

3.3 Factors Influencing Commutation Time

As a consequence of the natural commutation of inverter thyristors the commutating duration can be attributed to four dominant and other more moderate parameters, briefly discussed below.

Load Current

Increased levels of phase current protract commutation. So, commutation is significant when the system is running at full load drawing maximum current.

Machine Phase Voltage

Commutation relies upon the voltage available at the motor terminals to force thyristors off. By augmenting the motor excitation a shorter commutation can be achieved.

Inverter Firing Angle, β

Advancing the firing angle, β, increases the line-to-line voltage applied across the thyristor to be switched off. Therefore, commutation time contracts as β increases.

Commutation Reactance, x_c

The rate of transfer of current from one phase to the next is restricted by the reactance of the two commutating phases. The larger the reactance the longer commutation takes.

The Influence of Other Parameters

The stator winding and thyristor resistances will generally be negligible, their effect on commutation nominal.

Low values of link impedance will upset the synchro-inverter stability [16]. Rectifier switching will propagate through to the inverter side disturbing inverter switching and vice versa. Oscillation of link current can also arise as a result of small choke values.

Thyristor re-triggering can take place if sufficient time is not allowed after commutation for the thyristor to recover its full blocking capability. The required interval for thyristor recovery is not a constant but a function of several parameters including the thyristor characteristics [17].

Simple Calculation of Commutation Time

The dependence of commutation time, μ, upon the four main factors of β, I_{dc}, V_{ph} and x_c is demonstrated by the well known equation [8],

$$\mu = \beta - \cos^{-1} \left\{ \cos\beta + \sqrt{2}\,\frac{I_{dc}\, x_c}{3\, V_{ph}} \right\} \qquad (3.1)$$

Of the four main factors influencing commutation time all are known for a particular operating point except for x_c which must be calculated or measured.

3.4 The Value of Commutation Reactance

For a machine with a laminated rotor the commutation reactance can generally be taken as the average of the subtransient reactances x_d'' and x_q''. Even so this may not be a sensible assumption since the variation of machine subtransient reactance with rotor angle may be considered typically as in fig 3.4. It may be more accurate to choose a value for a curve such as fig 3.4 knowing β and rotor load angle.

For a solid rotor machine the problem becomes more complicated since eddy currents and the complex distribution of flux makes parameter calculation difficult.

To address the problem it is useful to study the magnetic conditions present in the motor during and in between commutation.

3.5 Influence of Commutation on the Motor Magnetic Field

The sudden movement of stator current around the machine windings six times every electrical cycle significantly upsets the normal motor flux pattern. An examination of the magnetic field movement is undertaken for a general motor and consideration of the solid rotor pole case is outlined.

3.5.1 Influence of Commutation on a Two Pole Motor Magnetic Field Pattern

Commutation may be best visualised for a two pole machine so that electrical and mechanical degrees may be equated. Fig 3.5 shows a machine cross section with m.m.f. components for the instant just

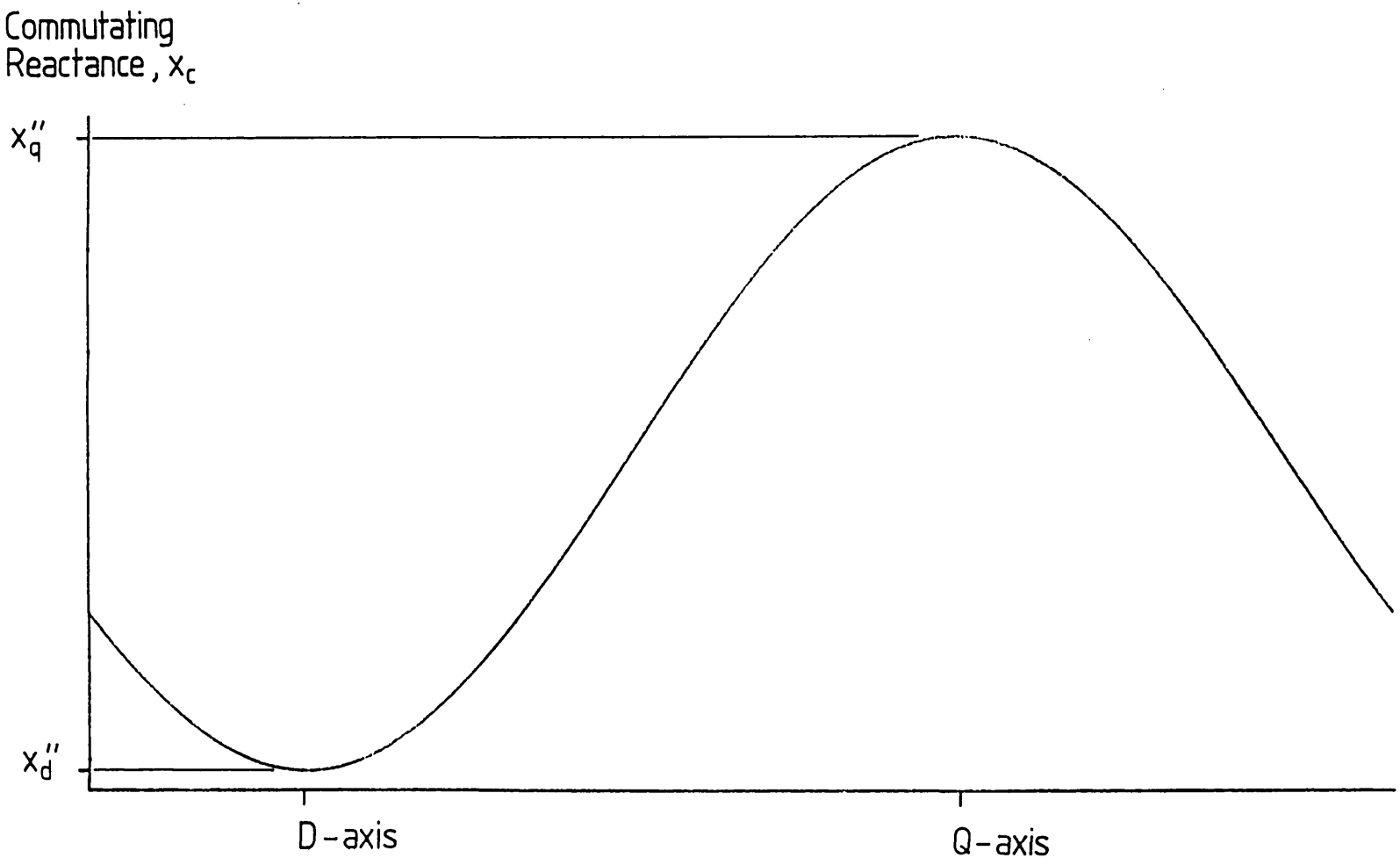
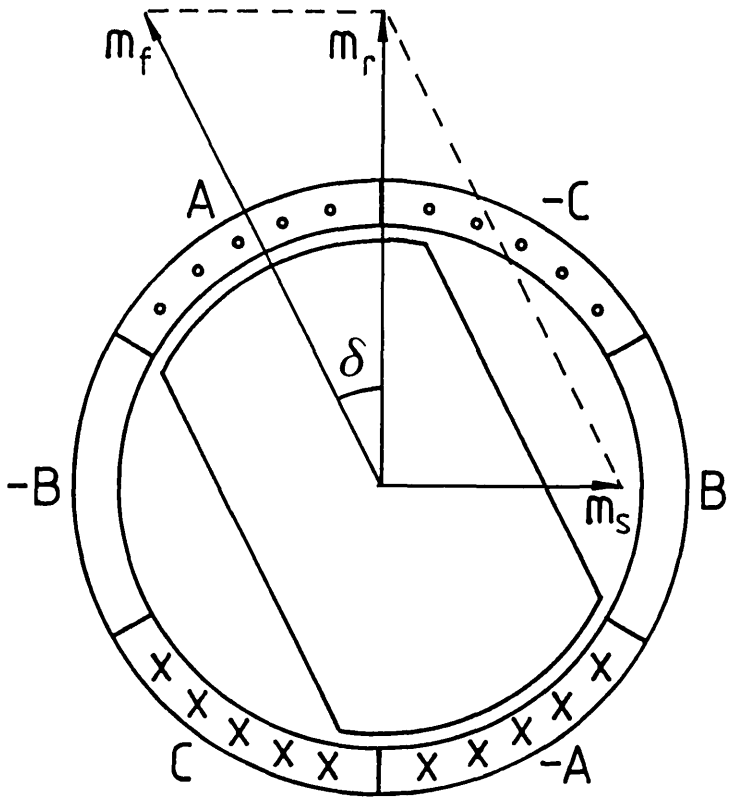


Fig.3.4. Machine Subtransient Reactance as a Function of Rotor Angle.



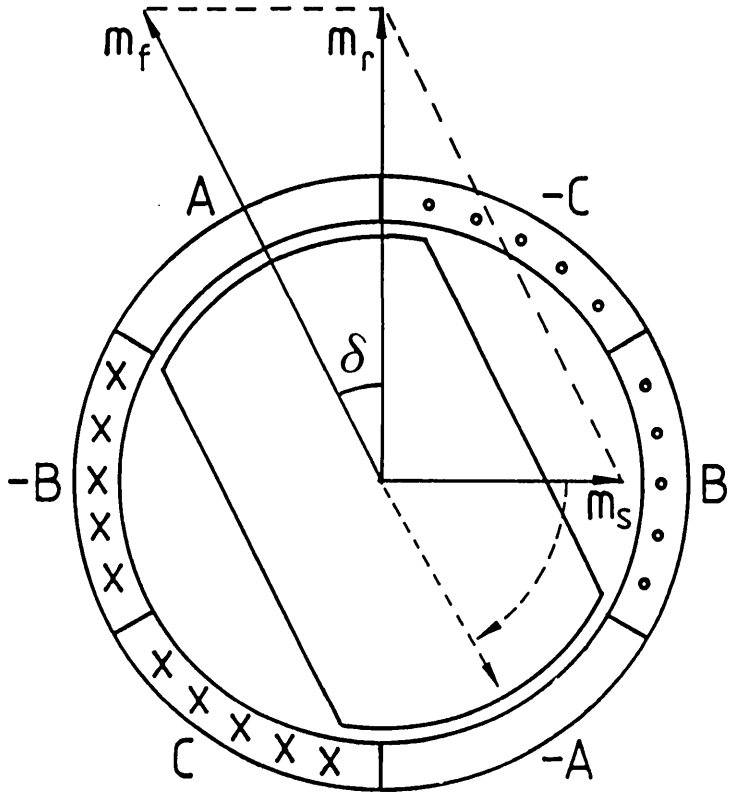
m_f= field m.m.f.

m_r= resultant m.m.f.

m_s= stator m.m.f.

Fig. 3.5. Motor Cross Section

(a) m.m.f. space phasor and current pattern at t_1.



m_f= field m.m.f.

m_r= resultant m.m.f.

m_s= stator m.m.f.

Fig. 3.5. Motor Cross Section
(b) m.m.f. space phasor and current pattern at t_2.

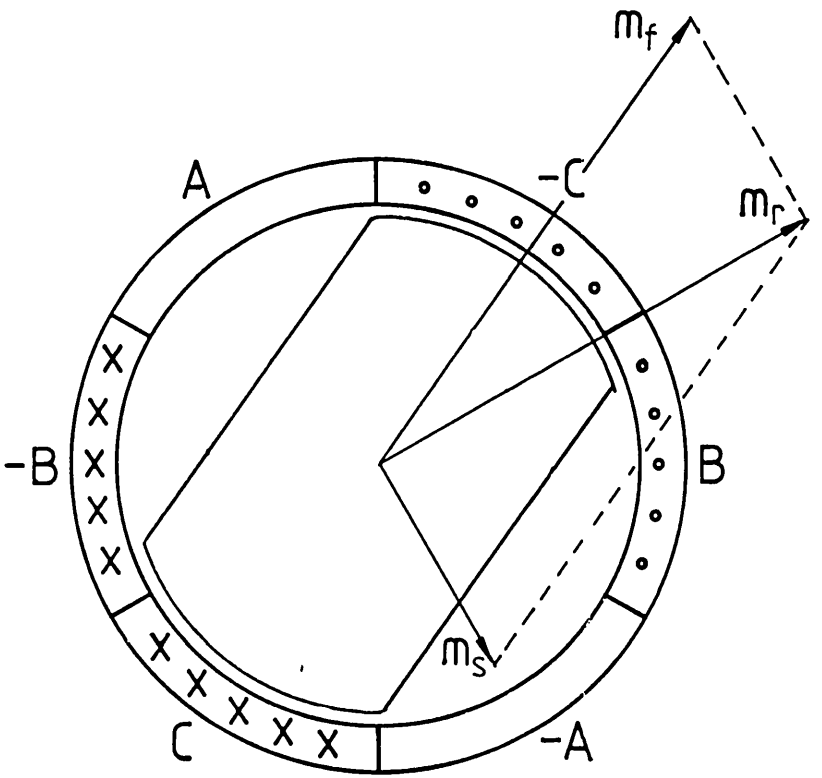


Fig. 3.5. Motor Cross Section
(c) m.m.f. space phasor and current pattern at t_3.

prior to commutation (t_1, of fig 3.3(a)). The resultant m.m.f. corresponding to fig 3.3(a) will be aligned with the combined a-c axis. Therefore, the field m.m.f. will be in the direction shown assuming an arbitrary load angle, δ.

Assuming commutation to be short, rotor motion will be negligible so field m.m.f. remains stationary. Commutation transposes the stator current pattern sixty degrees clockwise implying a corresponding stator m.m.f. rotation shown as a dotted line in fig 3.5(b). However, the resultant flux cannot move swiftly with respect to the rotor, being restrained by eddy currents in the poles. It therefore comes to the surface of the pole (from inside) at the same place, finds its way along the air gap, the adjacent stator flux leakage path across the tooth tips and the rotor surface and enters between the stator winding in the new advanced position. Fig 3.5(c) shows the instant prior to the next commutation, ie sixty degrees on in time from fig 3.5(b), when the m.m.f.'s have resumed their original relative positions.

This "jerky" advancement of stator m.m.f. and the relatively steady motion of the rotor can be likened to a kangaroo racing a cyclist [18]!

The abrupt advancement of stator m.m.f., which is not instantaneous, gives rise to a sixth harmonic ripple in the field current (experienced in actual tests and computer simultation). A torque ripple is also present when motors are used with synchro-inverters.

3.5.2 Stator Flux Distortion

It is possible to consider the stator flux distortion as superimposed upon the overall magnetic field condition. Fig 3.6 shows the stator

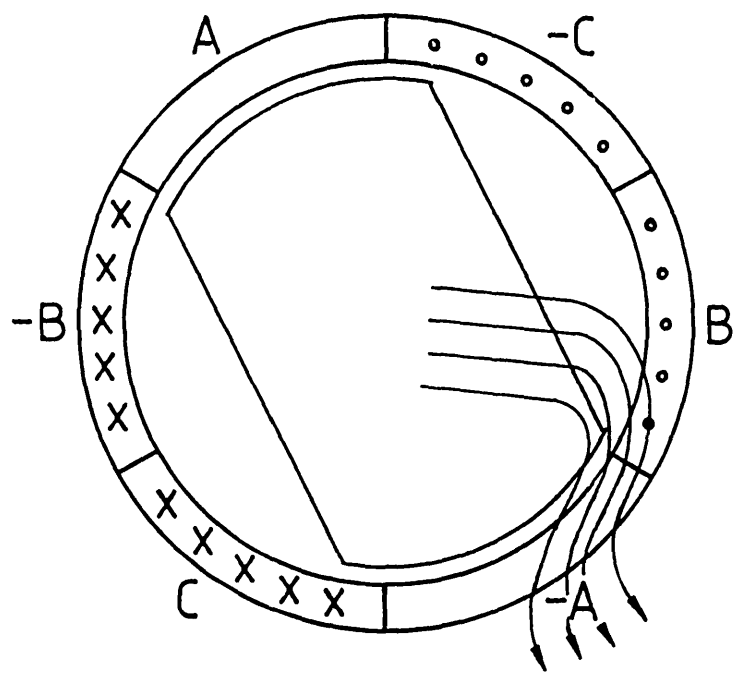


Fig. 3.6. Motor Cross Section. Stator Flux Pattern Corresponding to Commutation of Current from Phase a to Phase b.

flux and the effect of commutation. The sudden transition of stator current does not automatically force stator flux ahead by sixty degrees, but rather distorts as shown. The flux will be held out of the rotor pole by damping circuits which will only relent their influence relatively slowly compared to commutation time and the flux pattern may remain distorted until the next commutation occurs. The assumption of superimposing stator flux upon a loaded magnetic field condition has been considered later as a means of determining the rate at which phase current transfer can take place and hence for predicting commutation time.

An appraisal of how the flux pattern changes with commutation and the value of parameters to be attributed to an equivalent circuit model becomes complicated for a solid salient rotor machine. Solid iron eddy currents will resist any sudden flux pattern changes, the eddy currents themselves having complex paths. The gradual penetration of eddy currents and associated flux pattern at a solid rotor's surface can be very complicated [19].

3.6 Estimation of Overlap Angle Using Machine Reactances

It has been shown that commutation reactance can be considered proportional to the machine's substransient reactance when laminated rotor machines are considered.

A.C. Williamson [20] achieves close correspondence to actual commutation times with the numerical solution of the machine equations. He obtains further success by the use of the simple equation (3.1), assuming in both case that

$$x_c = \frac{x_d'' + x_q''}{2} \qquad (3.2)$$

Y. Takeda et al [21] solves the machine simultaneous differential equations and substitutes the leakage inductances of the armature windings as the commutating inductance.

Commutation is similar to a line-to-line short circuit. Solution to a generator subject to a line-to-line short circuit by Gopal-Reddy [22] also uses an approximate as well as a specific machine equations solution. He uses subtransient reactances obtaining good comparison between predicted and actual results.

Other authors [23,24,25] specifically concerned with converter fed synchronous drives have successfully used the subtransient reactances as a substitute for commutation reactance. Gayek [18] takes this further by allowing for the difference in x_d'' and x_q'' fig 3.4 depending upon rotor position.

An elegant solution using operational inductances and Fourier analysis is performed, by M.J. Hoeijmakers [16]. He shows how the length of commutation influences the magnitude of harmonics present in the Fourier series and that commutating reactance is therefore dependent upon length of commutation. The frequency dependence of the commutation inductance is considered further and he shows that

$$l_c(12\omega) = \mathrm{Re}\ \{\ (12\omega)\}$$

is a fairly good choice for commutation time prediction. Where l_c is the operational inductance and ω the motor frequency.

The idea of using operational inductances for the solution of a variety of machine transients is well documented. Widger and Adkins [26] use operational inductances to determine the starting performance of solid salient pole motors by inserting the frequency dependent impedances into equivalent circuits. Operational impedances are also used by Bharali and Adkins [27] for turbo-generator simulations allowing for rotor eddy current effects.

3.7 Conclusions

The presence of a solid salient rotor machine in the synchro-inverter system requires not only the consideration of the electrical switching but the solution of a magnetic field transient allowing for rotor eddy current effects. The unbalanced nature of the problem complicates any analysis so that referring magnetic into electric quantities and vice versa becomes difficult.

Periods between commutations must be considered when the motor flux pattern recovers from the last commutation, it is quite possible that the flux pattern does not fully recover. Several iterations of a solution may be required to reach a convergent solution.

The rate at which the flux pattern can change will be limited by eddy currents concentrating the flux and current near the rotor surface - the so-called skin effect. Therefore, the steep flux gradients at the rotor surface must be allowed for. Gradual flux penetration and general flux movements during the transitory commutation period will influence the reactance behind the stator electrical terminals so that using subtransient reactances to represent commutating reactance is an oversimplification.

A comprehensive solution to the inverter fed problem requires a motor cross section field solution coupled directly to an inverter representation. A technique which allows electric and magnetic quantities to be coupled forming a single complete model is introduced in the next chapter.

CHAPTER FOUR

THE MAGNETIC CIRCUIT MODEL AND LINKED INVERTER CIRCUIT

4.1 Introduction

The magnetic equivalent circuit modelling technique adopted here is developed from the work of L Haydock [6]. Haydock successfully extends the original work of C J Carpenter [7] applying the theory to model actual turbo-generator tests. Carpenter puts forward the important concepts of adopting rate of change of flux as a magnetic current and magnetic flux as analagous to electric charge. Carpenter's most fundamental and crucial concept is the treatment of linkage between a magnetic and electric circuit as a reciprocal parameter, rather than a number of turns.

The method stands between the simplified models of the two axis, or generalized theory, and the sophisticated, but complex, finite element methods. The networks developed are recognizable as machine geometries since the models are based on a machine's major flux paths. The reduction of a complex magnetic system to a distinguishable circuit of discrete elements gives economical computing times yet its coarseness may not make it as accurate as the finite element technique although topological definition can be as coarse or fine as necessary. The magnetic circuit analogue and its principles are detailed in depth by Haydock [6]. The fundamental ideas are adopted here to suit the synchro-inverter problem and to model the experimental system of chapter two.

The fundamental assumption discretizes the motor cross section into its major flux paths. For example, the air gap flux path between a stator tooth and opposite rotor section of equal pitch is lumped into a single element. Allowance is made for fringing although the effect of local permeance modification due to adjacent differences in Ampere-turns is ignored. End effects are accounted for by adding one air gap length to the machine active length for all calculations.

A method of analysing the system by inter-linking magnetic and electric circuits is sought. Magnetic aspects are commonly minimized by referring all effects to one set of terminals or in a transient analysis in terms of "inductances" immediately. These inductances may not realistically represent the magnetic conditions in the machine.

By representing the linkages explicitly as explained by Haydock a more lucid model is formed. For a synchro-inverter the three phases should be fully represented which complicates the "duality-referral" technique used by Haydock. The linkage equations are well known, it is a case of representing the equations in a discrete component form. The machine cross section is aleady in a discrete component form and by the use of a linkage device it is possible to represent the whole system network, electric and magnetic circuits as one. The modelling of the power electronics is a relatively trivial exercise once the machine is modelled.

4.2 A Simple Magnetic Circuit

The idea of a magnetic circuit is introduced in this section and the gyrator device explained in relation to the simple example considered.

Consider a simple C-core wound with N turns linking it to an electric source, v, as shown in fig 4.1. The iron core is assumed infinitely permeable, lossless and that there are no leakage paths or fringing.

Carpenter took Heaviside's [28] suggestion that the flow quantity or magnetic current, i_m, should be the time differential of flux

$$i_m \triangleq \frac{d\Phi}{dt}$$

If m.m.f. (f) is the magnetic voltage or potential

$$v_m \triangleq f$$

Magnetic permeance (Λ) is defined as having the properties of "magnetic capacitance" (C_m)

$$C_m \triangleq \Lambda$$

Then

$$v_m = \frac{1}{C_m} \int i_m \, dt \qquad (4.1)$$

exactly as for an electric circuit. This analogue is the direct magnetic circuit, fig 4.2. Magnetic flux (Φ) then becomes analogous to magnetic charge (q_m) and correctly represents energy storage. Energy storage is entirely in the air gap of the C-core example,

$$\Lambda_g = \frac{\mu_o a}{l_g} = C_m \qquad (4.2)$$

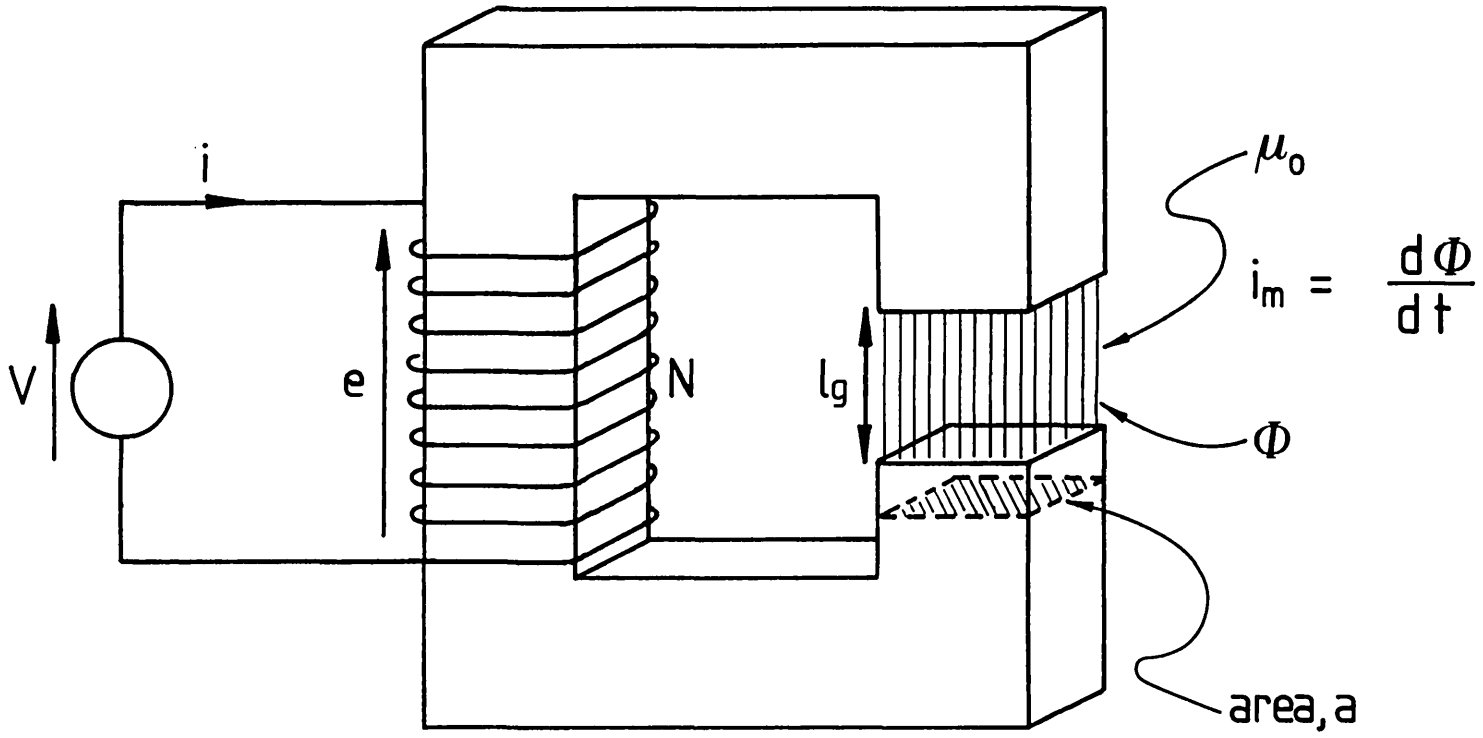
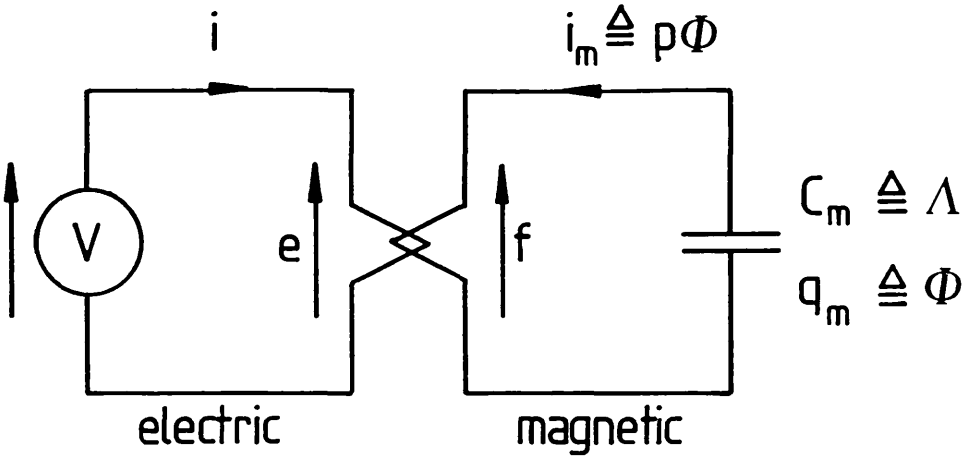
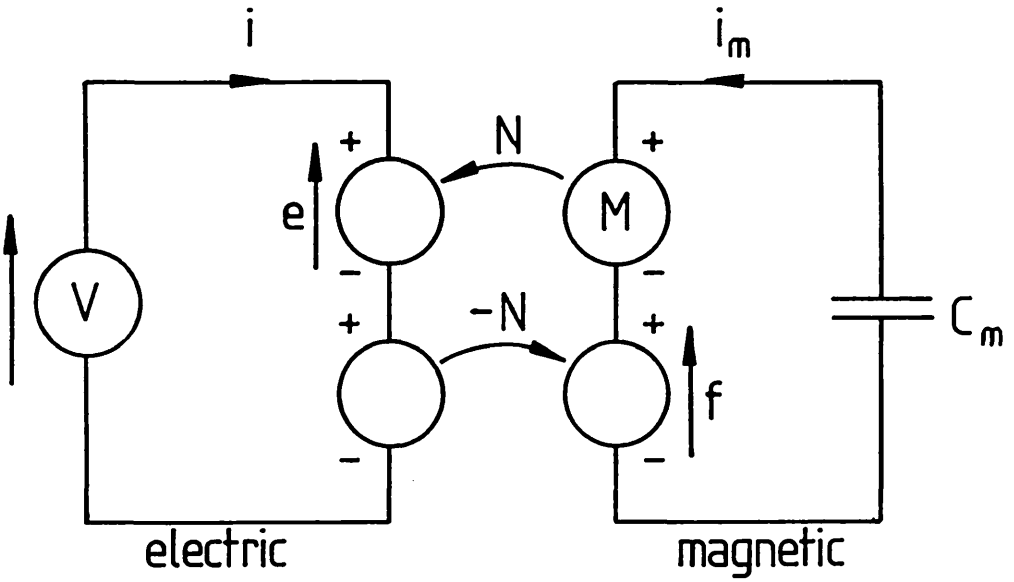


Fig.4.1. Electric Circuit Linking C - Core with N Turns.



(a) Linked magnetic and electric circuit.



(b) S.P.ICE.
Implementation

$$e = N.i_m$$
$$f = -N.i$$

Fig. 4.2. C-Core Equivalent Circuit.

4.3 The Gyrator, a Linkage Device

Magnetic and electric circuits can be represented together explicitly as shown by figs 4.1 and 4.2. Haydock shows how these circuits can be reduced by referring magnetic into electric circuits and vice versa. The intention here is to keep the electric and magnetic circuits separate but correctly linked.

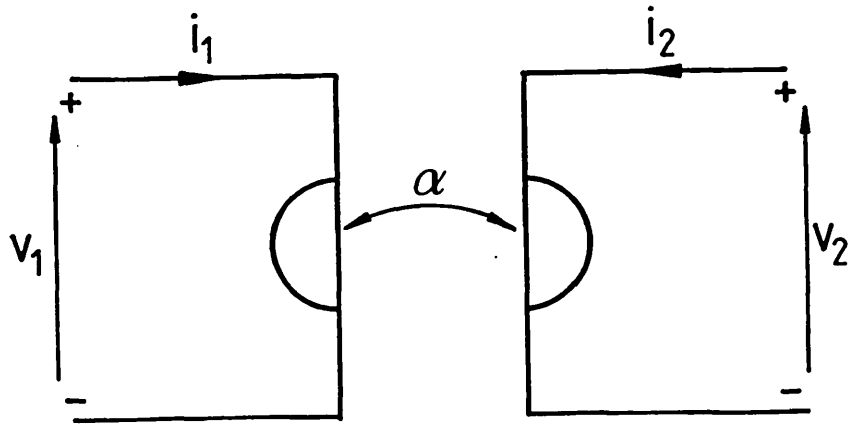
The magnetic and electric circuits of fig 4.2 are linked by the winding of N turns. The linkage equations are

$$e = N \frac{d\Phi}{dt} = N i_m \qquad (4.3)$$

and

$$f = - N i \qquad (4.4)$$

satisfying the circuit of fig 4.2. The equations 4.3 and 4.4 are of the same form as the gyrator equations, the linkage symbol in fig 4.2 representing a gyrator [29]. A gyrator is a two port element which is represented schematically as



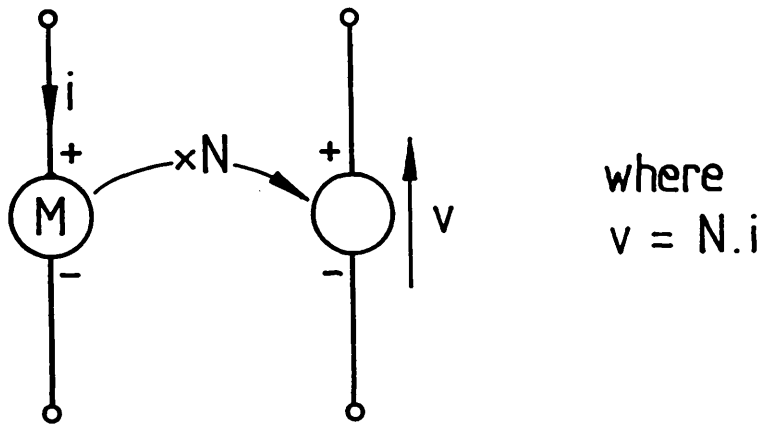
and the gyrator terminal voltage - current relationships are

$$v_1 = \alpha i_2 \qquad (4.5)$$
$$v_2 = -\alpha i_1$$

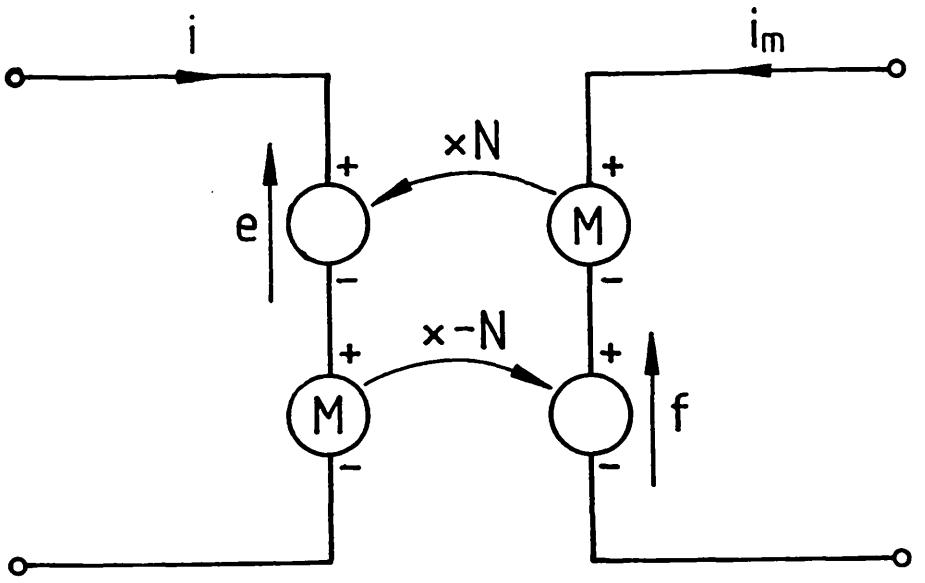
where α is a constant known as the gyration constant.

4.4 Gyrator Implementation in Discrete Element Form

To represent the gyrator set of equations 4.5 for network solution they must be in the form of discrete elements. This is possible with the use of current controlled voltage sources (appendix A), so for the circuit below, voltage, v, is a function of current measured, i.



Therefore two of these devices are necessary to satisfy the gyrator equations 4.5. A complete gyrator is realized in discrete element form as

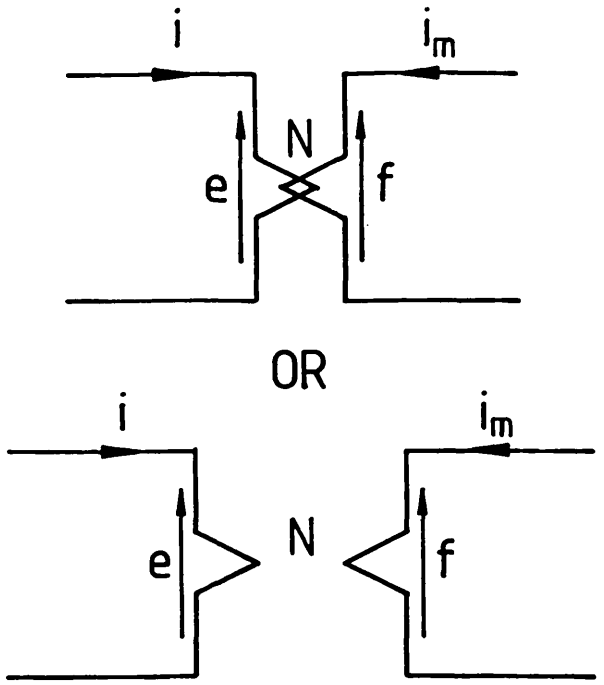


where



is purely a current meter having no influence upon the circuit. The C-core can therefore be modelled with discrete elements in network form as in fig 4.2(b).

To simplify later circuit diagrams the linkage symbol below is used to represent a gyration between magnetic and electric circuits.



4.5 Linkage of the Machine Stator to the Electric Circuit Using Gyrators

The Mawdsley's Stator, fig 2.11, has a set of three phase bands distributed in the manner shown in fig 2.12. These windings have to be represented with gyrators to link the electric and magnetic circuits, and hence it is possible to imitate exactly the double layer phase band distribution. The supposition of linking the electric and magnetic circuits of the simple C-core example is more apparent than the comparatively complex attribution of linkages required for a distributed stator winding.

Application of the "tearing principle" [6] determines the insertion of linkages. That is, if the conductors are pulled towards their equal and opposite conducting partner until they meet, linkages are inserted every time the conductors cross a defined flux path. The method of separation is arbitrary and the linked circuits may be distorted before the tearing principle is applied.

The first step is to define the motor's major flux paths. The stator core, assumed to be infinitely permeable, has the possible flux paths as shown in fig 4.3, with the stator winding in place. There are two possible ways of drawing together stator conductors of equal and opposite sign, and they are:

1. To draw the conductors towards each other around the circumferential centre line of the conductors as in fig 4.4(a). Linkages are then inserted at points denoted by *'s, fig 4.4(b).

2. The other way, results in a less complex and more lucid circuit. By drawing the conductors out of the back of the stator core as shown by fig 4.5(a) and resulting linkages (denoted by *'s) are formed as in fig 4.5(b).

Both methods were checked against each other and gave identical results.

The magnetic circuit model was composed to represent two pole pitches of the Mawdsley's motor cross section. Implementation of the second "tearing" method resulted in the stator circuit of fig 4.6. Appropriate linkage values are also shown.

Each phase band can now be linked with the appropriate stator electrical terminals through the correct number of turns figs 4.6 and 4.7. Each slot must be linked to the relevant stator phase terminals by the correct linkages, so that phase a voltage, v_a, is the sum contribution of the magnetic linkages

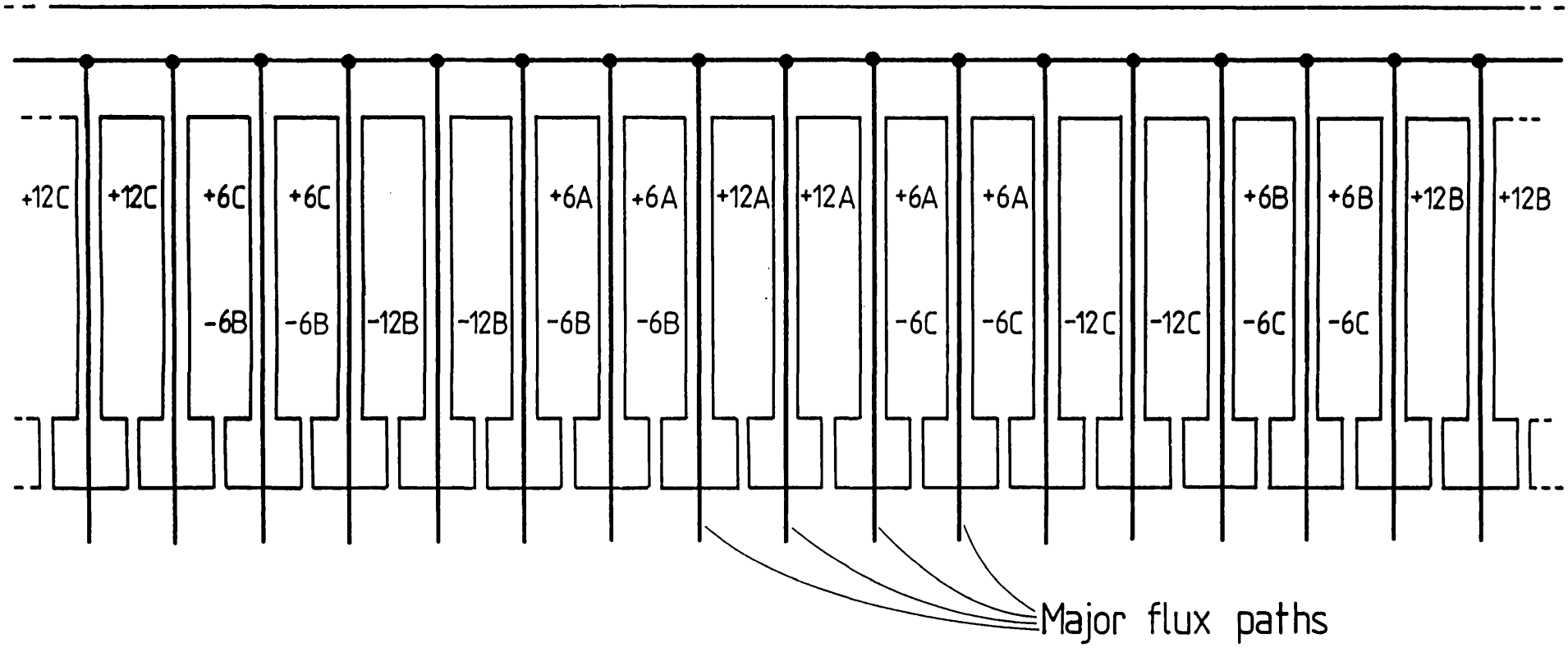
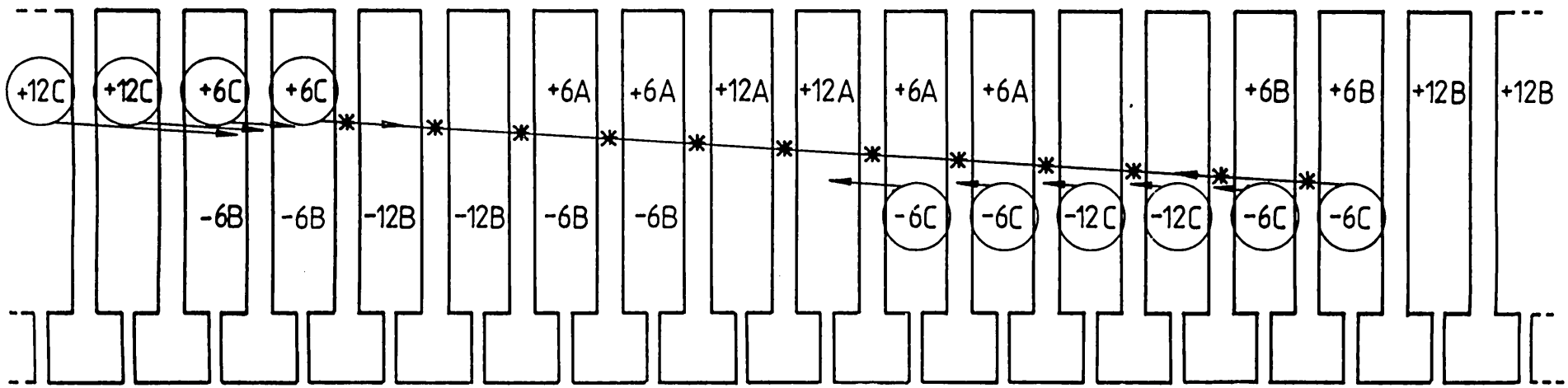


Fig.4.3. Stator Magnetic Circuit.

(a)



(b) Phase c linkages formed by "tearing" conductors as above. Similar linkages exist for phases a and b.

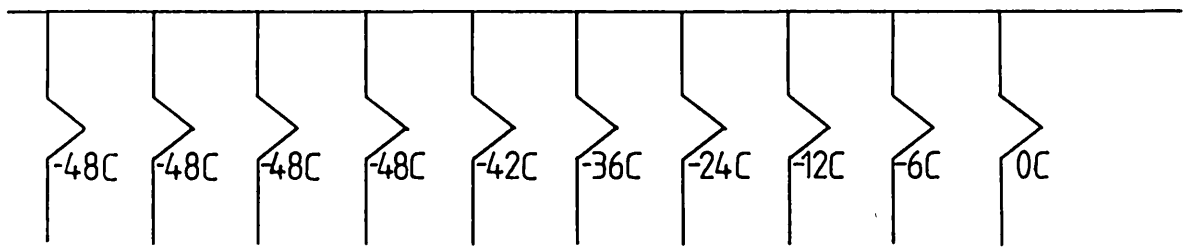
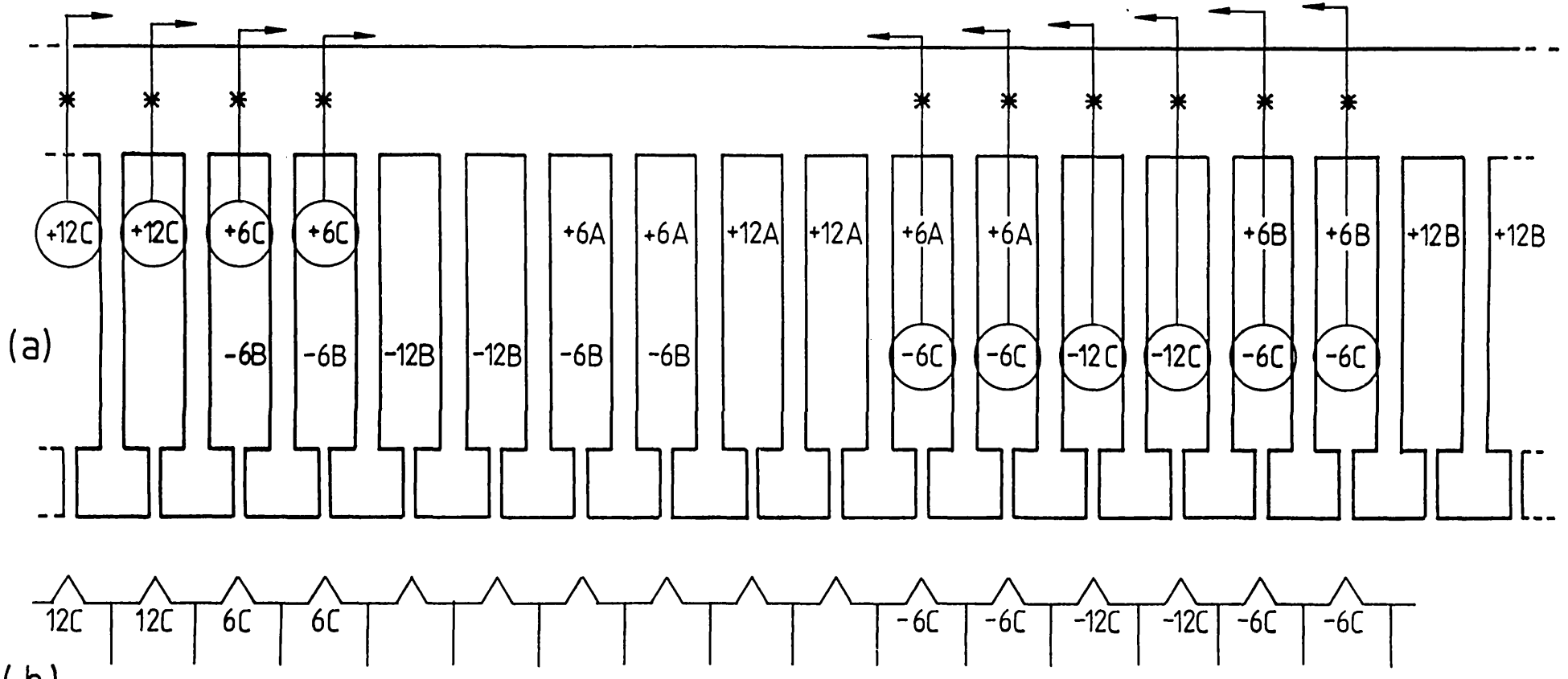
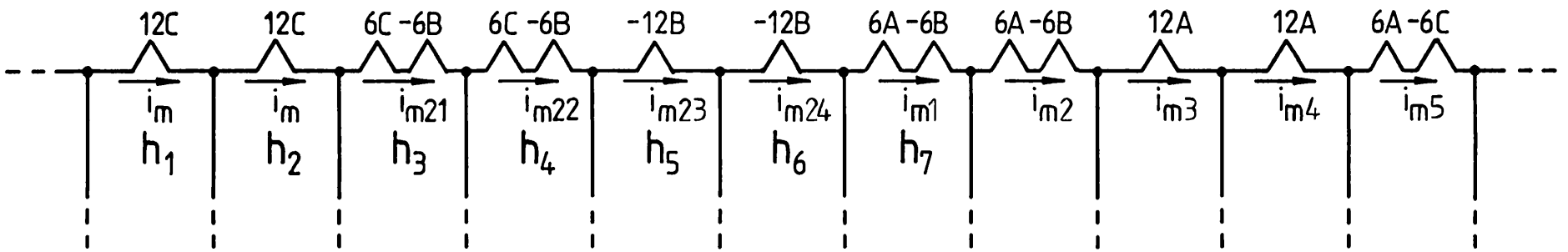


Fig.4.4. Stator Magnetic Linkages.



(b) Phase c linkages formed by "tearing" conductors through the stator core back. Similar linkages exist for phases a and b.

Fig.4.5. Stator Magnetic Linkages.



i_{12} to i_{24} exist in h_{12} to h_{24} respectively.

Fig.4.6. Stator Linkages.

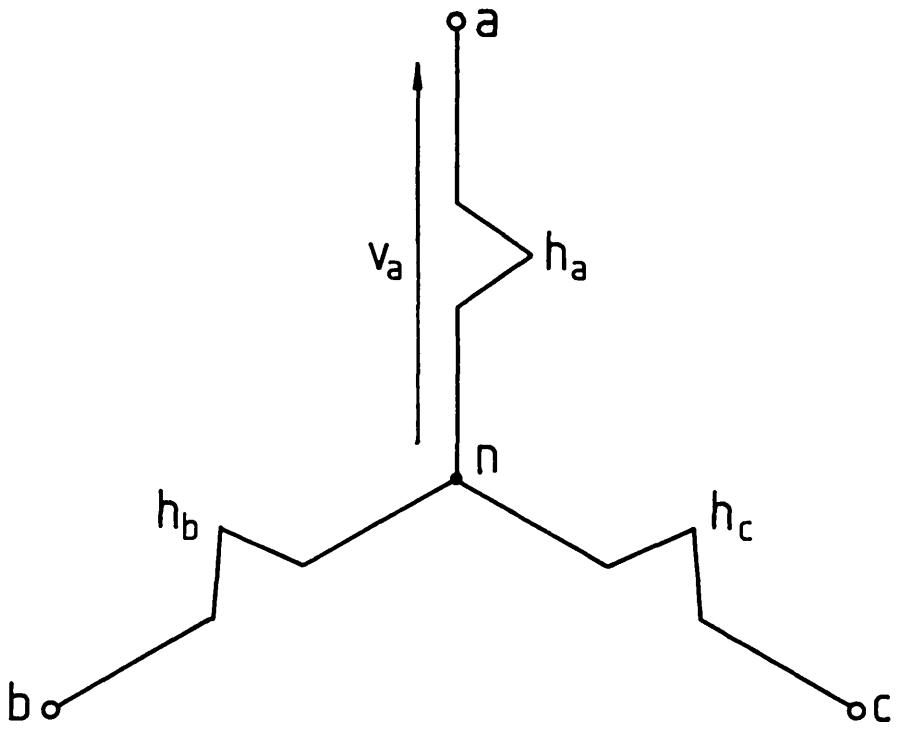


Fig.4.7. Stator Electric Circuit Linkages.

$$v_a = i_{m1}\ 6A + i_{m2}\ 6A + i_{m3}\ 12A + i_{m4}\ 12A + i_{m5}\ 6A + i_{m6}\ 6A - i_{m13}\ 6A - i_{m14}\ 6A - i_{m15}\ 12A - i_{m16}\ 12A - i_{m17}\ 6A - i_{m18}\ 6A \qquad (4.6)$$

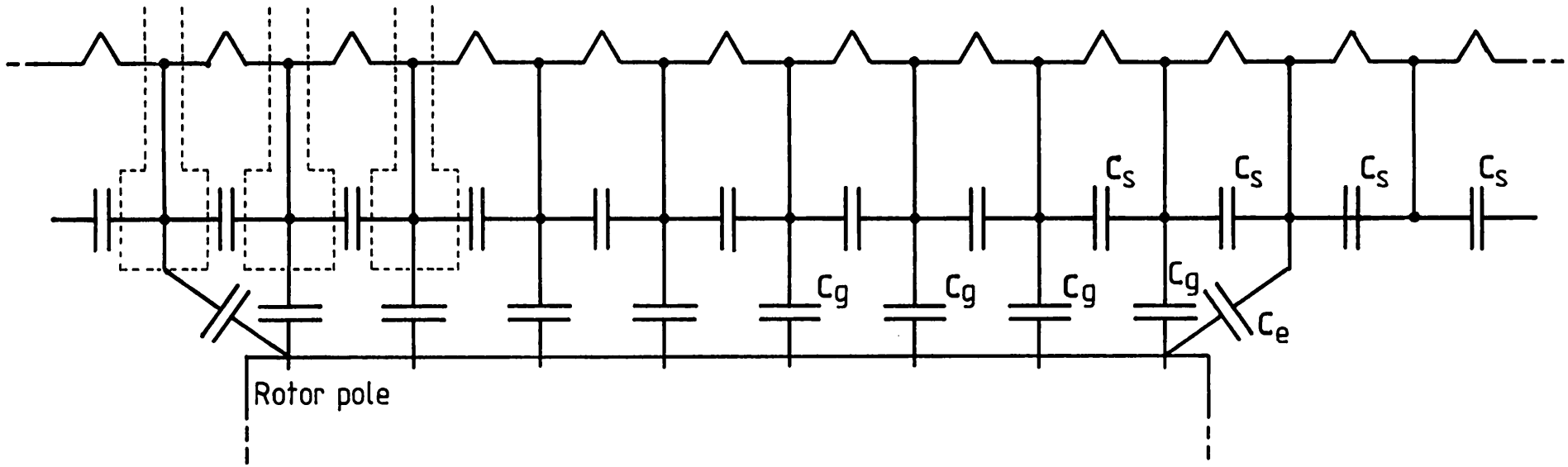
Where i_{m1-6} and i_{m13-18} are the magnetic currents of fig 4.6.

Obviously, only one pole pitch need be considered since the voltages produced by each stator pole are equal, due to symmetry. Therefore, the first six terms of equation 4.6 are used and multiplied by two. Similar equations exist for the other two phases, b and c. The linkages in the electrial circuits, fig 4.7, are represented by single current dependent voltage source devices, h_a, h_b and h_c, as detailed in appendix A. The stator electrical terminals now fully link the actual stator magnetic core with the exact phase winding distribution of the actual machine.

4.6 Permeance Representation

All permeance calculations are based on the machine's geometry using equation 4.2.

Calculation of the stator tooth leakage paths and the air gap permeances is straight forward. To allow for fringing of flux, calculations are modified using Carter's coefficient [30]. This increases the stator tooth-to-tooth permeance by 8%. Similarly air gap permeances allow for fringing and an extra permeance is added at pole edges (about 25% of a single mid pole air gap permeance value). Fig 4.8 illustrates the connection of fringing capacitors and tooth leakage paths.



Not to scale.

Fig.4.8. Magnetic Circuit Stator Leakage and Air Gap Permeances.

The stator and air gap paths are now fully represented. The stator iron is assumed infinitely permeable so that stator core paths are effectively short circuits. Stator slots are virtually closed, fig 2.11, so slot leakage permeances are readily definable. The air gap paths are split into section's equal to the stator slot pitch and the rotor surface is split into the same sections, ie the rotor has the same effective number of teeth as the stator.

4.7 The Solid Rotor

The easily recognizable flux paths of the air gap and stator do not exist in the solid iron poles of the rotor. A means has to be found of defining not only flux paths and associated permeances but also eddy current paths.

4.7.1 Solid Iron Permeances

As discussed in chapter three the rotor flux distribution is complex and distortion is significant at commutation. The field pattern has been described and is assumed to be two dimensional although in practice it has a three dimensional distribution.

The rotor poles resist any sudden change of flux pattern due to eddy currents. The resulting skin effect concentrates flux at the rotor surface when commutation takes place. To represent the steep flux gradients a two dimensional mesh of permeances is required of fine definition at the rotor surface. The same technique is implemented in finite element work [31] where fine meshes are used in air gaps and solid iron surfaces experiencing swift changes in flux density. The method used here is not as refined as that with finite element where

the rotor surface would be dissected into several hundred triangular sections.

Fig 4.9 shows a portion of the rotor sectioned into a lamination of 0.5 mm depth at the surface, and subsequent layers doubling in depth towards the rotor centre. Permeances based on these laminar portions and connecting the flux paths extending down from the air gap (shown dotted fig 4.10) are calculated from

$$C_{mi} = \frac{\mu r \, \mu o \, \text{area}}{\text{gap}} \qquad (4.7)$$

For the "horizontal" permeances, fig 4.11

$$\text{area} = d_i \times l_m \quad (i = 1 - 5)$$

$$\text{gap} = d_s$$

$$l_m = \text{machine active length}$$

In the absence of any data on the rotor material a fixed value of relative permeability, μ_r, of 100 has been chosen. The value was selected to allow for a degree of saturation, based on the observations of Turner [31] and Haydock [6], that "freezing" permeabilities at their initial saturated value throughout a transient seems to accurately model a machine fault or test.

Permeances are inserted to connect the horizontal capacitor layers completing the flux paths shown dotted in fig 4.10. These capacitors are set with increasing values of relative permeability as a function of increasing pole depth. The body permeance is set to infinity. This has been found necessary since a fixed value of μ_r throughout the pole

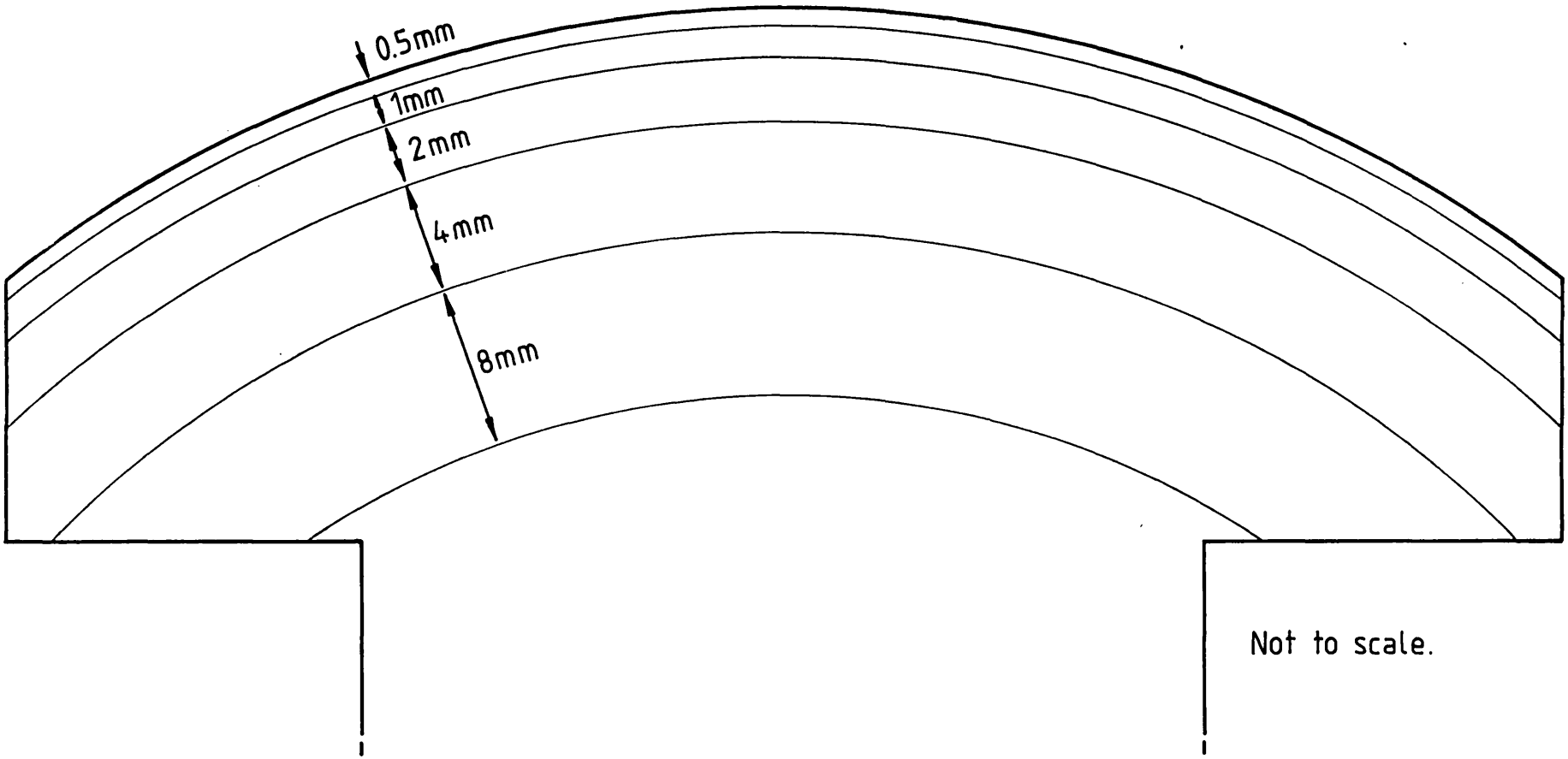


Fig.4.9. Division of Solid Rotor into Permeance Layers.

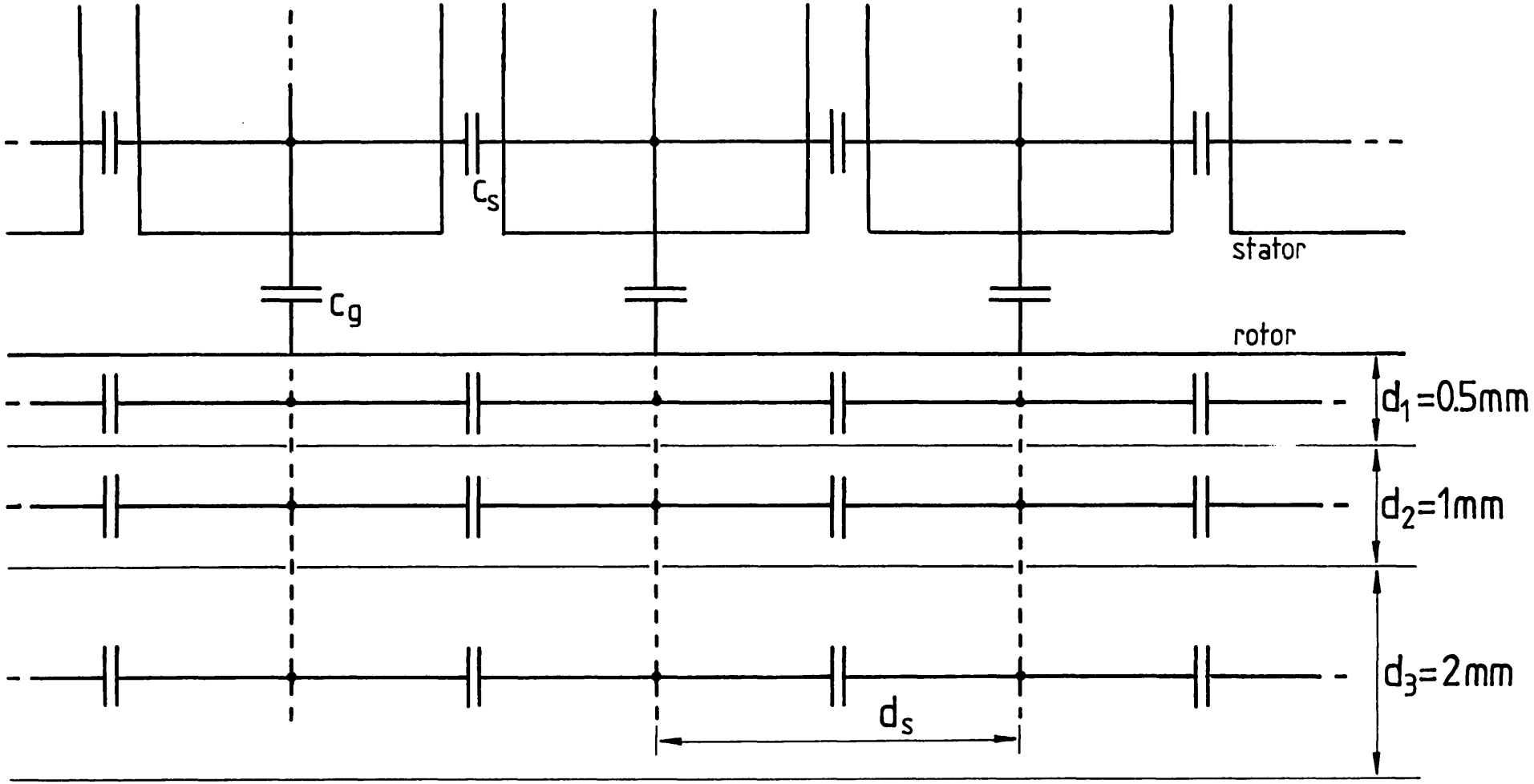


Fig.4.10. Solid Rotor Horizontal Permeances.

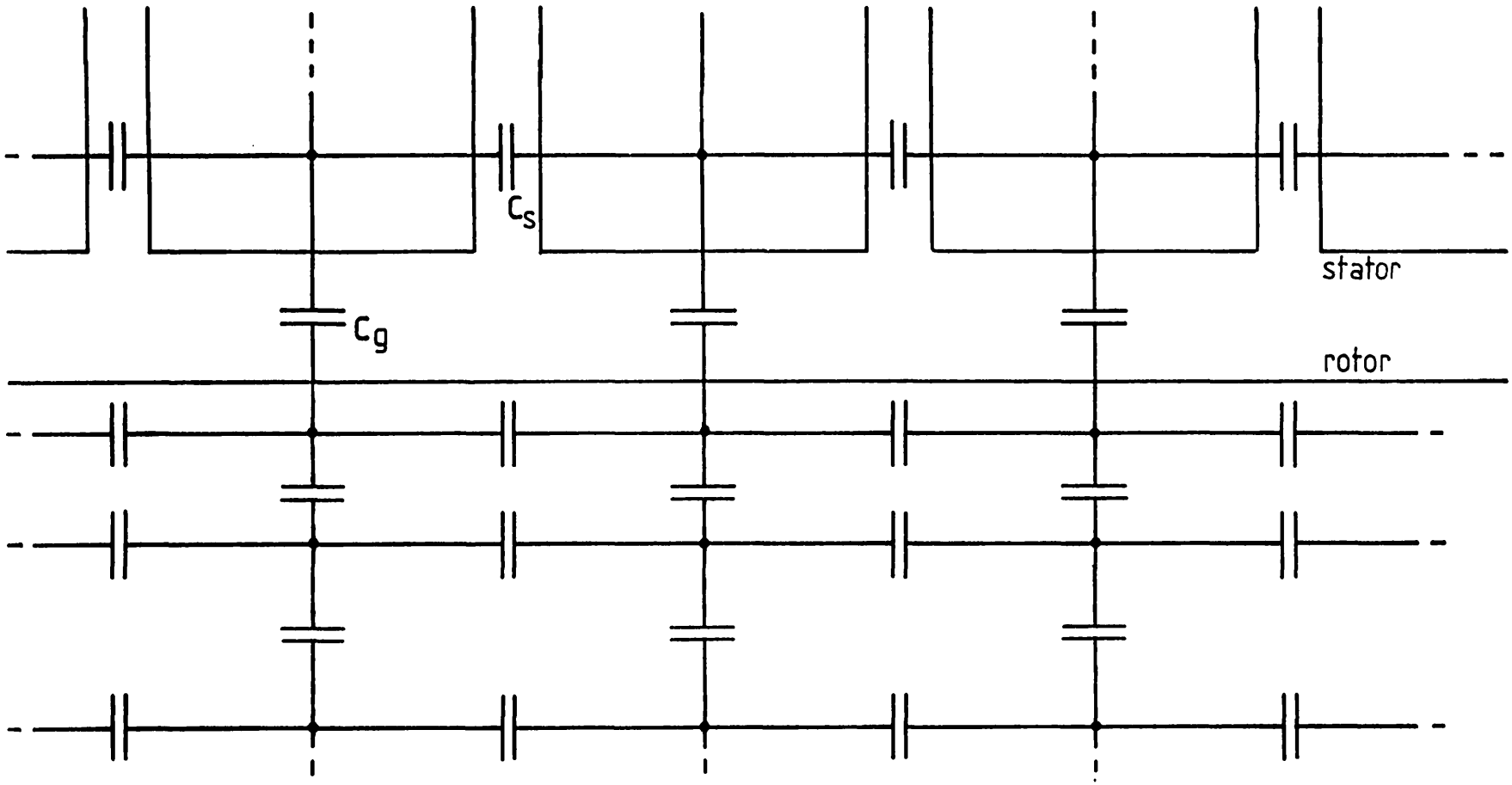


Fig.4.11. Solid Rotor 2-D Permeances.

produces a collapse of generated back e.m.f. when the motor is loaded. The increased values of permeance do not affect the transient flux disturbance or the commutation times, and prevents the generated e.m.f. from collapsing. The resulting grid, fig 4.11, allows for two dimensional fluxes in the top portion of the rotor pole.

4.8 Rotor Eddy Currents

Rotor eddy currents are assumed to exist at right angles to the cross section of the machine (in practice eddy currents will probably flow in three dimensions in a complex manner). The damping effects of these eddy currents are considered and a method of representation set out for the solid rotor.

4.8.1 Basic Concepts and Assumptions

The rotor eddy currents will link the magnetic flux paths in the same manner as a real winding or a damper cage. However, the eddy current paths are not readily definable and attribution of eddy current paths to a particular portion of iron is speculative especially for the case of an unbalanced fault and the associated asymmetrical field distribution. The possible conducting paths though, flowing at right angles to the section, ie axially along the motor, were defined as essentially a set of "rotor bars". These "bars" were put inside each of the squares formed by the permeance grid of fig 4.11, and shorted at the rotor ends, resulting in fig 4.12.

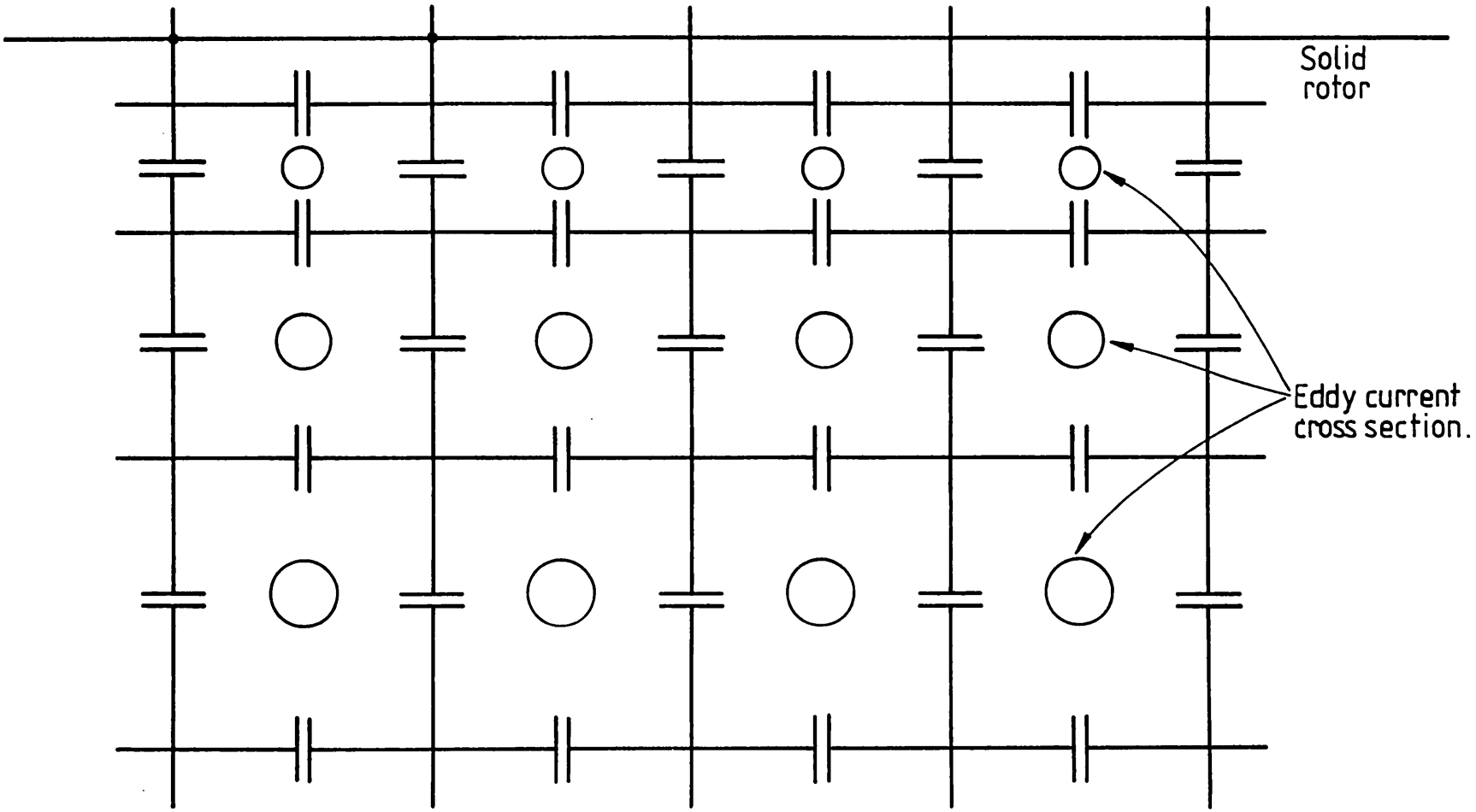


Fig.4.12. Insertion of Eddy Current Paths.

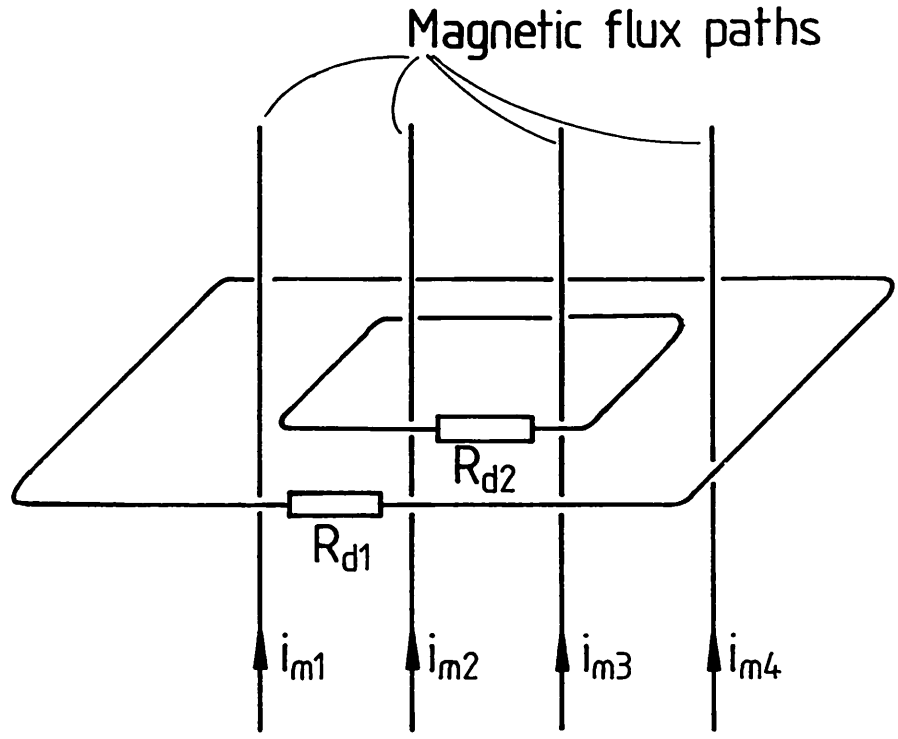
4.8.2 Solid Rotor Eddy Current Paths

To appreciate the attribution of damping currents to particular flux paths it is useful to re-iterate the simple case [6] of two damping coils linking several flux paths. Fig 4.13(a) shows two damping coils (these could be the dampers of a cylindrical machine) which have four flux paths passing through them. The resistances of the single turn coils are R_{d1} and R_{d2}.

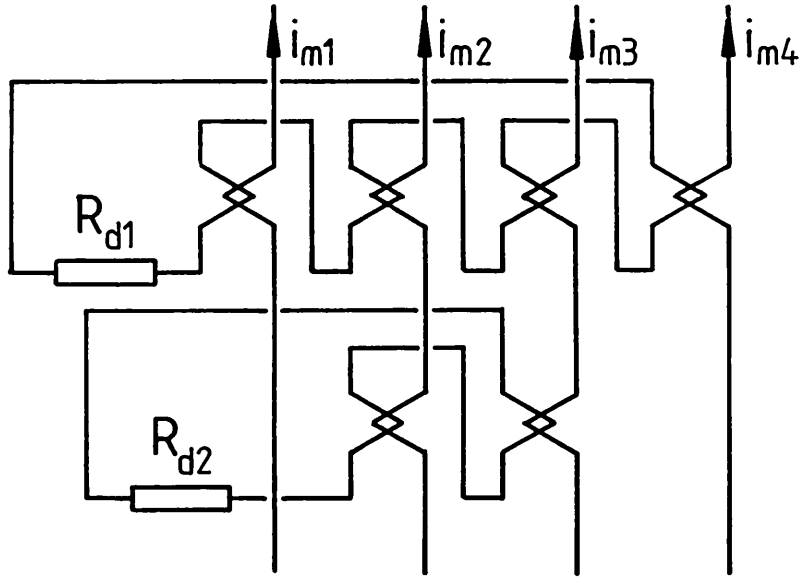
Application of the "tearing principle" produces the linkages, as shown in fig 4.13(b), by pulling the conductors towards the centre of the flux paths.

Both electric currents of fig 4.13(b) link all four flux paths so that there is a mutual coupling of magnetic currents via the damping circuits. To fully represent the correct damping effects of R_{d1} and R_{d2} the circuit should be represented fully as shown, since in general $i_{m1} \neq i_{m2} \neq i_{m3} \neq i_{m4}$. For the solid rotor material many flux paths will be linked by numerous eddy current paths making the problem even more complex.

The object of putting layers of damping, or "dampances", in the solid rotor pole is to represent the influence of commutation on flux occurring near the rotor surface (shown as Φ_a below)

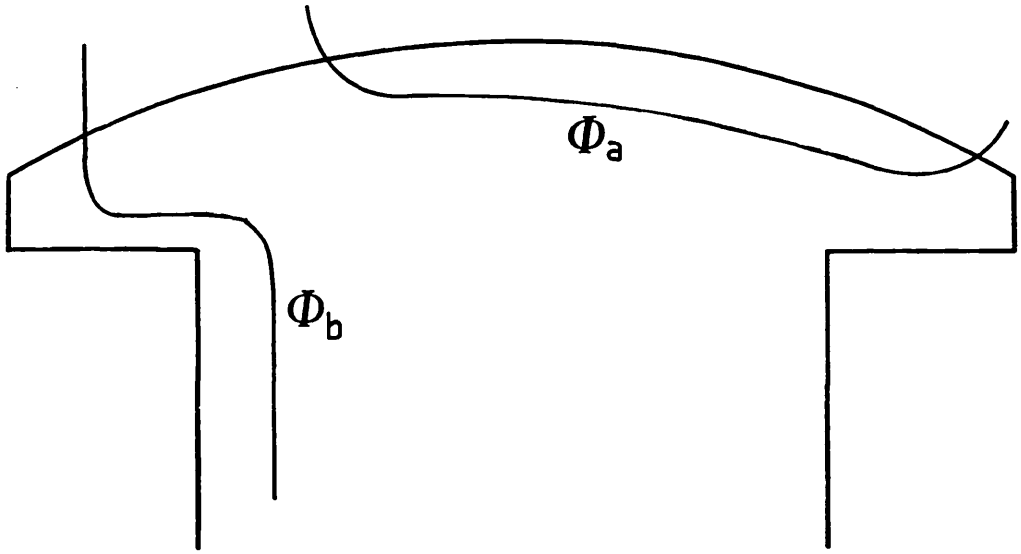


(a) Electric damper circuits linking magnetic flux paths.



(b) Magnetic circuit of (a).

Fig.4.13. Linkage of Discrete Electric Dampers to Magnetic Flux Paths.



Also, a secondary effect which causes pulsations in the field winding should be allowed for (shown as Φ_b above).

The poles of the machine have an axis of symmetry on the axis of rotation of the rotor. Pulling the eddy current paths of fig 4.12 through to the rotor centre to meet their equal and opposite conductor results in linkages formed similar to fig 4.14(a). The damping effects of region 1 couples all four flux paths below it and similarly eddy current 2 couples flux paths below its own region. A full representation thus requires the complex coupling of each electric damper to several flux paths.

The damping resistance R_{d1} is "shared" by all four flux paths so that the flux paths are mutually coupled. An approximation of damping effects is required if the electric resistances are to be referred into the magnetic circuits as magnetic dampances. It is desirable to refer in the electric resistances since the circuit then becomes less complex.

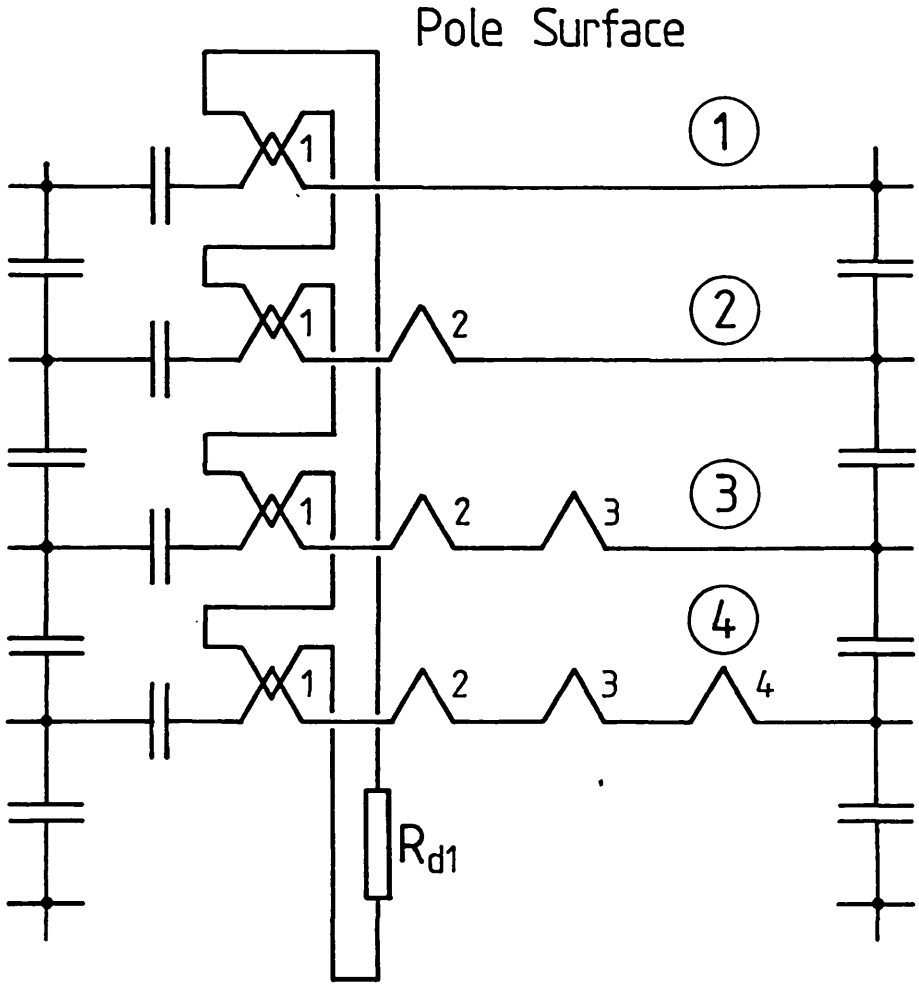


Fig.4.14 (a). Portion of Solid Rotor Showing Linkage of Each Layer to an Eddy Current Circuit.

The approximation is made by ignoring the mutual linkage effect, assuming each eddy current links each flux path individually, fig 4.14(b). Referral of the electric resistance is then straight forward so that the equivalent magnetic dampance [6] is

$$R_{mdi} = \frac{1}{R_{di}} \qquad (i = 1 \text{ to } 4)$$

for each flux path linked, resulting in fig 4.14(c).

Now, the dampance of the top layer is an eighth of the value of the fourth layer so the upper eddy currents have a reduced effect upon flux movement in lower layers of the rotor pole. Therefore, any mutual coupling effects will have little influence upon major flux movement. Also, mutual coupling may not be present anyway since flux may only be changing in, for example, the top most layer (the skin effect) so that i_{m1} = non-zero, $i_{m2} = 0$, $i_{m3} = 0$, $i_{m4} = 0$. In general magnetic currents may not appear together, hence no mutual coupling via the damping circuits.

The eddy currents of a solid pole are not restricted to known coils, as the current is in a damper cage of a laminated motor, and several return paths may exist. However, the eddy current flowing in a small rotor area will be equal and opposite to the current flowing in a similar area but on the opposite pole. Fig 4.15 shows an elemental eddy current $+i_e$ flowing in the top left corner of a north pole and an equal and opposite current, $-i_e$, flowing in the south pole. These currents form a current loop which links the flux paths crossing through the loop. By drawing such pairs of conductors together the linkages are formed, or dampances inserted, every time a conductor

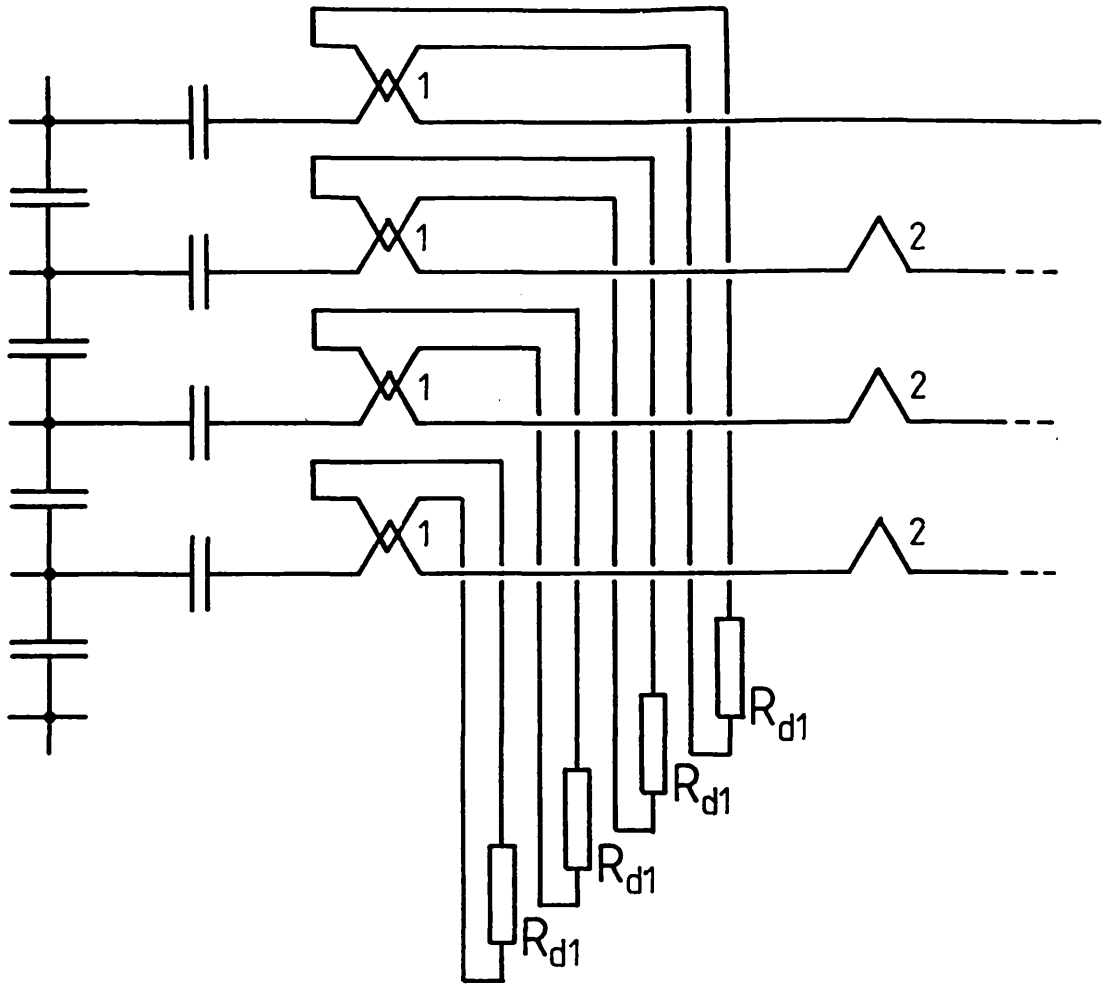


Fig.4.14(b). Approximation of Eddy Current Damping Effects.

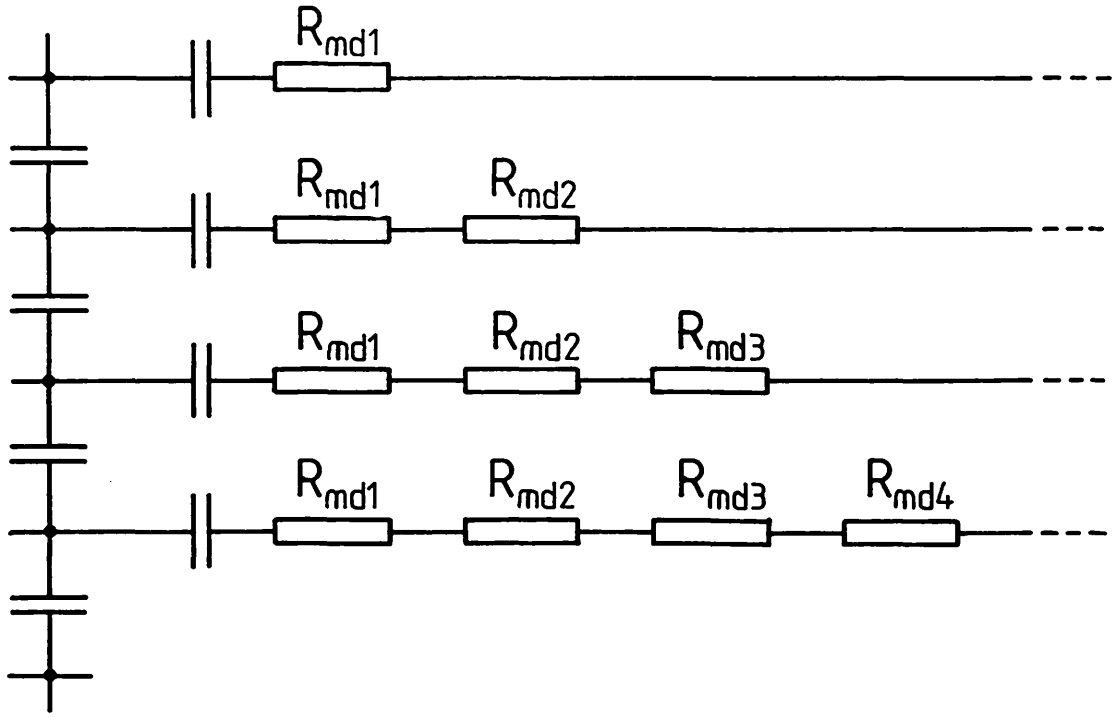


Fig.4.14(c). Damping Resistances Referred into the Magnetic Circuit.

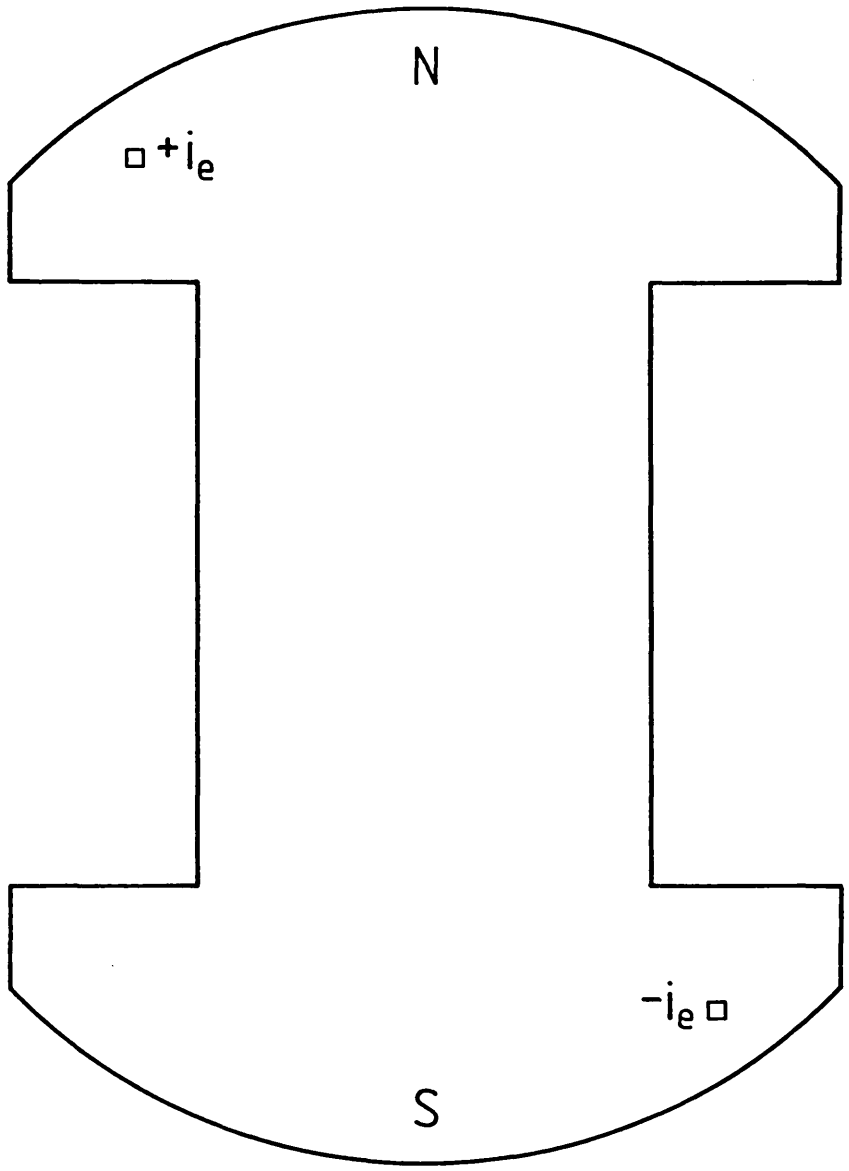


Fig.4.15. Axial Symmetry of a Two Pole Rotor Cross Section.

crosses a flux path.

Eddy currents in the pole corners, fig 4.16, are first pulled in toward the pole centre line and then into the body centre. The final rotor pole circuit is shown in fig 4.17 with the additional body flux paths and associated dampances inserted. The pole dampances are of a relatively large value since not only do the body eddy currents link the body flux paths but so do all the eddy currents which have been pulled in from the two pole extremities. Damping reduces in value further away from the pole until at the rotor surface only one eddy current loop links the top flux path. Intuitively the increase of dampance towards the rotor hub is correct since fluxes deep in the rotor body cannot move as fast as fluxes at the rotor surface.

The addition of the field circuit completes the rotor magnetic circuit, fig 4.17. A single pole pitch is shown.

It is necessary to fully represent two pole pitches of the motor since no sufficient means could be found of representing boundary conditions for a single pole pitch. Simply setting the voltages to be equal and opposite at the boundaries does not satisfy the boundary conditions.

4.9 The Inverter Power Electronics

The models' electric stator terminals are connected in star configuration, fig 4.7. Connection of the electric network is straight forward since the circuit solver, S.P.I.C.E. (discussed later), is an electronics circuit solver. The inverter, d.c. link, and rectifier could all be readily modelled using S.P.I.C.E.

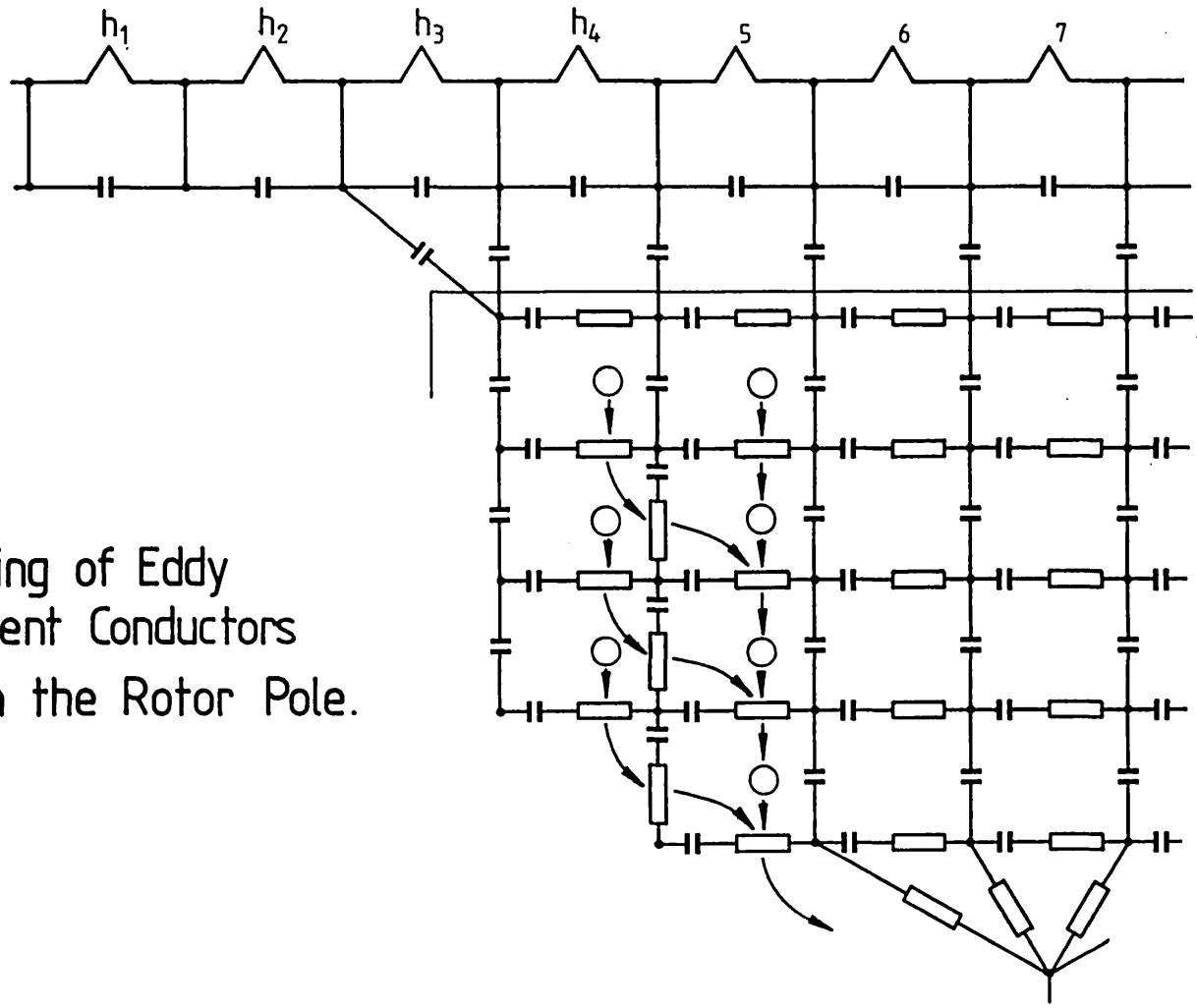
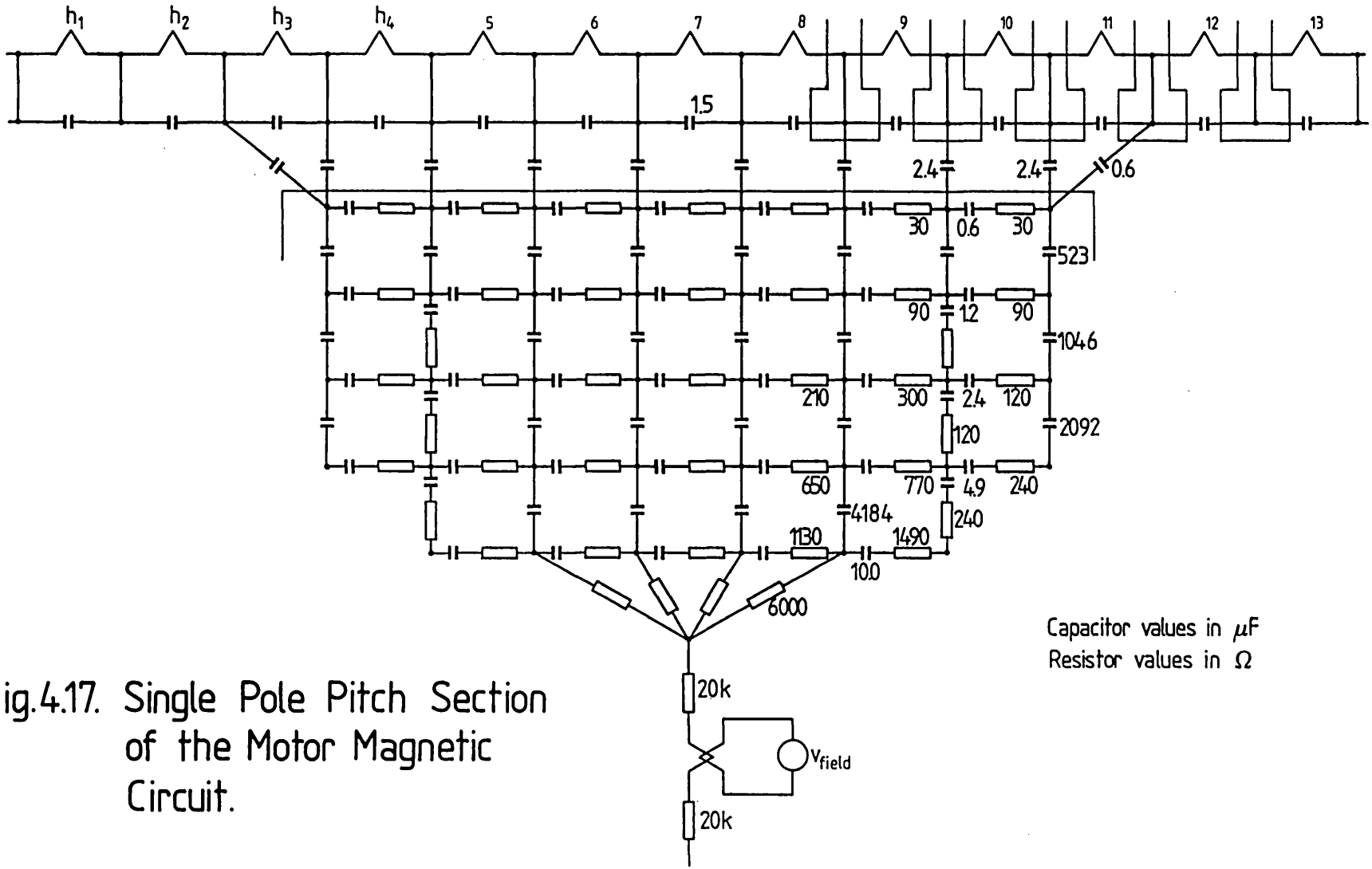


Fig.4.16. Tearing of Eddy Current Conductors from the Rotor Pole.



Capacitor values in μF
Resistor values in Ω

Fig.4.17. Single Pole Pitch Section of the Motor Magnetic Circuit.

4.9.1 A Thyristor Model

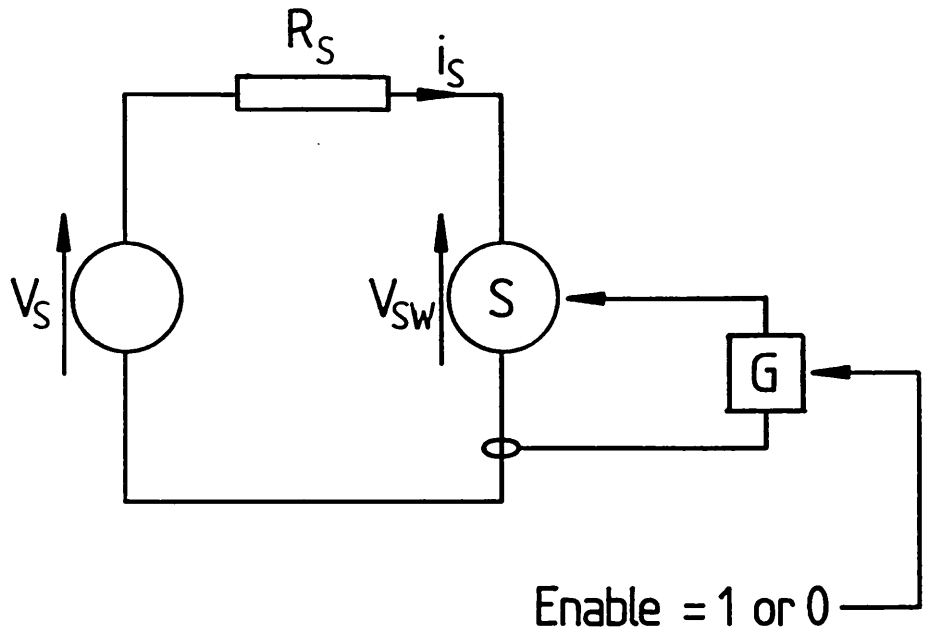
A Thyristor model does not exist in the current version of S.P.I.C.E. A two transistor model [32] has been tried in simple practical circuits but convergence errors make the model unsuitable. Other models [33, 34,35] which implement dependent sources to simulate switching have also been of very limited success when connected in practical power electronic circuits. The unpredictable behaviour of these models is put down to their complexity, and so recourse to developing a more simple model has been undertaken. A simple switch does not exist in S.P.I.C.E. so the first task is the development of a switching device.

4.9.2 A Simple Switch

To model a switch the device must "hold off" the applied voltage when in an "OFF state" and be a short circuit, zero voltage across the device, when in an "ON state". The device can be likened to a voltage source which is zero to represent a closed switch and has a voltage equal and opposing the applied voltage when open. This idea is shown schematically in fig 4.18 where the switch, S, is connected in series with a d.c. source voltage, V_S, and a resistance, R.

Negative feedback holds the voltage V_S across S when open circuit. When S is closed V_{SW} goes to zero. The ON state is straight forward, the "enable" forces V_{SW} to zero and current i_S flows equal to

$$i_S = \frac{V_S}{R_S}$$



$V_{SW} = V_S$ $\quad i_S = 0$ $\quad$ S is open circuit

$V_{SW} = 0$ $\quad i_S = \frac{V_S}{R_S}$ $\quad$ S is short circuit

Fig. 4.18. An Ideal Switch.

In the OFF state i_s is monitored and when G is enabled the magnitude of V_{SW} equals that of V_S. G is the gain of the feeback path so that

$$V_{SW} = G \times i_S$$

If G is large the current i_s (effectively the leakage current) is small. G acts as a resistance and is very large when enabled, zero when disabled.

The S.P.I.C.E. implementation of the switch is shown in fig 4.19. V_{TH} is a current controlled voltage source, of a polynomical type (appendix A) and for the circuit of fig 4.19 has the equation

$$V_{TH} = i_{TH} \times i_{GT} \times G \qquad (4.9)$$

If i_{GT} is arranged to be 1A (for the OFF state) equation (4.9) becomes

$$V_{TH} = G \times i_{TH}$$

Values of G = 100,000 and R_{TH} = 1 satisfy the switching requirements of a nearly ideal switch. The addition of a series diode, fig 4.20, translates the simple switch into a thyristor model. The diode prevents reverse current flowing when the device is reverse biased. The anode, A, cathode, K, and gate, g, terminals are all identifiable.

The resultant device is a thyristor of zero forward resistance and about 100,000 k Ω reverse resistance. Satisfactory results have been achieved when the device is implemented in a full thyristor bridge model, fig 4.21. Modification to allow for thyristor characteristics is possible although refinements at this stage of development would be unnecessarily elaborate.

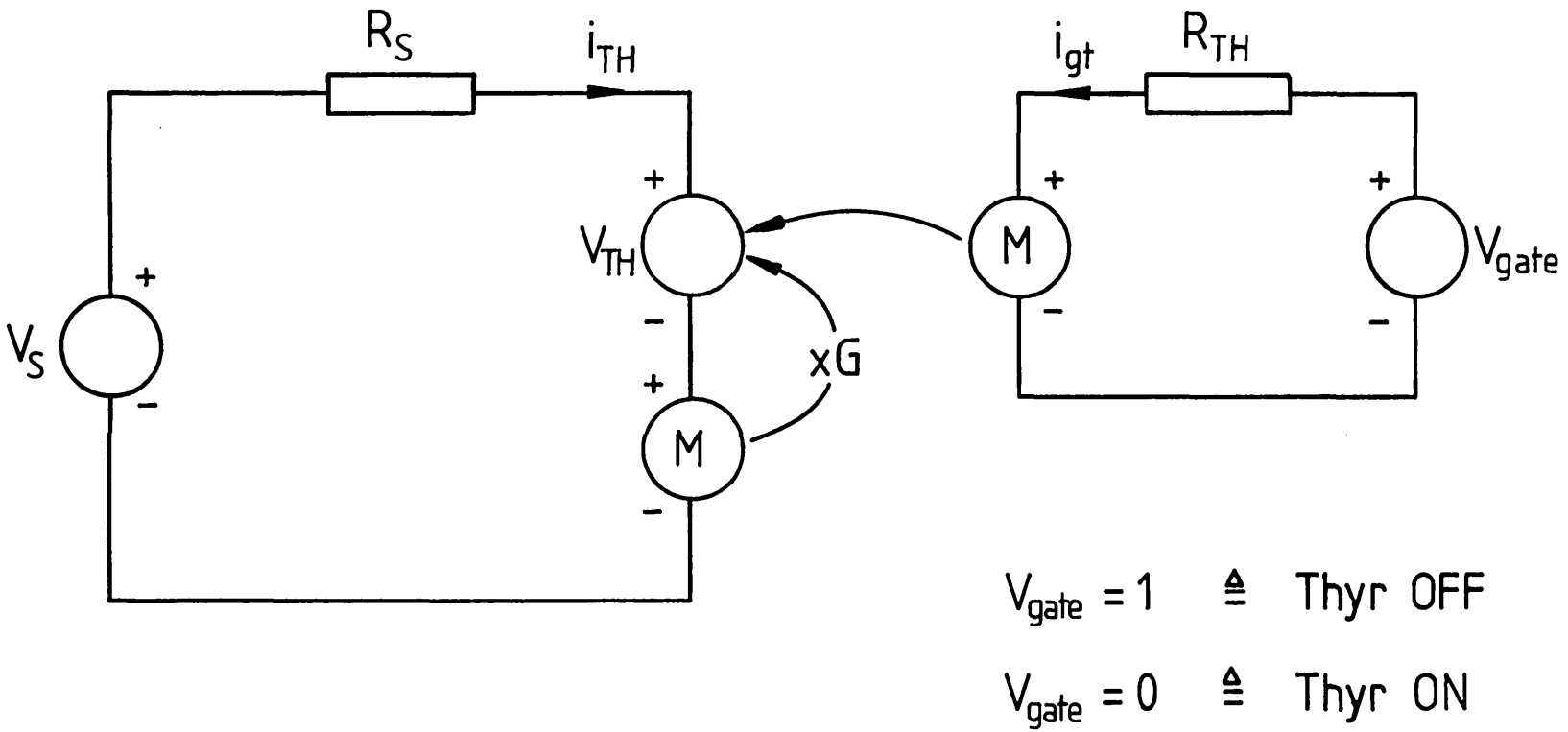


Fig. 4.19 S.P.I.C.E. Implementation of an Ideal Switch

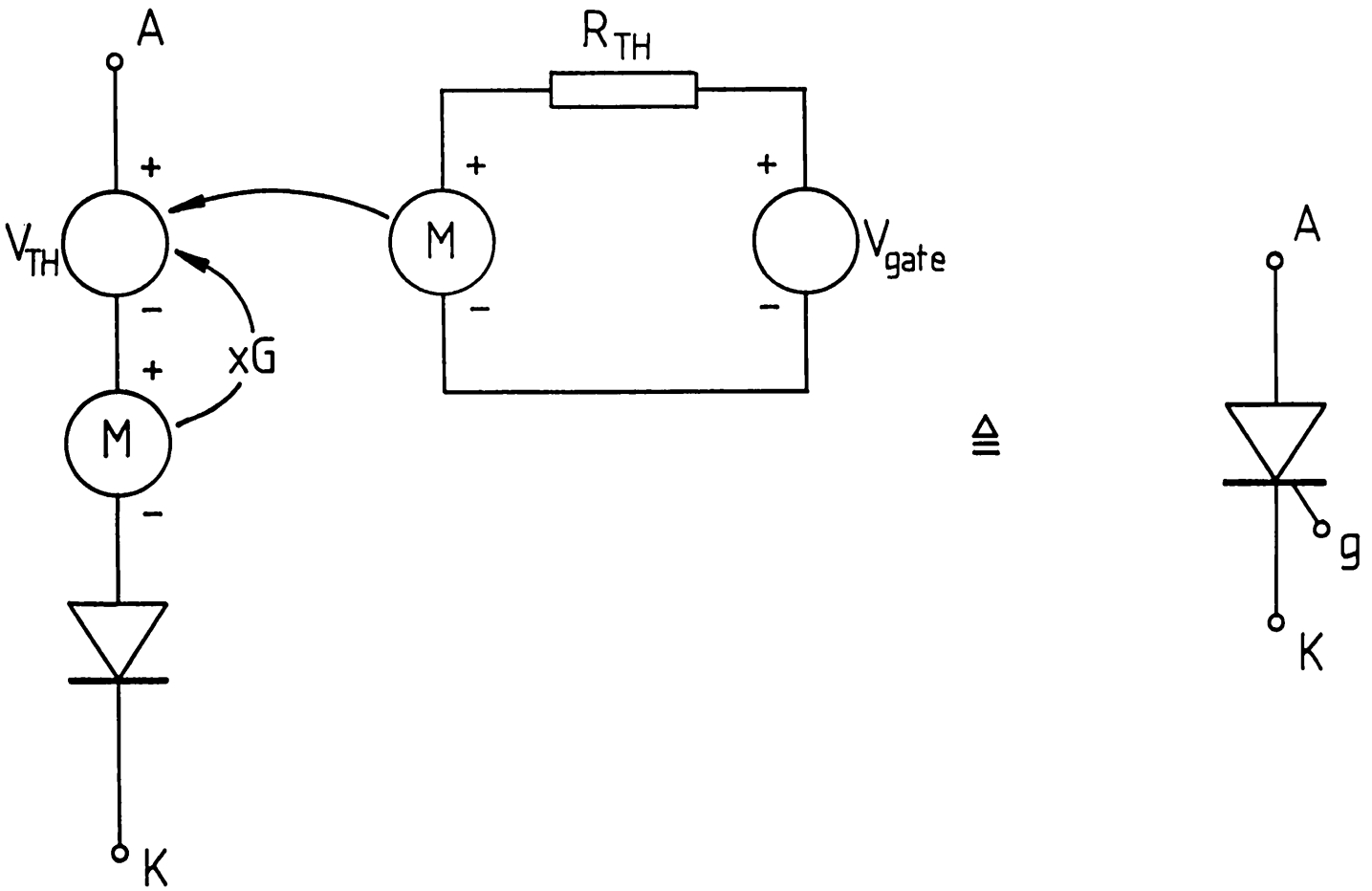


Fig. 4.20. S.P.I.C.E. Implementation of an Ideal Thyristor.

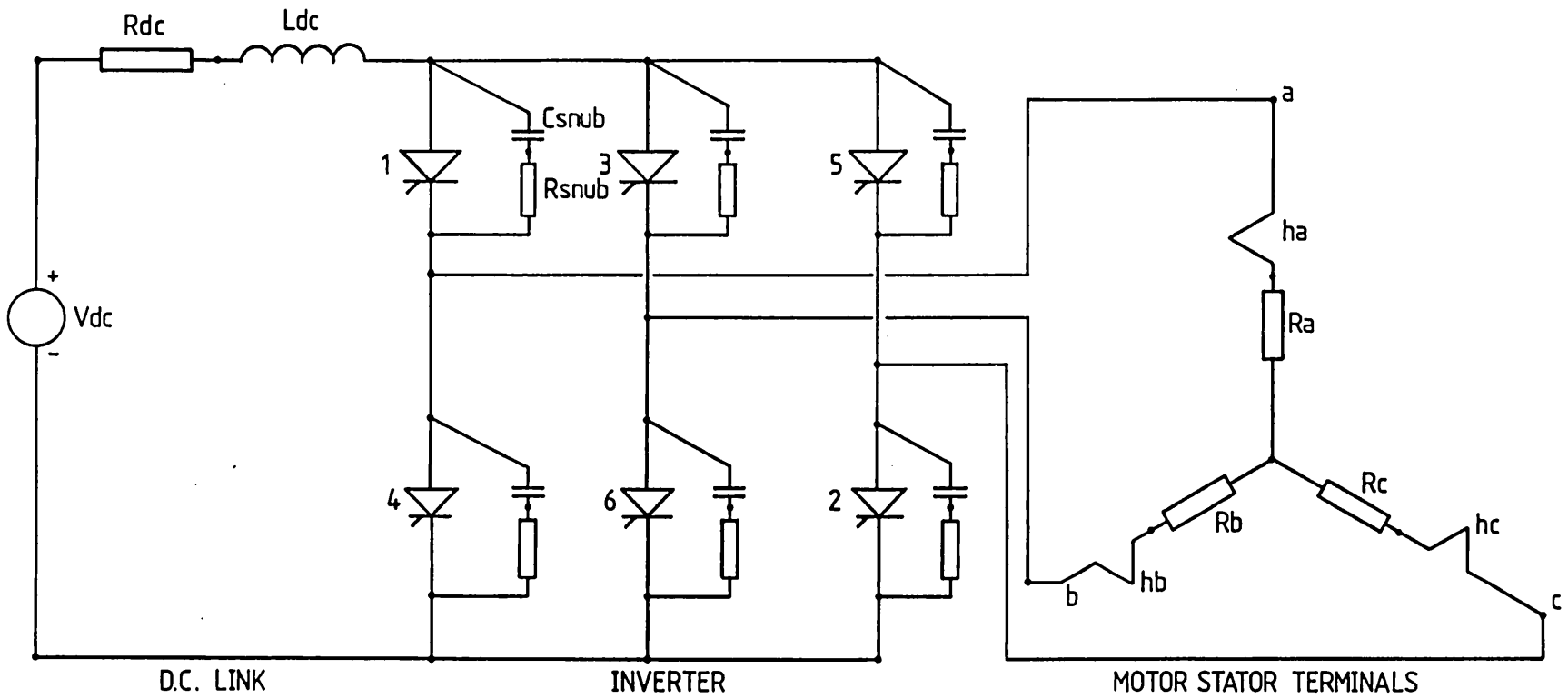


Fig.4.21. S.P.I.C.E. Inverter Model (thyristors modelled as in fig.4.20.).

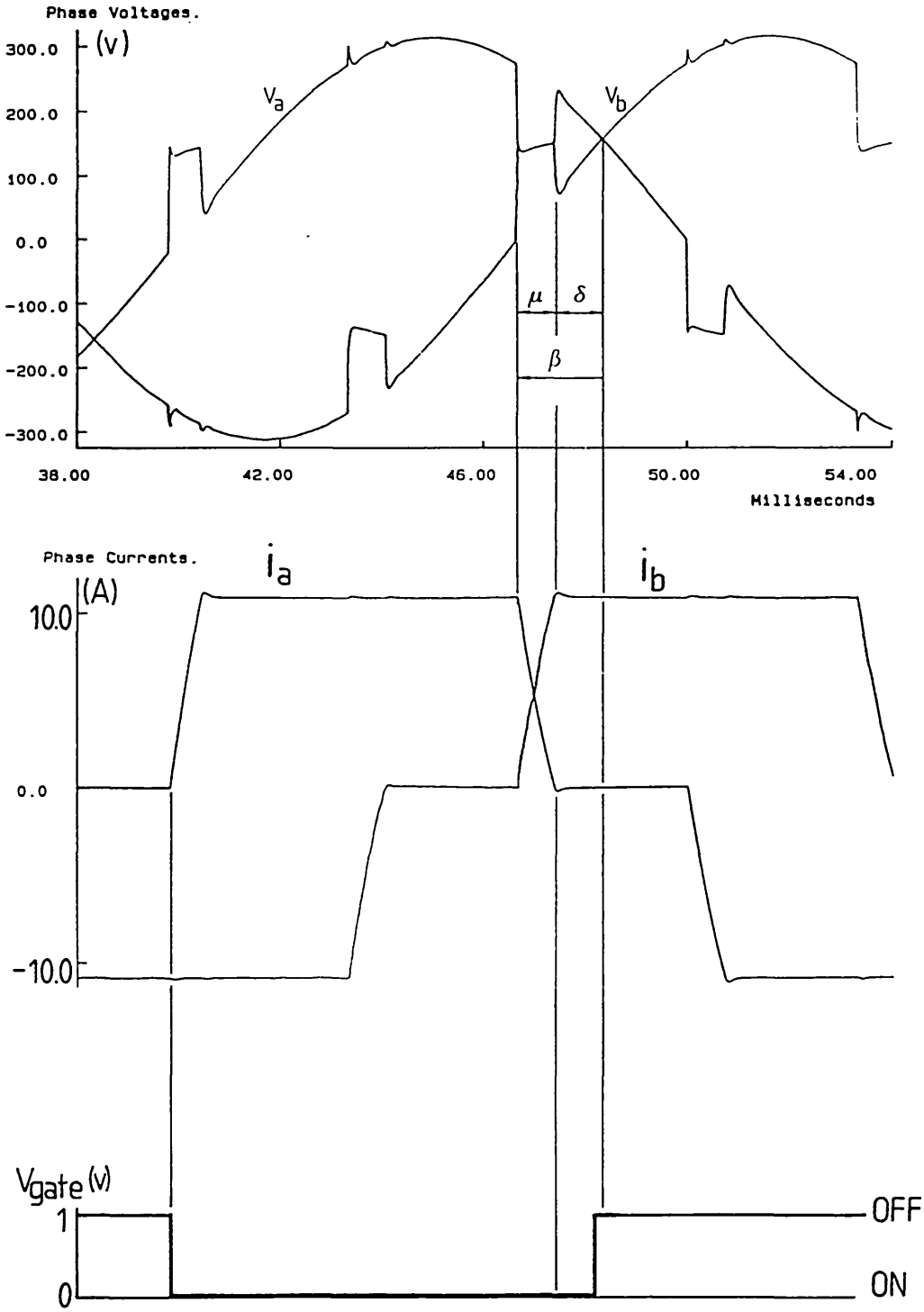
The sequencing of thyristor switching is simply arranged by using pulse functions as the gate signals, V_{GT}. However, unlike a real thyristor the model developed here does not "reset" the gating signal, V_{GT}, to zero once thyristor current has fallen below the holding current. V_{GT} pulse functions therefore have to disable a short time after commutation is complete, fig 4.22.

4.9.3 The Inverter

The full inverter circuit is shown in fig 4.21, gating circuits are omitted for clarity. Snubbers are connected just as in the actual circuit to prevent switching transients. The link choke, and associated resistance, connect the inverter to the voltage output. V_{dc} was set at a constant value corresponding to the average rectified output since rectifier/inverter interaction is minimal by L_{dc} being large. It is a simple case to simulate rectifier switching as is shown later. Connection of the inverter to the motor terminals completes the system model.

4.9.4 Additional Components

All the diagrams shown so far, and following, omit all the dummy resistances that are required for circuit solution. S.P.I.C.E. demands that each node must have a d.c. path to the ground, zero node, thus requiring the insertion of large resistors (100kΩ) across most capacitors. Also, loops of capacitors with no resistance in series with them make solution impossible since infinite currents would flow with voltage applied to the circuit. Small resistances (0.001Ω) have been inserted in capacitive loops.



Gating signal for thyristor 1.

Fig.4.22. Computer Model Thyristor Gating. Gate Disables Just Before v_a v_b Crossover.

4.10 The Circuit Solver, S.P.I.C.E.

S.P.I.C.E. is a digital computer program that simulates the electrical performance of semiconductor circuits. It was developed by Nagel [36] in the mid-70's for application to a wide range of practical circuit simulation problems. The program has been updated several times and the version used here is S.P.I.C.E. 2g.5 [37]. The program can determine the quiescent operating point, the time-domain response, or the small-signal frequency-domain response of a specified electronic circuit. S.P.I.C.E. contains models for the common circuit components and is capable of simulating most electronic circuits.

The analyses carried out here use the time-domain transient analysis for simulating the actual synchro-inverter operation, and the a.c. analysis solver for the static frequency response tests. The option of setting the circuit initial voltage conditions is available and is discussed in the next chapter.

4.11 Conclusions

A complete static magnetic circuit cross section of the Mawdsley machine with solid rotor has been developed. The motor model is exactly linked, as the actual motor is, to the electronic inverter using gyrators to represent magnetic/electric linkages. Allowance is made for stator tooth leakage paths and the rotor is dissected into flux paths. Rotor discretization allows for flux concentration near the rotor surface and vertical permeances complete the two dimensional representation of the possible flux paths. Eddy currents are represented with "magnetic dampances" and the problem of defining eddy current return paths is resolved by pulling the eddy current paths to

the "neutral" centre point of the rotor hub.

A thyristor device has been developed enabling the representation of a dynamic inverter model. Other electronic circuit components are easily modelled in S.P.I.C.E. so that the synchro-inverter simulation is complete except for machine motion.

CHAPTER FIVE

RELATIVE MOTION BETWEEN ROTOR AND STATOR

5.1 Introduction

In the previous chapter a technique for modelling a motor cross section having a solid salient rotor has been outlined. The resulting network is only valid though for stationary machine tests such as the static frequency response test or a simple step response analysis. No allowance is made for the generation of motor back e.m.f.'s or the variation in stator reactances due to the relative rotor position. It is possible to set up separate models having different relative rotor angles although continuous or part motion is not possible with the model as it stands.

The variation of commutating reactance due to rotor position for long commutation intervals may be significant, and the initial rotor angle (dependent on β and load angle) will also influence commutating reactance. Allowance should be made for commutating reactance variation in any analysis, especially for motors with solid salient poles.

The recurrent magnetic field distortions, due to commutation, may well coalesce to result in a permanently distorted magnetic field in the steady state. This phenomenon would be allowed for in a rotating model and could be examined by studying the calculated magnetic field pattern. It would also be of interest to study the penetration of flux to see if flux distortion is held out of the main pole body

volume or whether the flux pattern as a whole is disturbed.

More importantly, the generation of motor back e.m.f. facilitates the coupling of the inverter, fig 4.21, to the motor magnetic circuit. A full simulation is then possible for an indefinite number of electrical cycles and an opportunity to study rectifier/inverter interaction is provided. Computed waveforms are then available for direct comparison with actual phase quantities and field currents.

5.2 Representing Motion by Varying the Air Gap Permeance

The air gap permeances of the motor model developed in the previous chapter have a constant value. By the addition of further air gap capacitors, linking the rotor to the stator teeth, and allowing all air gap permeances to vary as a function of rotor angle back e.m.f.s at the stator terminals will be generated. The analytical justification for adopting this approach is given below.

5.2.1 Analysis of Varying Air Gap Permeance

The generation of e.m.f at the stator terminals is a function of the rate of change of flux linkages due to transformer and rotational effects. The transformer effect is already allowed for and the rotational e.m.f. is dealt with here.

The motional e.m.f, e_r, in a winding of N turns results from the movement f at angular speed ω_r of its conductors through the gap flux, Φ_g.

$$e_r = N \cdot \frac{d\Phi_g}{dt} \qquad (5.1)$$

Equation 5.1 can be written as

$$e_r = N \cdot \frac{d\Phi_g}{d\Theta} \cdot \frac{d\Theta}{dt} \qquad (5.2)$$

and

$$\frac{d\Theta}{dt} = \omega_r$$

for a constant angular velocity.

So equation 5.2 becomes

$$e_r = \omega_r . N . \frac{d\Phi_g}{d\Theta} \qquad (5.3)$$

Now,

$$\Phi_g = f_g . \Lambda_g \qquad (5.4)$$

where f_g is the air gap m.m.f. and Λ_g the air gap permeance.

Assuming a constant air gap m.m.f. equation 5.4 can be substituted in equation 5.3,

$$e = N.\omega_r . \frac{d\Lambda_g}{d\Theta} . f_g \qquad (5.5)$$

Thus, e is a function of rate of change of air gap permeance with rotor angle. For the simple machine of fig 5.1 e_r will be a maximum when Λ_g (capacitance in magnetic circuit terms) is a minimum.

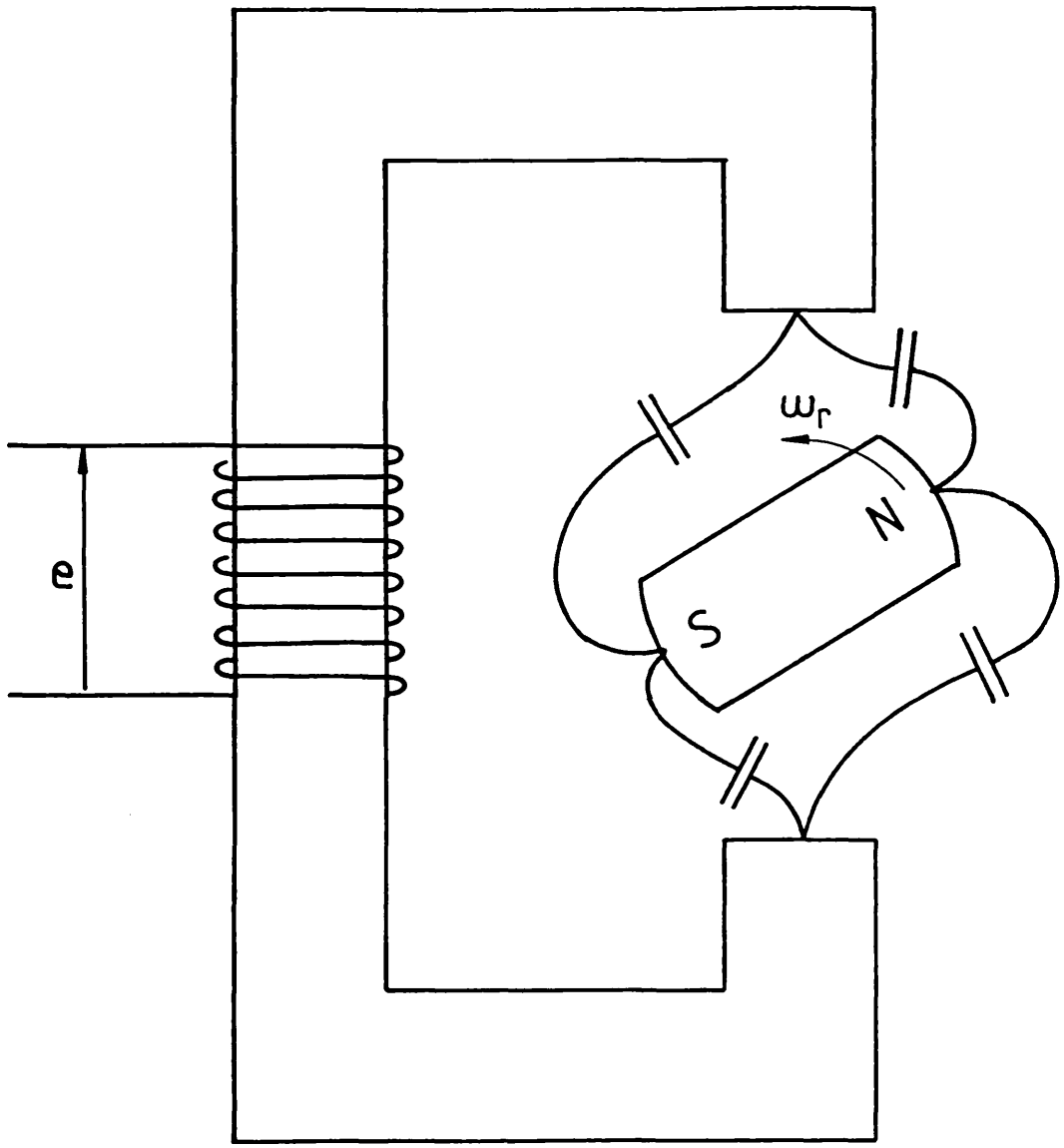


Fig.5.1. A Simple Machine.

5.2.2 Other Work

The variation of air gap permeance to model rotor motion is used successfully by Sutton [38] to model a "Flux Switching", a.c. generator and by Ostovic [39, 40] who models induction and permanent magnet machines. Both authors utilize air gap permeances which vary as a function of rotor angle. In each case the permeance between maximal and minimal (zero) value is approximated with a sinusoidal function figs 5.2(a) and (b). The assumption of a sinusoidal permeance function is shown to be valid by Sutton when compared to actual flux versus rotor angle plots.

Sutton's machine has a simple magnetic circuit geometry, with only four air gap permeances, implementing the permeance variation of fig 5.2(a). A complete rotor revolution necessitates the bonding of each stator tooth with every rotor tooth with a variable gap permeance.

Ostovic's induction motor [39] requires many more air gap permeances to satisfy the union of each stator tooth with all the rotor teeth. Fig 5.3 shows a developed section of Ostovic's complex air gap structure, with other permeances omitted for clarity. He uses the permeance variation of fig 5.2(b) so that maximum permeance occurs when a rotor tooth is directly opposite a stator tooth. The shape of the permeance function therefore inherently emphasizes the tooth ripple. The formulation of Ostovic's models is similar to the technique used here, that is, the major flux paths are identified and relevant permeances inserted. He then develops his own set of equations from the magnetic network for solution. The technique enables the study of machine transient, dynamic and starting behaviour as well as steady state operation.

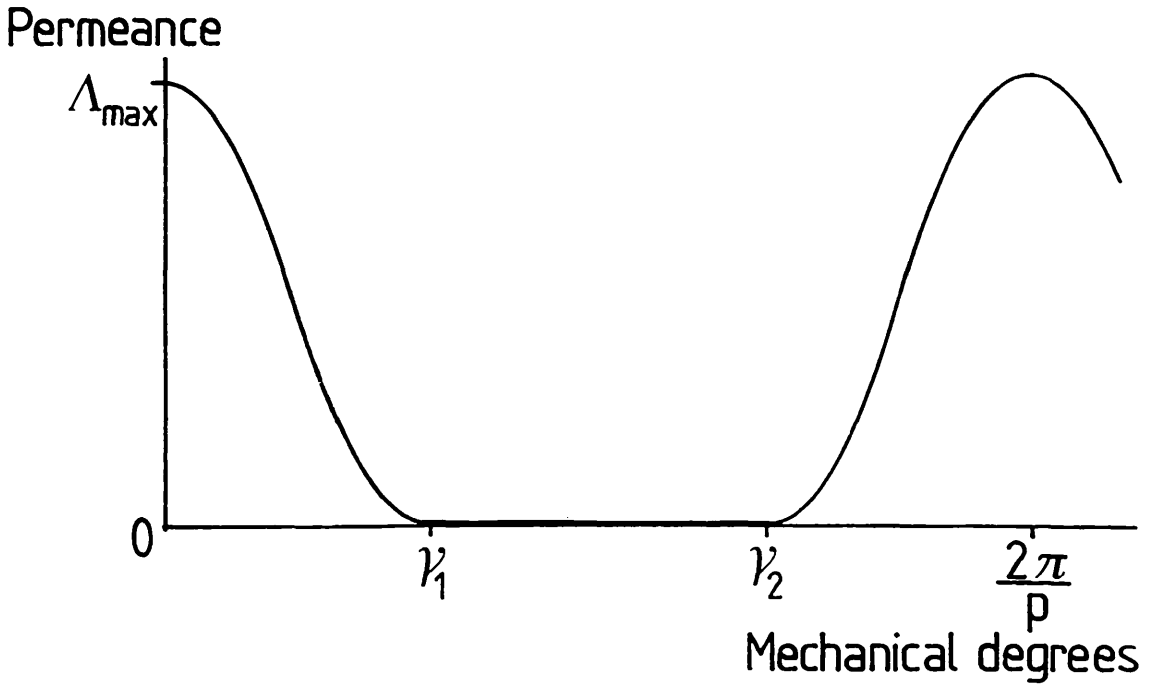


Fig.5.2(b). Air Gap Permeance vs. Rotor Angle used by Ostovič.

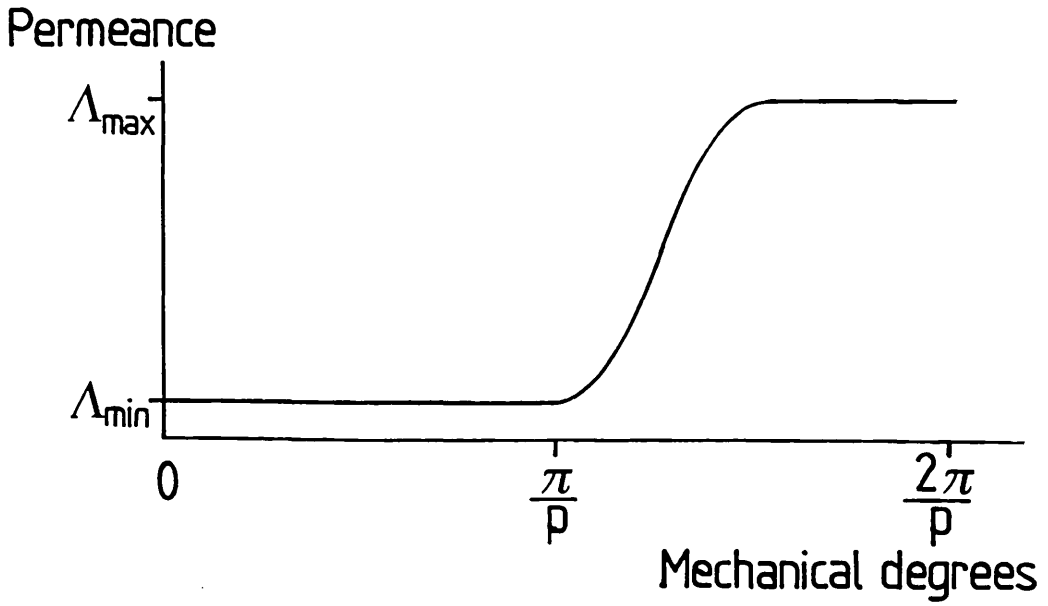


Fig.5.2(a). Air Gap Permeance vs. Rotor Angle used by Sutton.

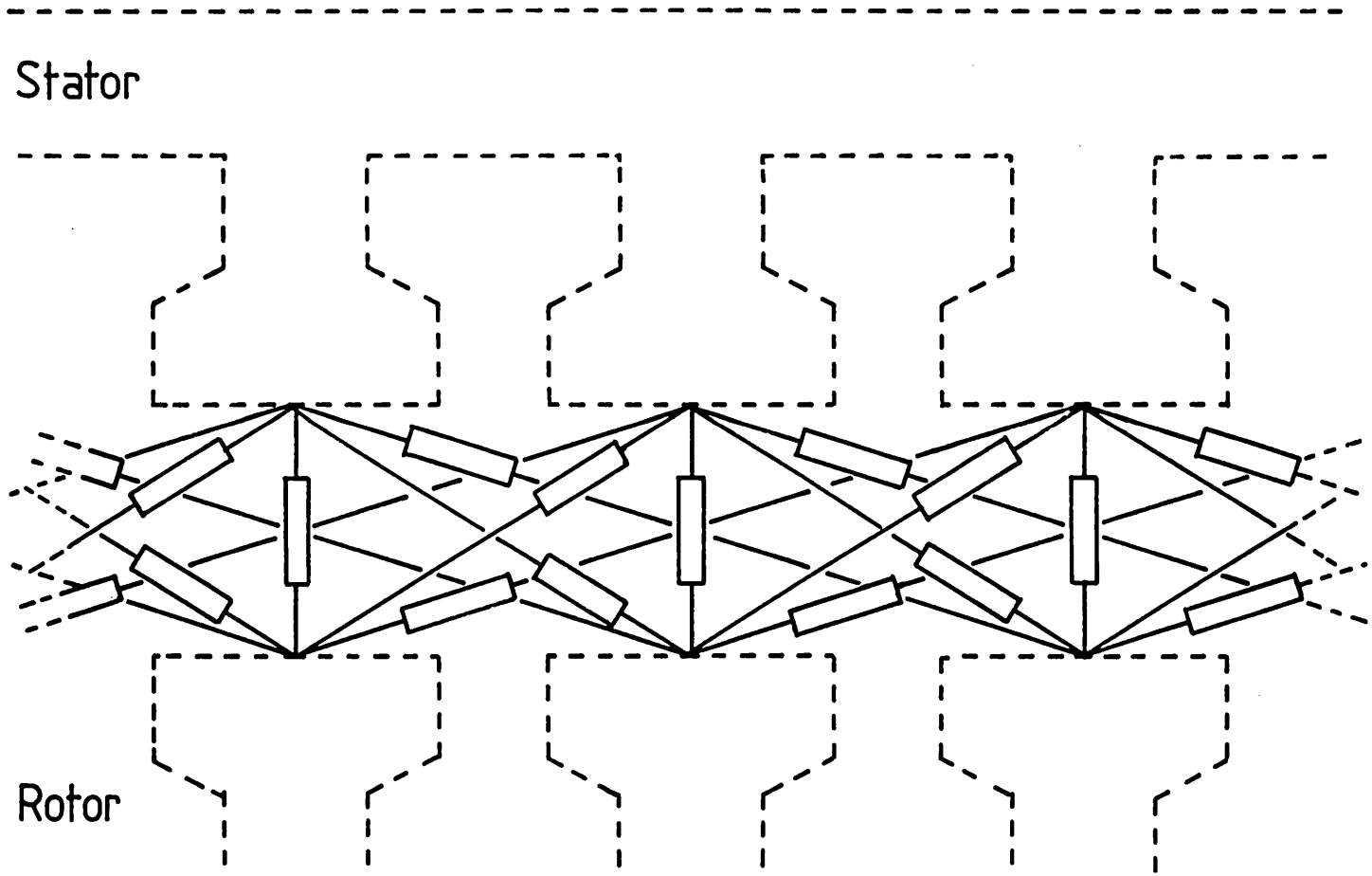


Fig.5.3. A Section of Ostovics Induction Machine Equivalent Magnetic Circuit. Air Gap Permeances Illustrated.

5.2.3 Variable Air Gap Permeances of a Simple Machine

Simple machine geometries and various air gap permeance functions have been experimented with. A single phase machine, depicted in fig 5.4, with purely sinusoidal permeance functions, fig 5.5(a), produces a sinusoidal output voltage of expected magnitude and phase. All stator teeth are connected to the two rotor poles, only three air gap permeances are shown in fig 5.4 for clarity. An air gap permeance variation such as fig 5.5(b), similar to Ostovic's produces an output voltage with pronounced slot ripple, fig 5.6(a). The permeance (capacitive) waveforms, figs 5.5(a) and 5.5(b), are drawn for the associated capacitors of fig 5.4, with the rotor starting as shown at t = 0 and rotating clockwise. A sinusoidal gap function fig 5.5(a) eliminates slot ripple as shown in fig 5.6(b).

5.3 The Solid Rotor

The solid rotor surface has already been discretized into flux path sections of the same pitch as each stator tooth, fig 4.8. Eight paths into the rotor exist, necessitating the coupling of sixteen (for both rotor poles) rotor paths to twenty four stator teeth, ie, 384 time variant capacitors. However, S.P.I.C.E. does not have such time variant elements. It was found that a time dependent capacitor could be modelled from seven circuit elements as outlined in appendix B. 384 x 7 elements though would probably have been too many elements for S.P.I.C.E. to cope with, let alone other circuit elements.

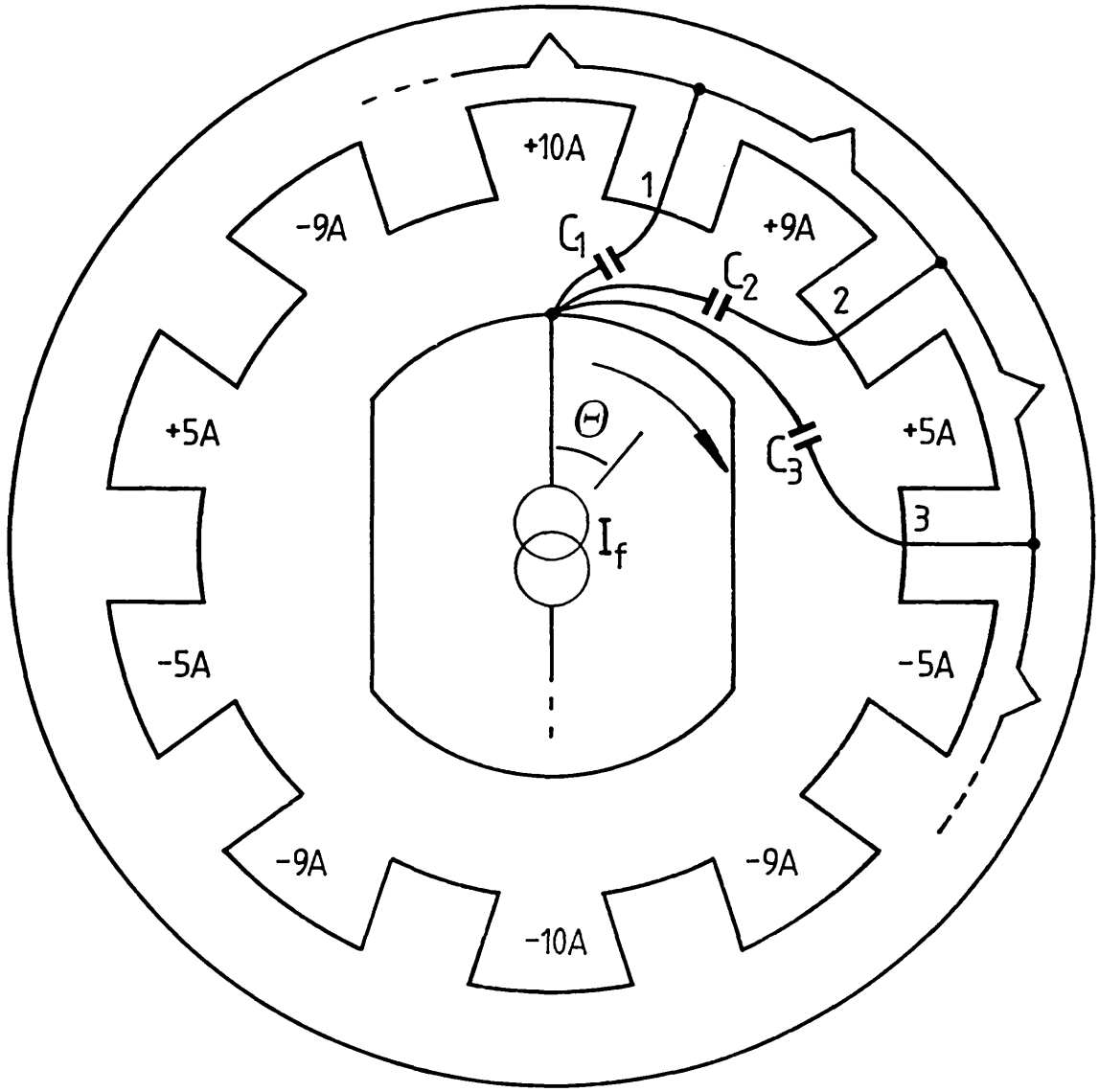
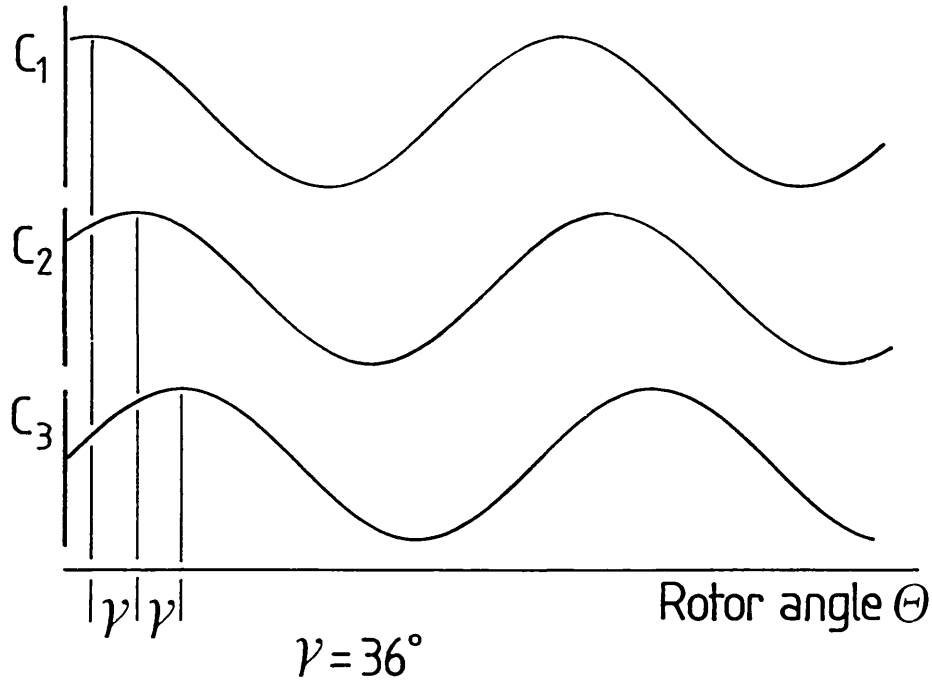
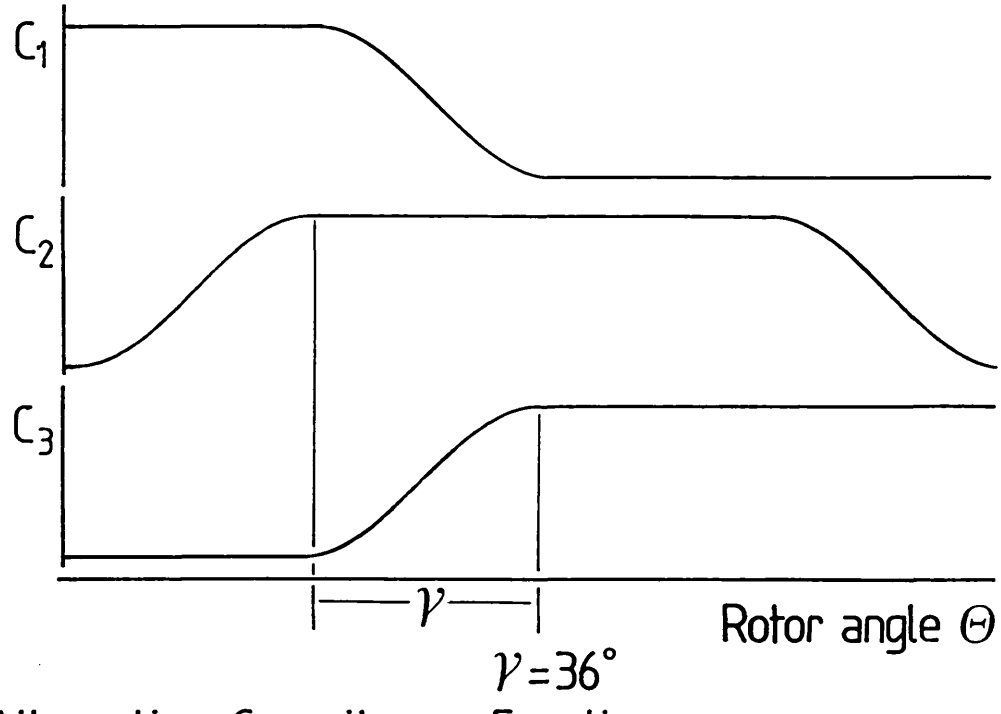


Fig.5.4. Single Phase Machine. Only Three of the Required Twenty Air Gap Capacitors are Shown.

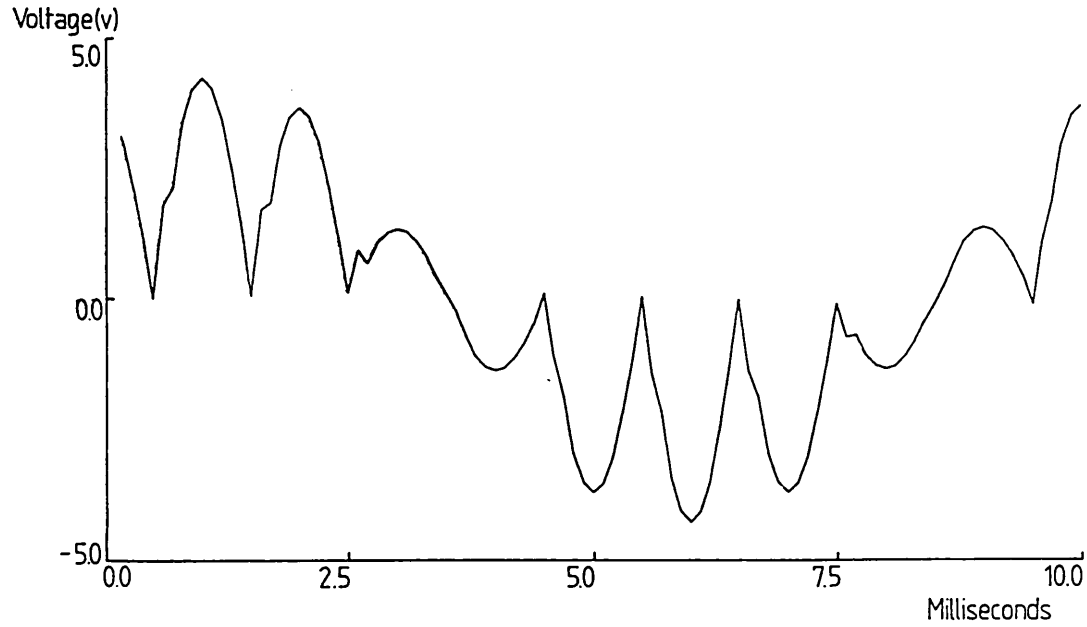


(a) Sinusoidal Capacitance Functions.

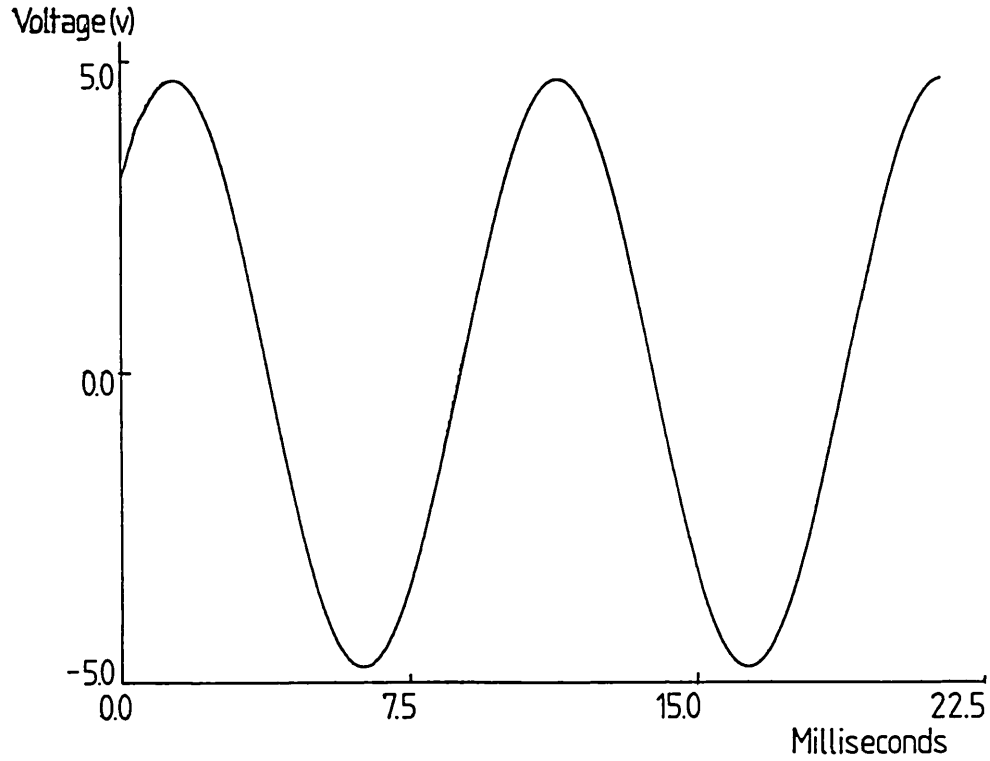


(b) Alternative Capacitance Functions.

Fig.5.5. Air Gap Capacitance Variation as a Function of Rotor Angle for the Machine of Fig.5.4.



(a) Using Air Gap Capacitor Functions of Fig.5.5(b).



(b) Using Air Gap Capacitor Functions of Fig.5.5(a).

Fig.5.6. Open Circuit Phase Voltages for the Simple Machine of Fig.5.4.

5.3.1 A Means of Reducing the Number of Air Gap Permeances

For a complete motor revolution, over two and a half thousand S.P.I.C.E. elements would be required. To reduce the number of gap capacitors it is assumed that a stator tooth more than one slot pitch away for a particular rotor section results in a minimum capacitance and is set to zero capacitance. Motion is also limited to moving the rotor by one stator slot pitch, ie 15 electrical degrees, thus requiring only thirty two variable capacitors. The final results then become the initial conditions for a program representing the next fifteen degrees of movement.

Figs 5.7 to 5.9 show developed stator and rotor sections for a rotor movement of 15^{o}. For clarity only air gap capacitors are shown. At the start, $\theta = 0^{o}$, capacitors C_{jb} are at zero permeance, while C_{ja} are at a maximum value (j = 1 to 8), fig 5.7. The rotor moves to the right so at $\theta = 7.^{o}5$, fig 5.8, the half way stage, all gap capacitors are of equal value. Finally, at $\theta = 15^{o}$, fig 5.9, the capacitors C_{jb} have reached maximum permeance value while the C_{ja}'s have fallen to zero (j = 1 to 8). The final node voltage values for this 15^{o} portion of movement are then used to set the initial conditions for a program simulating the next 15^{o} of movement, fig 5.10, and so on. So the next "new" circuit starts with new C_{ja}'s inserted and the old, zero value, C_{jb}'s removed (final voltages across C_{ja} are used as initial voltages for C_{jb}, ie the old C_{ja}'s become the new C_{jb}'s). In fact, the new circuit, fig 5.10, is exactly the same as fig 5.7 except the stator windings are shifted to the left by one slot pitch.

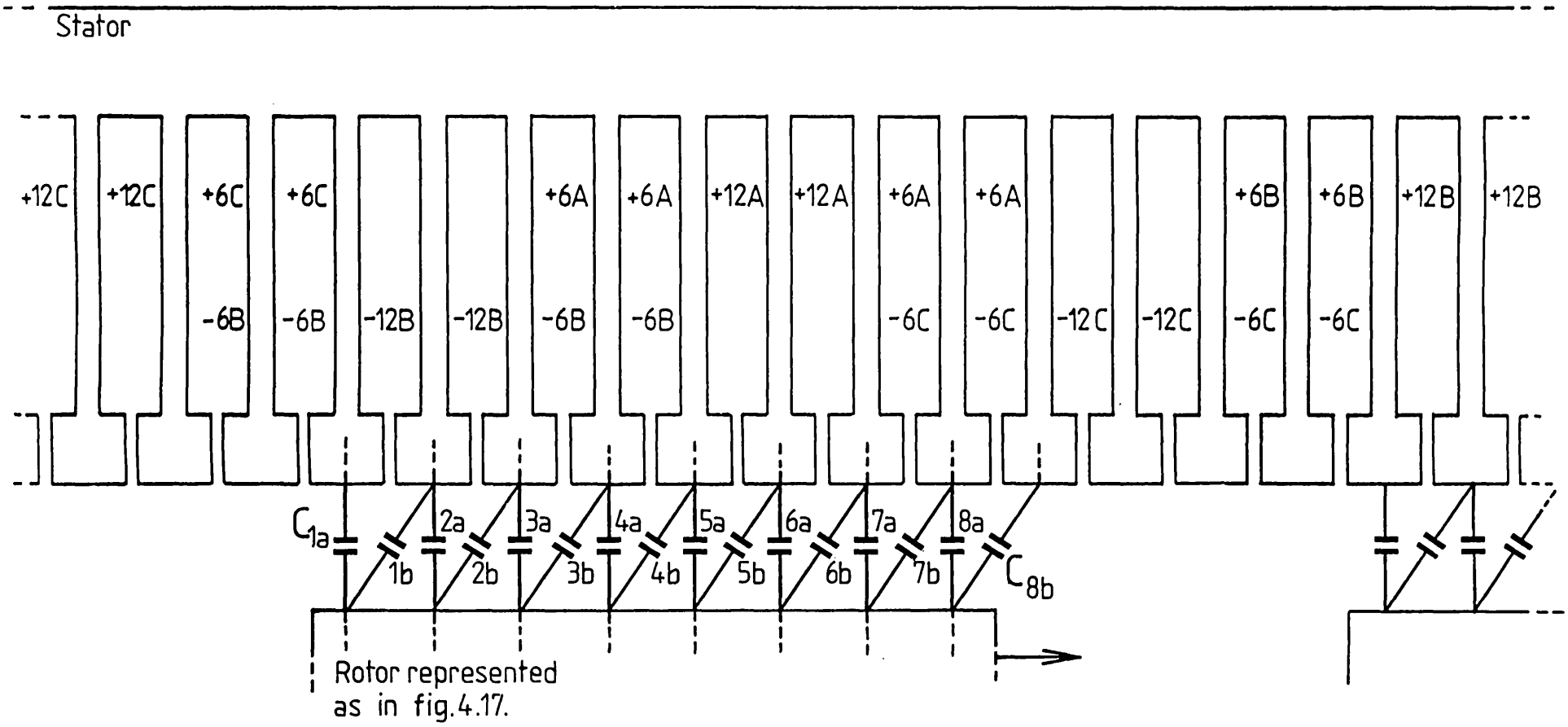


Fig.5.7. Rotor Motion Represented by Air Gap Capacitors Varying as a Function of Time. Initial Rotor Position $\Theta = 0°$.

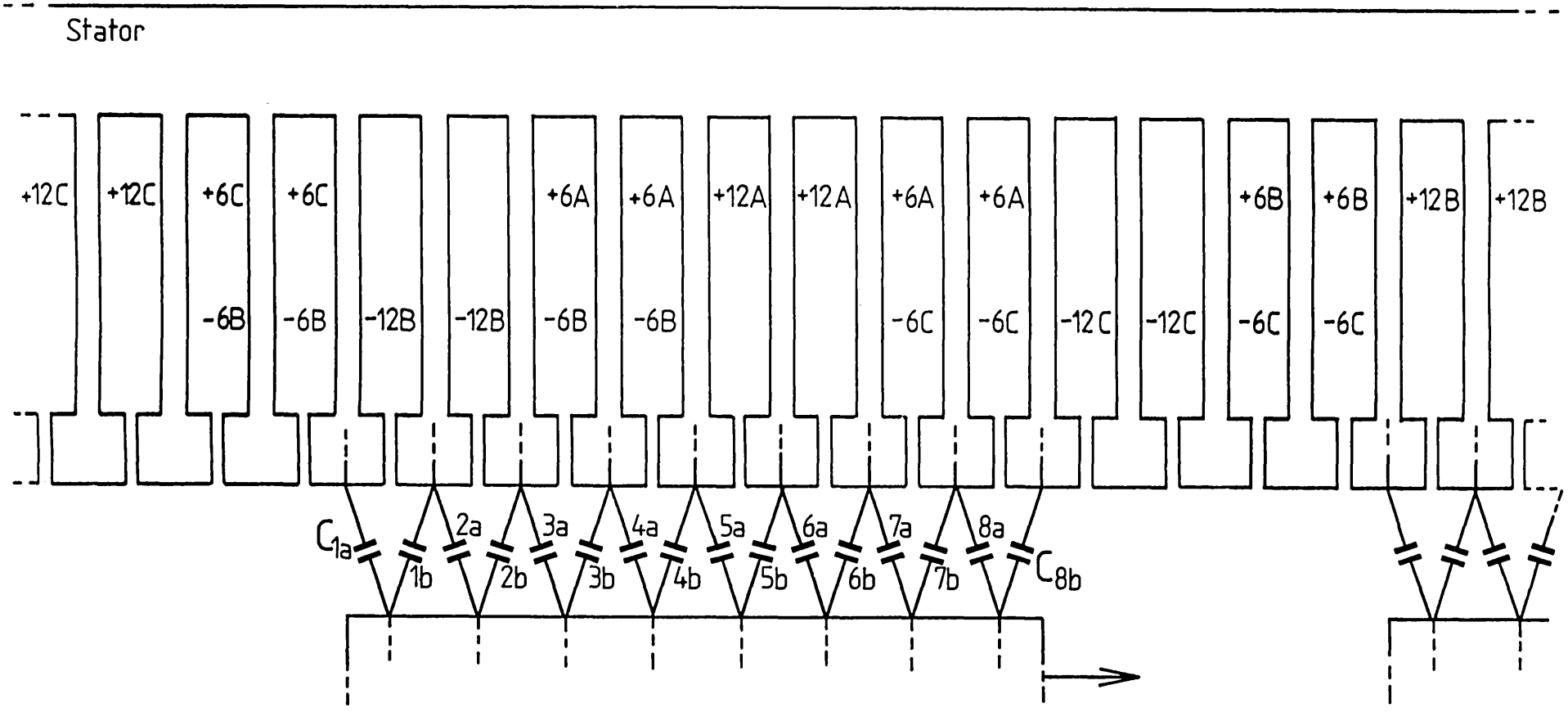


Fig.5.8. Rotor Position $\Theta = 7^{\circ}.5$.

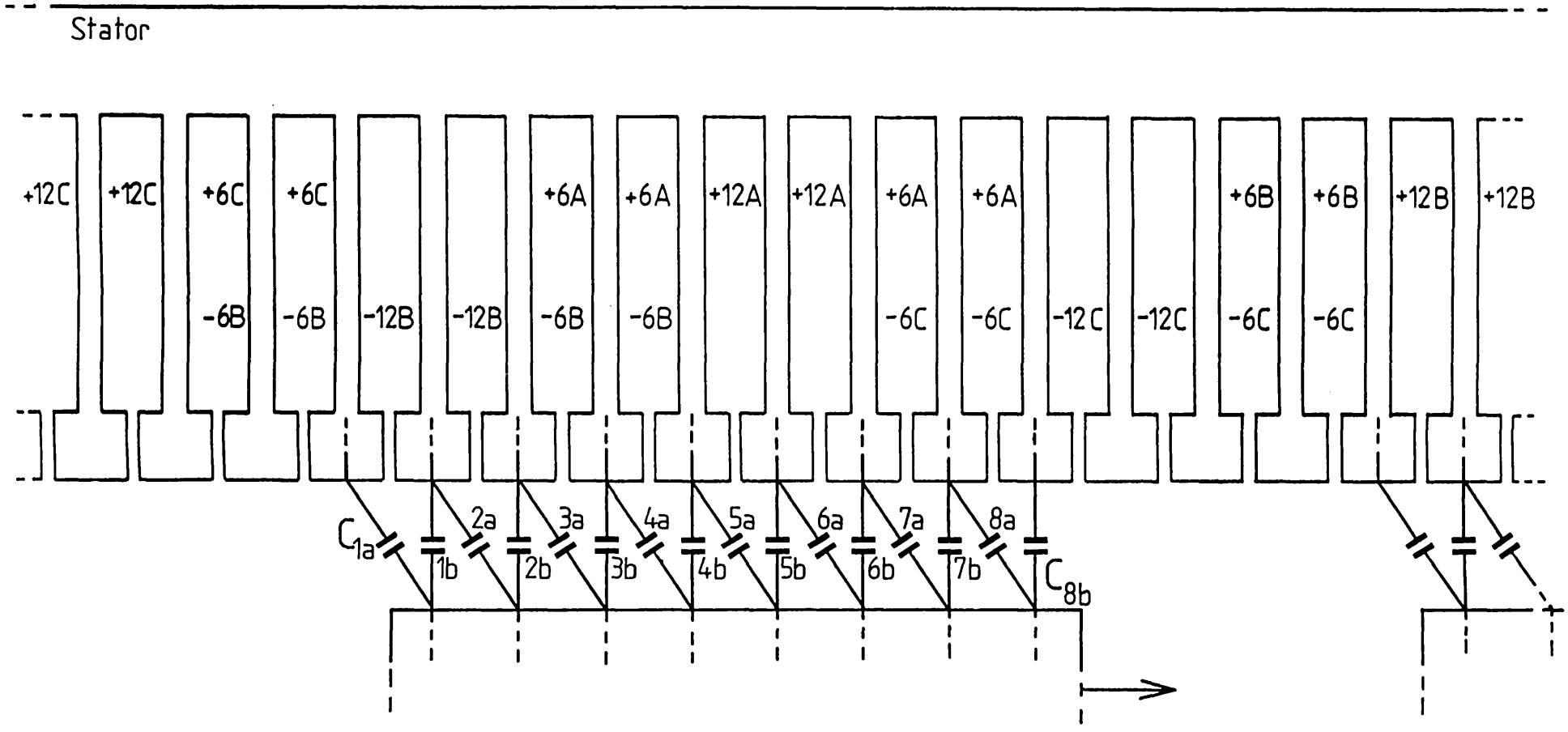


Fig.5.9. Rotor Position $\Theta = 15°$.

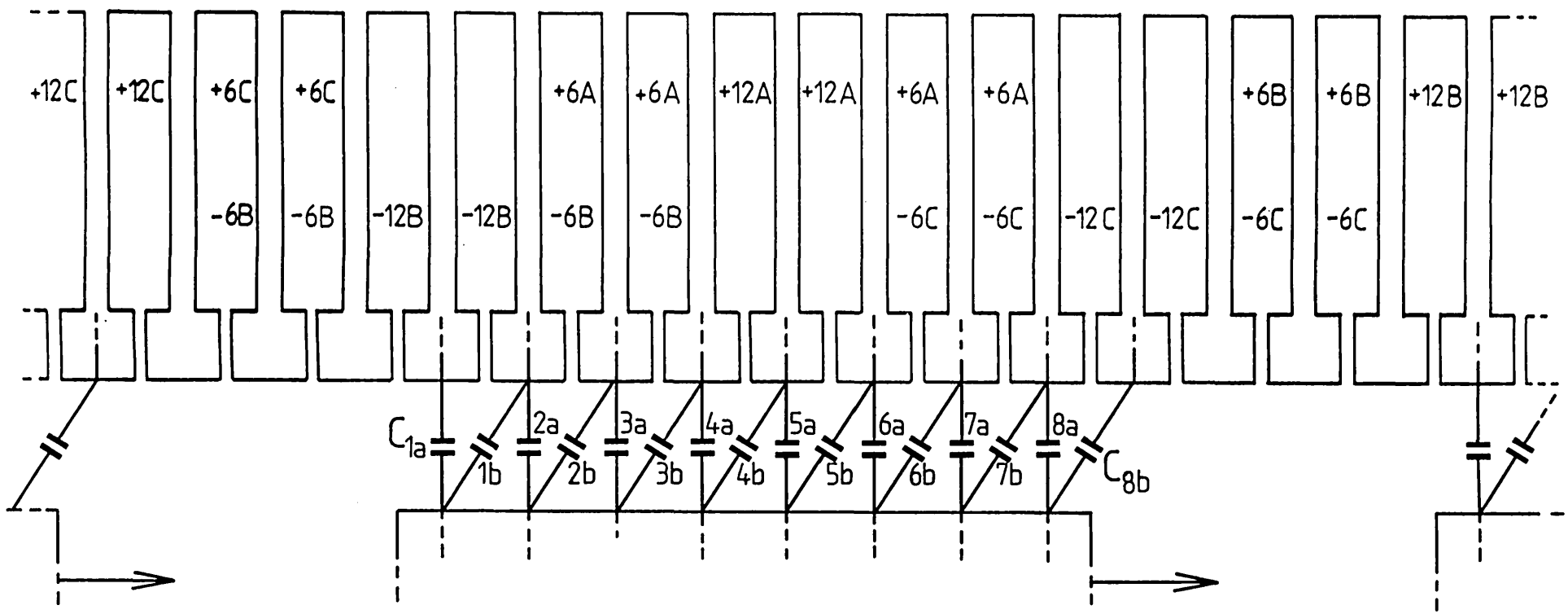


Fig. 5.10. Initial Rotor Position for Next 15° of Motion Continuing from Fig. 5.9, $\Theta = 15°$ to 30°.

5.3.2 Selection of an Air Gap Permeance Function

A relevant air gap permeance function must be chosen for the air gap capacitors detailed in 5.3.1. A sinusoidal function, fig 5.12, produces an open circuit voltage of the correct form but with very pronounced slot ripple similar to fig 5.6(a). To understand how this problem is overcome it is necessary to appreciate how the stator back e.m.f is generated from the magnetic circuit.

Fig 5.11 shows a portion of the rotor section and stator. As in fig 5.7 the rotor starts from $\theta = 0^o$. Each C_{ja} capacitor has an initial charge q_j of polarity as shown while capacitors C_{jb} have zero charge. Movement of the rotor to the right results in a charge redistribution from the "a" capacitors to the "b" capacitors since

$$q = c.v$$

and m.m.f. (v) is assumed constant. Thus a magnetic current, i_m, will flow discharging the capacitor C_{1a} at the left hand pole edge and charging the capacitor C_{8b} at the opposite pole edge. The magnetic current forms a loop around the core back and zig zags through the gap capacitors. Since i_m represents rate of change of flux an e.m.f. is induced in the stator electric terminals the magnitude of which depends upon the level of i_m.

The flow of i_m will be dependent upon the rate of change of air gap capacitors since

$$i_m = v_g . \frac{dC_g}{dt} + C_g . \frac{dv_g}{dt} \qquad (5.6)$$

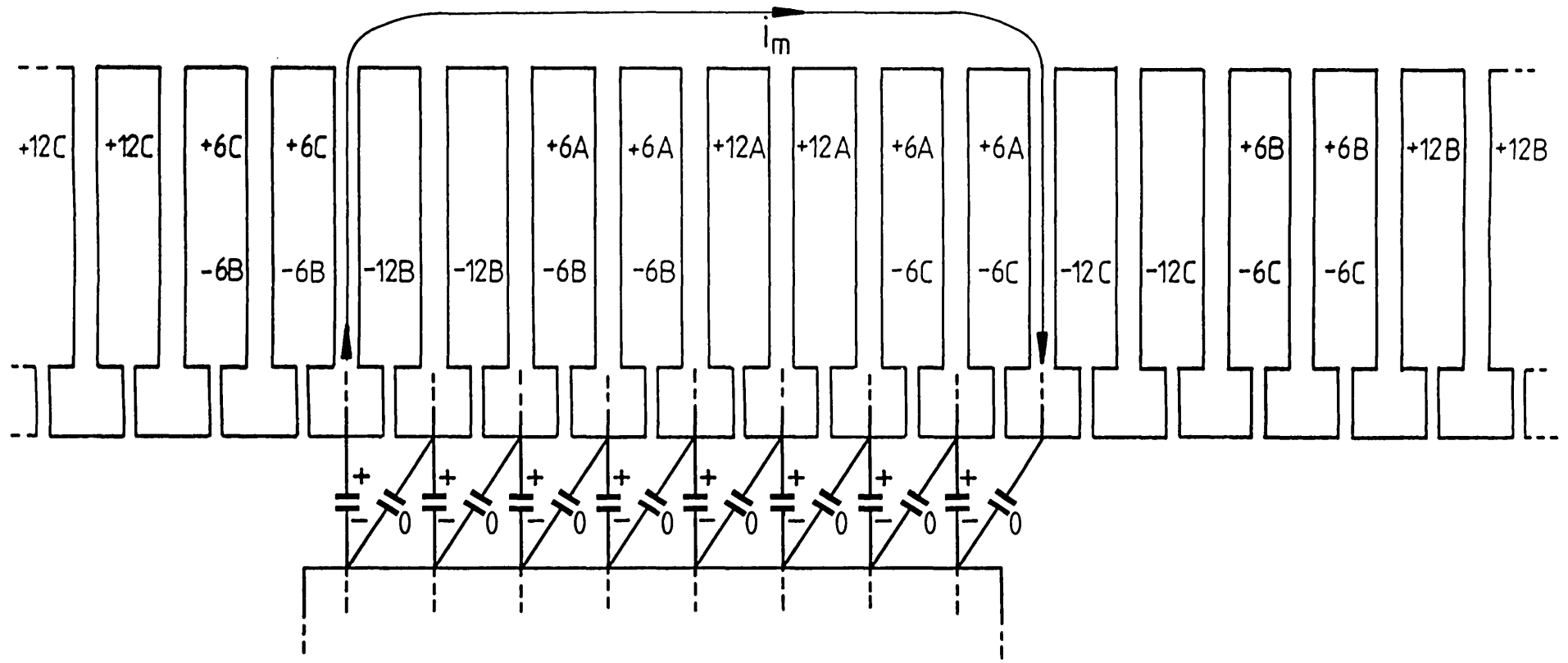


Fig.5.11. Magnetic Current Flow due to Rotor Movement.

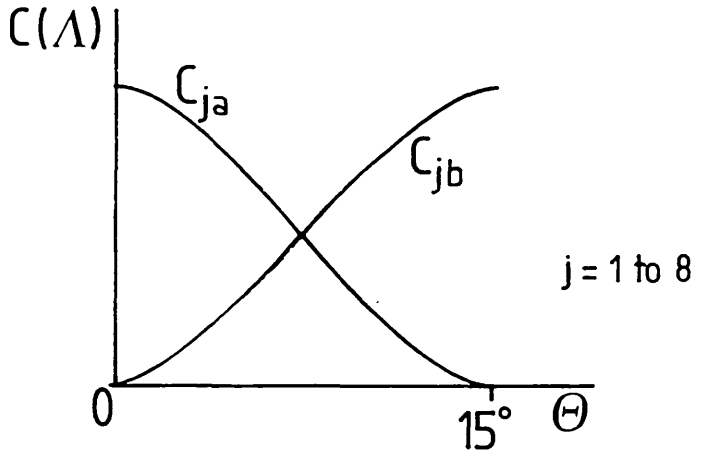


Fig.5.12. Sinusoidal Air Gap Permeance Functions.

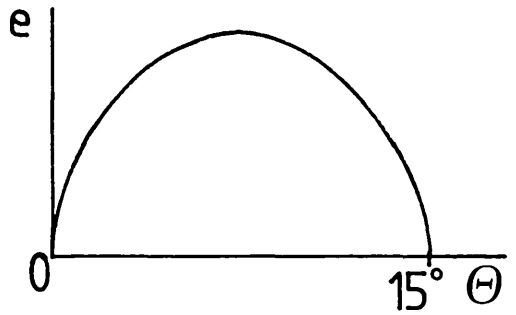


Fig.5.13. Generated e.m.f. Using Air Gap Capacitors of Fig.5.12.

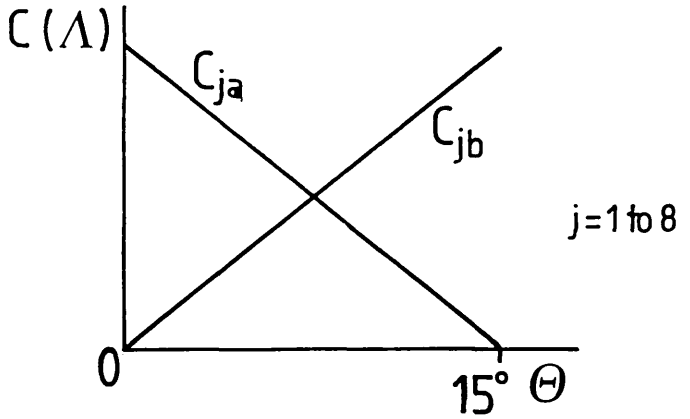


Fig.5.14. Linear Air Gap Permeance Functions.

Where v_g is the gap voltage (m.m.f.) and C_g the gap capacitance.

Air gap m.m.f. remains constant, therefore

$$i_m = v_g \cdot \frac{dc}{dt} + \text{zero}$$

For the sinusoidal gap capacitance function of fig 5.12,

$$i_m = 0 \quad \text{at } \theta = 0^o \text{ and } \theta = 15^o$$

since

$$\frac{dC_g}{dt} = 0$$

i_m = maximum at $\theta = 7.^o5$

since

$$\frac{dC_g}{dt} = \text{maximum}$$

And the sinusoidal nature of C_g causes i_m and therefore generated e.m.f., e, to be of the form shown in fig 5.13 for 15^o of rotor motion.

It is obvious from the above that variation in rate of change of gap capacitance should be avoided. Also, the condition must be satisfied that total air gap permeance under the pole must be invariant. The sinusoidal function keeps total gap permeance constant, but exaggerates slot ripple. A ramp function, fig 5.14, yields i_m constant and therefore e = constant over 15^o of movement. However,

for a complete electrical cycle (360°) the waveform of fig 5.15 is obtained for the stator voltage. As can be seen voltage is indeed constant for each 15° section of rotor angle, but stepping in the voltage waveform arises at the transfer points between each 15° section. The magnetic current, i_m, flows at a constant rate around a path such as fig 5.16(a) and (b) for a 15° section. Now, the next 15° section has shifted the magnetic current along one slot pitch, fig 5.16(c) so that current flows through the next tooth along linking a different pattern of stator conductors. Thus, i_m suddenly jumps along one slot pitch every 15° and so slot ripple is again prominent.

It is apparent that i_m will be virtually constant in the stator core above the pole centre but at the pole edges gradually spread into the rotor. Fringing of the permeances at the pole edges can improve the current distribution as is shown.

Capacitors are added at pole edges as shown in fig 5.17(b). Their permeance functions, fig 5.17(a) are modelled to prevent the sudden jumping of magnetic current at each 15° program transition. The initial (or final, depending on whether the capacitor is at the rotor's leading or trailing edge) slope of C_{e1} is zero and gradually increases in slope until the slope is equal to that of the ramp function of fig 5.14. The resulting open circuit voltage is a sinusoid with negligible steps in voltage at program transitions.

The transitory steps though become pronounced, fig 5.18, when the motor model is connected to the inverter system, that is, with an applied stator load current. Armature reaction and magnetic flux distortion cause the ripple. However, two other factors are thought to contribute to the problem as outlined below:

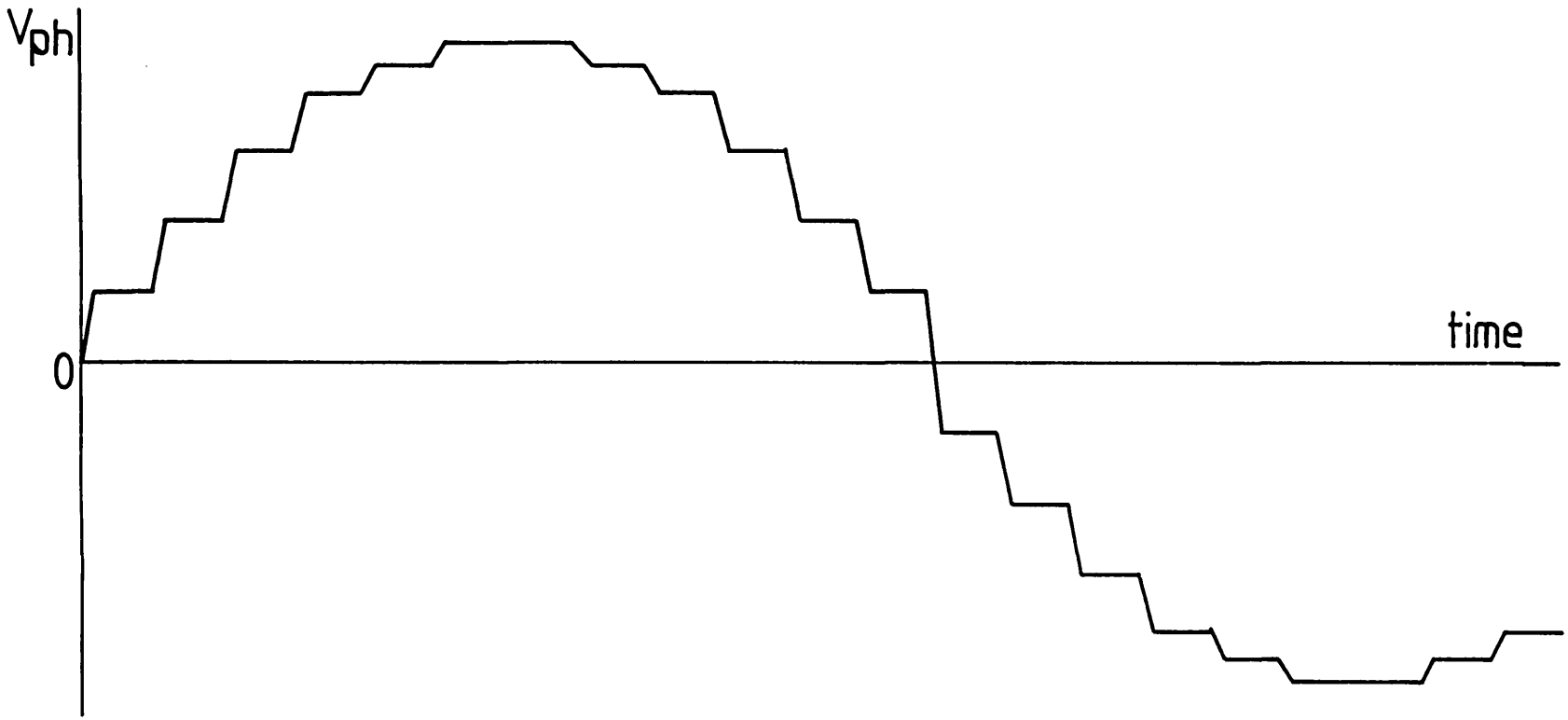


Fig.5.15. Motor Magnetic Model Open Circuit Phase Voltage, Using Air Gap Capacitors having a Time Function of Fig.5.14.

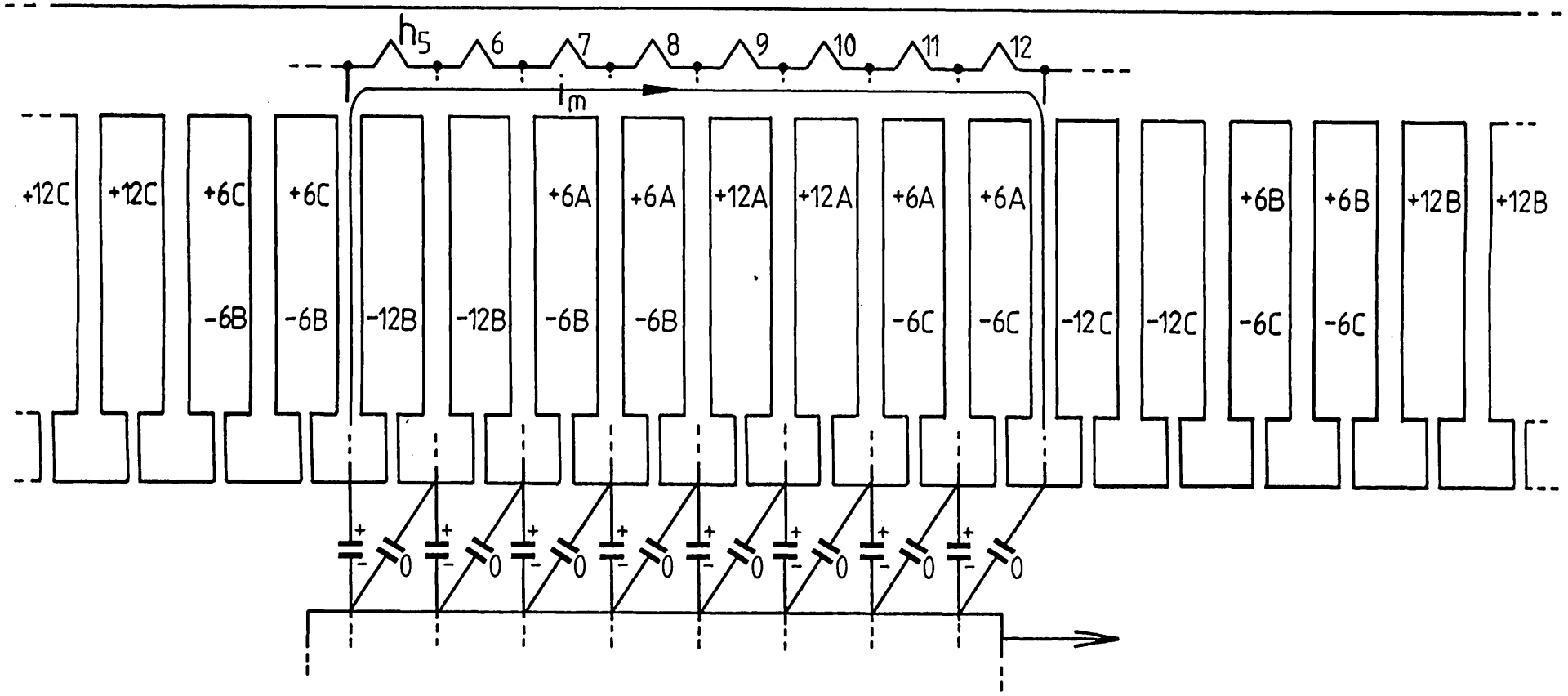


Fig.5.16(a). Stator Magnetic Current due to Motion. $\Theta = 0°$.

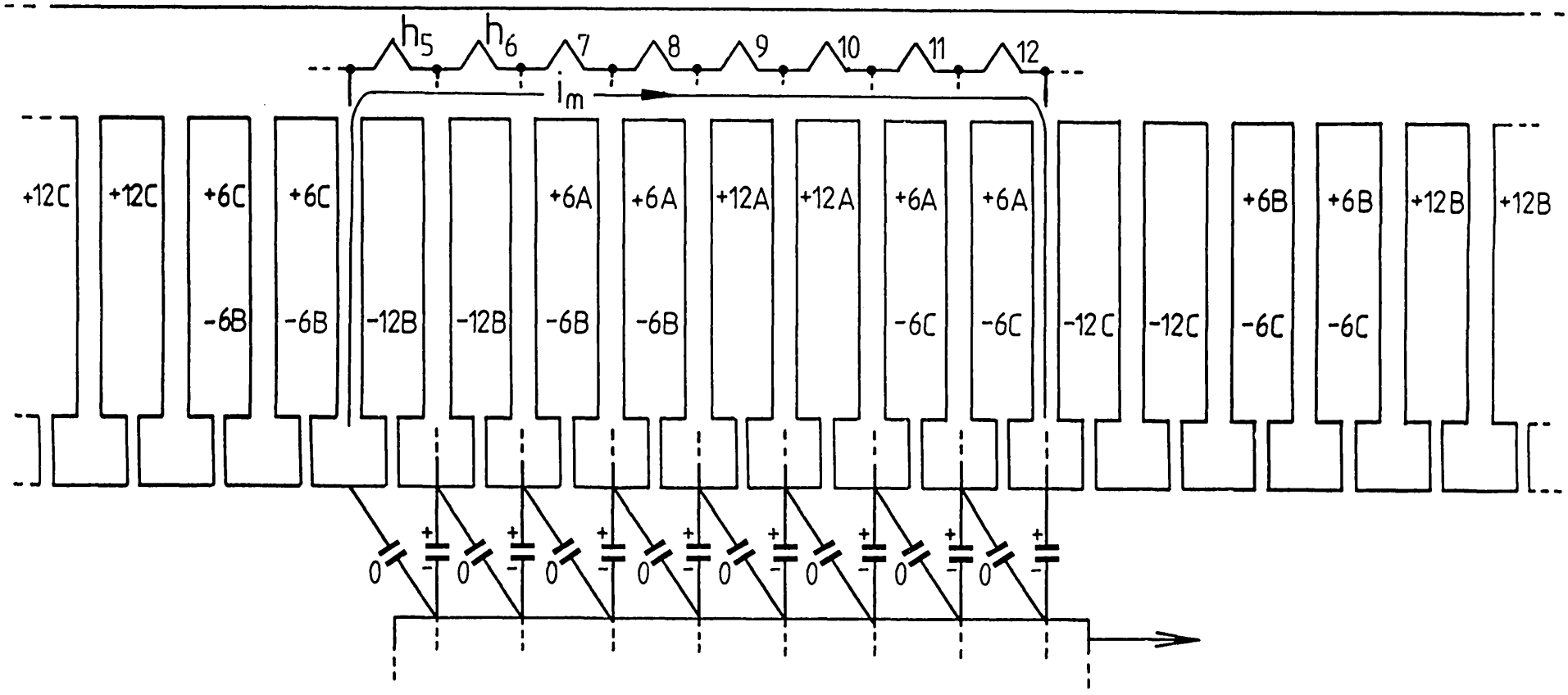


Fig.5.16(b). Stator Magnetic Current due to Motion. Θ=15°.

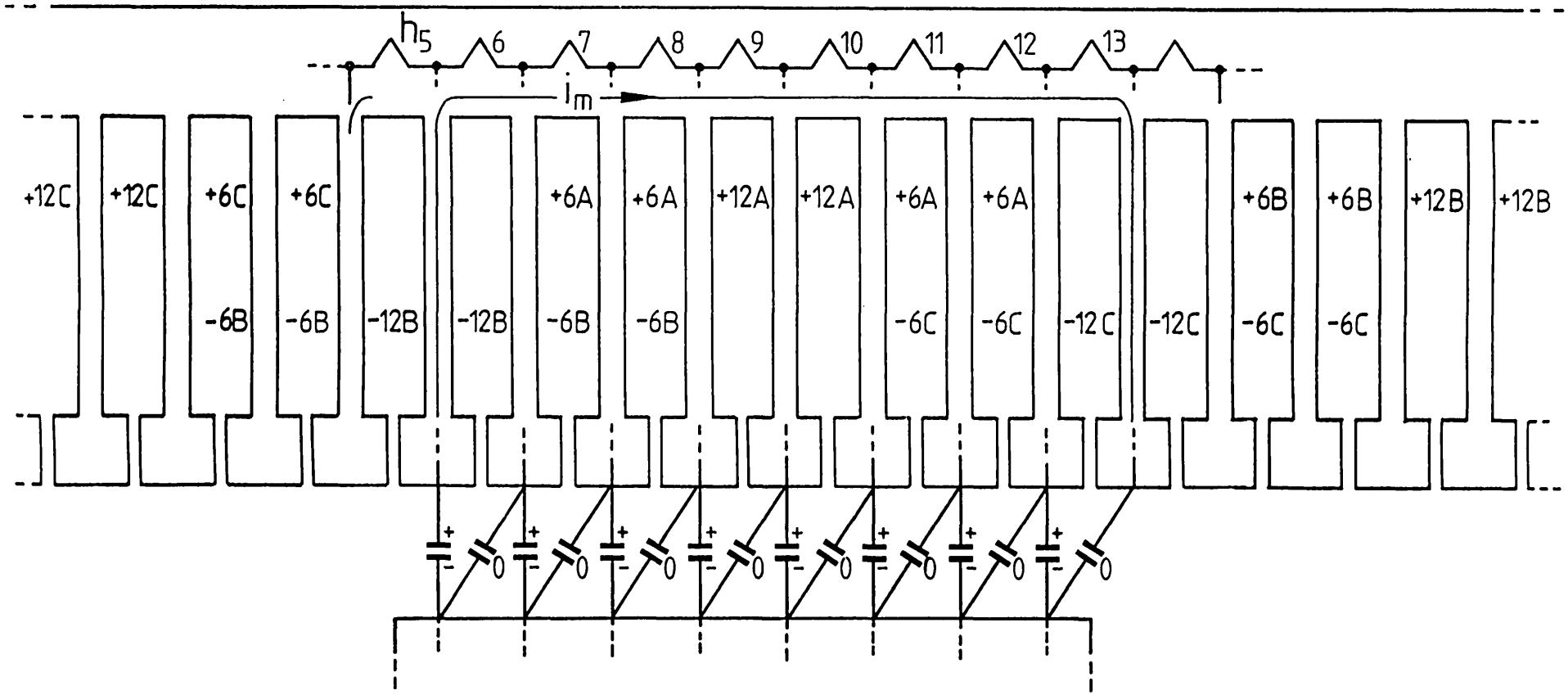
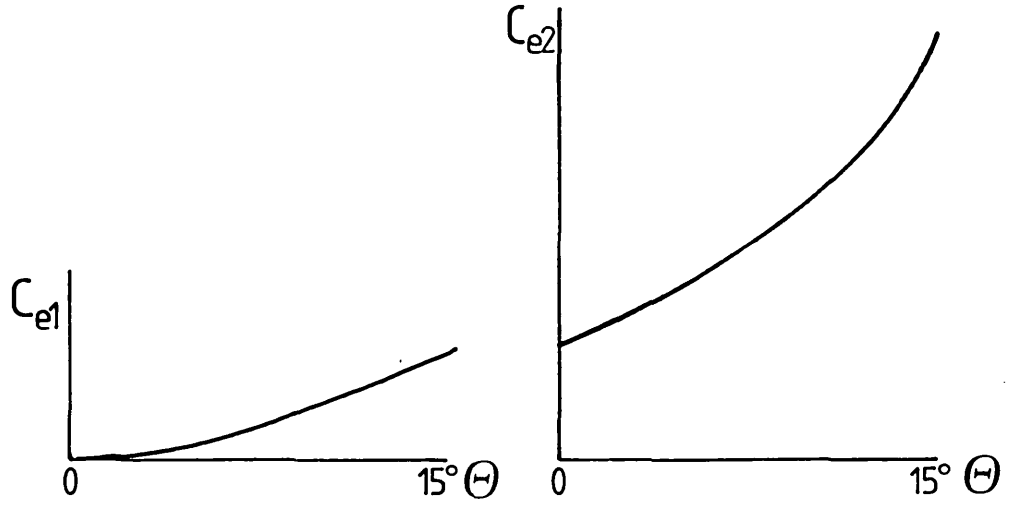
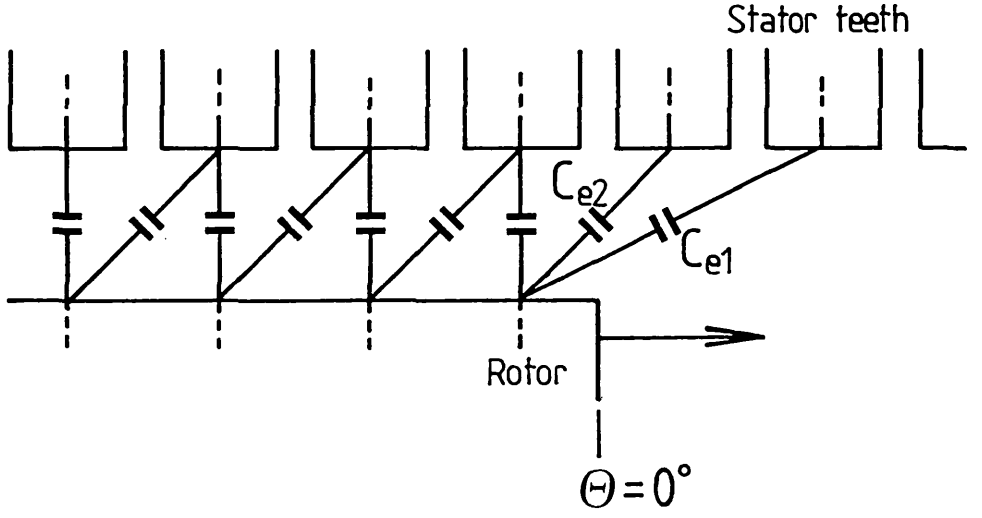


Fig.5.16(c). Stator Magnetic Current due to Motion in the Magnetic Circuit Succeeding that of Fig.5.16(b). $\Theta = 15°$.



(a) Variation of Pole Edge Capacitors with Rotor Angle.



(b) Magnetic Circuit Connection of Pole Edge Capacitors.

Fig.5.17. Pole Edge "Fringing" Capacitors.

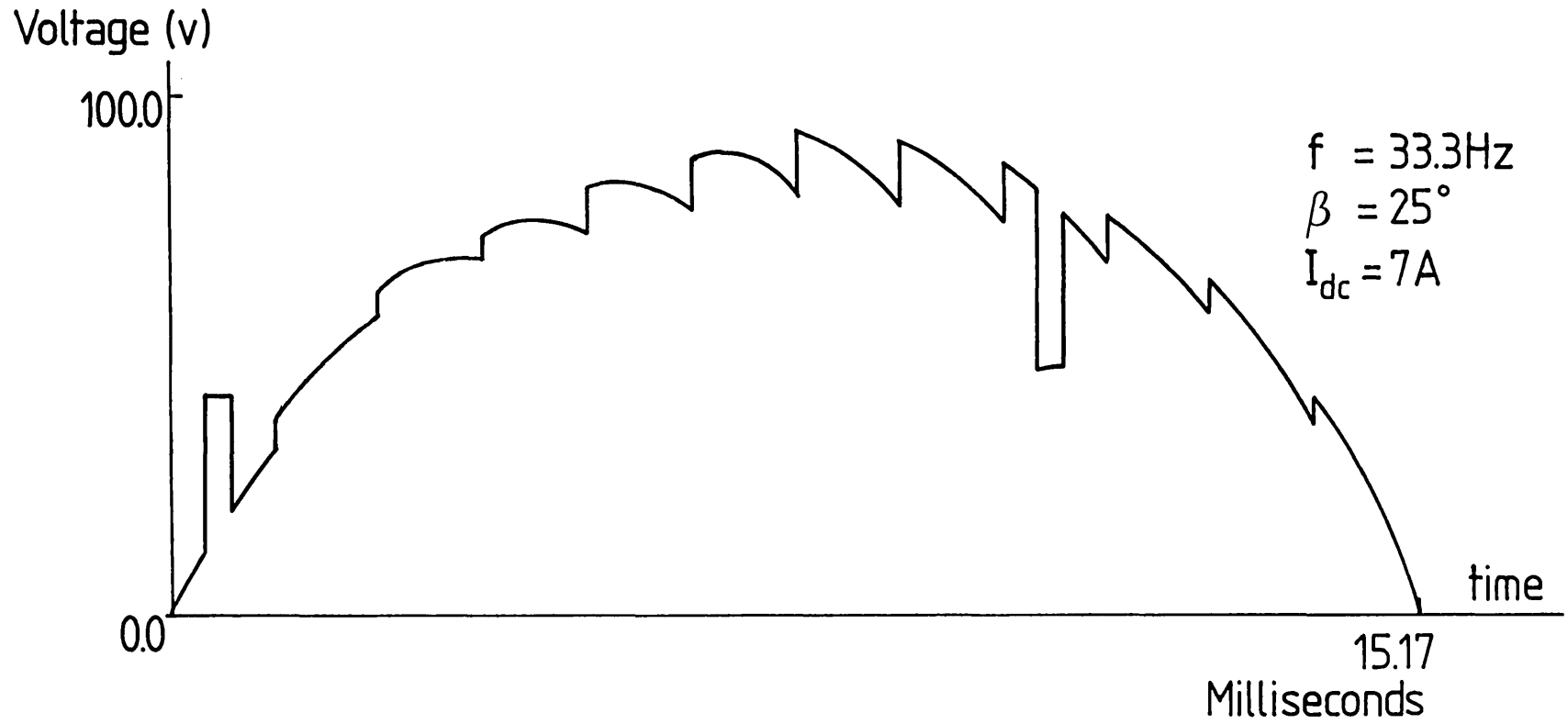


Fig.5.18. Typical Motor Phase Voltage for Variable Air Gap Permeance Model.

1. The objective is to model a continuous system as a "lumped" magnetic model. Discretization of the rotor surface into essentially a structure having a similar number of teeth as the stator will by nature accentuate slot ripple.

2. The initial, and final, gap capacitor values are zero, fig 5.14. The charge which then has to be attributed to such capacitive values becomes ambiguous ie

$$q = C.V \qquad c = 0$$

Therefore,

$$q = 0.x\,V \quad ?$$

Thus, initial capacitor current values are ambiguous. It is apparent from fig 5.16 that the current in a gap capacitor at program transition suddenly changes direction. The sudden change in the rate of change of capacitance from a positive to a negative slope causes the change in current direction, equation 5.6. Fig 5.16(a) and (b) shows the capacitors C_{jb} charging at a positive rate. After transition to the next program C_{ja}'s become C_{jb}'s so that the current effectively reverses direction suddenly. New capacitors suddenly appear that are expected to immediately carry current. Only node voltages can be set as initial conditions in S.P.I.C.E. so that initial current flows are uncertain.

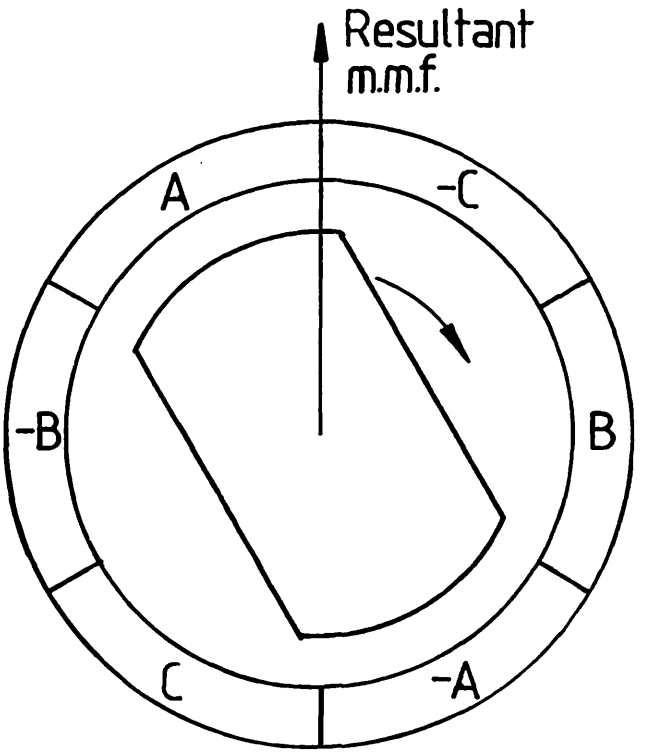
The main cause of discontinuity at program transition is put down to the effects of machine flux distortion. The slot ripple became worse for higher load currents, ie significant armature reaction.

As discussed in chapter three, section 3.5, the resultant m.m.f. and therefore flux are heavily distorted to one side of the rotor pole, as shown in fig 5.19. In magnetic circuit terms there will be a concentration of magnetic charge (q) on the gap capacitors towards the right hand side of the pole, fig 5.20. With charge mainly concentrated to one side the magnetic current will flow in a loop concentrated on the path shown in fig 5.21. Current i_m is approximately constant since the ramp functions of the main pole region capacitances dominate. This current flows for the periods from $\Theta = 0^o$ to $\Theta = 15^o$ and links the stator turns, B, C and D etc. The next 15^o of movement starts with the next program, at $\Theta = 0^o$ as in fig 5.22. However, i_m has suddenly leapt one slot forward to link stator, turns C, D and E etc. The spontaneous change of flux linkages results in waveforms of fig 5.18.

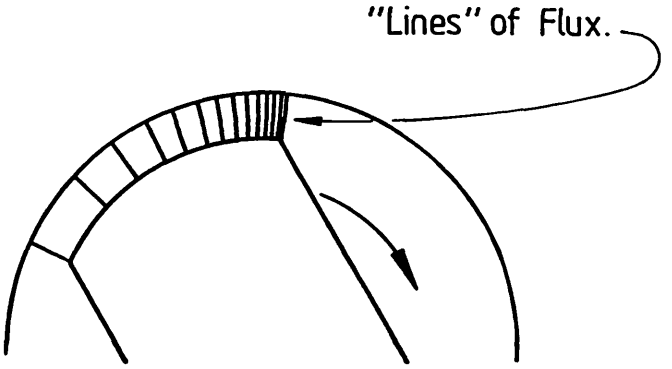
In spite of the badly distorted phase voltage waveforms the voltage magnitude and shape are correct. The link current converges to the value expected, and commutation times are of the correct order. However, the method is cumbersome, each 15^o section of movement requiring forty minutes computer processing time so that one electric cycle took sixteen hours to compute. An alternative method of modelling motion is therefore considered next.

5.4 Move the Stator Conductors

An approach is described which instead of moving the rotor with respect to a stationary stator the stator conductors are rotated around the stator core while the rotor remains static. Thus, the linkages are moved around the stator. The method is similar to that used by Turner [41] in finite element simulations of turbo-generator



(a) Resultant m.m.f. Space Phasor Corresponding to Similar Conditions of Fig. 3.5. (a).



(b) Flux Concentrates Towards Leading Pole Edge.

Fig. 5.19. Simple Motor Cross Section Showing Flux Distortion.

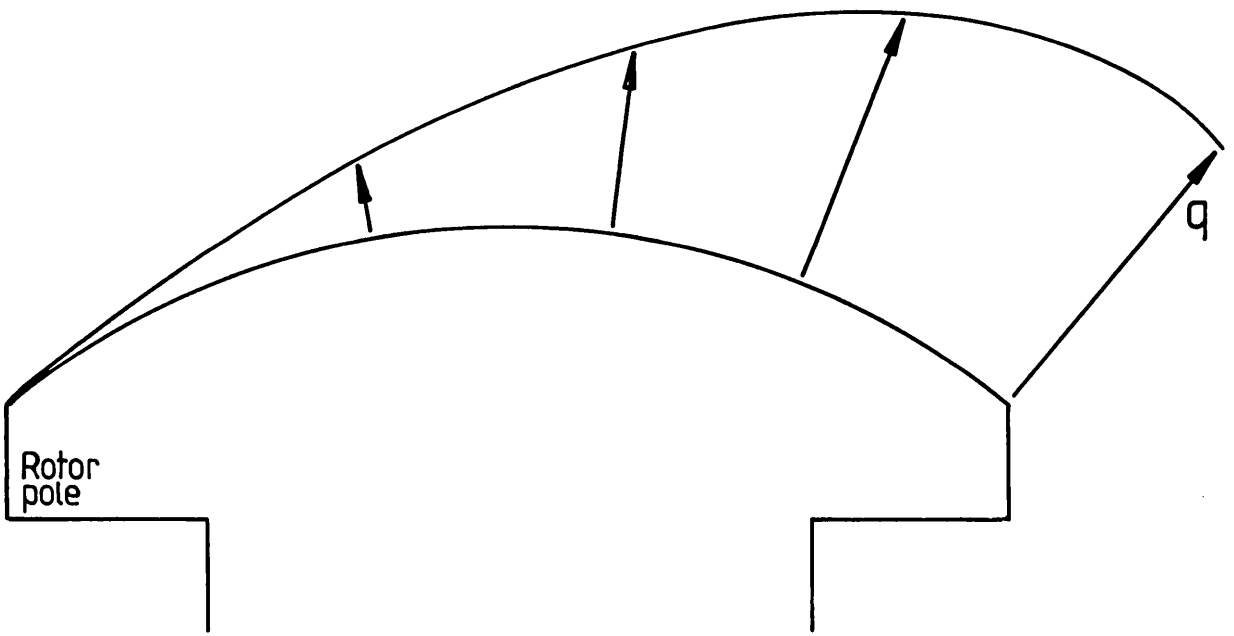


Fig.5.20. Rotor Cross Section Representing the Distribution of Air Gap Flux (Magnetic Capacitor Charge, q) When the Motor is Loaded.

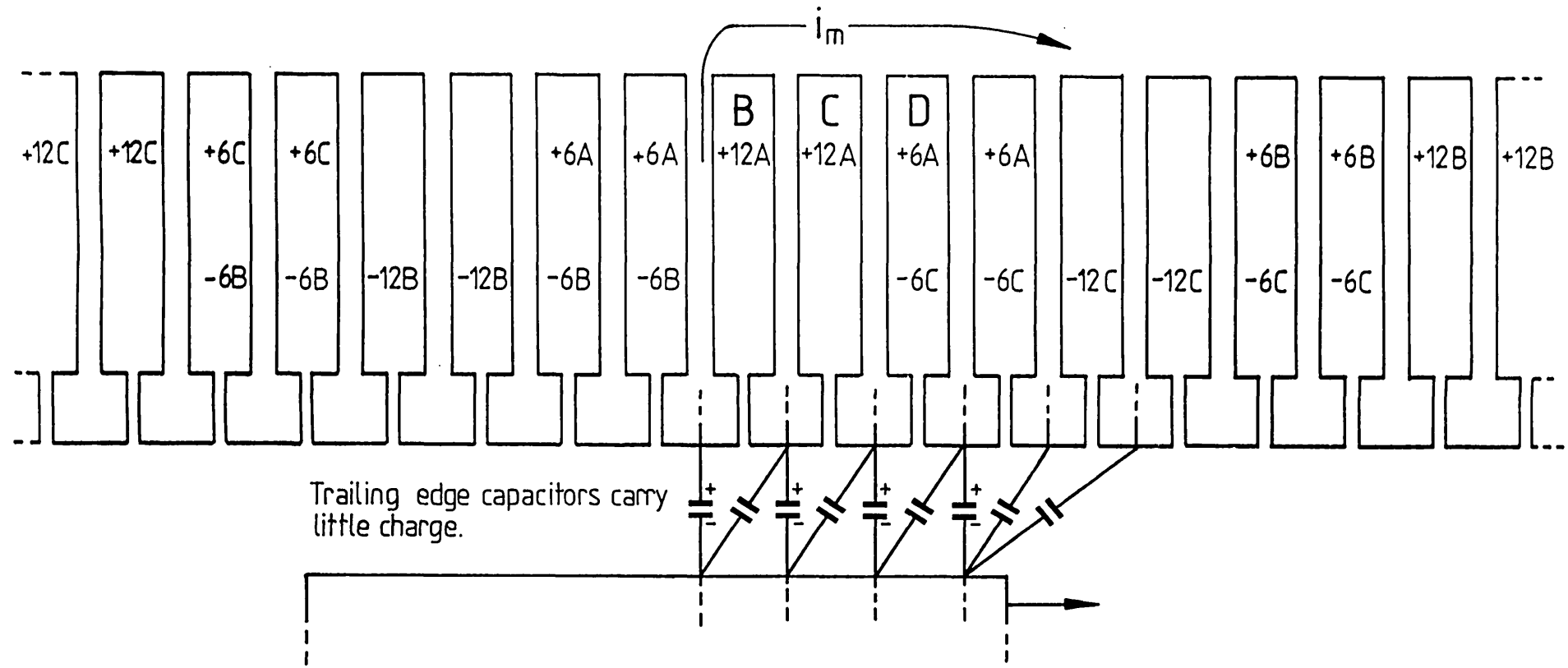


Fig.5.21. Armature Reaction Concentrates Flux and Magnetic Current Towards the Rotor's Leading Edge (corresponding to fig.5.20). $\Theta = 0°$.

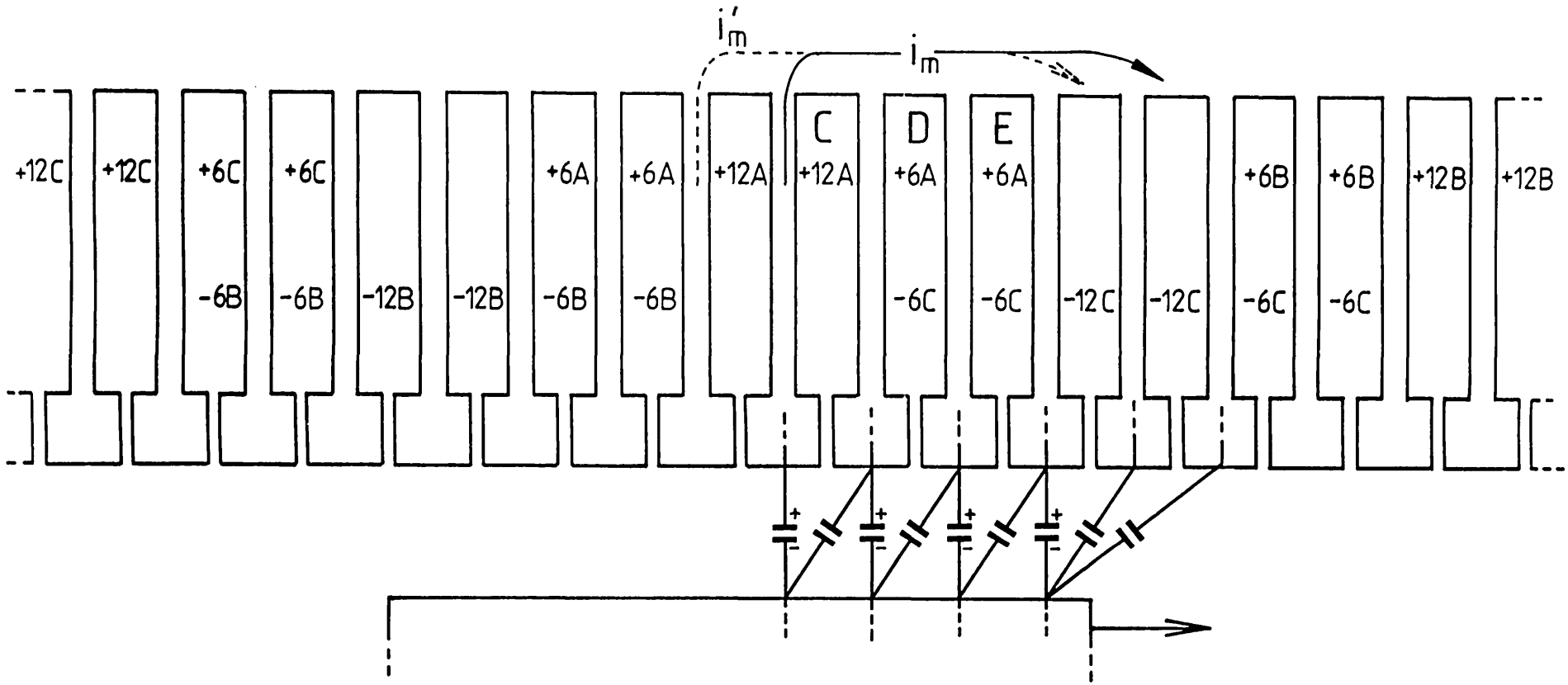


Fig.5.22. Magnetic Circuit Succeeding that of Fig.5.21 for Θ=15°. i'_m is the Magnetic Current Flowing in the Preceding Circuit of Fig.5.21.

transients.

Turner moves the stator m.m.f. pattern between each time step calculation and calculates the induced voltages at each time step from the rate of change of flux linkage. The effects of rotational and magnetic field effects are allowed for in the stator winding voltage equations. The method produces results that compare well with actual tests and the model provides a true picture of the flux and current distribution at any instant during a transient analysis. Turner also states the benefits to be gained from using such a technique over the conventional d-q axis calculations.

Chapter four shows how a motor can be represented in magnetic circuit form with stator linkages correctly represented. Nevertheless the model represents a static machine. Moving the stator conductors implies that the stator linkages must be a function of time (or rotor angle).

5.4.1 Linkages Represented as a Function of Time

If flux linkage is made to change, an e.m.f. is induced in the electric circuit as

$$e = N \cdot \frac{d\Phi}{dt}$$

The change of linkages may occur in three ways:

1) Supposing the flux constant, a coil of N turns may move through it.

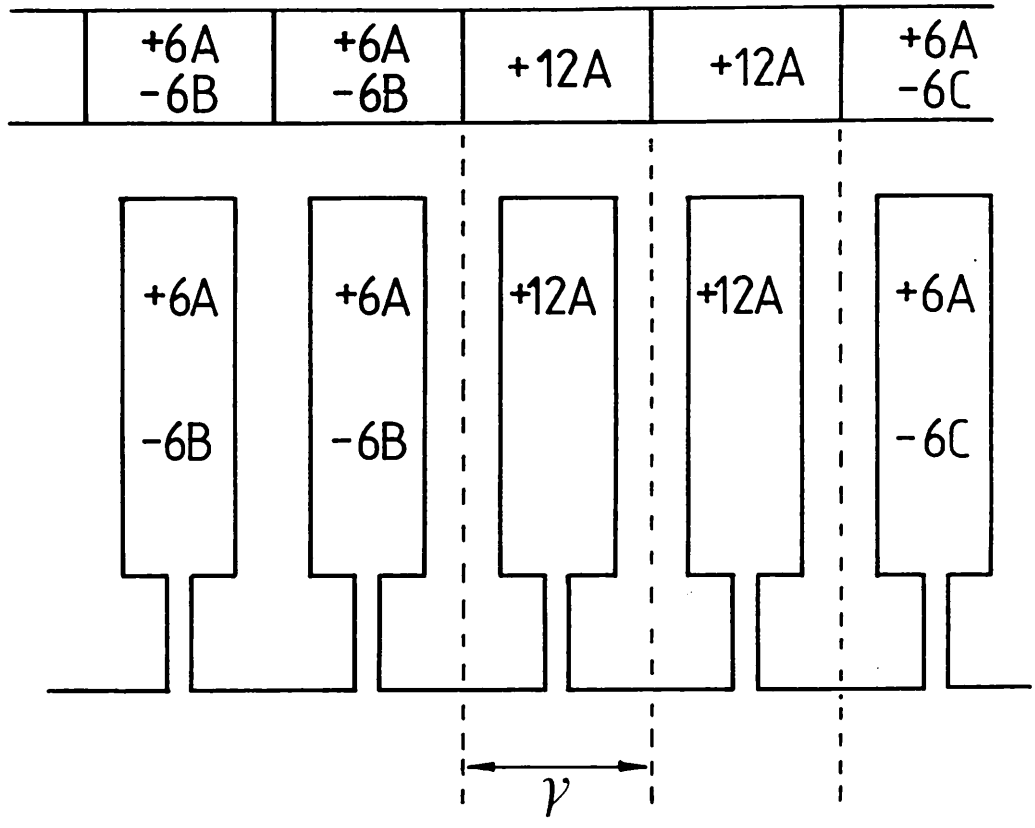
2) Supposing the coil stationary, the flux may vary in magnitude.

3) 1 and 2 may occur together. The coil may move through a time-varying flux.

(2) is already included in the circuit model as it stands. To represent the effects of (1) the stator linkages must vary as a function of time.

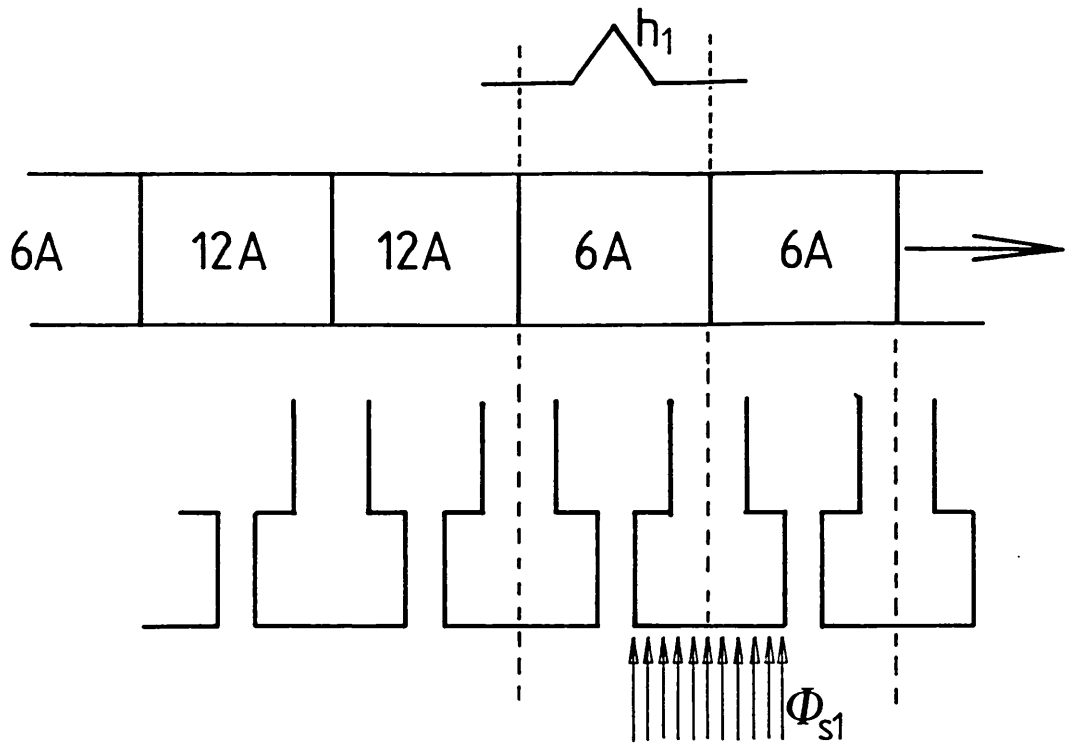
The conductors within a particular slot are assumed to span a complete slot pitch as depicted in fig 5.23. To represent the rotation of these phase bands around the stator core the linkage of each gyrator must be a function of time. Fig 5.24(a) shows the stator phase bands moving to the right through the gyrator shown. The instant shown is at $t = t_1$ and there are six turns of phase a in slot one at $t = t_1$. Moving the phase bands to the right increases the linkages of "a" and the increase is assumed to be linear so that the linkage function for slot one with phase a passing through it is as shown by fig 5.24(b). The other two phase bands must be accommodated and the complete set of linkage functions for phases a, b and c passing through linkage one are shown in fig 5.25.

Instead of a constant number of phase turns linking stator and electric circuits the turns are a function of time. The linkage functions for each slot will not be the same, they will be the same shape as in fig 5.25 except that each subsequent gyrator linkage function will be delayed by 15° from the previous one for a clockwise progression from h_1. At first sight this appears to be a large number of separate linkage functions to be represented. However, only twelve are necessary since an "extra twelve" are gained by negating the

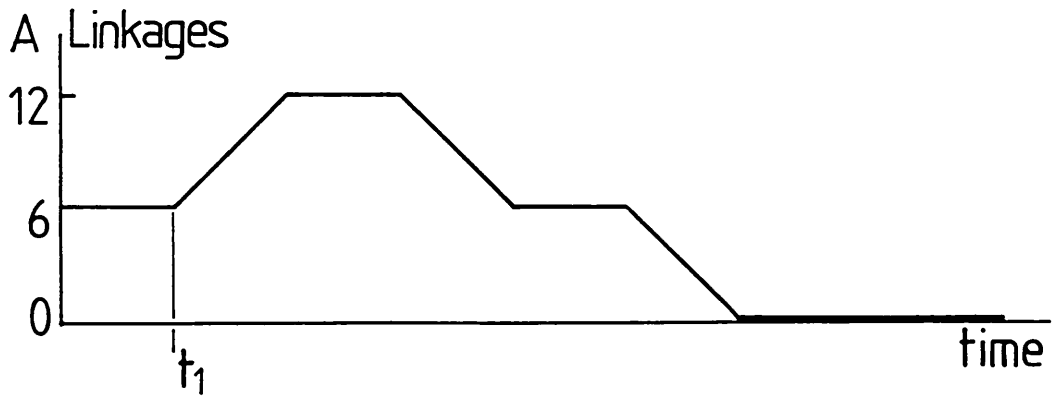


γ = slot pitch = 15° (electrical)

Fig.5.23. Stator Conductors Pulled Out of Slots and Assumed to Occupy a Complete Slot Pitch.

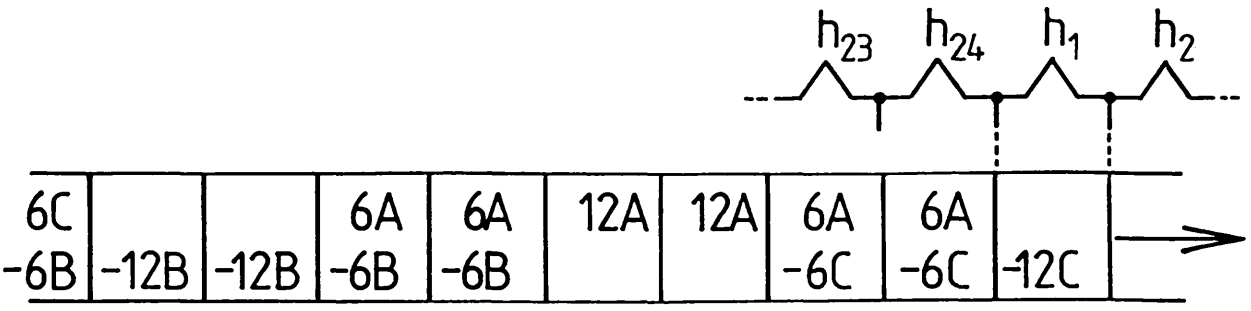


(a) Phase Band A Moving Through Slot h_1. Position Corresponds to t_1 Below.



(b) Number of Phase A Linkages at h_1 as a Function of Time.

Fig.5.24. Movement of Stator Conductors.



Stator Phase Bands Move Through h_1 so that its Linkages Vary with Time as Below.

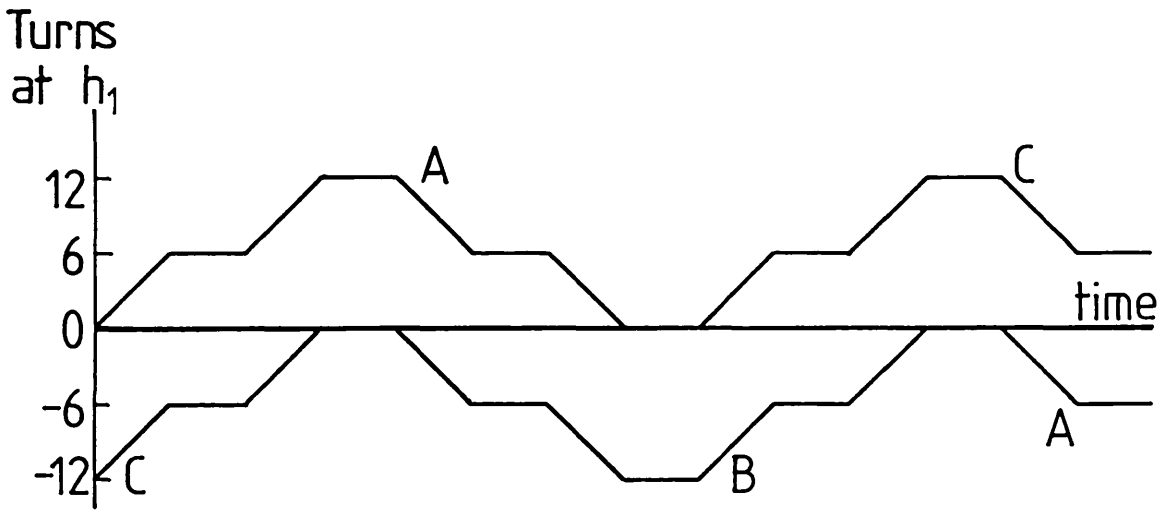


Fig.5.25. Linkage Functions Required in a Single Slot Gyrator to Represent Stator Phase Band Rotation.

twelve already defined.

5.4.2 S.P.I.C.E. Implementation of Stator Movement

A gyrator with fixed N has already been successfully modelled for a general linked electric and magnetic circuit, figs 5.26. N must be made to vary as a function of time. To do this a polynomial current controlled voltage source [37] is implemented. Fig 5.27(a) shows the linkage function of fig 5.27(b) implemented as a time varying voltage source which replaces the multiplication constant N of fig 5.26. So that

$$e = -i_m \cdot i(t)$$

and

$$f = i_e \cdot i(t)$$

This now requires the insertion of one current controlled voltage source per phase per slot and a stack of current controlled voltage sources for each electrical phase as in figs 5.28 and 5.29.

The movement of the stator windings around the core is not in itself sufficient to induce e.m.f. due to motion. It merely provides a means of aligning the stator windings to link the magnetic field and respond to changes in magnetic flux to produce e.m.f. To induce e.m.f. due to rotation the stator conductors must cut flux, in the case of the magnetic circuit analogy a magnetic current must flow in the stator core back to emulate the rate of change of flux. To calculate i_m the flux cutting rule is used as follows.

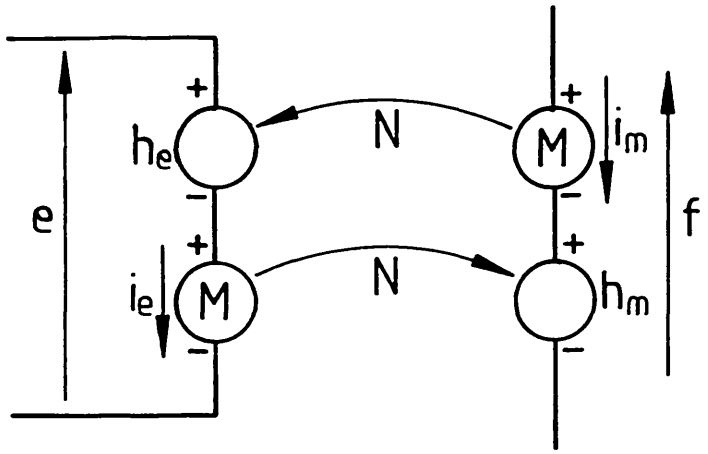
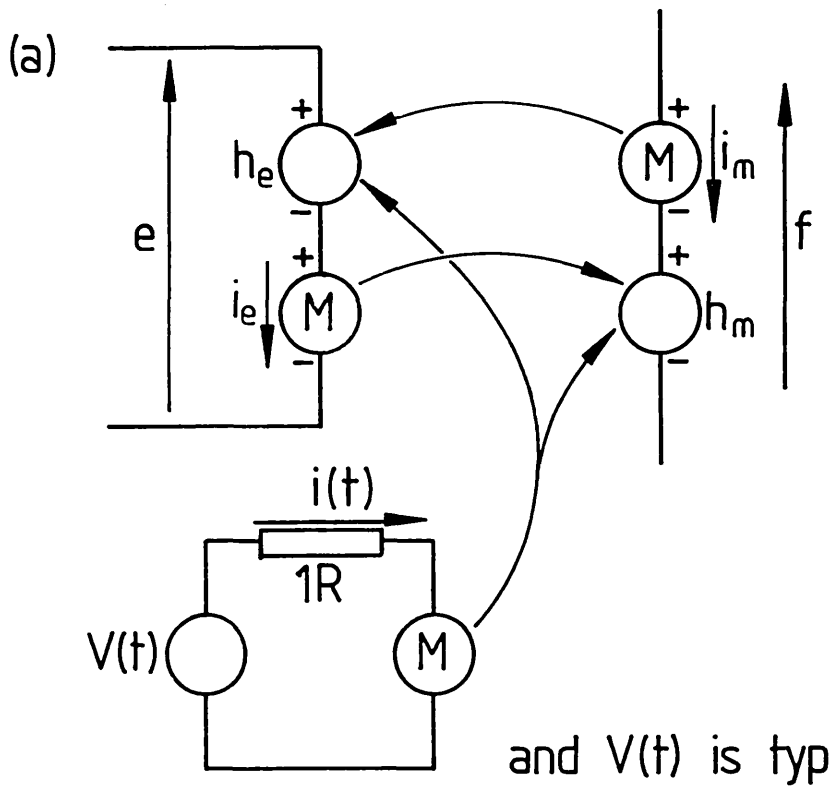


Fig.5.26. Gyrator with Constant Linkages N.



and V(t) is typically :

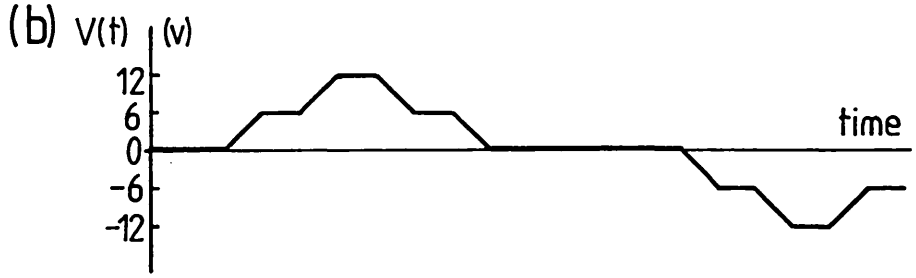


Fig.5.27. S.P.I.C.E. Implementation of Time Varying Linkages.

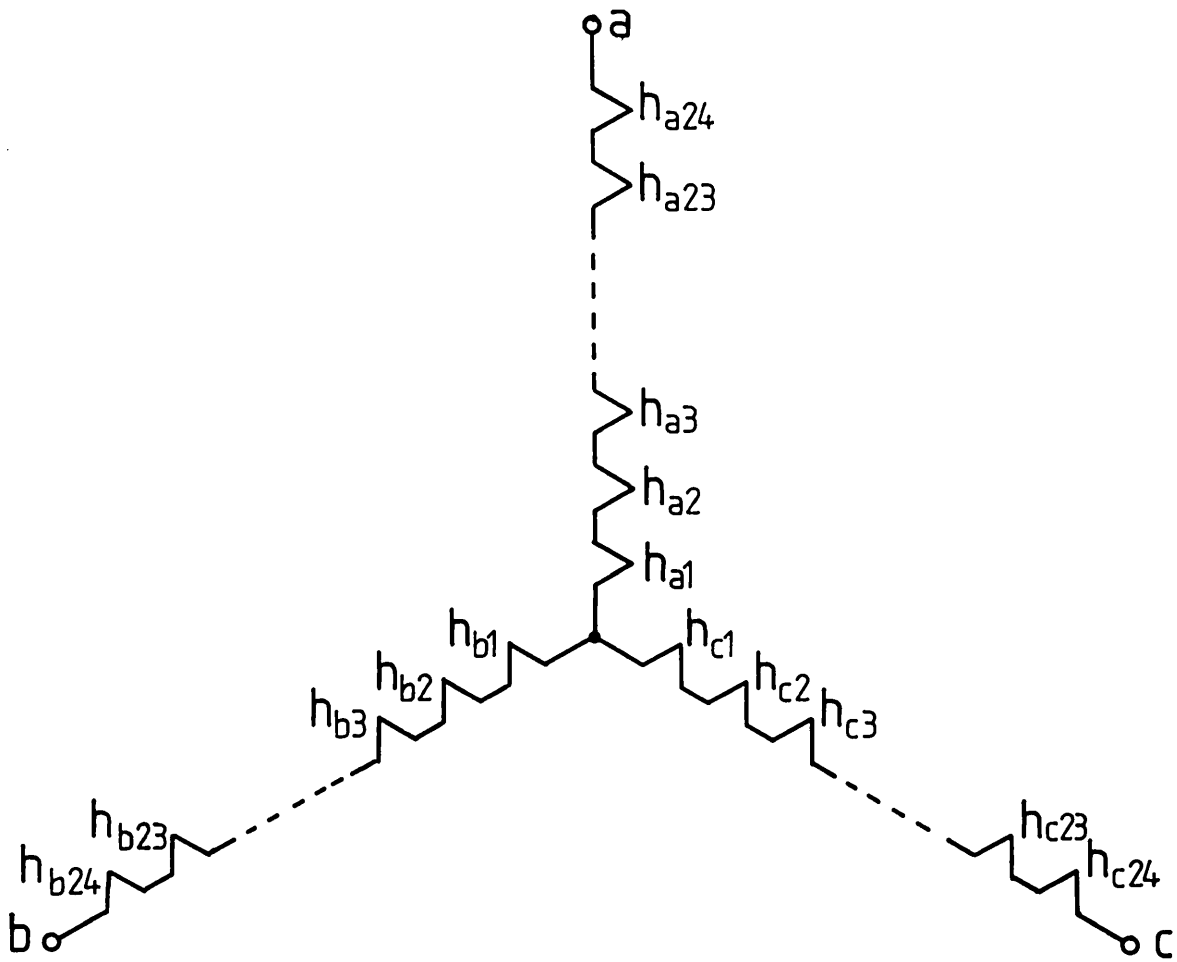


Fig.5.28. Stator Electric Windings. Gyrators Link Windings to each Stator Slot of Fig.5.29.

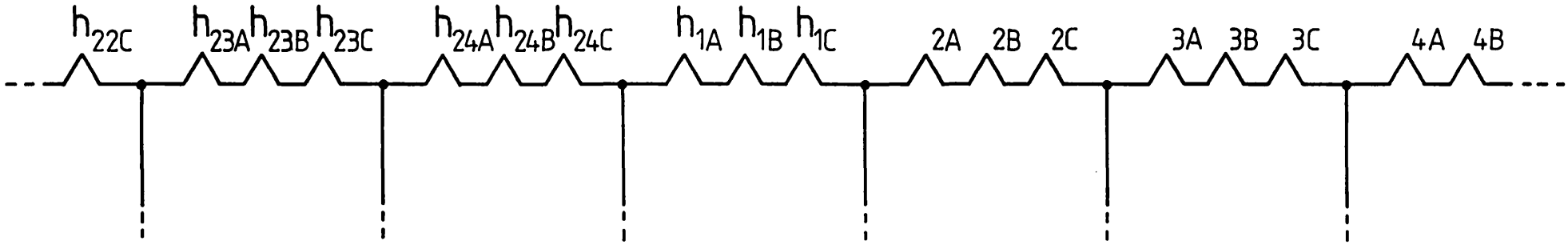


Fig.5.29. Gyrators Represent Each Phase in All Magnetic Circuit Stator Slots.

5.4.3 The Flux Cutting Rule and its Application

"The e.m.f. in a single conductor of length l calculated from the rate at which it cuts across a magnetic field of uniform density B when moving at speed u in a direction at right-angles to the direction of flux" [42] is the flux cutting rule:

$$e = Blu \qquad (5.7)$$

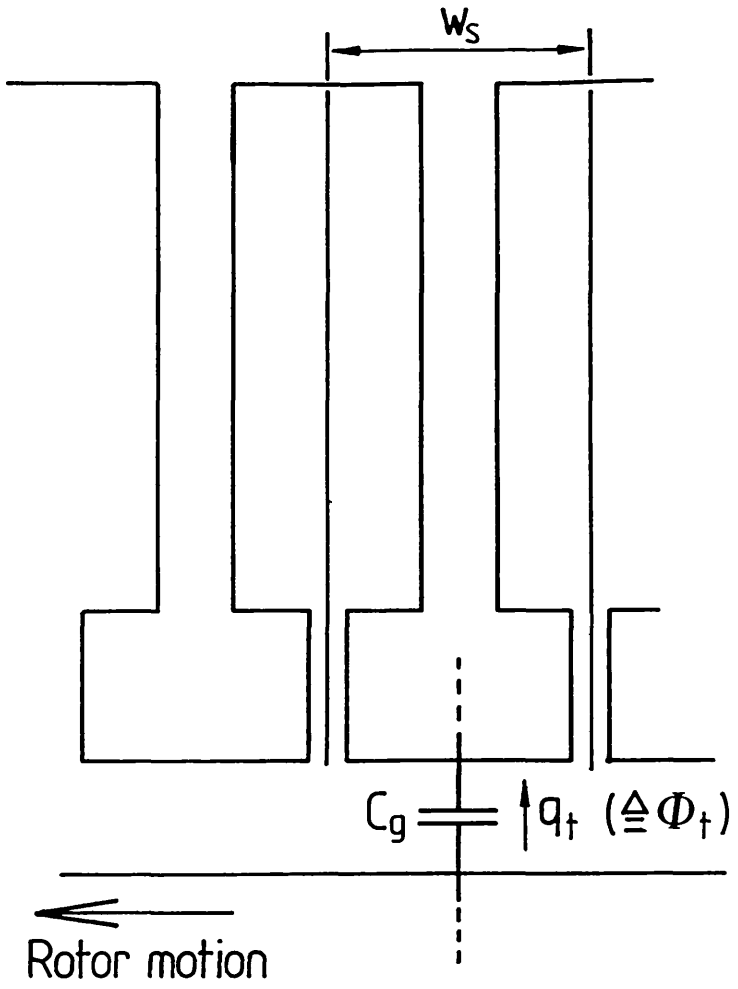
This is the motional e.m.f., always associated with the conversion of energy between the mechanical and electrical forms.

The flux cutting rule is used here to calculate the required magnetic current to induce e in each stator conductor. It is assumed that flux crosses the air gap perpendicular to the rotor and stator tooth surface and that the e.m.f. induced in a slot conductor can be calculated from the flux under the relevant tooth. Flux density is also assumed uniform under each tooth.

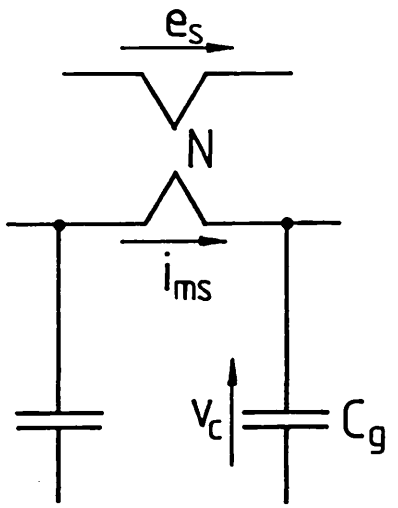
Consider a single slot and associated gap capacitor, illustrated in fig 5.30(a). Since the slots are virtually closed let the tooth width = w_s, the slot pitch. The requirement is to define e as a function of speed and charge, q_t, across each tooth air gap capacitor.

$$B = \frac{\Phi t}{w_s \cdot l_m} \qquad (5.8)$$

Where l_m = machine length.



(a)



(b)

Fig.5.30. Gap Flux of Capacitors Ahead of Each Slot is used to Calculate Rotational e.m.f..

A point on the rotor will rotate past twenty four slots per electric cycle or

$$24.w_s.f \quad (m/cycle)$$

For a frequency of f(Hz) the velocity can be expressed as

$$u = 24.w_s.f \quad (m/s) \tag{5.9}$$

e can now be written in terms of speed and flux by combining equation 5.8 and 5.9,

$$e = \frac{\Phi t}{w_s.l_m} .l_m.f.24.w_s$$

$$= \Phi_s.f.24 \quad (volts/conductor)$$

For N conductors in a slot

$$e_s = N.\Phi_s.f.24 \tag{5.10}$$

To express e_s as an analagous magnetic current; For N conductors in a slot

$$e_s = N \frac{d\Phi_s}{dt} = N.i_{ms} \tag{5.11}$$

Equating 5.10 and 5.11

$$N.i_{ms} = N.\Phi_s.f.24$$

so

$$i_{ms} = \Phi_s . f . 24$$

$$\Phi_s \triangleq q_s ,$$

and

$$q_s = C_g \, v_c$$

Where v_c is the voltage across C_g, so that

$$i_{ms} = C_g . v_c . f . 24 \qquad (5.12)$$

i_{ms} is the magnetic current required to flow in the slot linkage h1 to induce the voltage e_s through N turns as shown by fig 5.30(b).

The rotational and the transformer effects are now included in the circuit model.

Fig 5.30 depicts the rotor moving from right to left. This is the same as moving the stator conductors from left to right, fig 5.31. At h_1 the linkages, or turns, start to cross over into the region w_s and begin "cutting" the flux q_1 across C_1. Therefore, the charge on C_1 is assigned to the linkage h1 in determining the magnetic current to flow in h1 as a result of the Blu rule. That is, voltage in each slot is generated from the conductors of that slot cutting the flux across the capacitor in front of the conductors. So the voltage across C_1 is used in equation 5.12 to calculate the magnetic current to flow in h1 to generate e due to motion.

The direction, or polarity, of the magnetic currents in each slot is yet to be defined for a particular direction of rotation and field polarity. Some basic polarity rules are therefore defined.

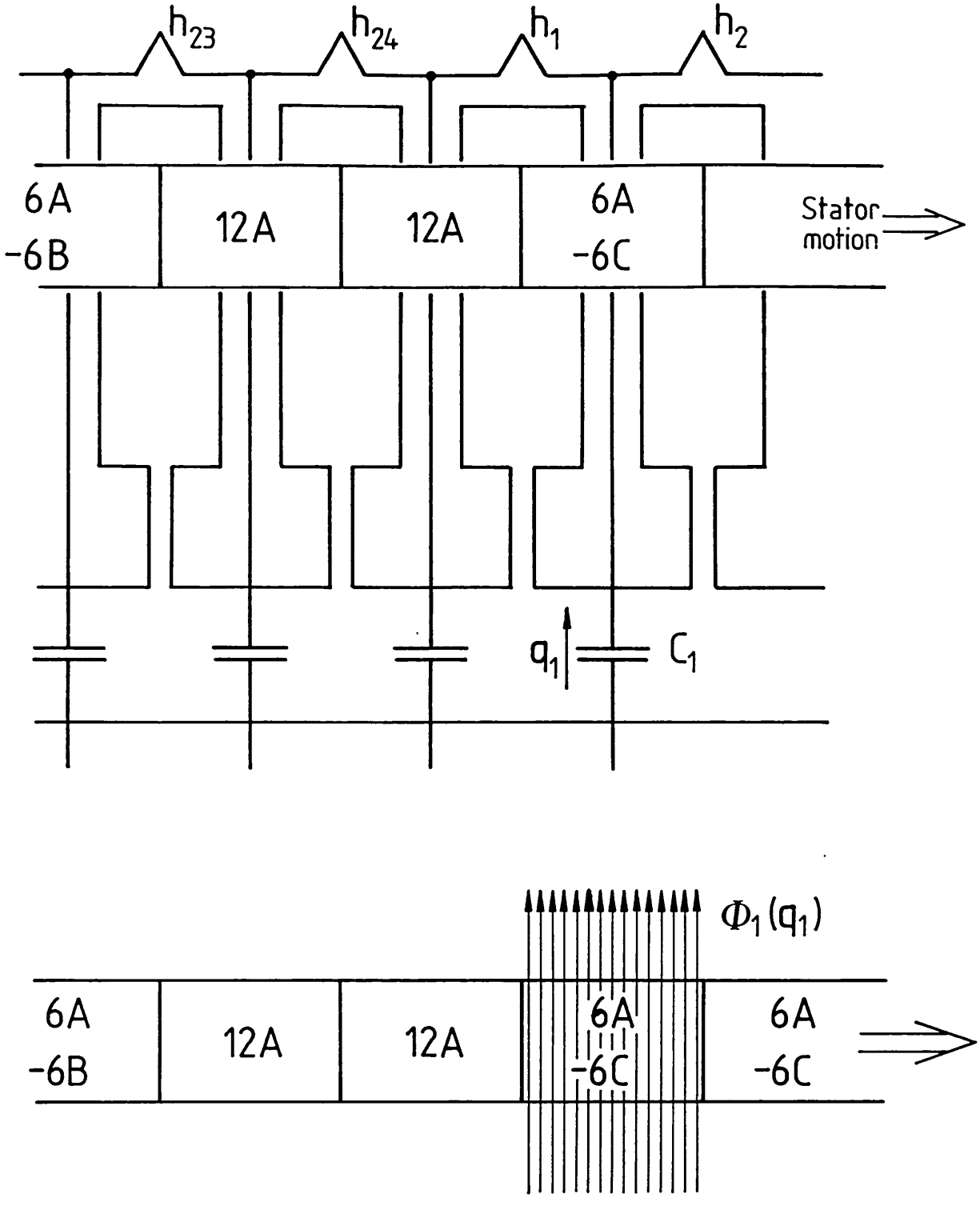


Fig.5.31. Stator Conductors Move Through Slots and Cut the Flux (Charge) Across "Leading" Air Gap Permeances (Capacitors).

5.4.4 Polarity of Rotational e.m.f.

Consider a general machine, fig 5.32, rotating at a constant speed, stator terminals open circuit, constant field voltage and infinitely permeable rotor and stator iron. The rotor rotates anti-clockwise. The machine's cross-section can be represented as the magnetic circuit of fig 5.33. Assuming the field sets up a magnetic voltage polarity, as shown, then each gap capacitor will assume a polarity as shown. Now, referring back to the idea of the gap permeance varying with rotor angle, section 5.3, the permeance (capacitance) C_1 connecting tooth two to the top left corner of the rotor is increasing in value and therefore accumulating charge. To accumulate charge C_1 must have a current i_m flowing into it. A corresponding equal current flows out of a capacitor on the right hand side of the top pole. The stator core current therefore flows as depicted.

More simply, the constant air gap flux is moving as a whole with the rotor in an anti-clockwise direction. Since flux is equivalent to magnetic charge, then the air gap charge moves in an anti-clockwise direction. To shift air gap charge of polarity shown then the current i_m depicted must flow.

To produce i_m current generators are connected across the slots with the polarity shown. The current generators derive the current from equation 5.12 and leading gap capacitors. The generators are an open circuit to all other circuit influences and the short circuit of the stator core means that i_m flows only through the stator core, all other paths having a relatively high impedance.

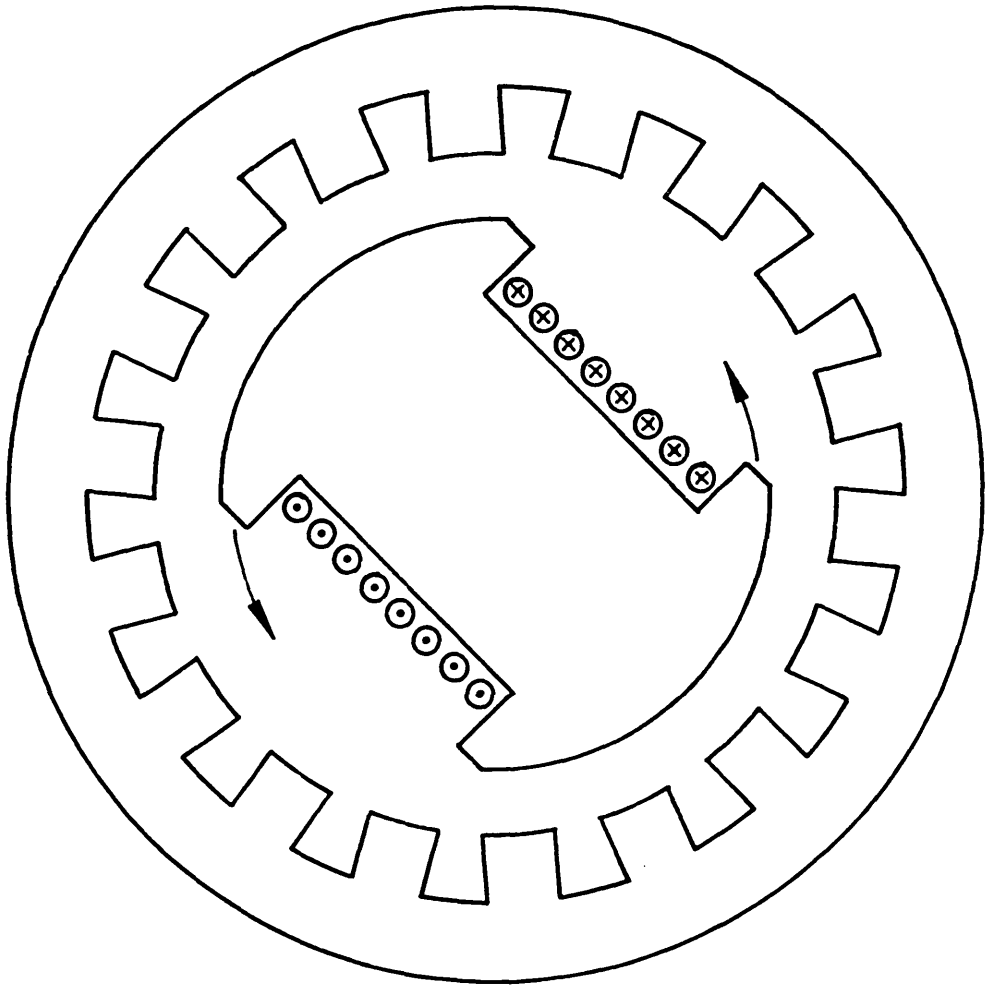


Fig.5.32. Simple Solid Salient Rotor Synchronous Machine Cross Section.

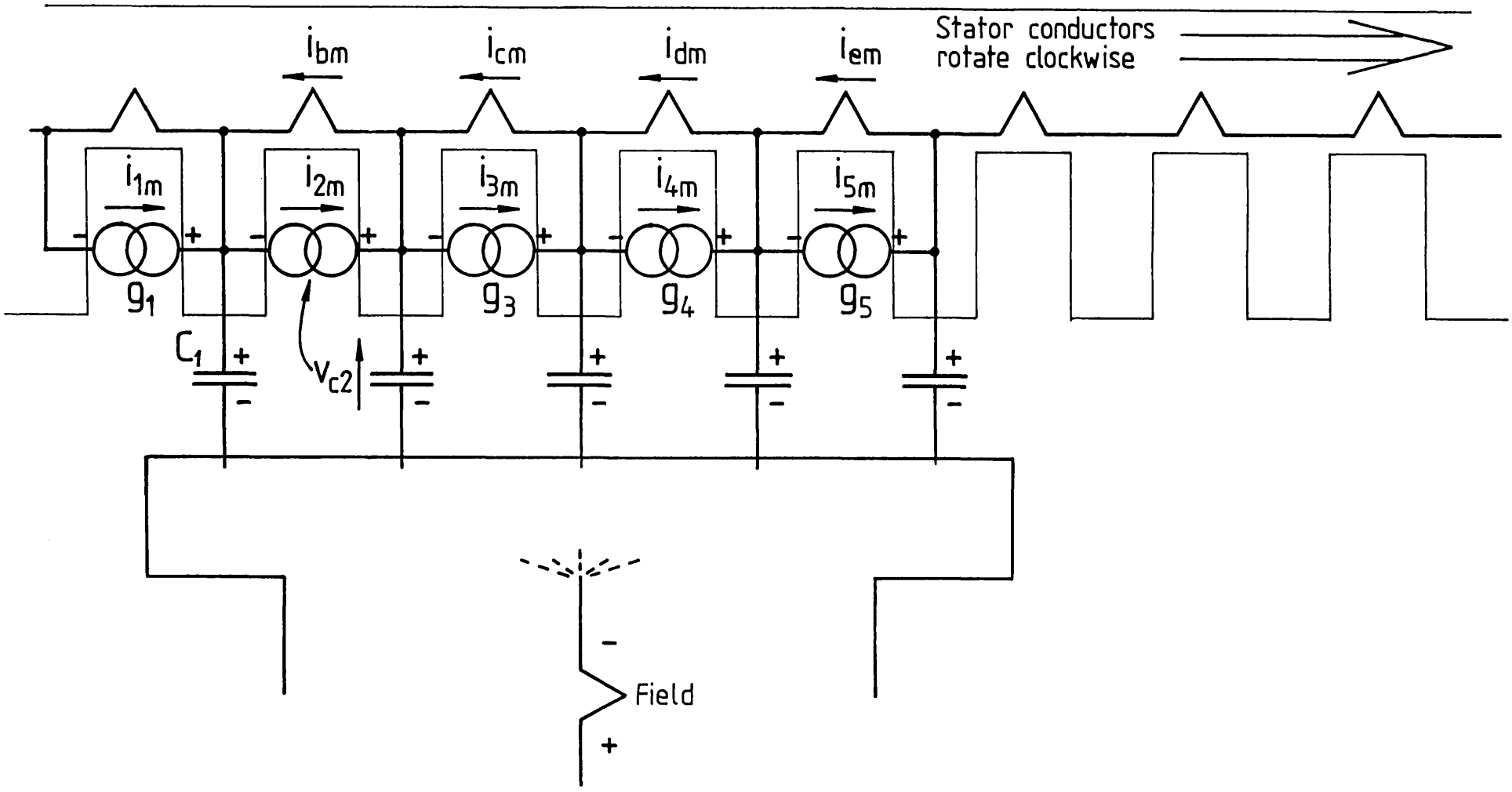


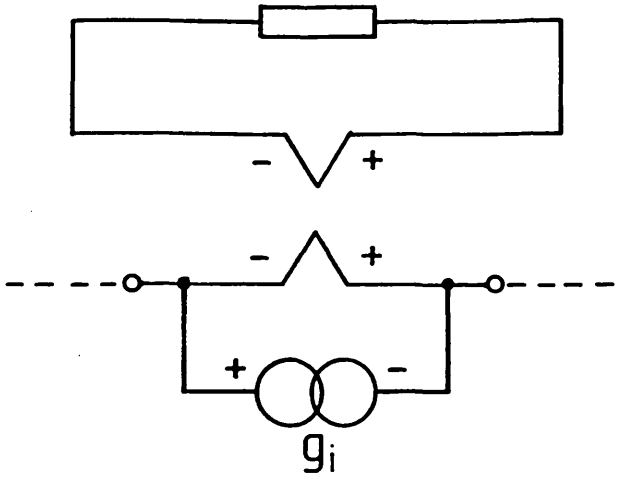
Fig.5.33. One Pole Pitch of Magnetic Circuit of Fig.5.32. Voltage Controlled Current Sources (g) Implement B.l.u. Rule.

An alternative to using the magnetic current generators is to refer the current generators through to the electric circuit, ie implement the Blu rule directly. Referring a parallel current generator [6] through a linkage is shown in fig 5.34. The result is a series voltage source appearing in the electric circuit with the polarity shown. This has to be done for all three phases. Each of these voltage sources must also be multiplied by the instantaneous number of turns (ie the linkage functions fig 5.25). Thus, resulting in twelve sources per phase, twelve more elements than the current generator method plus the complication of multiplying each voltage source with the relevant linkage function, for the laboratory motor.

5.4.5 Setting Up the Initial Field Pattern

It is necessary to set up the initial field pattern before transient solutions can take place. To allow for the long time constant of the machine reactance the field is energized with stator terminals open circuit. The motor is stationary during this time with fixed linkage terms and no generation of magnetic currents to set up rotational e.m.f.. The final node voltages of the static program were then inserted as initial conditions for loaded machine simulations with the inverter connected.

There are over one hundred final voltage values to be transferred from the static program to the actual synchro-inverter system simulation. The output file format is of a different form to that of the initial condition format. A "C" [43] program has been written to remove voltage values from output files and insert these values into the corresponding node initial conditions of a S.P.I.C.E. input file. The "C" program is able to cope with an unspecified number of node voltage



Referring Rotational Magnetic Current Source into Electric Circuit:

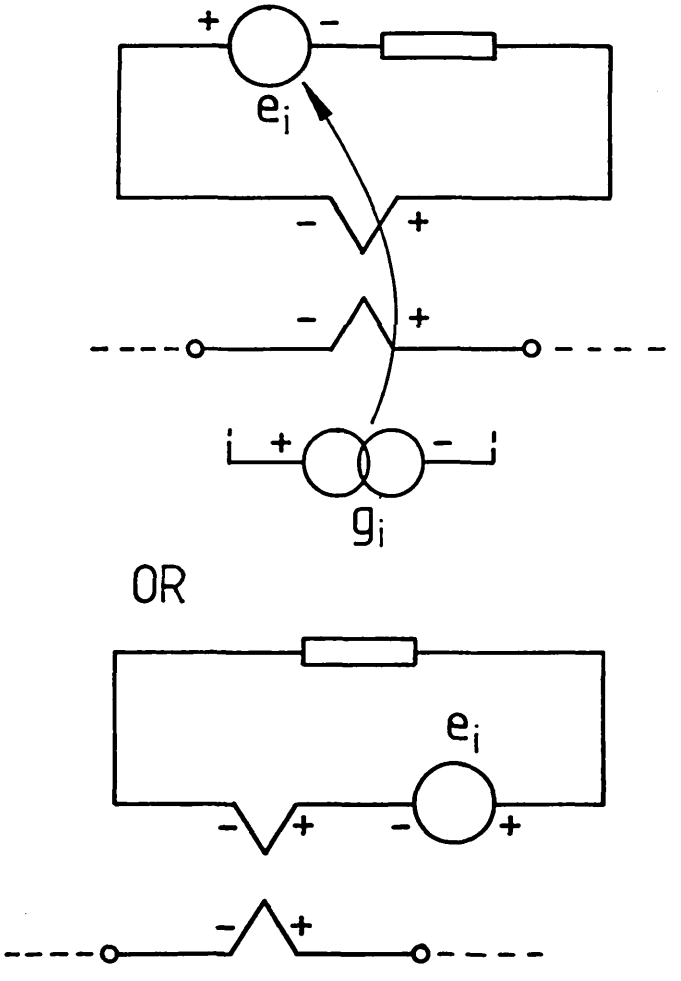


Fig.5.34. Rotational e.m.f. Represented Directly in the Electric Circuit.

substitutions. This flexibility does not require the S.P.I.C.E. files to be of a fixed format or continuous updating to allow for magnetic circuit changes.

The S.P.I.C.E. programs were ran on a "Digital Microvax" computer running on the UNIX system. UNIX's command structure is written in "C" so that the use of "C" for character manipulation and program initialization is relatively straight forward.

5.5 Conclusions

Techniques for representing motion in a magnetic circuit model and the generation of e.m.f. due to motion have been discussed.

The first method implements a gap permeance which varies as a function of time. The method has been used to great success by at least two authors [38,39,40]. The nature of S.P.I.C.E. though is not conducive to the representation of capacitors as a function of time. S.P.I.C.E. was originally developed as an integrated circuit analysis package and not as a magnetic circuit solver. The topologies and requirements of magnetic circuits and integrated circuits are very different. In spite of the difficulties encountered in using S.P.I.C.E. to solve the "varying air gap capacitor" simulations reasonable results were obtained. However, the slot ripple caused on voltage waveforms created errors in commutation time when a program transition occurred in the middle of commutation and the ripple on the line-to-line voltage gave rise to errors in commutation times (since commutation is dependent on the available line-to-line voltage, equation 3.1). Also the cumbersome nature of solution led to the abandonment of this technique.

The second method of representing motion uses a technique similar to Turner [41], where the rotor and stator core are stationary and the stator phase bands rotate around the stator core. Modelling motion in this way allowed the rotation of the motor for indefinite periods whereas the first method was restricted to solving 15° sections of rotor angle at a time. The generation of e.m.f. due to motion requires the application of the "Blu rule" and its application is shown to be straight forward. The technique yields results comparable to laboratory tests, as is shown in chapter six.

The representation of motion enables the full inverter circuit to be connected, the link inductance and a representation of the rectifier. Solution times for a full machine and inverter systems having 661 elements and 418 nodes were between three to four hours for two electrical cycles depending on circuit parameters, time step length, and length of run.

Before dynamic simulation could take place the field pattern had to be set and allowed to settle for a particular field excitation level. The "C" programming language's flexibility lent itself to the character manipulation necessary to set initial conditions in an input file from the data of an output file.

CHAPTER SIX

SIMULATION OF THE SYNCHRO-INVERTER SYSTEM AND A COMPARISON WITH CONVENTIONAL CALCULATIONS

6.1 Introduction

Previous chapters have outlined the basic operation and construction of a laboratory syncho-inverter system. Also, the necessity for calculating commutation time for performance analysis and the development of a syncho-inverter computer model has been discussed. In this chapter conventional methods of calculating overlap angle are compared with actual overlap times. Actual and computed frequency response tests are compared and the validity of choosing machine reactances from these tests is assessed. It is shown how static step response tests on a magnetic circuit model allowing for rotor eddy currents, improves upon the conventional calculation of overlap time.

A linked electric/magnetic model of the complete synchro-inverter system is used to compute waveforms for comparison with actual waveforms obtained from the laboratory test rig. The model allows for motion and the generation of machine back e.m.f.s. Calculations are compared with a number of system operating points to check the validity of the computer model.

6.2 Static Frequency Response Analyses

The experimental set up for the standstill frequency response test is detailed in chapter two. The measured frequency plots for the machine

are shown in figs 6.1 and 6.2 and compared with computed results using a S.P.I.C.E. model. By adjusting the linkage factors of the static computer model of fig 4.17, the stator and rotor axes could be aligned as appropriate for the d and q axis tests. The connection of the computer model is the same as the actual test rig and the "a.c. card" [37] in S.P.I.C.E. was used to perform the frequency analysis. Solution time for a.c. analysis of the magnetic circuit took about thirteen minutes.

Both the measured and calculated curves exhibit the typical characteristics of such frequency responses although there are substantial differences between them. The measurement of the small phase angles at low frequency was of uncertain accuracy. Although the computer model is a coarse representation of the actual machine circuit with discretized eddy current paths and permeances, values of inductance calculated from machine operation using equation 3.1 gave values closer to the high frequency computed $L(\omega)$ then the measured $L(\omega)$.

6.3 Calculation of Commutation Time, using an Operational Inductance

At low frequencies $L(\omega)$ tends to the steady state machine inductance and at high frequencies $L(\omega)$ approximates to the machine's subtransient inductance. Values of μ are calculated using equation 3.1 taking the commutation reactance to be the average of $L_d(\omega)$ and $L_q(\omega)$ from the frequency response curves (for f = 1kHz). The calculated values are then compared with overlap angles measured directly from the laboratory system.

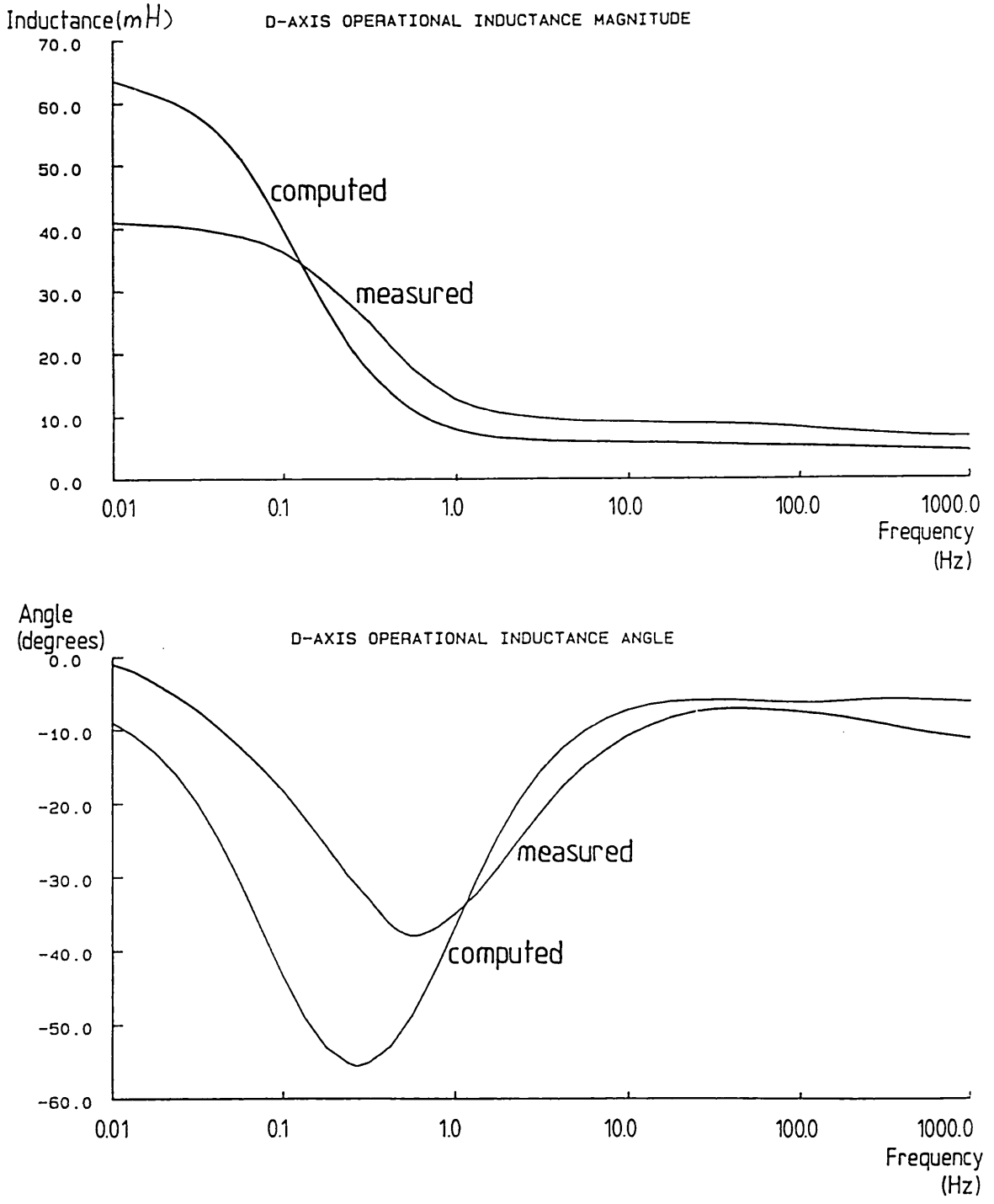


Fig.6.1. Computed and Measured D-Axis Static Frequency Response Curves.

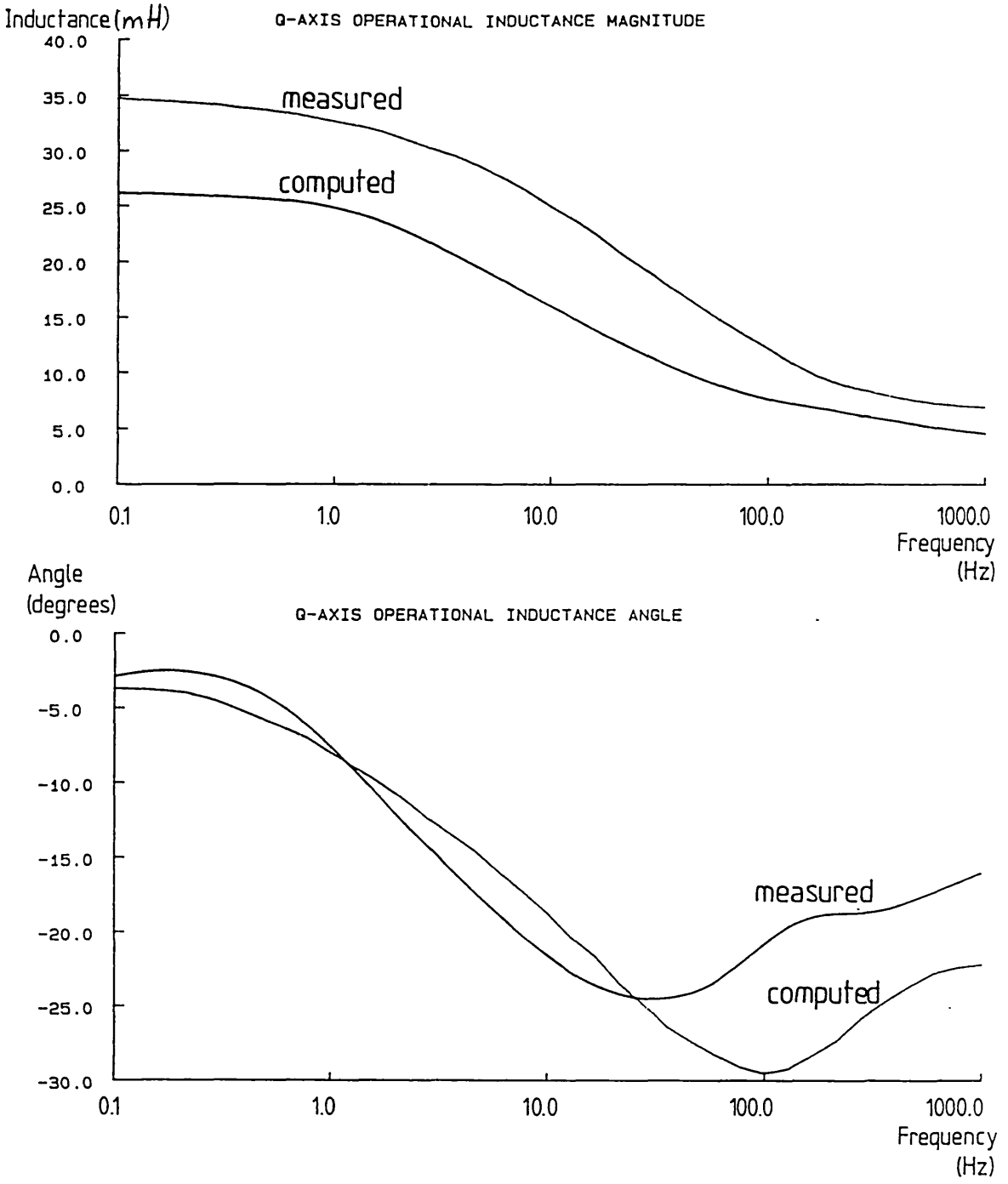


Fig.6.2. Computed and Measured Q-Axis Static Frequency Response Curves.

Preliminary tests were performed on a synchro-inverter system incorporating a motor having a laminated rotor with a discrete damper cage. The aim was to check the conventional means of calculating overlap angle and also to test the inverter and associated control electronics. The machine was a Mawdsley's Microalternator of similar rating to the solid rotor machine although the laminated machine had one more slot per pole than the solid machine's stator.

The difference between the variation of μ for a laminated and solid rotor machine is shown in fig 6.3. The laminated rotor curve has an almost linear variation compared to the solid rotor curve. It is apparent that commutating reactance in the solid rotor machine is increasing with commutation time due to the penetration of flux into the solid rotor.

Calculating the corresponding curves using equation 3.1 and the subtransient inductance values measured from the frequency response tests yields commutation angle as shown in fig 6.4. For the laminated rotor this calculated x_c value gives μ very close to the measured curve. However, the actual measured variation of x_c with commutation time is manifest for the measured μ for the solid rotor. The variation of x_c is even more pronounced in fig 6.5 where the firing angle is reduced to 30^o. The calculated curves are virtually linear, and do not allow for increase in x_c.

It has been suggested that a multiple of the machine frequency (6 or 12) can be used to find a value of commutating inductance from frequency response curves [16]. Actual frequency response curves are used to find L_c (6ω) and $L_c(12\omega)$ taking the average of direct and quadrature axis values. The results are shown for $\beta = 40^o$ in fig 6.6.

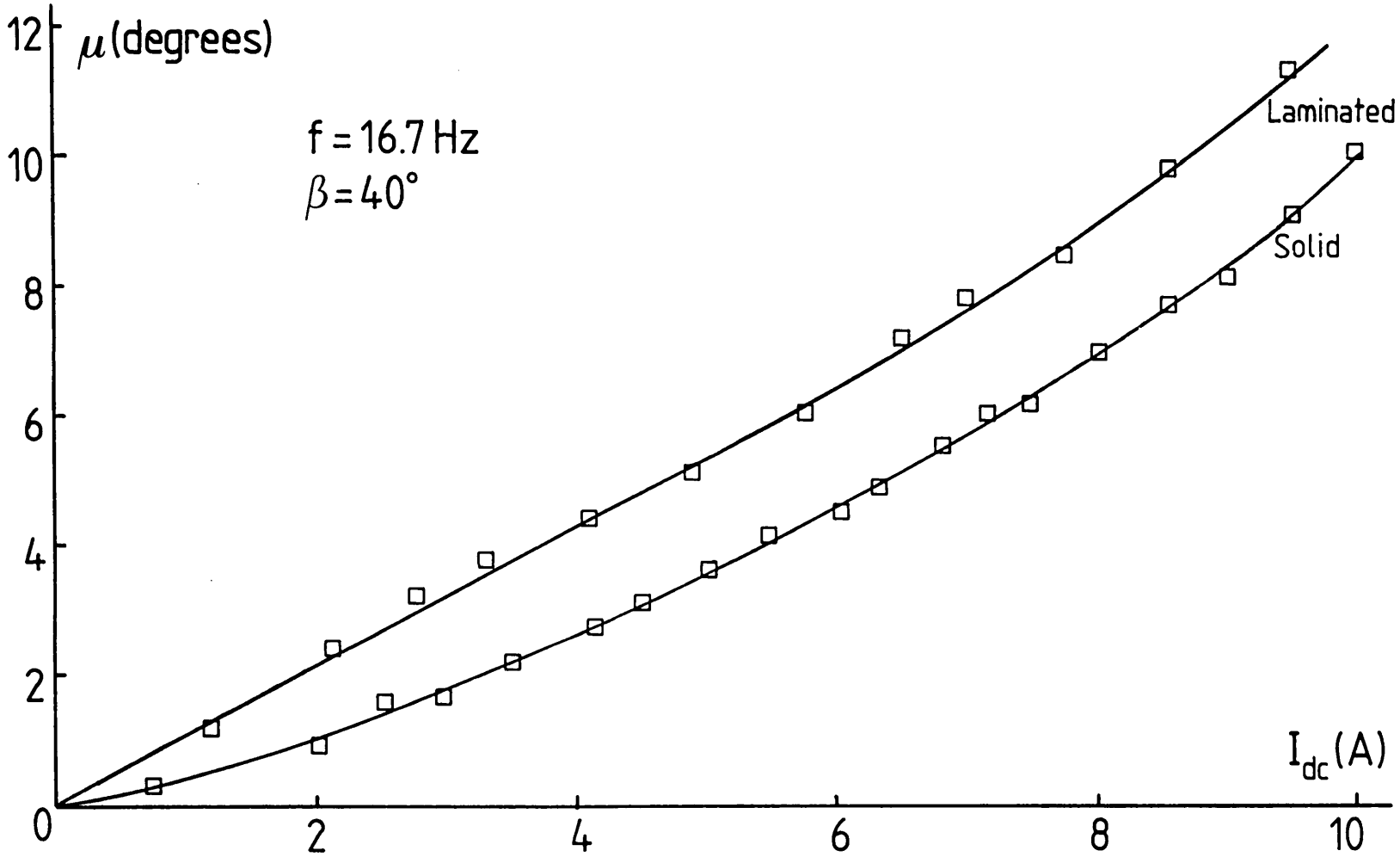


Fig.6.3. Measured Commutation Time vs. Link Current for Solid and Laminated Rotor Machines.

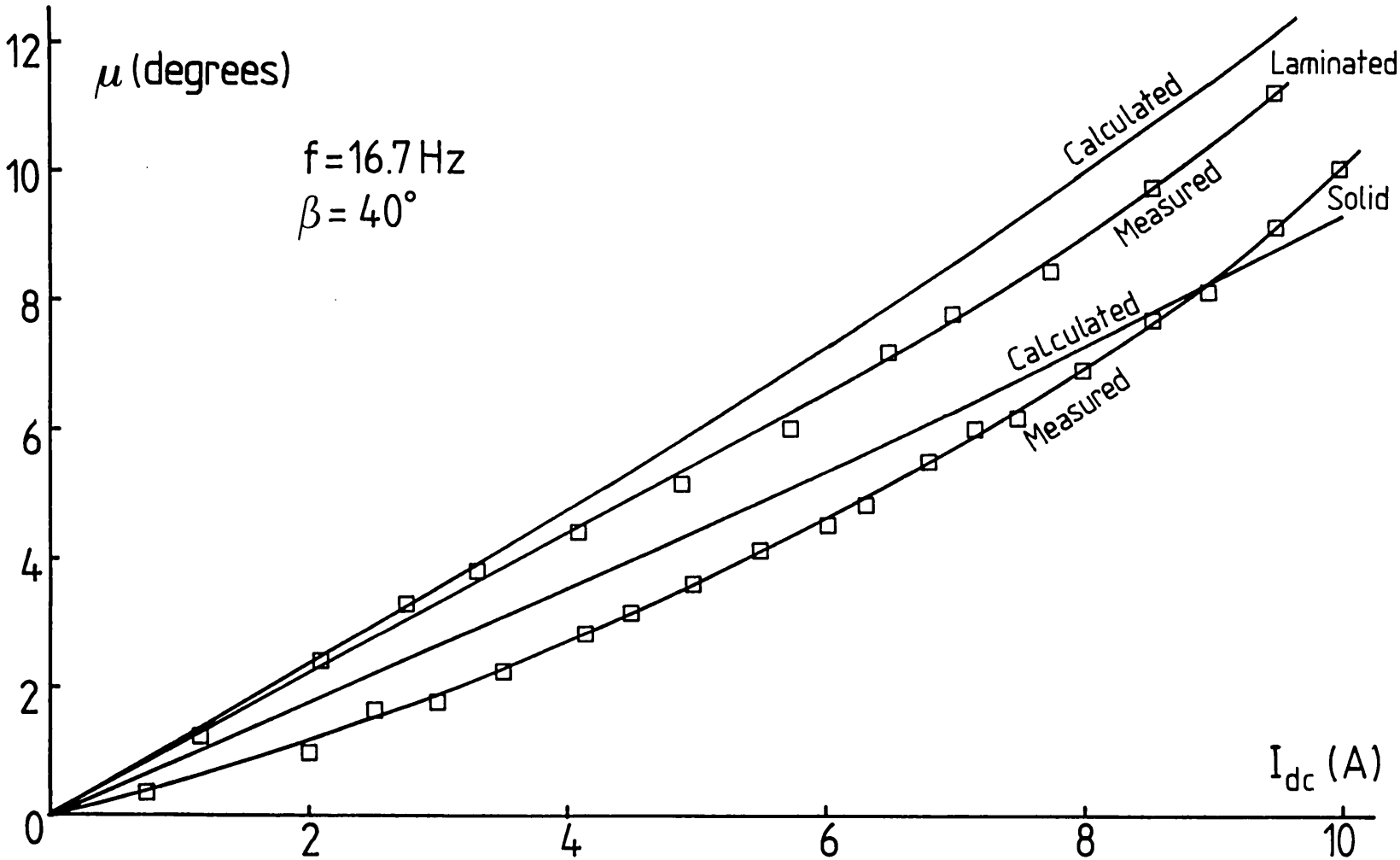


Fig.6.4. Commutation Time vs. Link Current. Calculated Curves use the Average of the Subtransient Reactances.

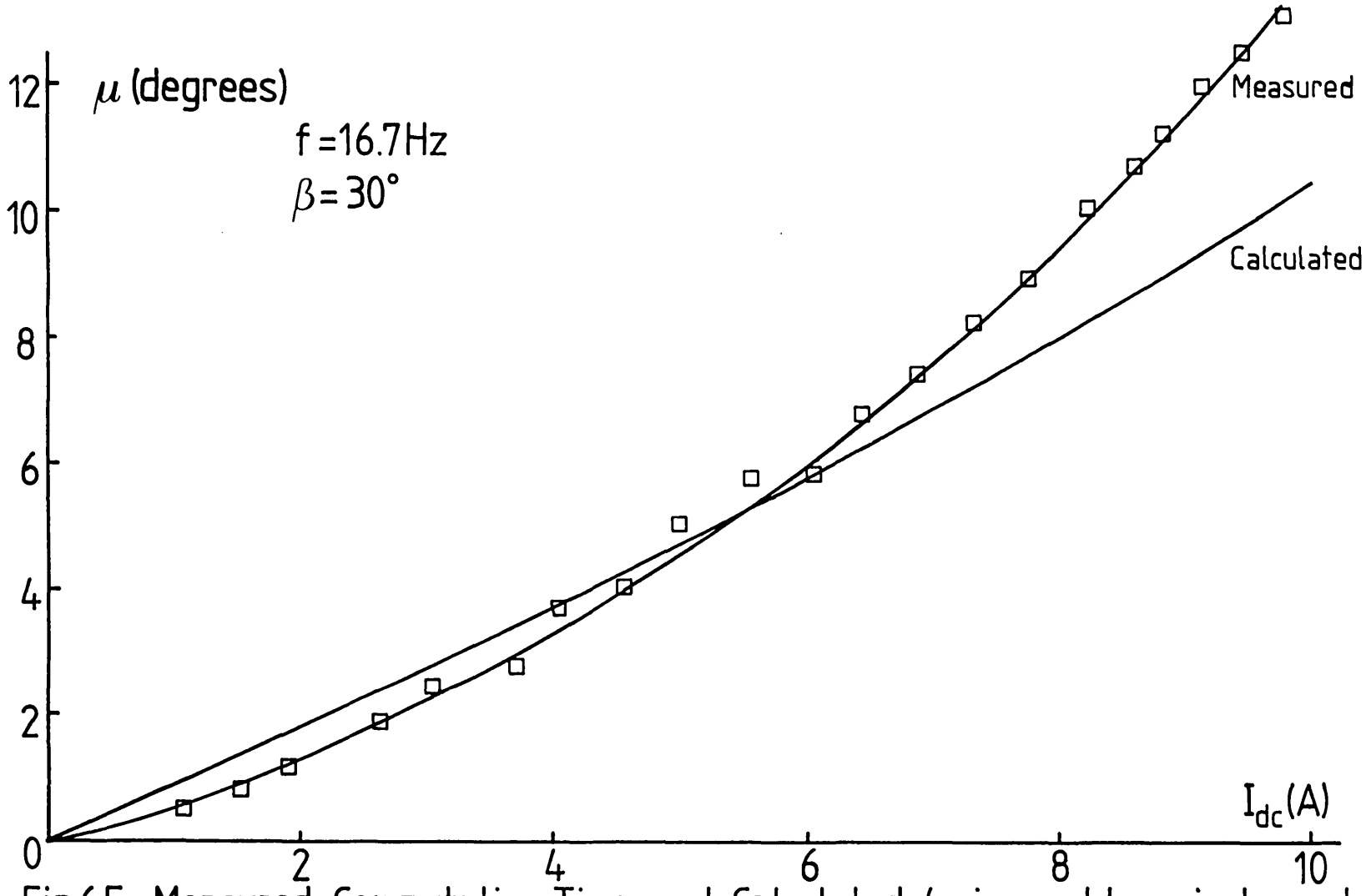


Fig.6.5. Measured Commutation Time and Calculated (using subtransient reactances) for the Solid Rotor Machine.

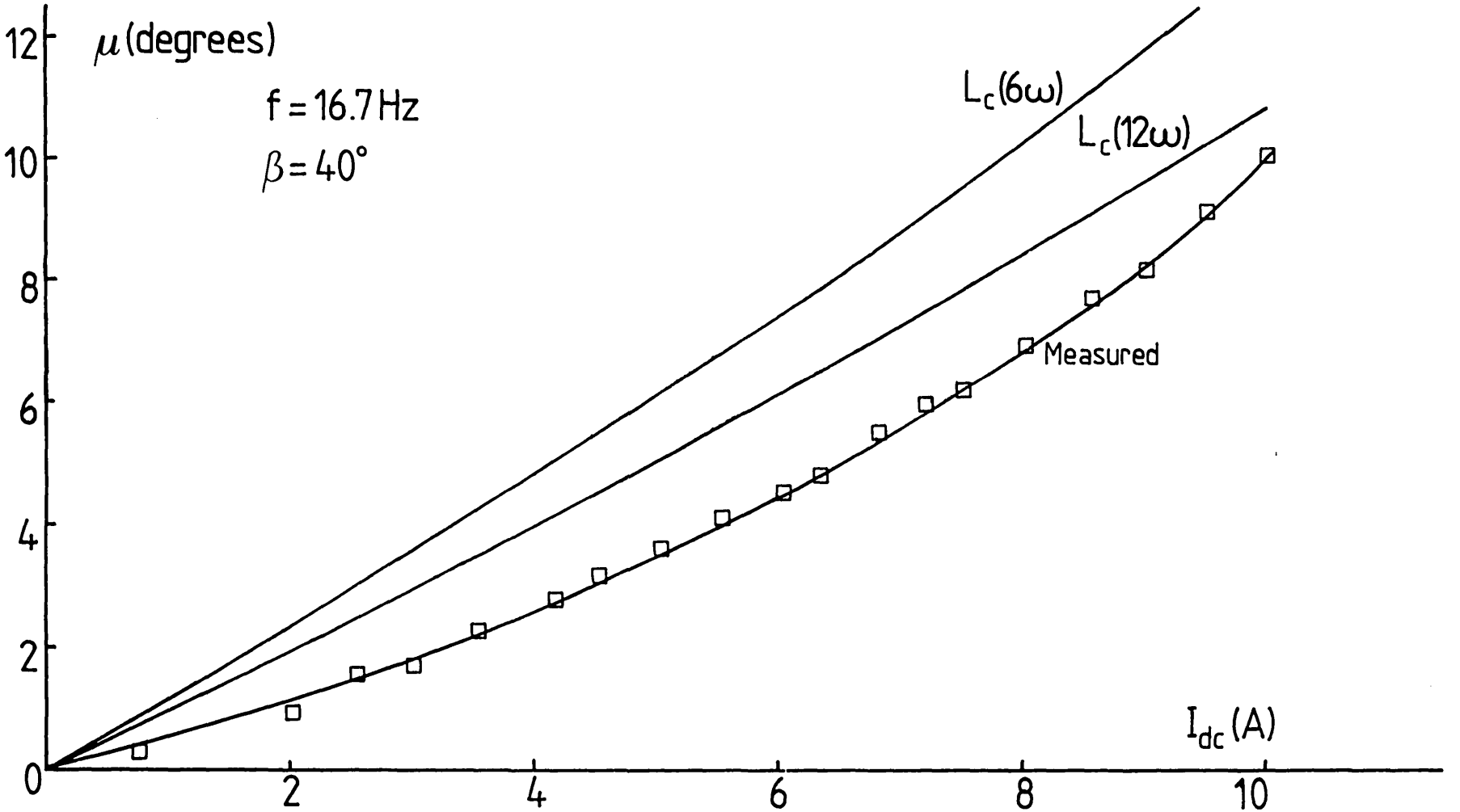


Fig.6.6. Calculated (using operational inductances, 6 and 12 times motor frequency) Compared With Measured Curves. Solid Rotor Results.

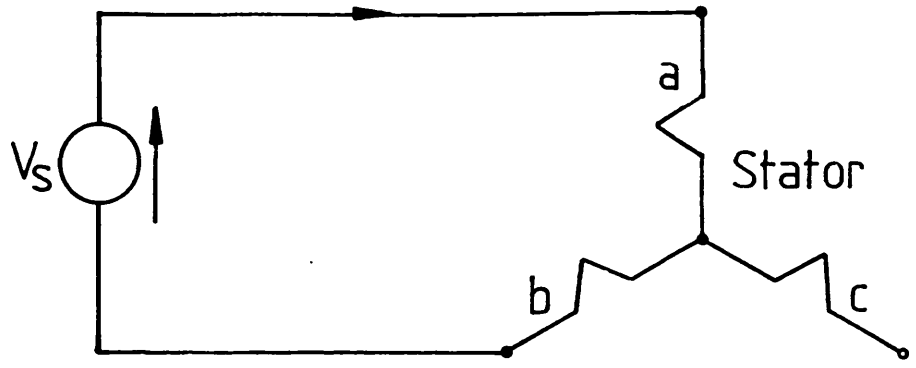
Again, the calculated curves have an almost linear variation and the error between calculated and actual results is considerable.

From fig 6.3 it is apparent that overlap angle is considerably lower for a solid rotor machine than for this laminated rotor machine of similar rating. The laminated rotor allows a more substantial flux pattern change at commutation, hence larger leakage paths, whereas the solid rotor surface eddy currents tend to hold flux changes out of the rotor. The commutating flux is therefore mainly limited to hopping across the stator teeth leakage paths for the solid rotor machine.

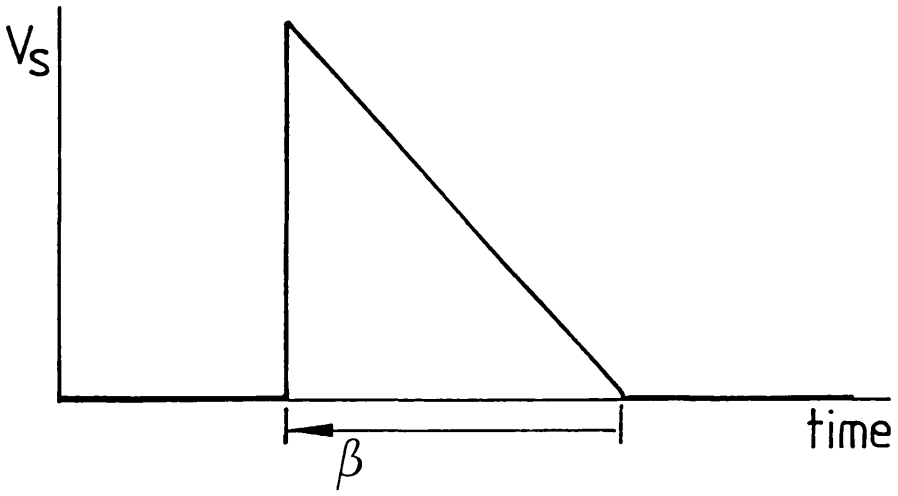
6.4 Line-to-Line Short Circuit Static Test

The commutation period can be likened to a line-to-line short circuit superimposed upon the loaded machine as discussed in chapter three. This analogy is used as the basis for line-to-line step response tests on a magnetic circuit model to calculate the variation of overlap angle with load current.

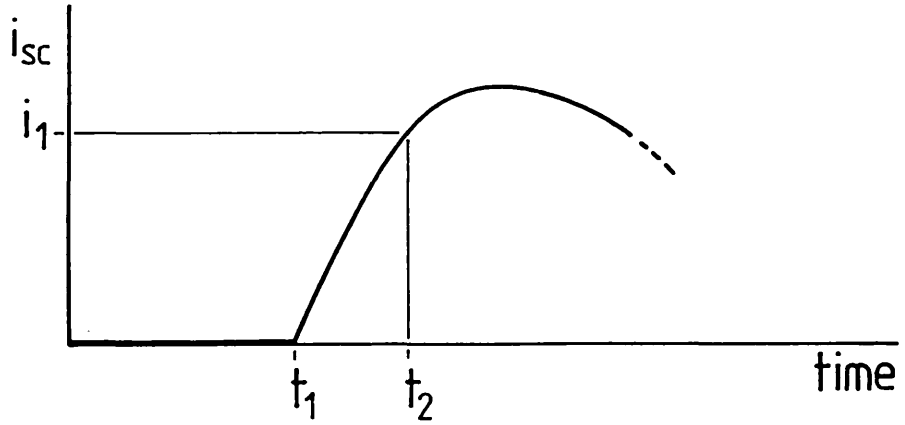
The static magnetic circuit model of fig 4.17 is used with the stator connected as in fig 6.7(a). Rotor motion is assumed to have little effect upon commutation and the motor back e.m.f. is applied externally as a voltage source. The voltage source, v_s, has a chopped sinewave step function of fig 6.7(b) representing the sudden application of line-to-line voltage across the machine terminals at commutation. The field circuit is short circuit. Short circuit current i_{sc}, typically as in fig 6.7(c), is measured for various frequencies, firing angles and phase voltages for a corresponding μ.



(a) Step response model circuit connection.



(b) Applied line-to-line voltage V_S.



(c) Short circuit current, $t_2 - t_1 = \mu$ for $i_1 = i_{dc}$.

Fig.6.7. Static Line-to-Line Step Response Test.

Results using this technique are shown in figs 6.8 and 6.9. In each case two rotor positions are chosen to calculate commutation time. It is apparent that commutation reactance is not only a function of time but also of initial rotor position and the movement of the rotor (for long commutation times). The magnetic circuit allows for eddy current and skin effects, thus improving upon the previous calculations. To make accurate calculations using this method information is needed on the motor's load angle and allowance made for motor movements during commutation. Obviously a full simulation of the synchro-inverter system will allow for these conditions.

6.5 The Full Synchro-Inverter Model

The synchro-inverter model discussed in chapter five is used to calculate overlap times for motor operating points as illustrated in figs 6.10 to 6.13. The improvement over the static model is apparent. Computer results compared extremely well with the actual curves. Field current is held constant for all tests at a value of i_f = 4A.

6.6 Comparison of Voltage and Current Waveforms and Observations

No data was available for the solid rotor of the laboratory model. An estimation of the field turns was made, allowing for packing, from a visual inspection of the rotor. The estimated turns of the computer model had to be reduced by 15 to 135 turns per pole to give a similar open circuit voltage magnitude to the actual value, as shown in fig 6.14. The computed waveform shape compares well with the actual voltage and even simulates the change in slope near voltage peaks.

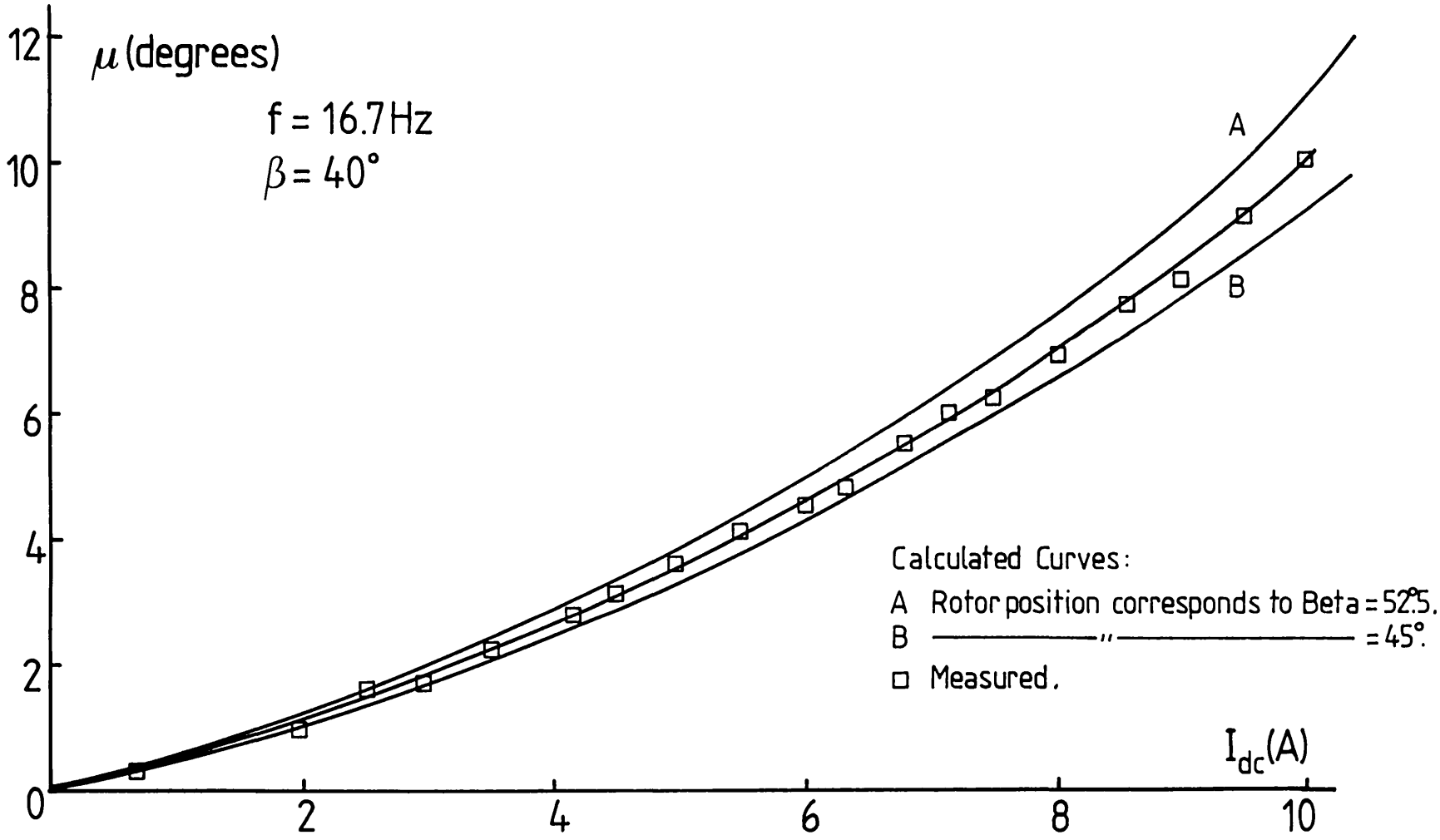


Fig.6.8. Line-to-Line Step Response Calculations and Measured Curve for Solid Rotor Machine.

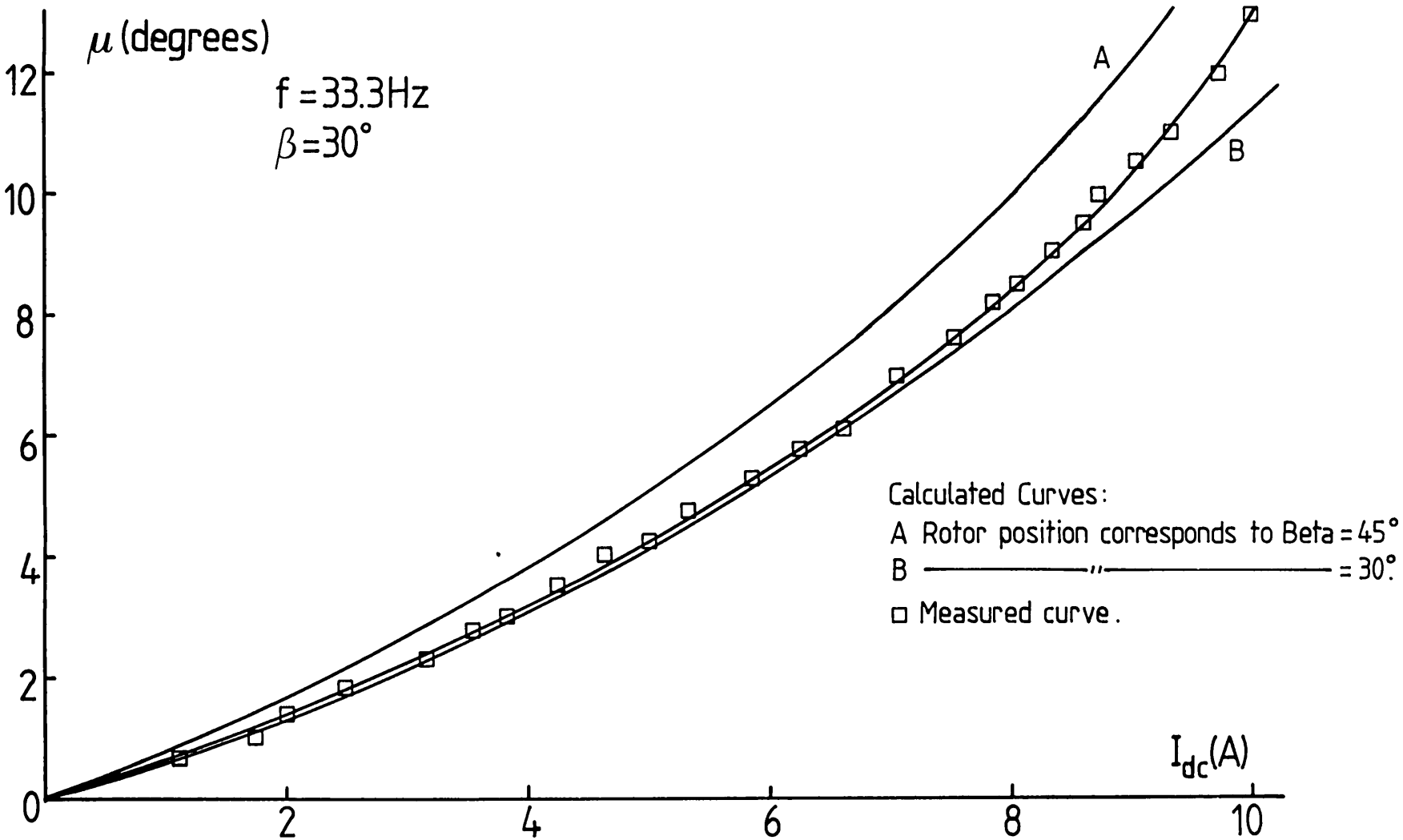


Fig.6.9. Line-to-Line Step Response Calculations and Measured Curve for Solid Rotor Machine.

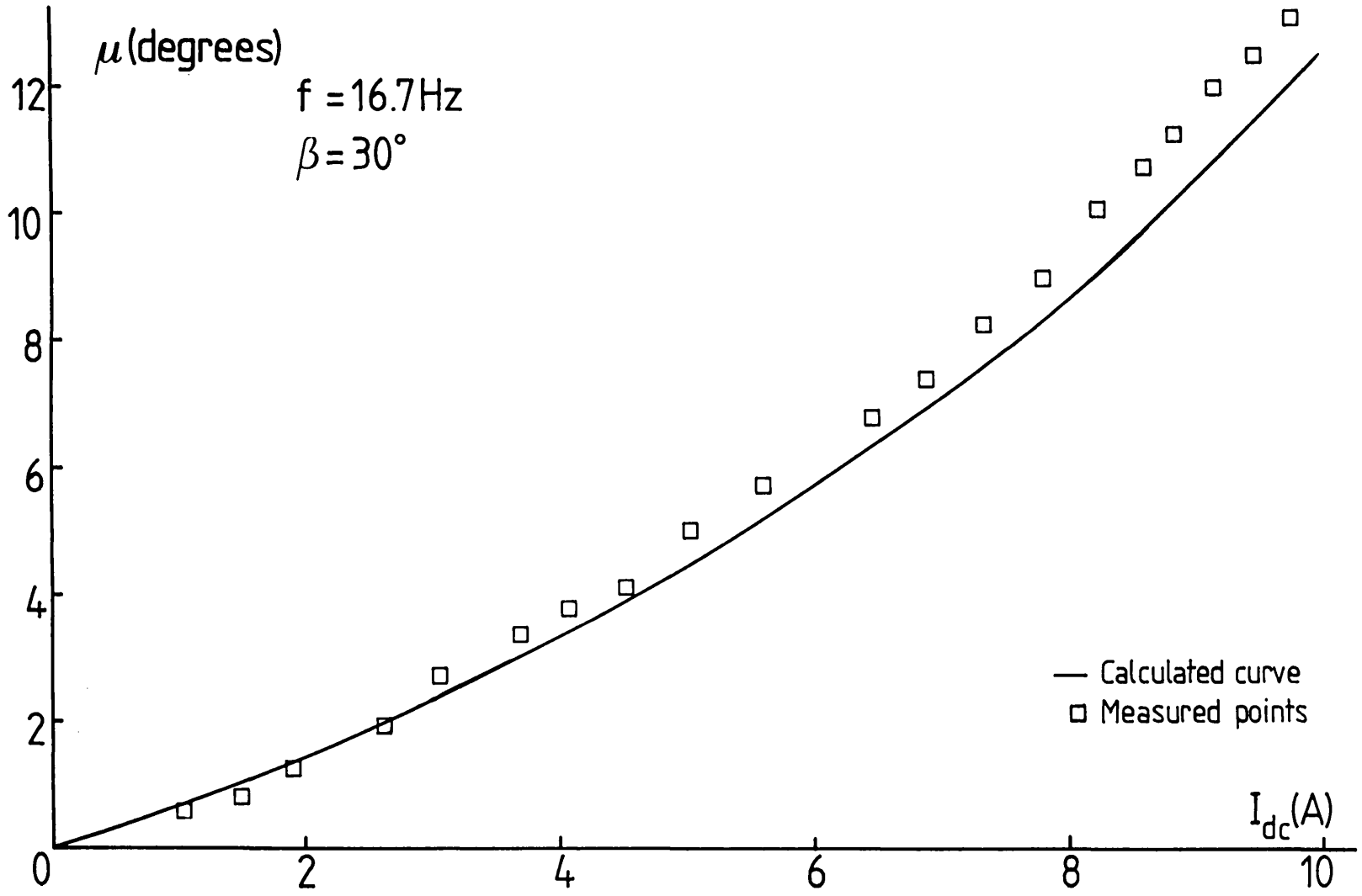


Fig.6.10. Commutation Time vs. Link Current Calculated from a Full Synchro-Inverter Simulation, with Measured Results.

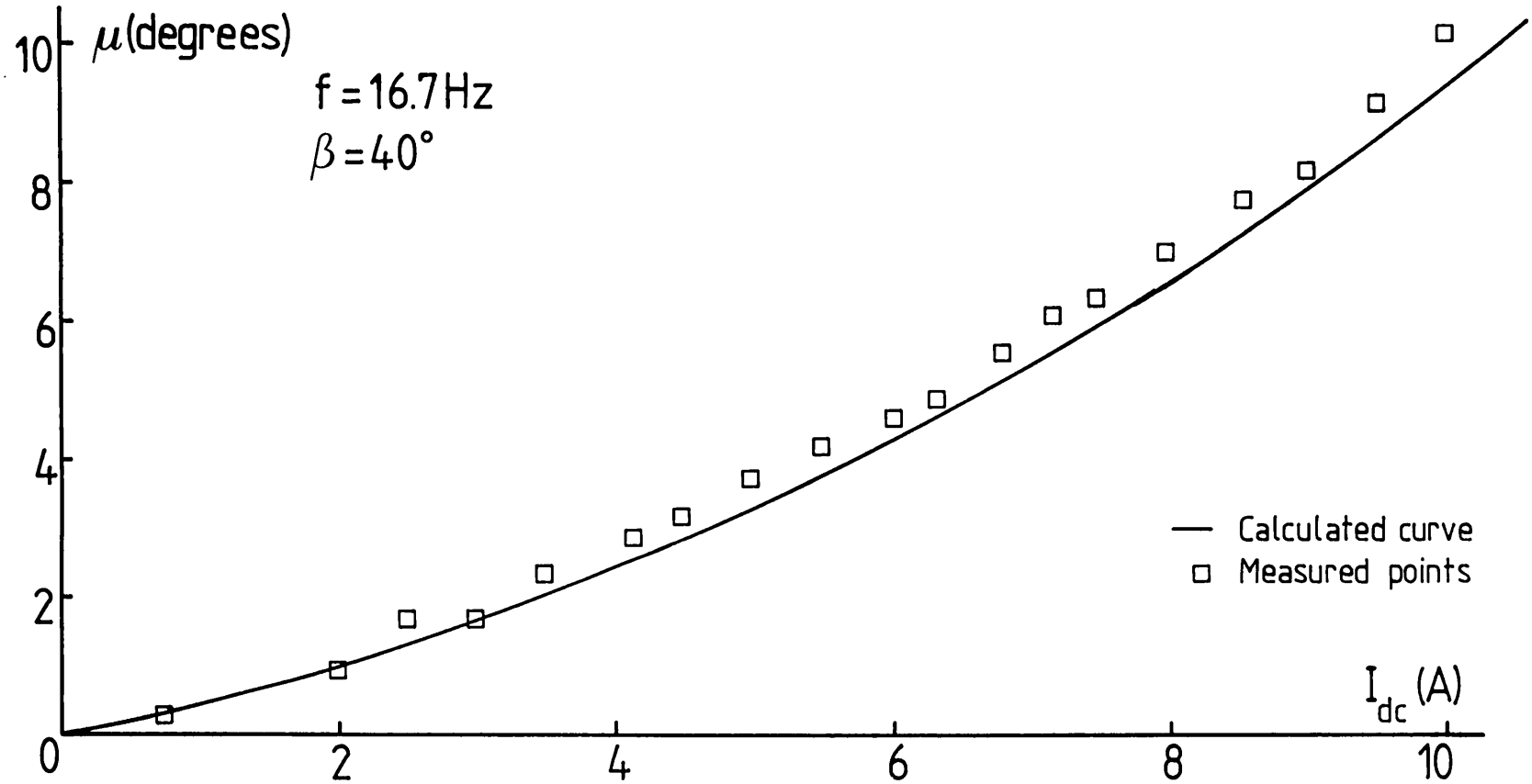


Fig.6.11. Commutation Time vs. Link Current Calculated from a Full Synchro-Inverter Simulation, with Measured Results.

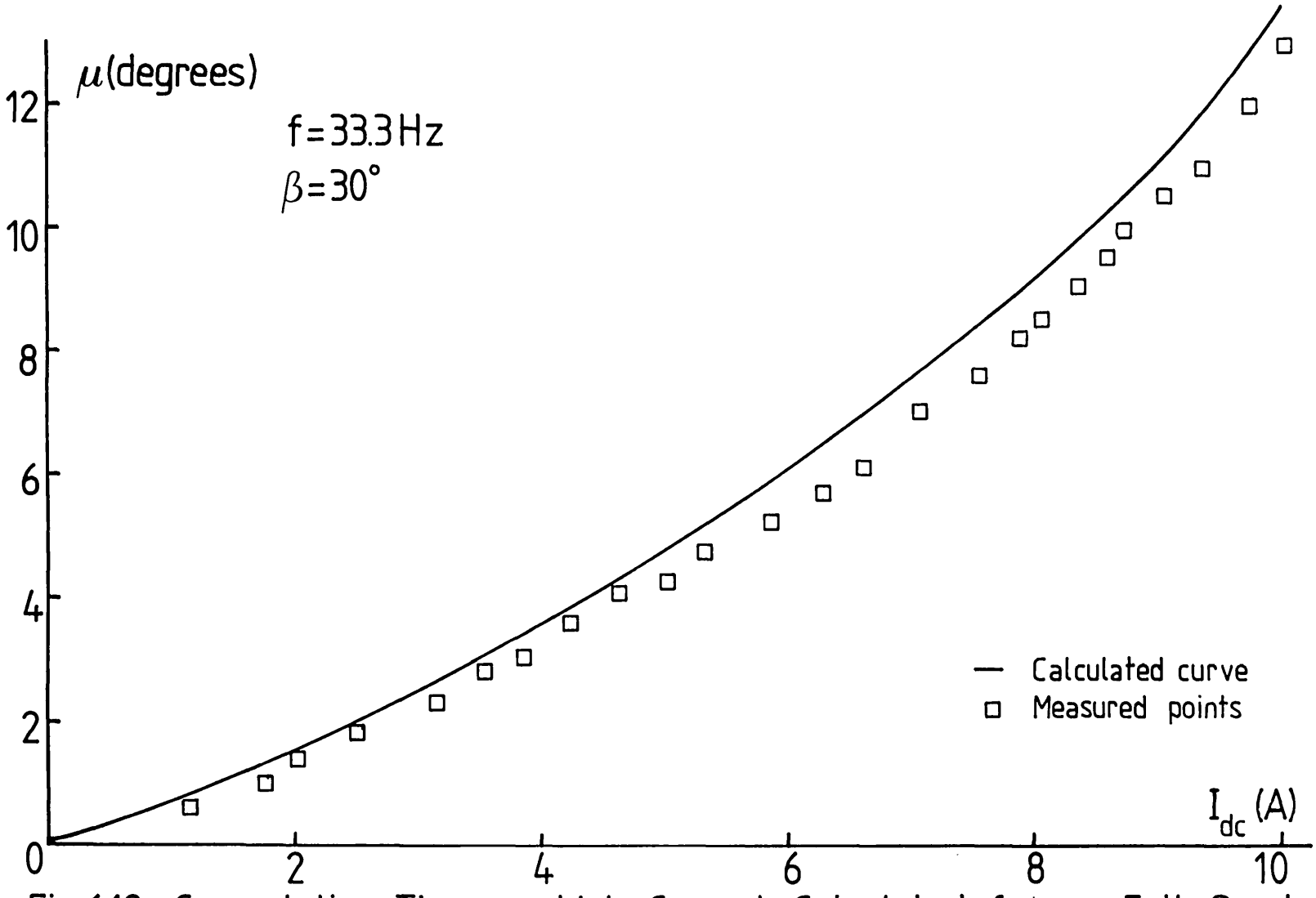


Fig.6.12. Commutation Time vs. Link Current Calculated from a Full Synchro-Inverter Simulation, with Measured Results.

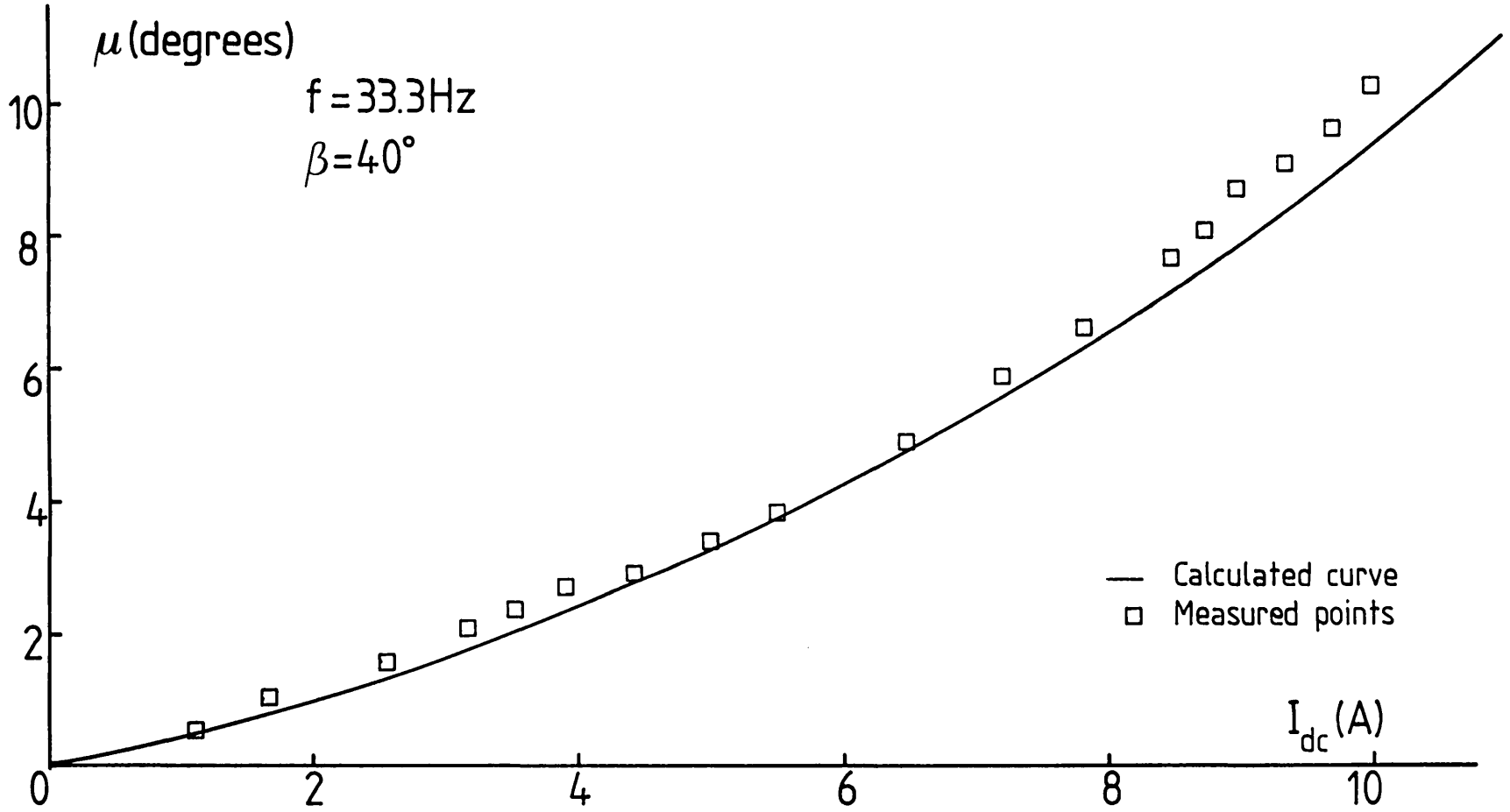


Fig.6.13. Commutation Time vs. Link Current Calculated from a Full Synchro-Inverter Simulation, with Measured Results.

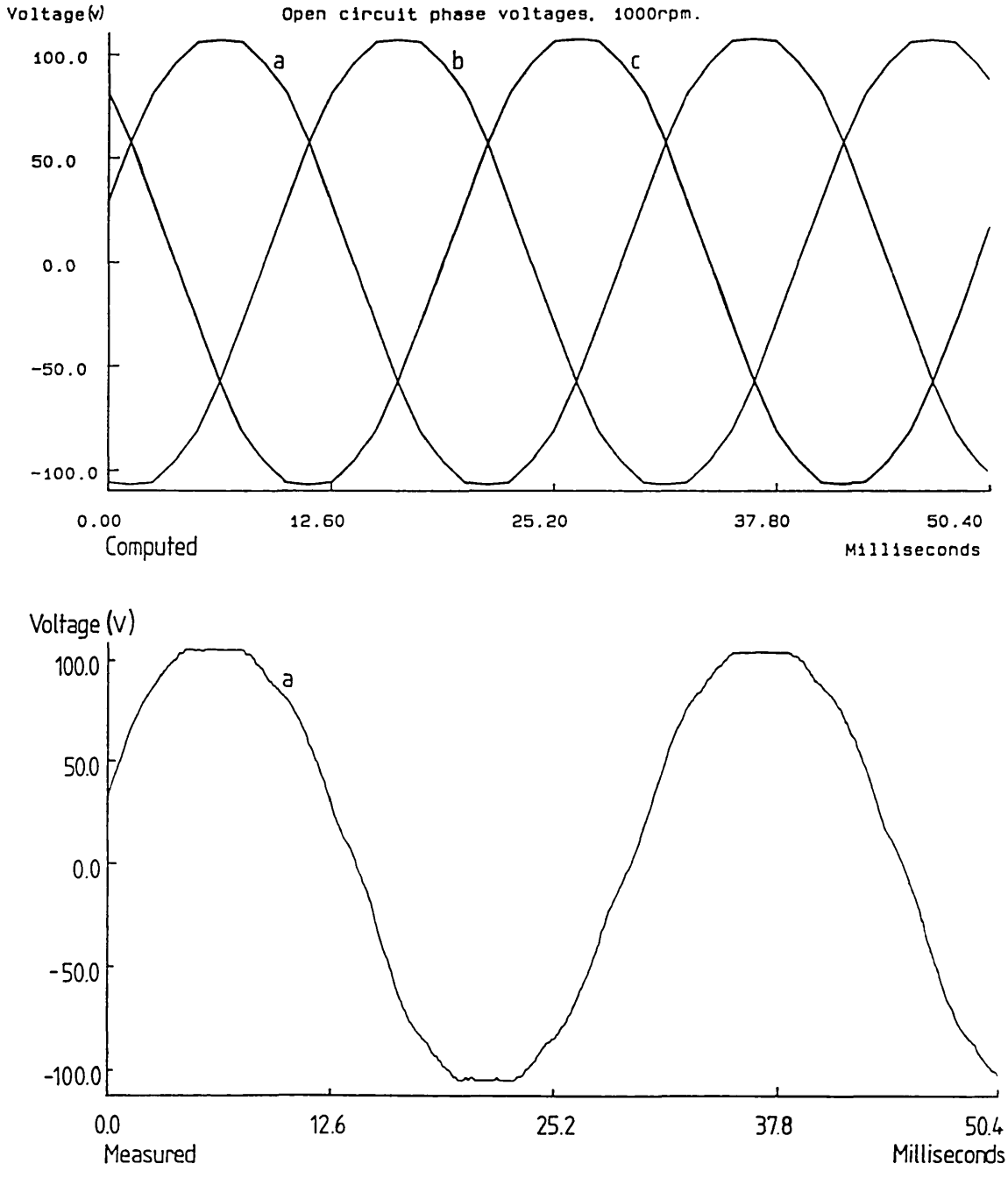


Fig.6.14. Motor Open Circuit Voltages.

The effect of armature reaction [44] is apparent in fig 6.15. As discused in chapter three the resultant flux will be distorted to one side so that the flux density will be approximately as shown in fig 6.16(a). This distortion gives rise to a steep leading edge to the voltage waveform and a gradual drop to zero as depicted in fig 6.16(b). This effect is noticeable in fig 6.15 by comparison with the corresponding open circuit voltage.

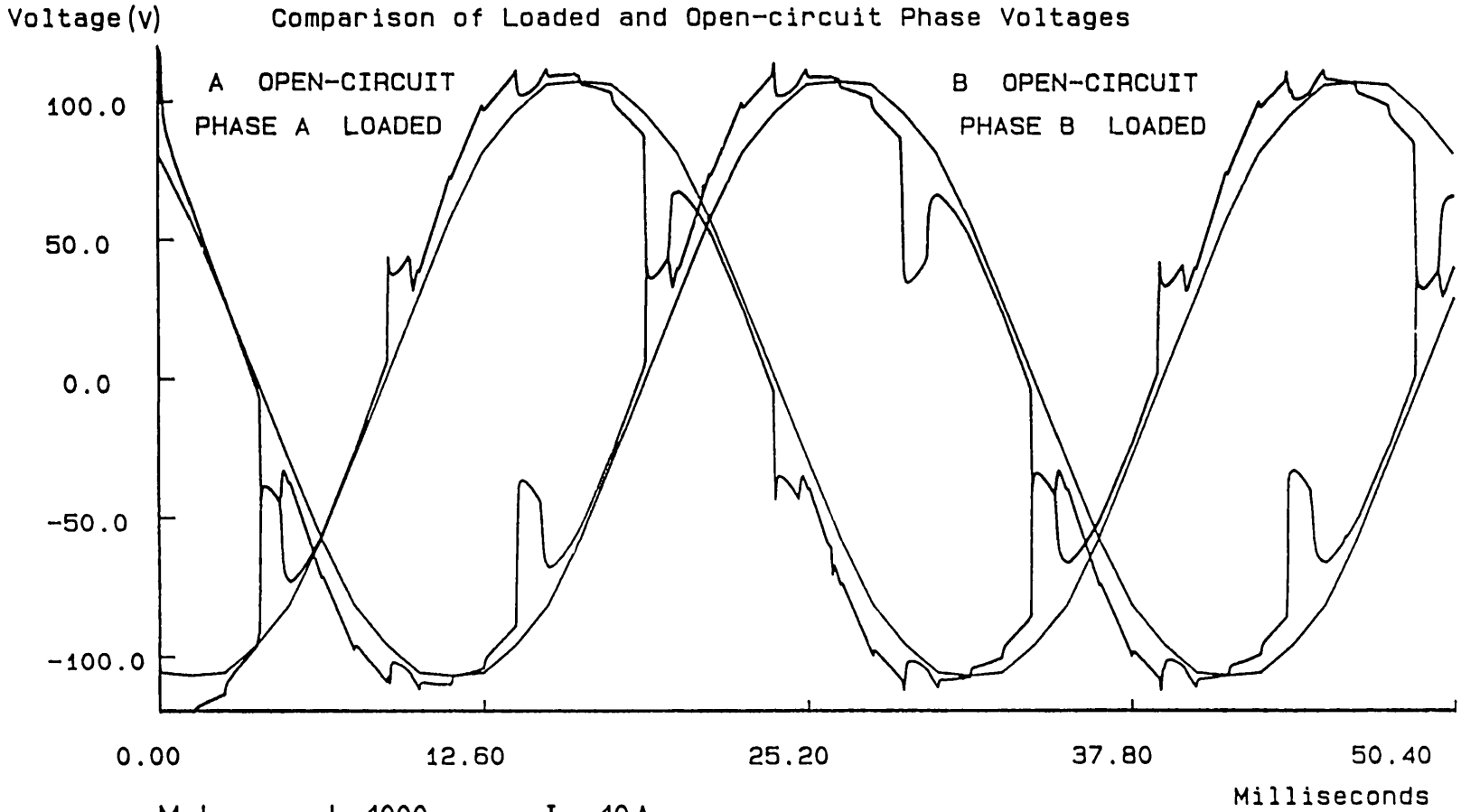
Fig 6.17 is a calculated curve which shows how the link current builds up from zero to settle at 10A. The increase of commutation time with current is also apparent.

For the following sets of waveforms the link current is set as an initial current in the link inductor for an appropriate link voltage, avoiding long computer runs to allow I_{dc} to converge. Field current is set constant at 4A for all tests.

The validity of the computer model is shown in fig 6.18 by overlaying actual and computed waveforms. Not only is there good agreement between commutation times but the general shape agrees well.

As mentioned above no value for rotor resistivity was available. An initial guess has been made for ρ to calculate the magnetic dampance values of the solid iron (the value chosen was $\rho = 2\ 4 \times 10^{-8} \Omega m$).

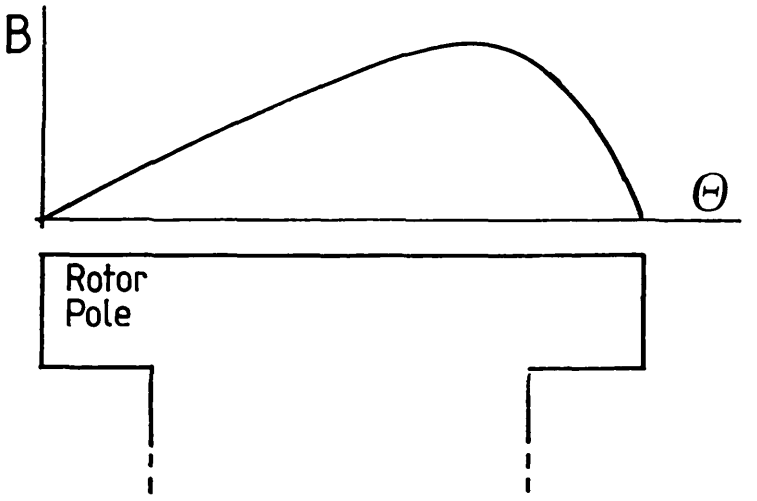
The computed field current ripple was found to be 1.8% (using the initial value of ρ) compared to an actual ripple of 7.5%. An overall reduction in the dampance values, to 25% of their initial value implying a corresponding increase in electric damping circuit resistance gave a computed field current ripple the same as the actual



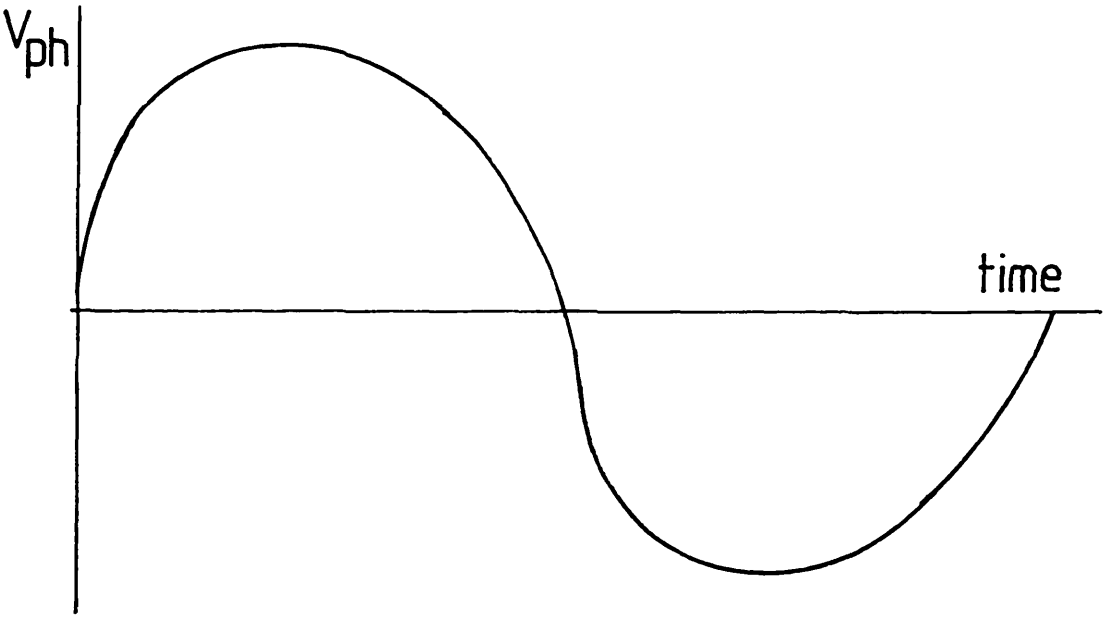
Motor speed = 1000 r.p.m. I_{dc} = 10 A.

$\beta = 30°$ $\mu = 13°.5$

Fig.6.15.



(a) Flux Density Along the Pole Face.



(b) Resulting Phase Voltage Distortion (exaggerated).

Fig.6.16. Distortion of Loaded Motor Phase Voltage.

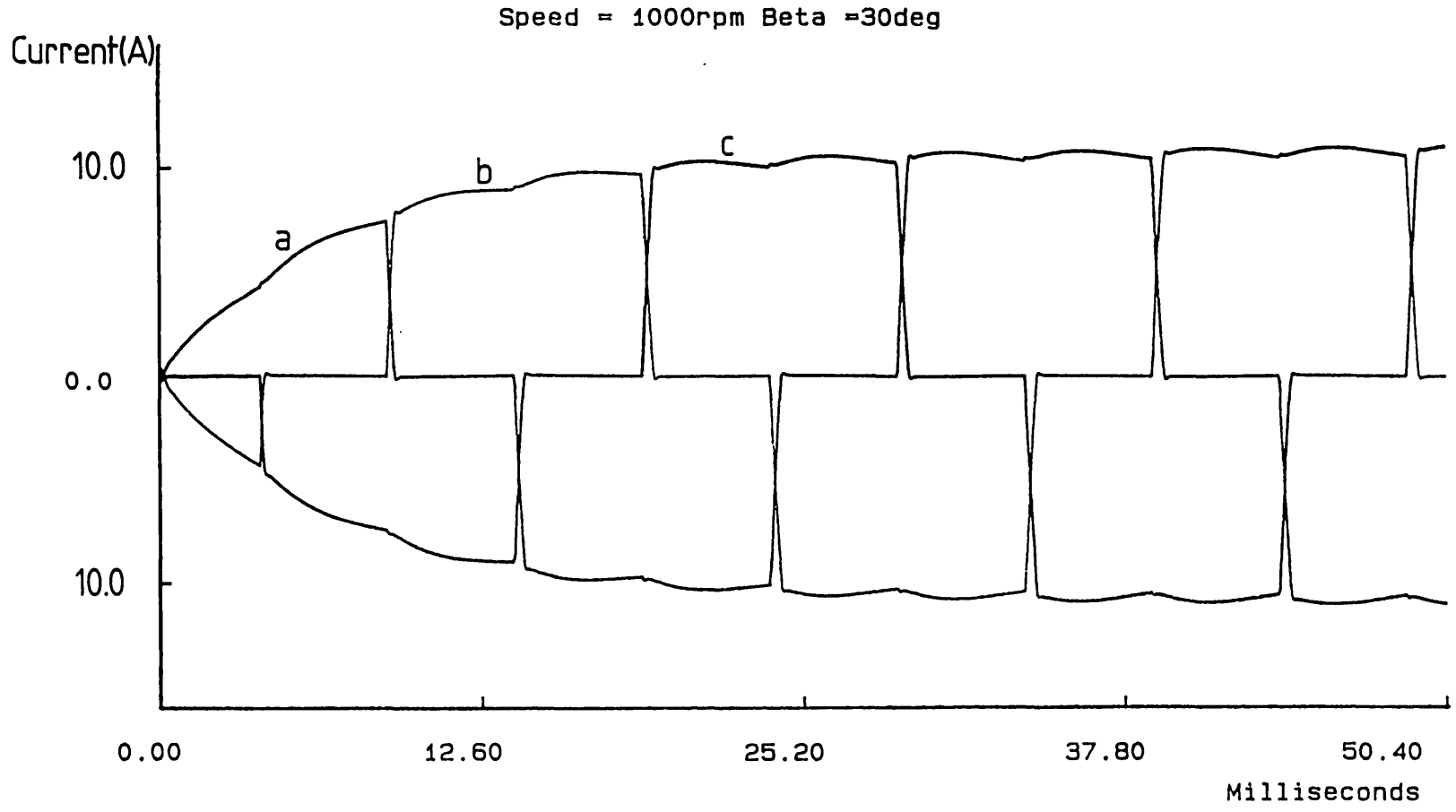


Fig. 6.17 (a). Increase of Link Current.

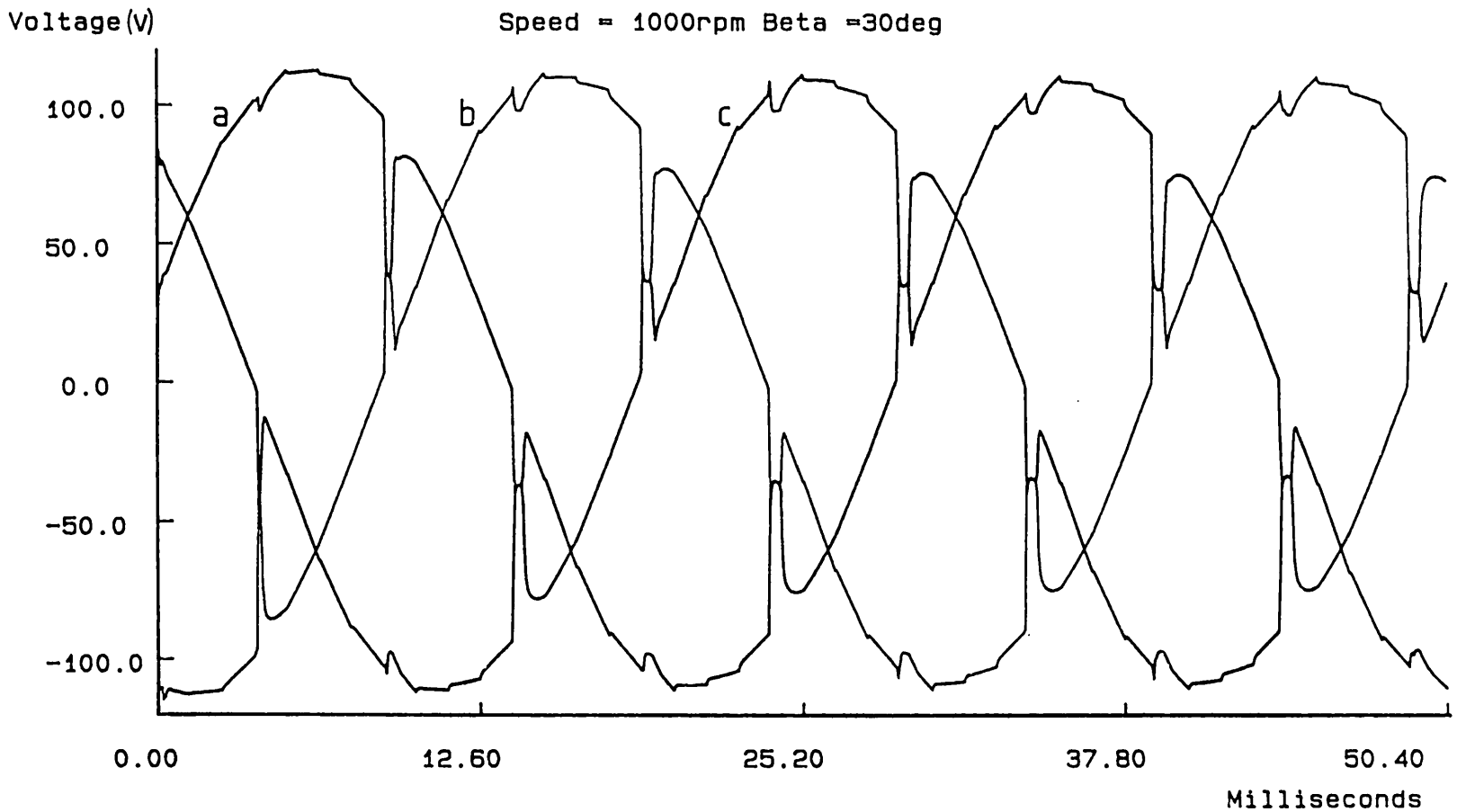


Fig.6.17(b). Increase of Link Current.

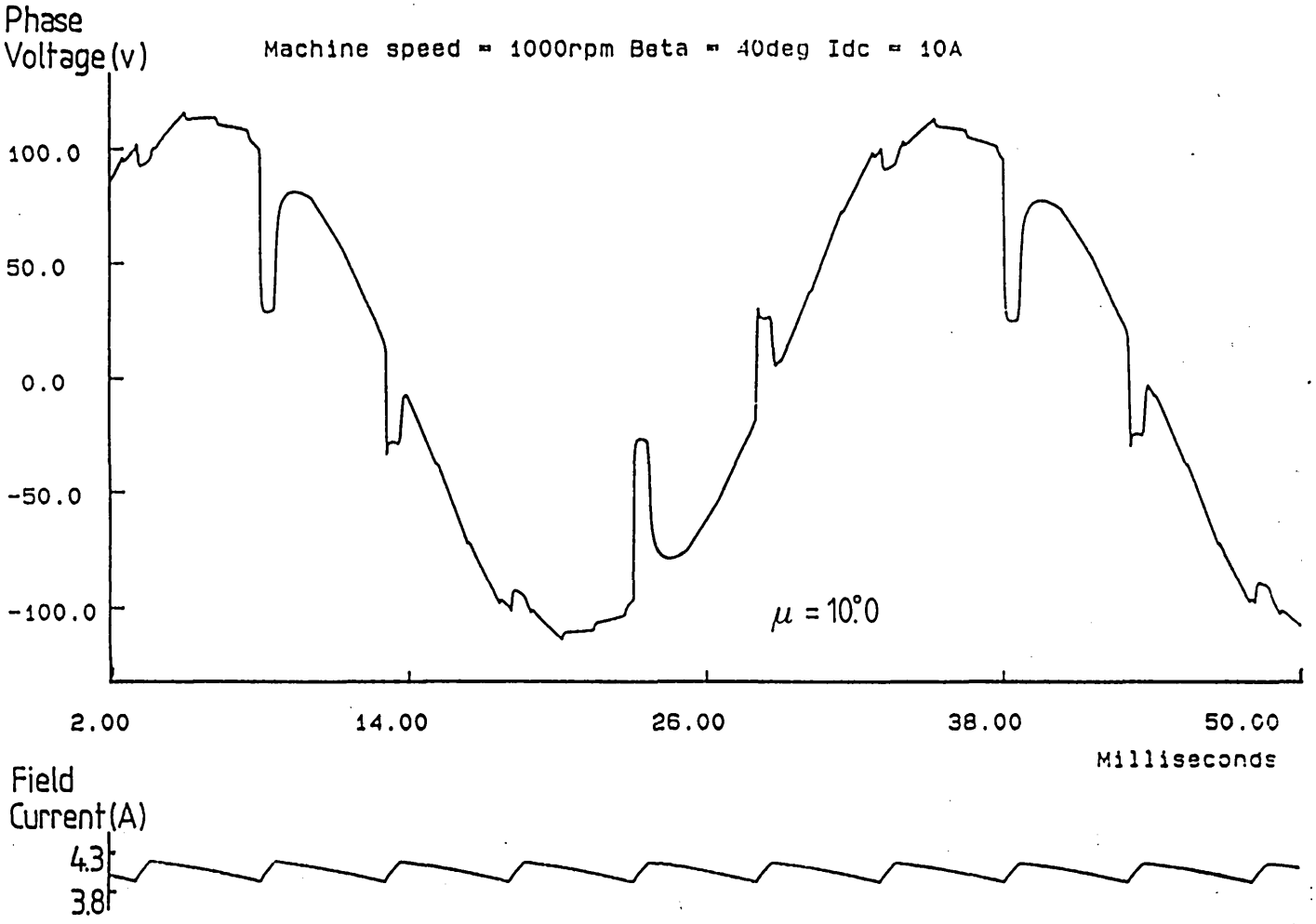


Fig.6.18. Computed Motor Waveforms for f=33.3Hz.

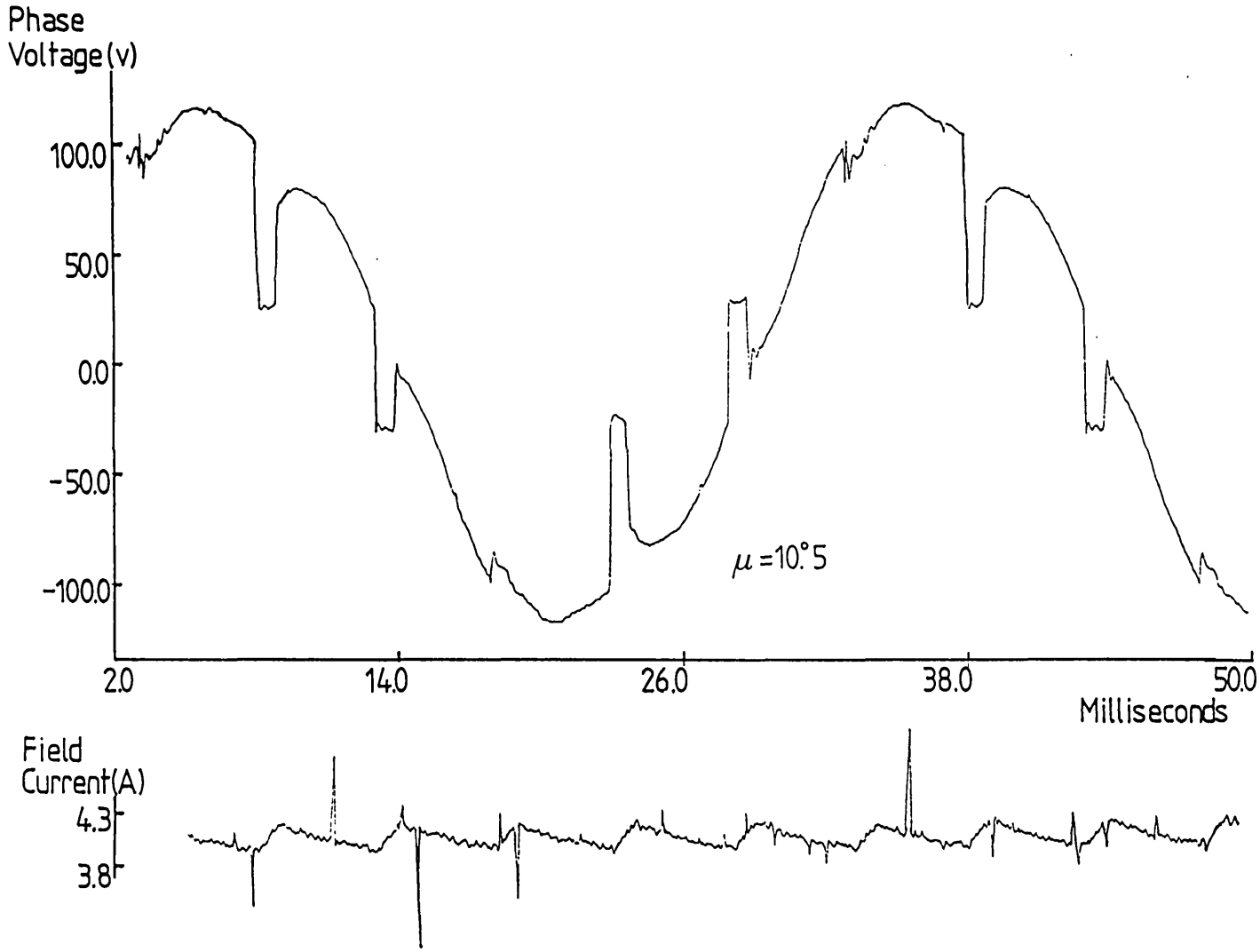


Fig.6.18. Measured Waveforms for f = 33.3Hz.

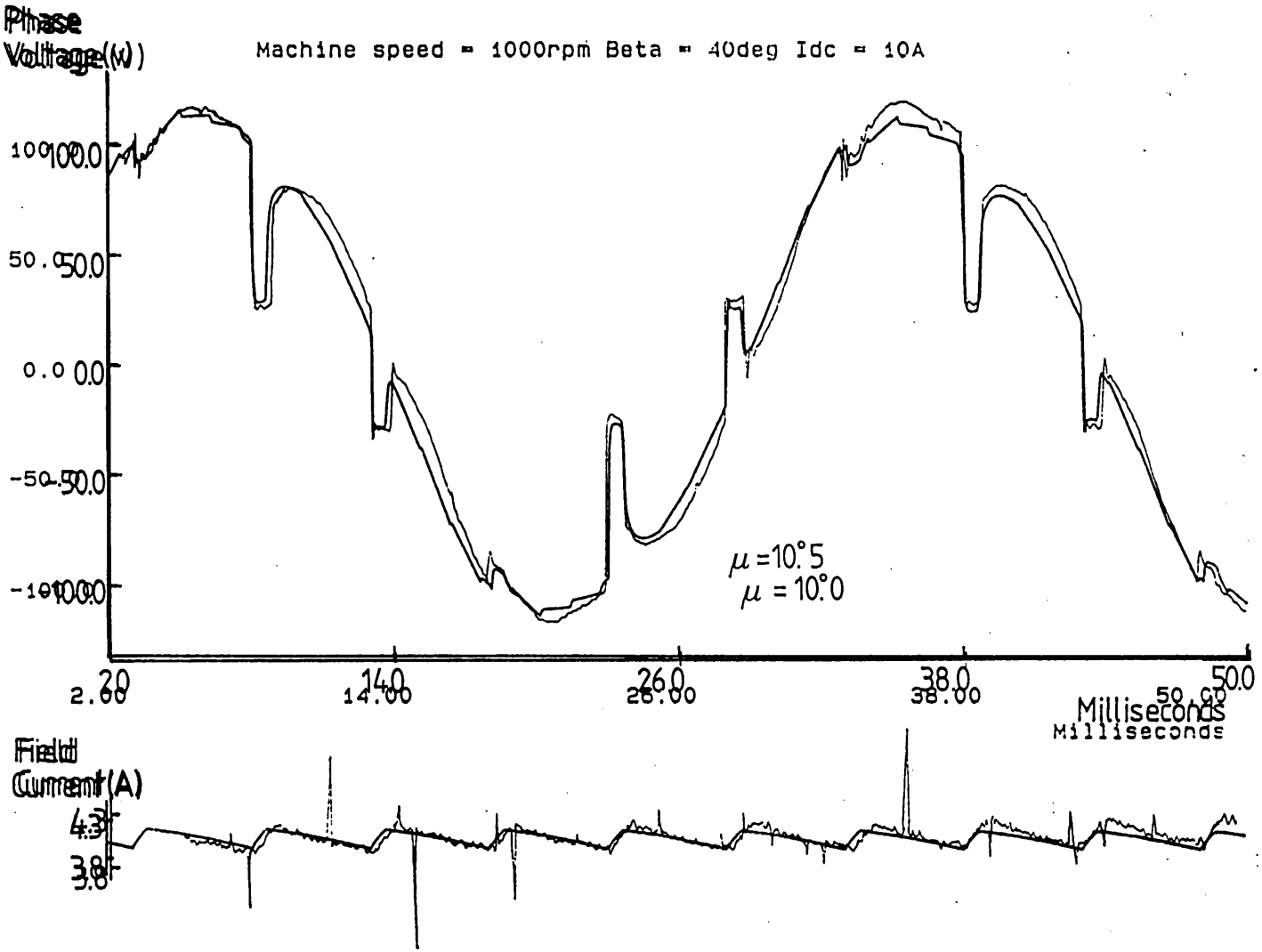


Fig 6.18. Measured Waveforms for f = 33.3Hz.

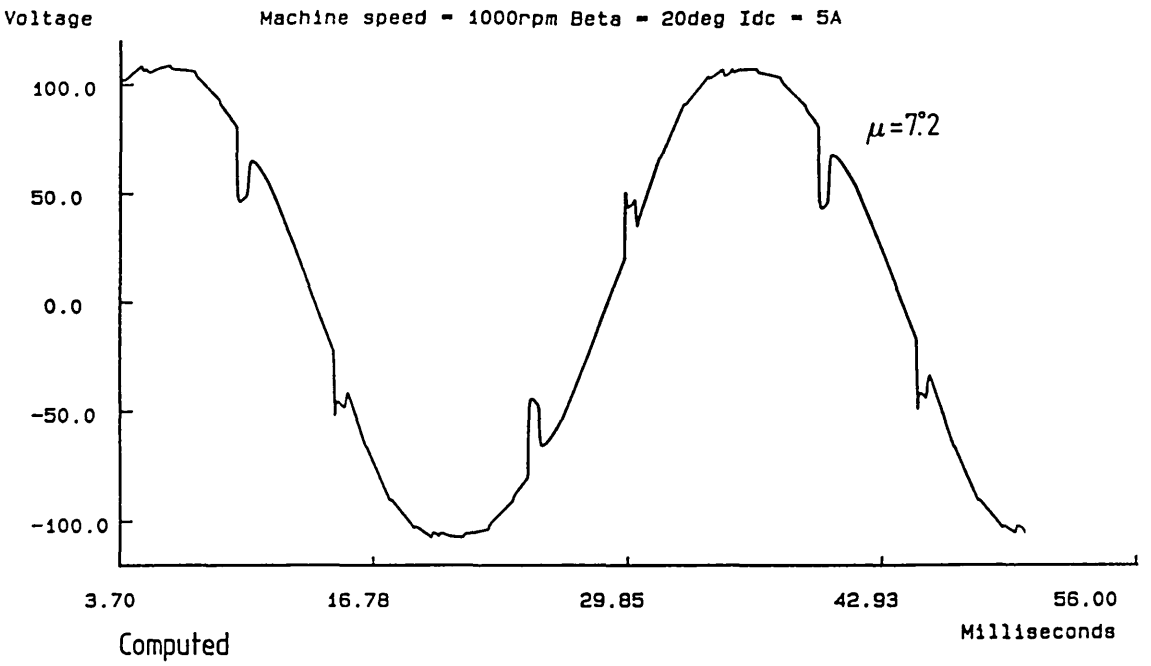
Fig 6.18. Computed Motor Waveforms for f = 33.3Hz.

value. The drastic change in dampance only increased commutation time by 12% and computed waveforms were generally unaffected. The discrepancy in the dampance values may be due to the rotor material having a much higher resistivity value, rotor end "ring" resistance may be large and no allowance is made for bolt holes. Neglecting mutual damping effects (section 4.8.3) may also contribute to the reduction of damping required.

As discussed in chapters two and three it is desirable to keep commutation as short as possible. A safety angle of at least ten degrees is needed to ensure safe commutation for the actual synchro-inverter. Tests have been conducted down to a firing angle of twenty degrees and the link current has been increased to a value where commutation failure occurred. Fig 6.19 is recorded for a maximum current level before commutation failure occurs. The relatively low current level does not distort either computed or actual waveforms as much as higher current, but the smaller firing angle results in comparatively longer commutation times. For fig 6.19 μ is about 7.5^{o}, almost twice the overlap angle for $\beta = 30^{o}$ which was 4.3^{o}.

It is possible to demonstrate a commutation failure, with the computer model, shown in fig 6.20. The computer model provides a much cheaper and less distressing(!) way of testing a synchro-inverter full capability.

An increase in firing angle to thirty degrees allows higher current levels to be tolerated. For the same speed of 1000 revs/min, fig 6.21 shows phase current and voltage waveforms. The result of using a large link inductance can be appreciated from the uniformity of the current waveform. The waveforms compare well although computed voltage



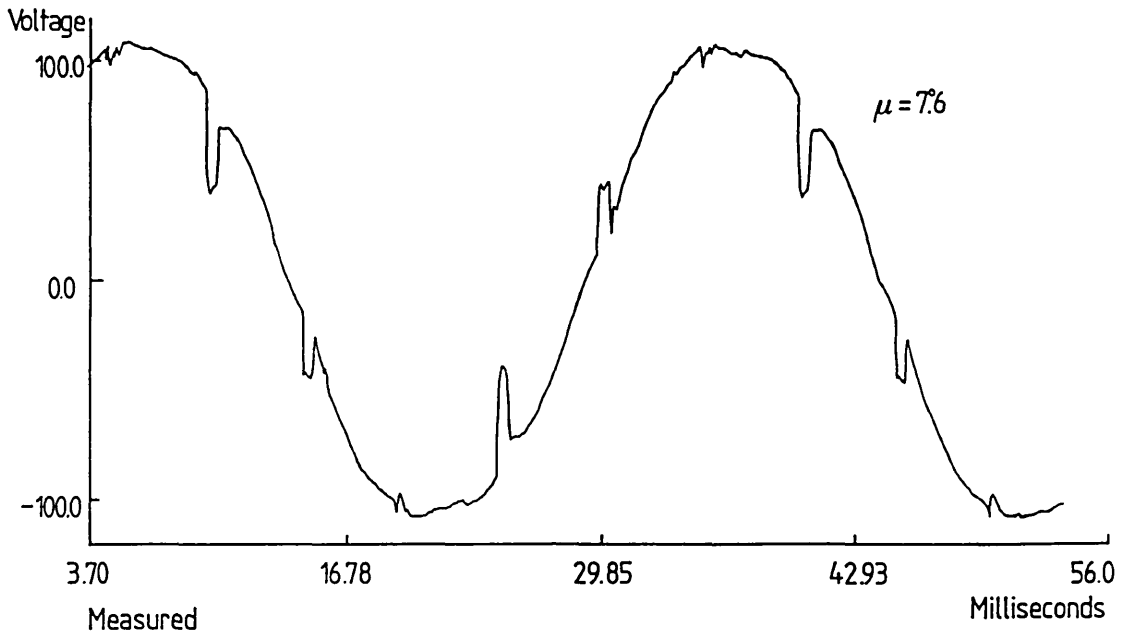


Fig.6.19. Motor Phase Voltages for f=33.3Hz β=20°

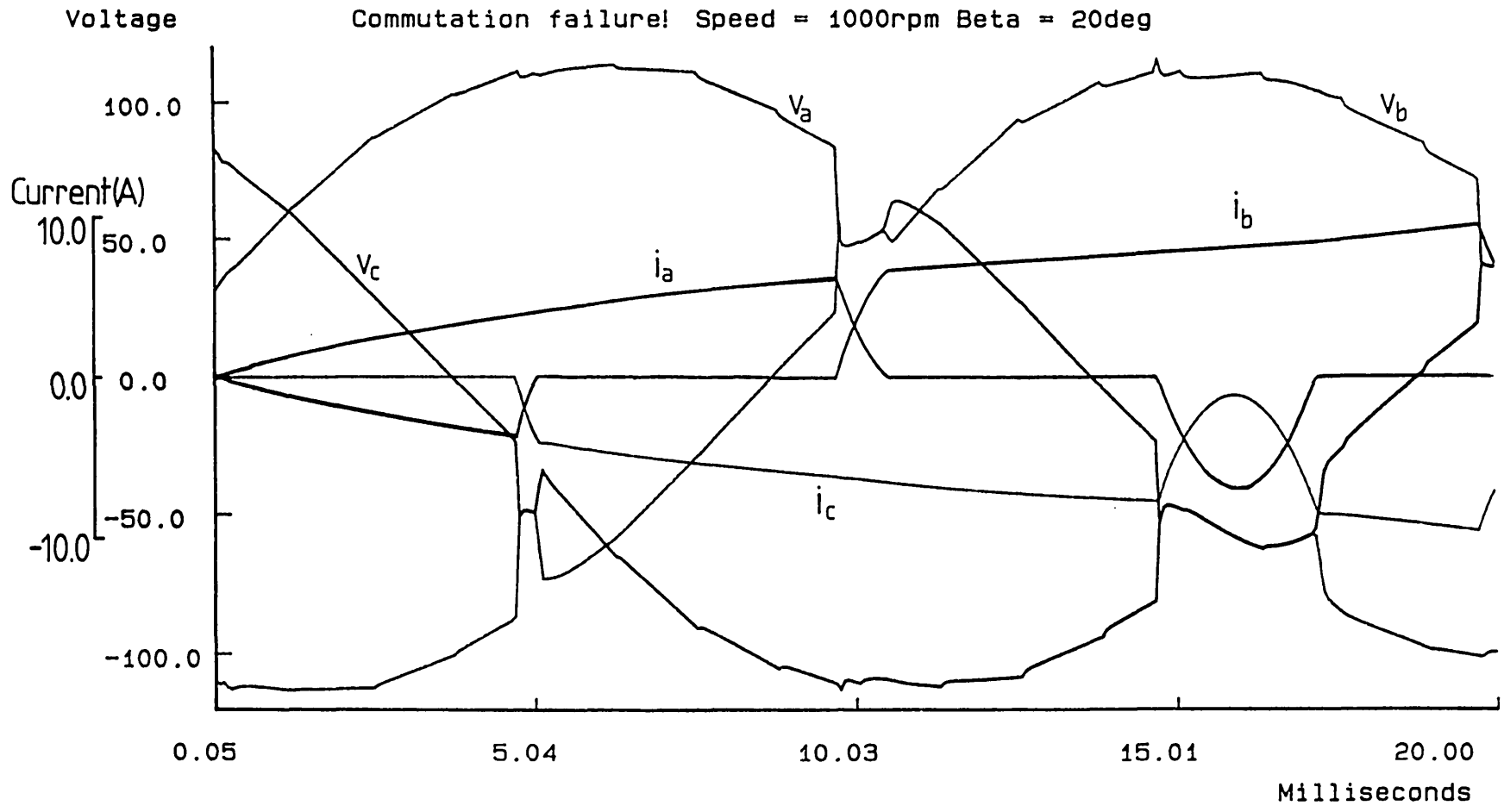


Fig.6.20. Computed Phase Voltage and Current. Simulation of Commutation Failure.

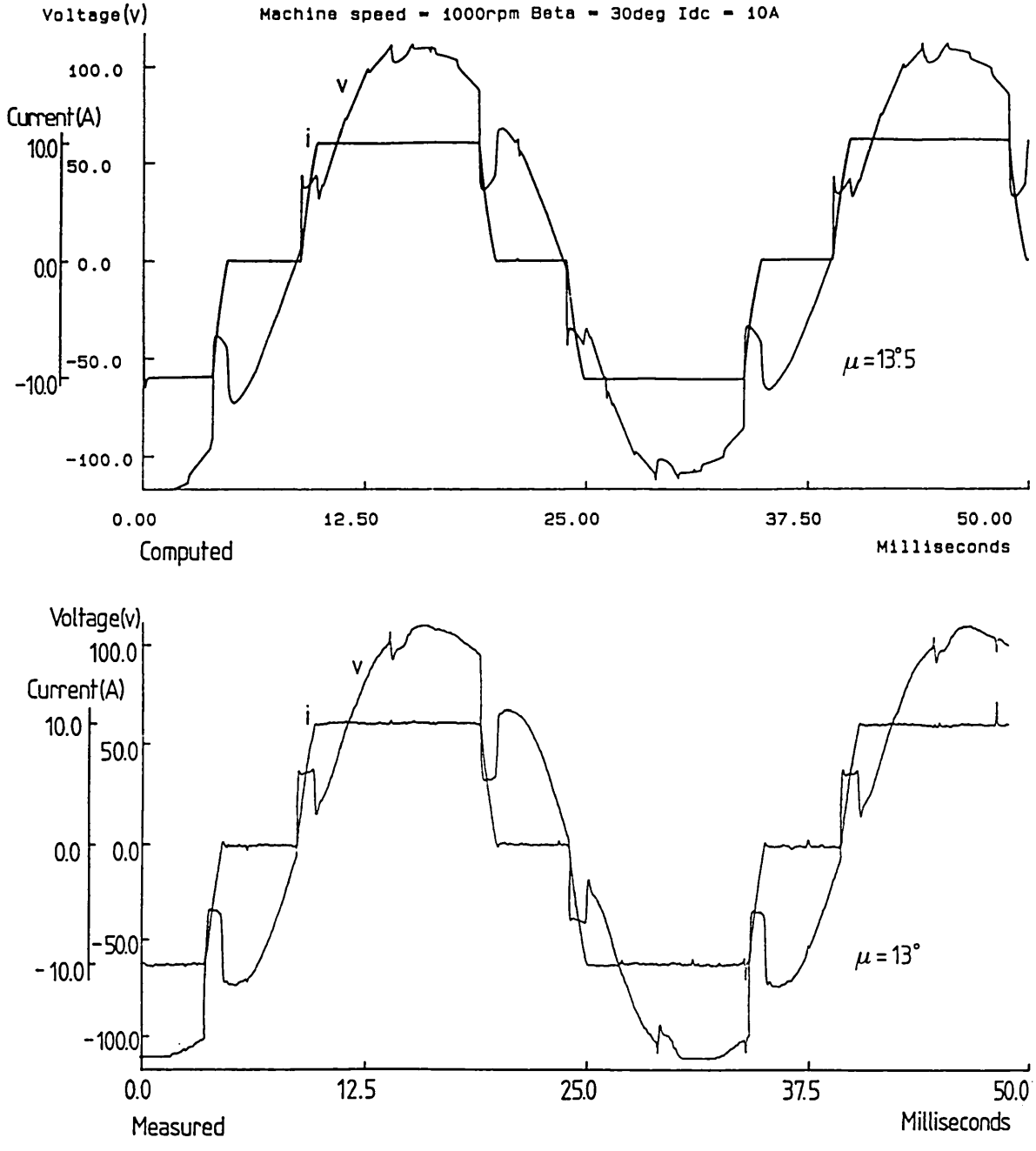


Fig.6.21. Motor Phase Quantities for f=33.3Hz β=30°

peaks drop at a faster rate than the actual waveform. This results in a computed voltage at commutation 6% lower than the actual voltage. Also, computed voltage recovery after commutation is not as "rounded" as the actual waveform.

The lower speed of 500 revs/min results in a lower voltage available for commutating the thyristors. Results are not available for a firing angle of twenty degrees since the line-to-line voltage was insufficient to commutate thyristors. However, a reasonable current level is achievable at $\beta = 30^{o}$, fig 6.22.

Mutual coupling between phases has been represented correctly in the magnetic circuit. Commutation causes a "mutual notching" in the phase not being commutated apparent in figs 6.22 and 6.23.

Secondary notching is insignificant at lower current levels as can be seen in fig 6.24. Overlap angle is again appreciable for $\beta = 20^{o}$ at the higher speed of 750 revs/min.

A commutation notch and current waveform are illustrated in fig 6.25. The initial voltage spike at commutation is predicted well although there is a discrepancy in the subsequent voltage slope. During commutation the two commutating phase voltages assume an average value. Differences between the computer model and actual system (phase impedances, thyristor characteristics) are thought to influence second order effects. The discrepancy does not detract from the overall computer model performance.

Incereasing β to 40^{o} for the same speed of 750 revs/min results in the waveforms of fig 6.26. For a similar link current the overlap angle

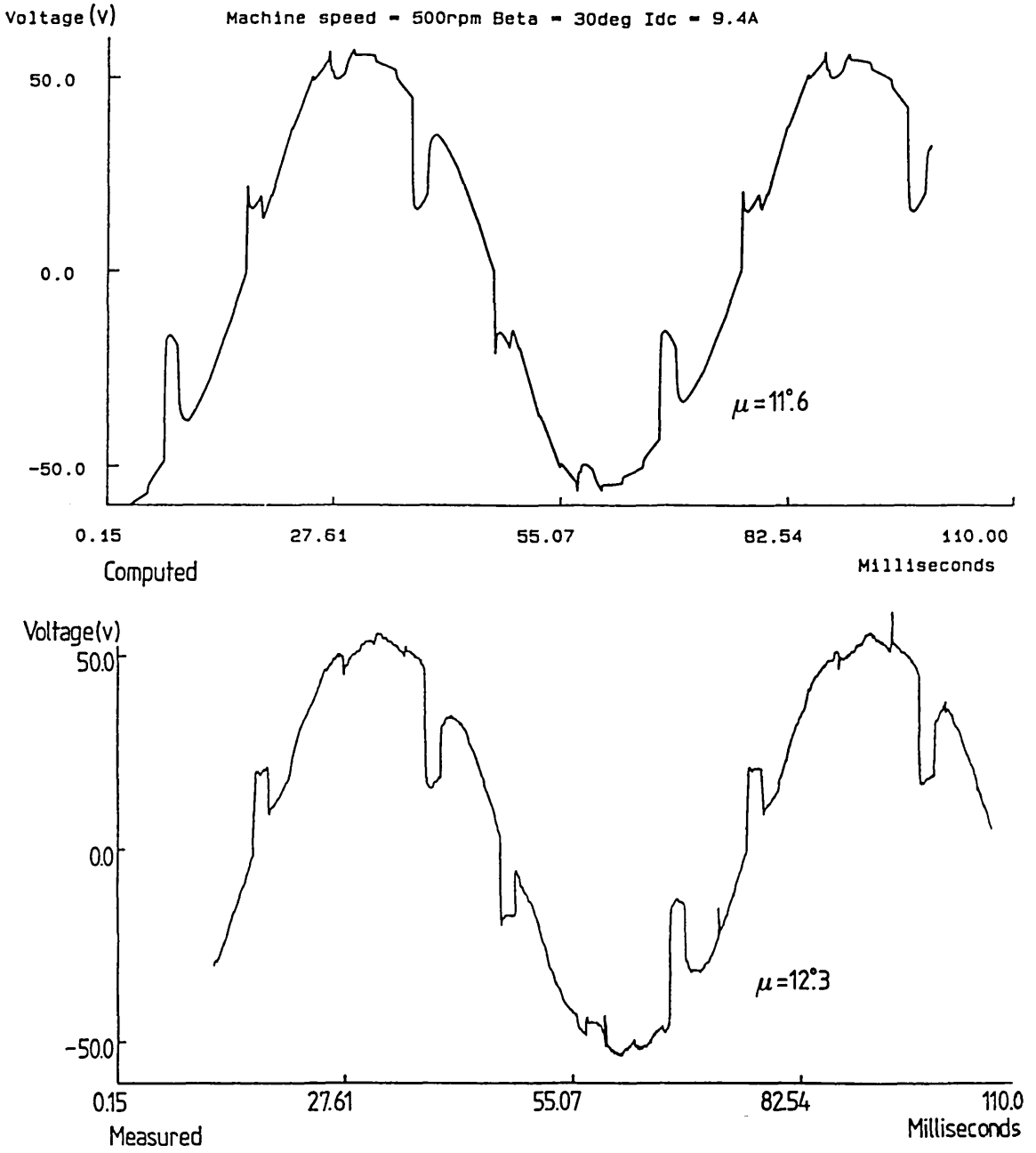


Fig.6.22. Motor Phase Voltages for f=16.7Hz $\beta = 30°$.

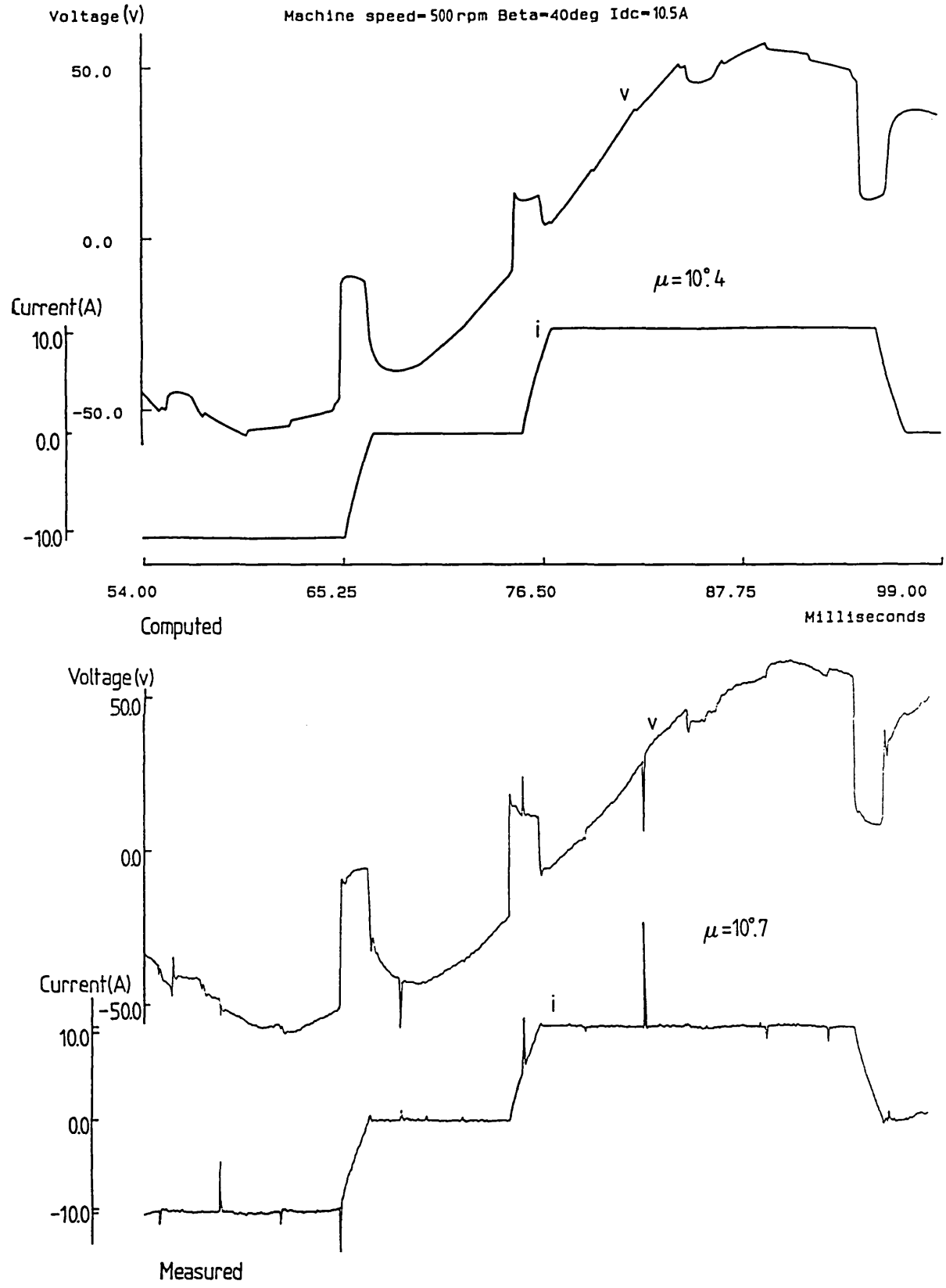
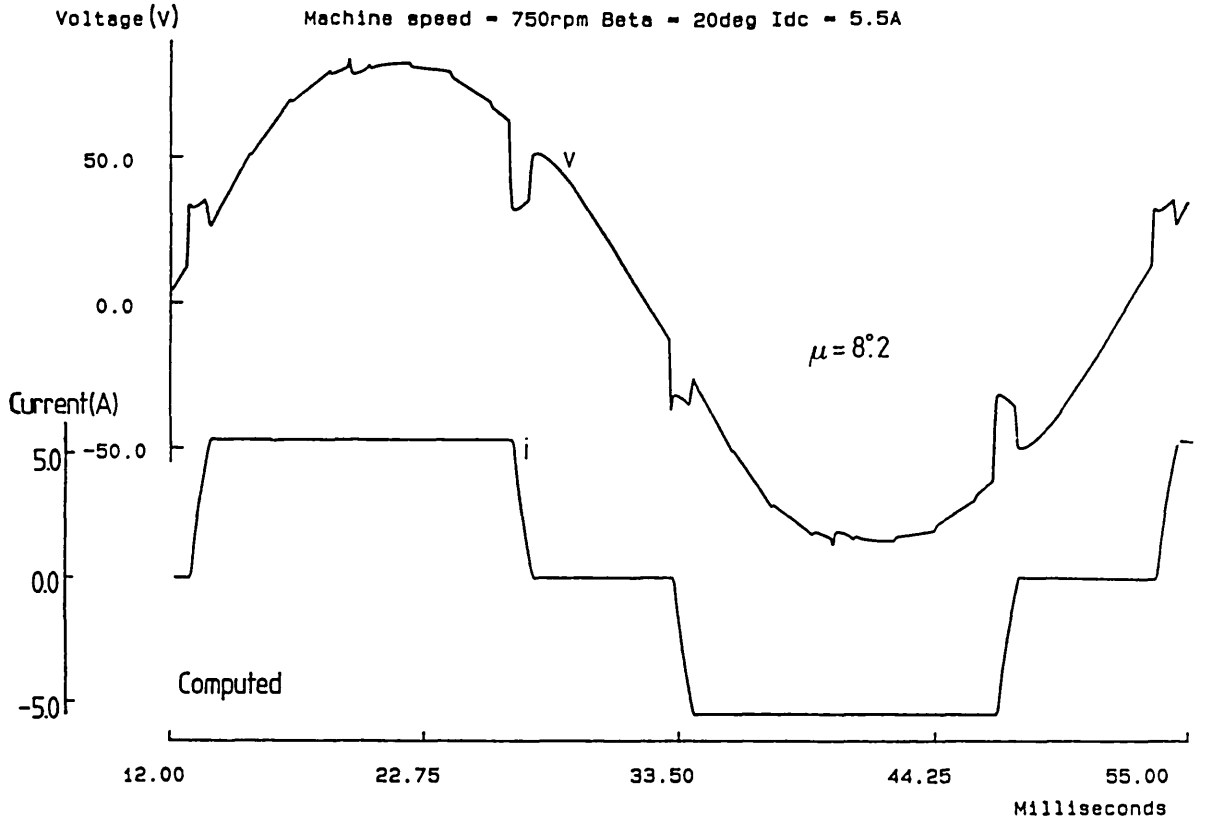


Fig.6.23. Motor Phase Quantities for f=16.7Hz $\beta=40°$



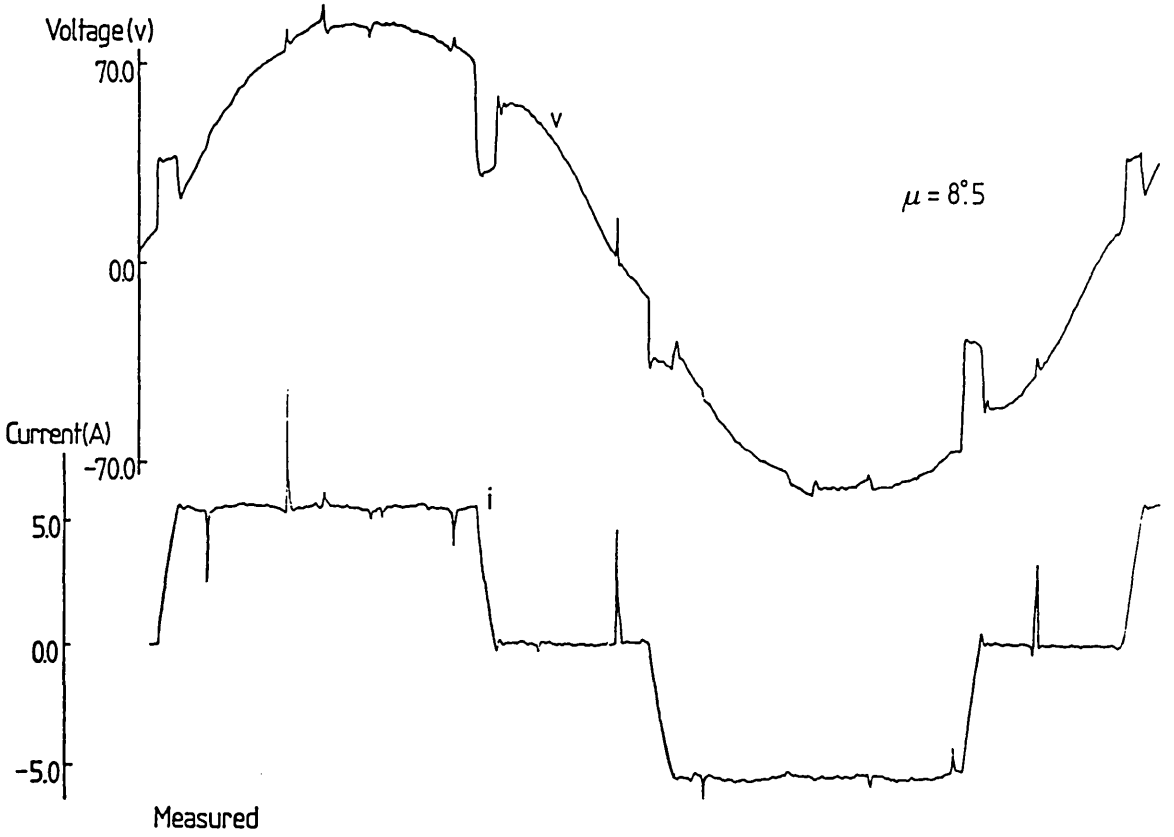


Fig.6.24. Motor Phase Quantities for f=25Hz β=20°.

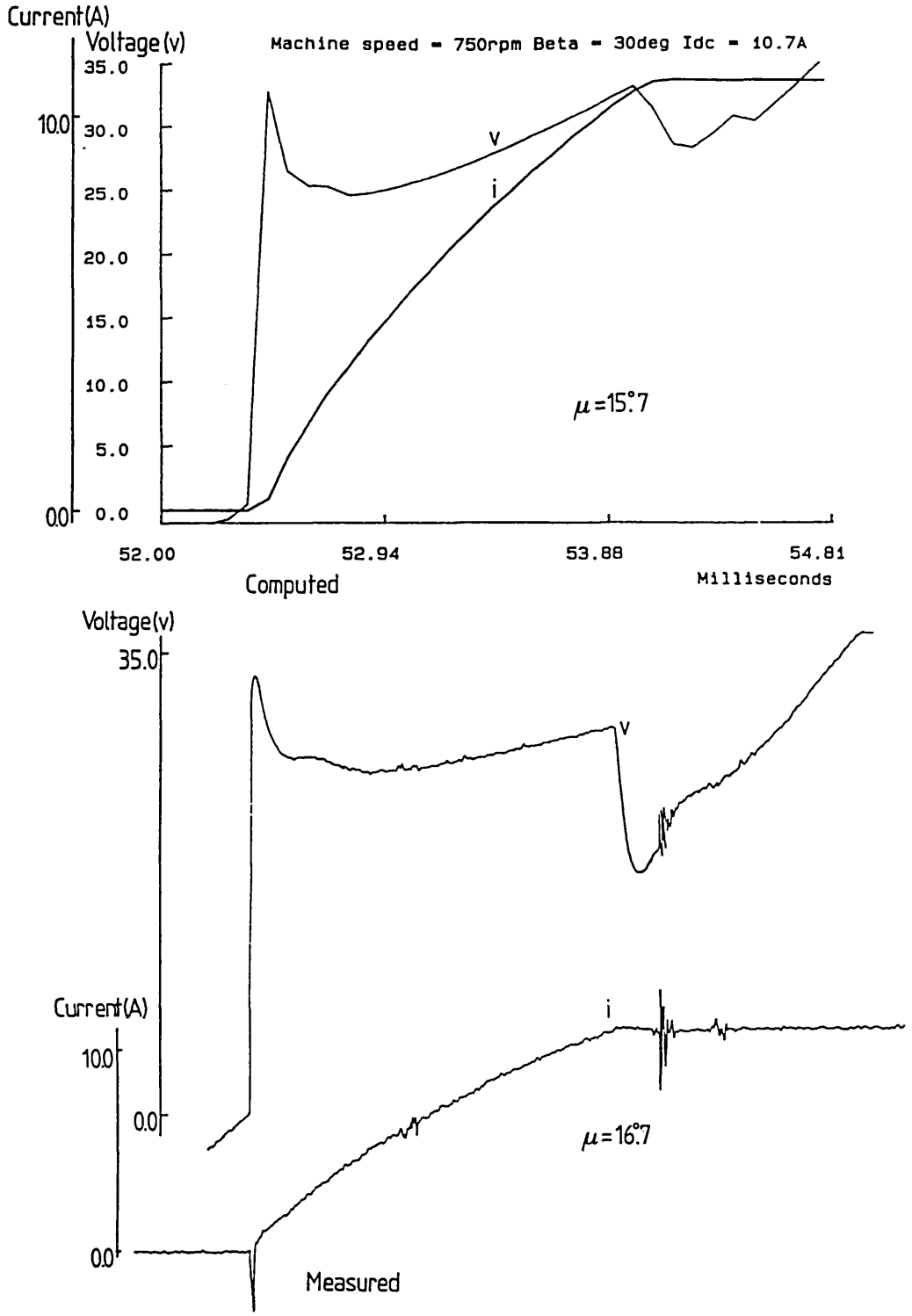
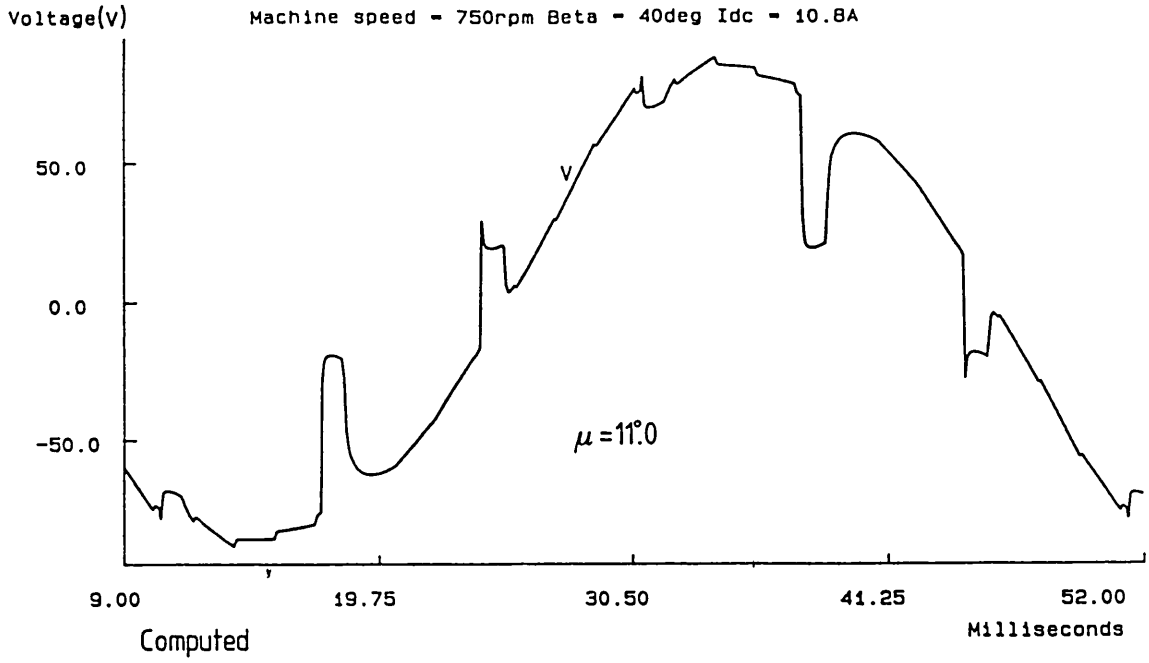


Fig.6.25. Motor Phase Quantities for f=25Hz $\beta=30.^{\circ}$



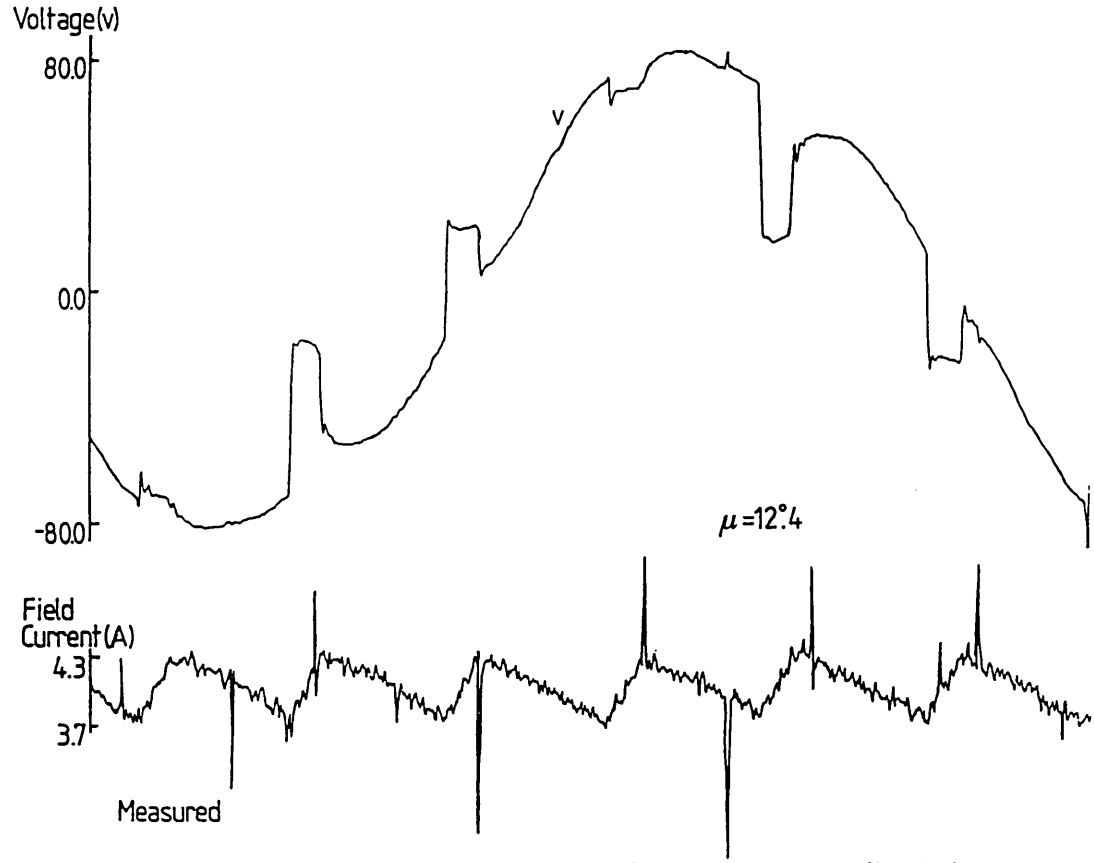


Fig.6.26. Motor Phase Voltage and Field Current for $f=25Hz$ $\beta=40°$.

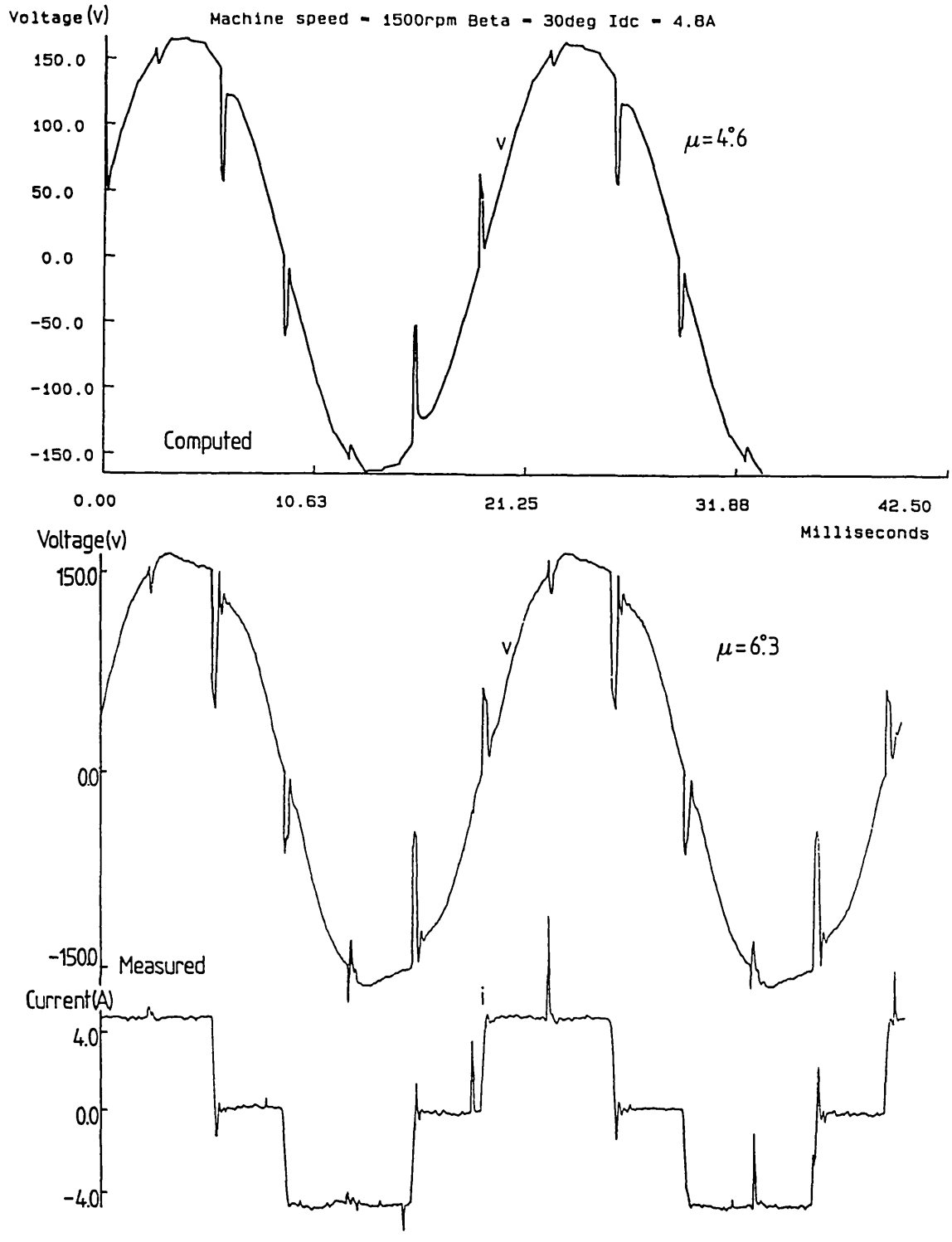


Fig.6.27. Motor Phase Quantities for f=50Hz $\beta = 30°$

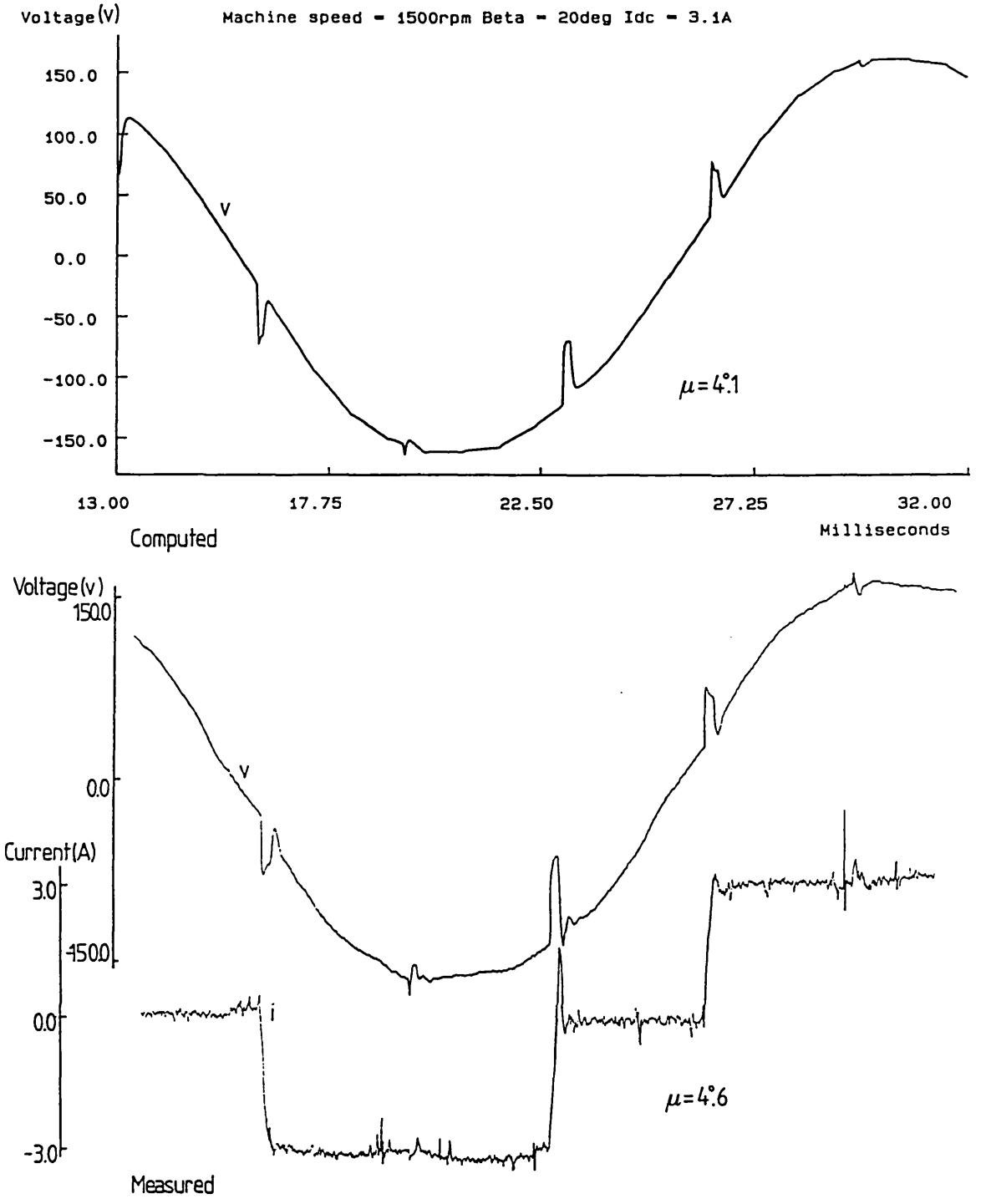


Fig.6.28. Motor Phase Quantities for f=50Hz $\beta=20°$.

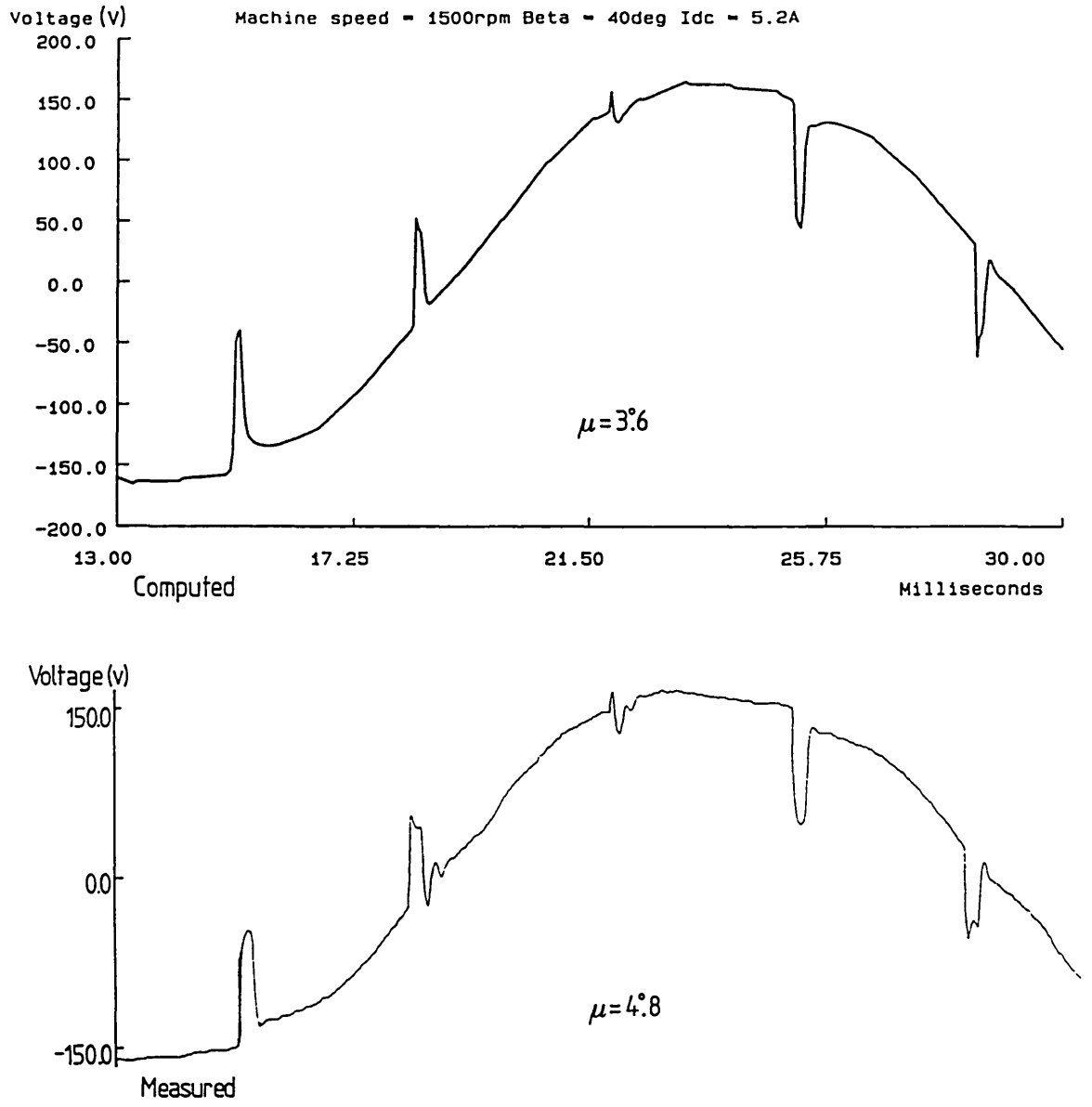


Fig.6.29 Comparison of Computed and Measured Phase Voltages for f=50Hz $\beta=40°$.

is reduced by 30%. However, the penalty is paid with a worse power factor.

The actual field current of fig 6.26 exhibits the influence of rectifier switching even when a large link inductor is used. The sharp spikes are of 50Hz frequency although no detremental effects are experienced in the machine's operating performance.

However, at a motor speed of 1500 rev/min (50Hz) rectifier interaction does take place. The rectifier and inverter lock into synchronism and it is thought this causes the discrepancies between actual and computed commutation times. The actual current waveform of fig 6.27 has large spikes coinciding at switching, and ringing is present at commutation on the voltage waveform. These effects are experienced at other firing angles, figs 6.28 and 6.29. In spite of the errors in computing commutating times the general wave shapes are comparable with the actual waveforms.

6.7 Conclusions

Actual and computed values of $L(\omega)$ are significantly in error over the whole frequency range. Values of inductance calculated from the actual overlap angles at low current levels correspond to the computed inductances $L(\omega)$ at ω = maximum. This suggests the computed frequency response is more accurate than the actual frequency response. The accuracy of the measurement of the actual response has already been questioned.

The assumption of a constant commutating inductance has been shown to be inadequate for solid rotor calculations. This is shown to be

apparent at high current levels. Choosing values of $L(\omega)$ from the frequency response tests did not result in good correspondence with actual overlap angles. By calculating the motor's step response a magnetic circuit model allowing for eddy currents gives much closer agreement with actual results than conventional means of calculating μ.

A model allowing for motion gives even closer agreement to actual results. The influence of the permanent distortion of flux can be studied with the full synchro-inverter simulation. Field distortion is apparent in the field current, it has an imposed ripple of about 7% and the voltage waveforms remain distorted after commutation.

At the time, it was not appreciated that the voltage waveform would distort in the manner shown in figs 6.15 and 6.16, subsequently no allowance was made for this when measuring the laboratory rotor load angle. Obviously, different load angles will be obtained depending on the point on the phase voltage where the stroboscope is fired. Further angular discrepancies may have arisen since the filtered voltage signal was used as the voltage reference for stroboscope firing. A more reliable means of load angle measurement is needed.

Slot ripple is present on the computed voltage waveforms. This is caused by the abrupt change in stator linkage functions every 15^{o}, fig 5.25.

CHAPTER SEVEN

THE INFLUENCE OF LINK INDUCTANCE AND MACHINE DESIGN ON SYNCHRO-INVERTER PERFORMANCE

7.1 Introduction

The machine topology of the magnetic circuit model used previously is adapted to analyse the influence of machine design changes. Damping is removed from the rotor circuit to examine the influence of a laminated rotor on the system. Also, air gap and stator tooth gap design changes for the solid rotor, are shown to influence the commutation angle. Rectifier/inverter interaction is analysed on the laboratory system, and the computer model, for a very low link inductance.

7.2 A Laminated Rotor

The solid salient motor magnetic circuit was adapted to model a laminated rotor without a damper cage (or a solid rotor with very high resistance value) by reducing the magnetic dampance values. The result is a marked increase in the commutating time for a similar load current. Fig 7.1 shows the resulting phase voltage waveforms and fig 7.2 the corresponding current waveforms, the maximum current 3.8A yields a commutating time of 10.3^{o}. This is over three times the commutating time of the solid rotor machine for the same conditions. Secondary notching is more pronounced as can be seen from fig 7.1, as is ringing at commutation cessation.

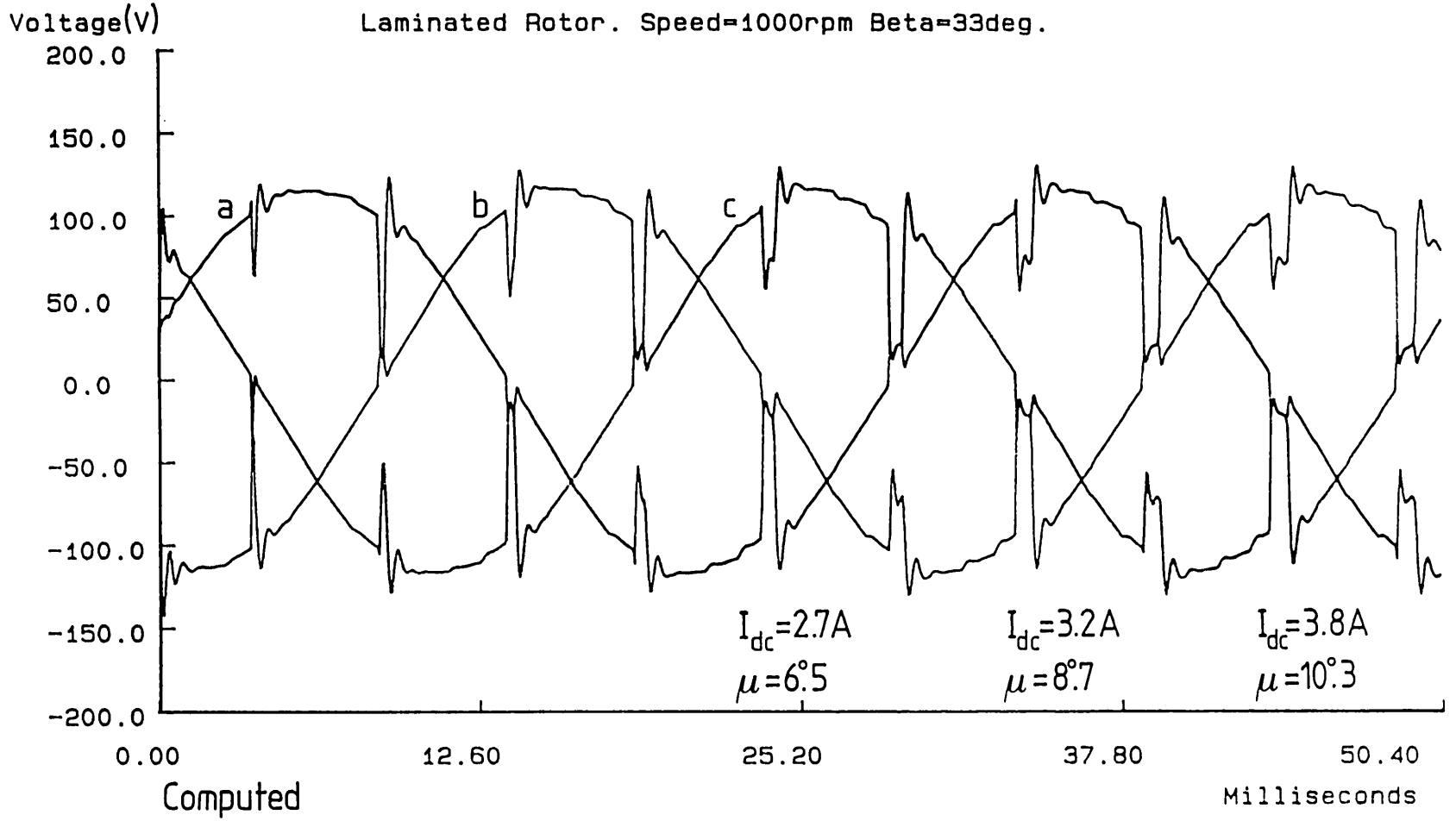


Fig.7.1. Phase Voltages of a Laminated Rotor Machine for I_{dc} Increasing.

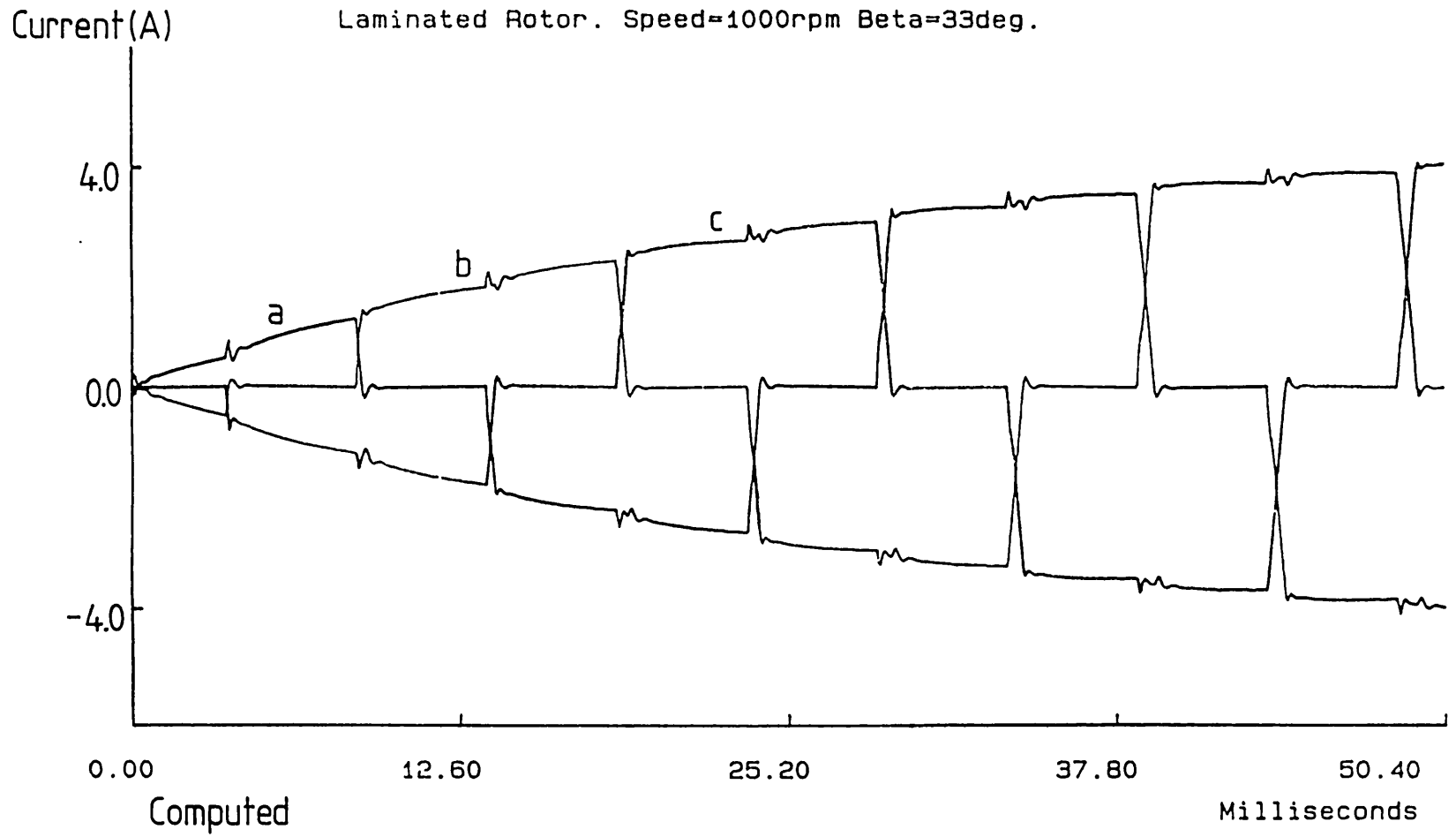


Fig.7.2. Motor Phase Currents Corresponding to Fig.7.1.

7.3 Reduction of Slot Leakage and Increase in Air Gap Length

To study the influence of reducing stator slot leakage the leakage capacitors, C_s fig 4.8, are reduced to 25% of their original value modifying the tooth cross section as shown below.

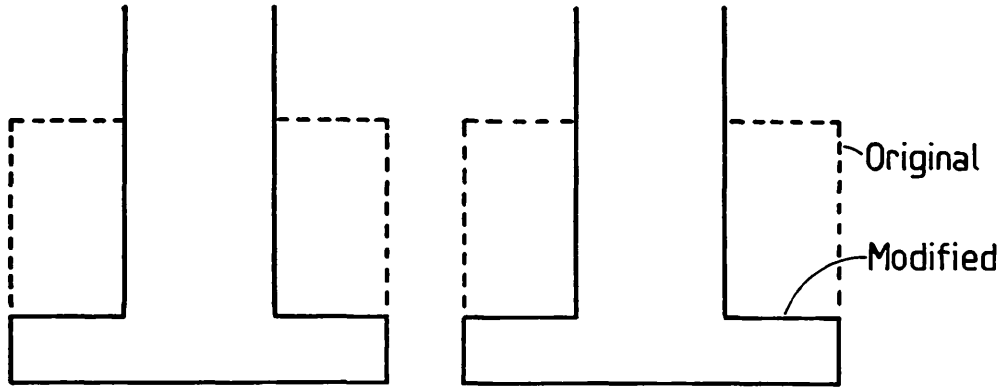


Fig 7.3 Reduction of Slot Leakage.

Resulting waveforms are shown in fig 7.4. By comparison with figs 6.12 and 6.21 the commutation time is considerably reduced, even with the load current level increased and β decreased, for a reduced slot leakage.

The effect of increasing the air gap length, with the original stator slot leakage, is shown in fig 7.5. The air gap length is increased to four times the original length and field current increased. The phase voltage is down by approximately 20%, and in spite of this the commutation time is reduced compared to figs 6.12 and 6.21.

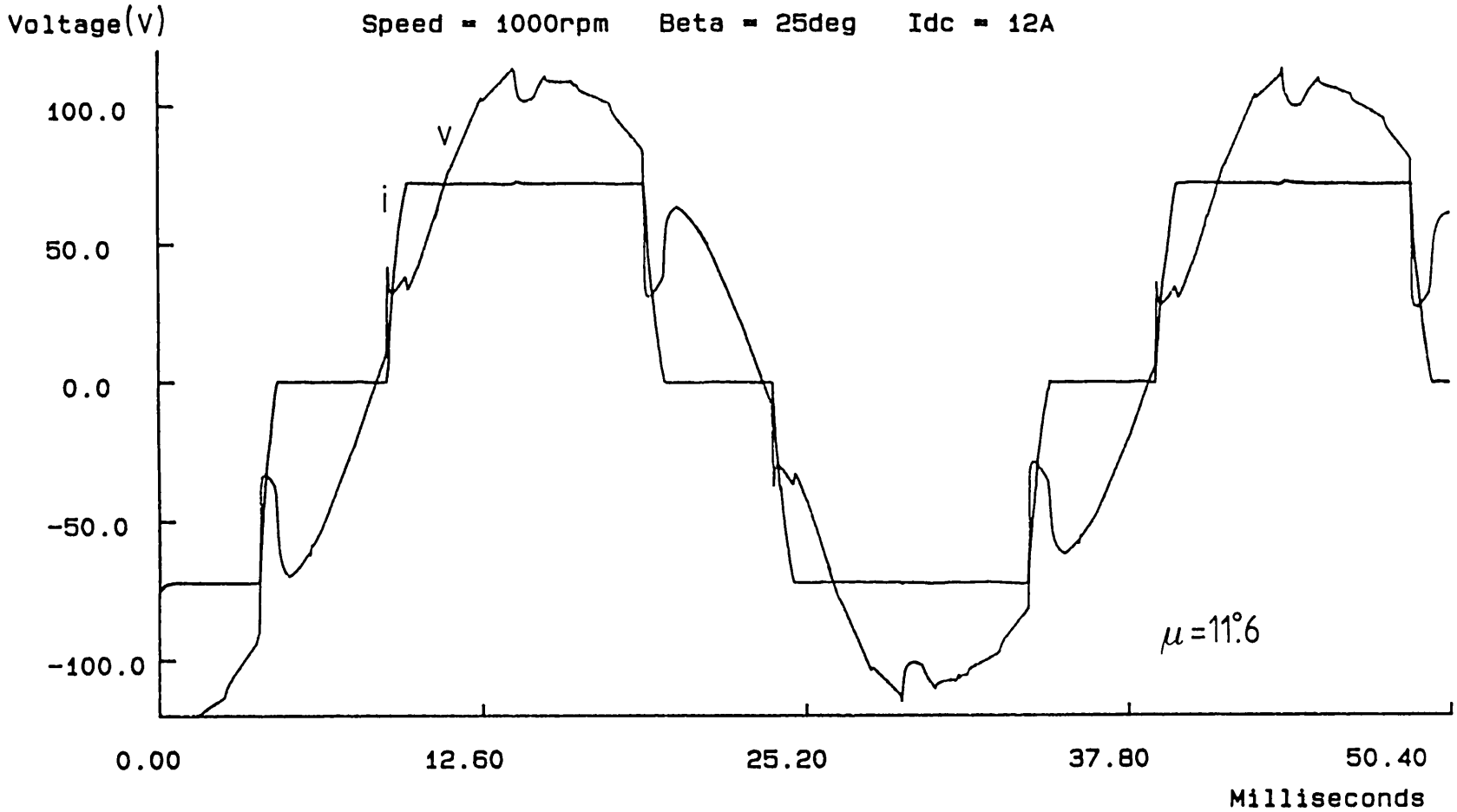


Fig.7.4. Computed Motor Phase Current and Voltage for Reduced Stator Tooth Leakage.

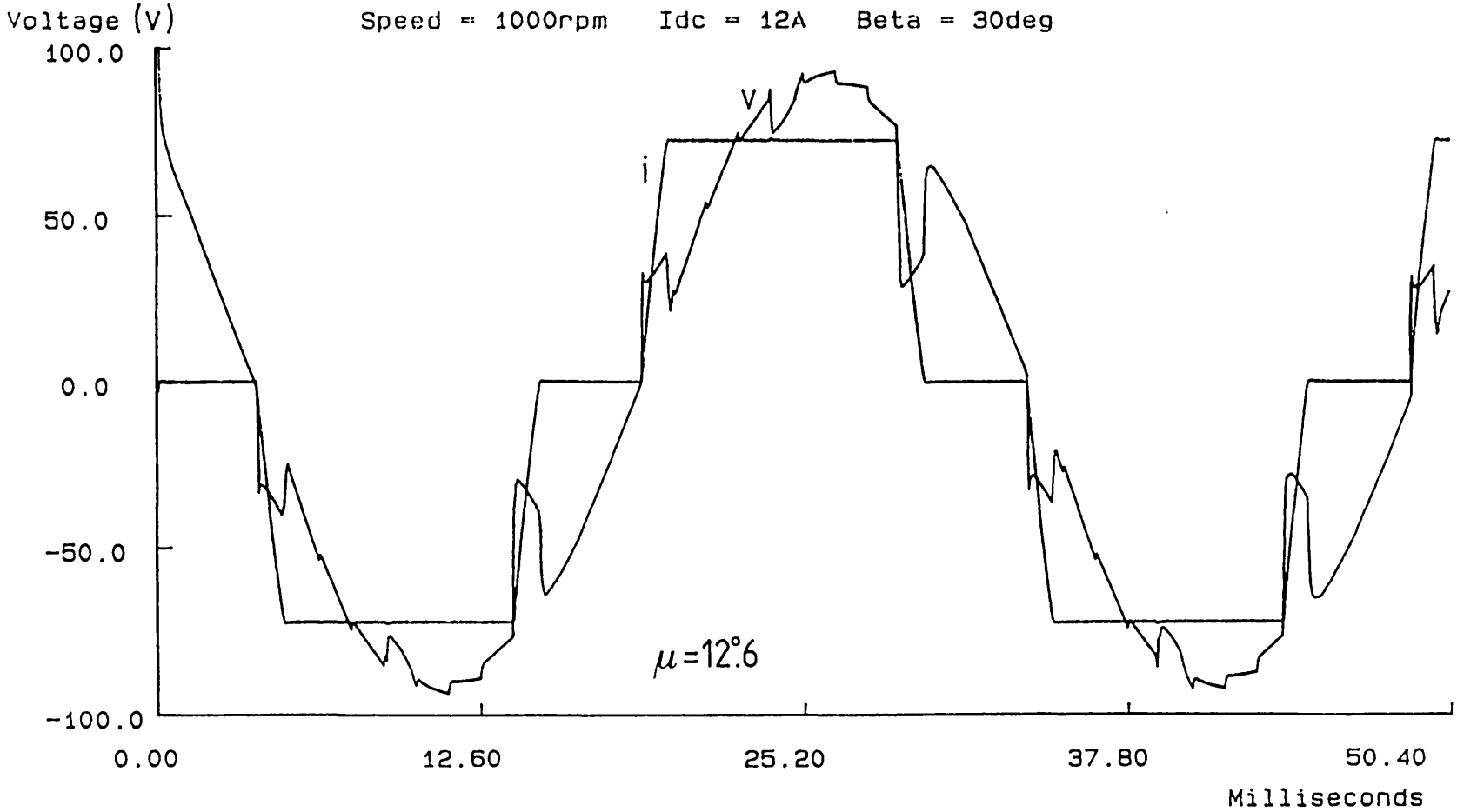


Fig.7.5. Computed Motor Phase Voltage and Current for Air Gap Length Increased by Four Times the Original Length.

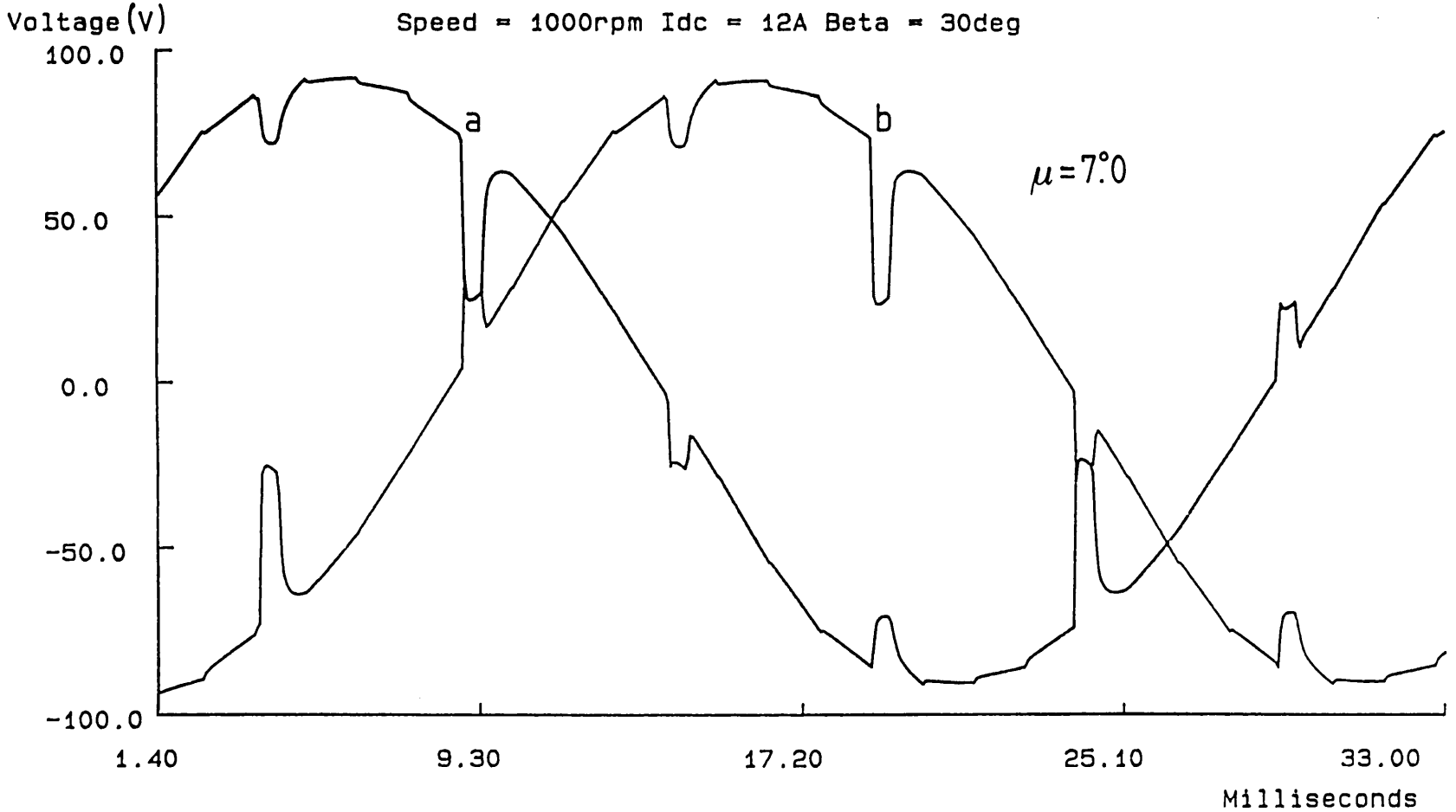


Fig.7.6. Computed Motor Phase Voltages for Reduced Stator Slot Leakage and Increased Air Gap Length.

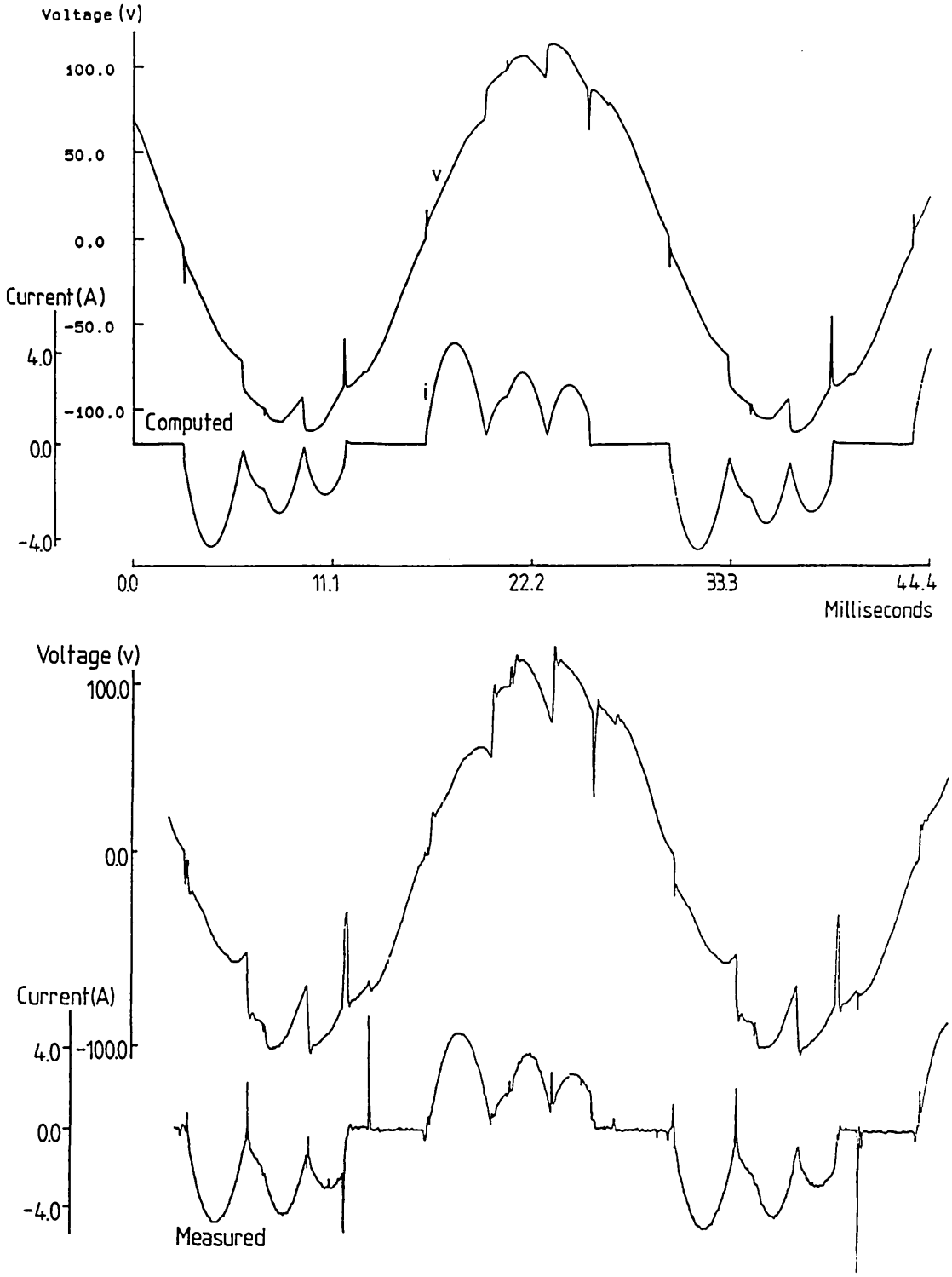


Fig.7.7 Motor Phase Quantities for f=37Hz, L_{dc}=0.03H, β=30°

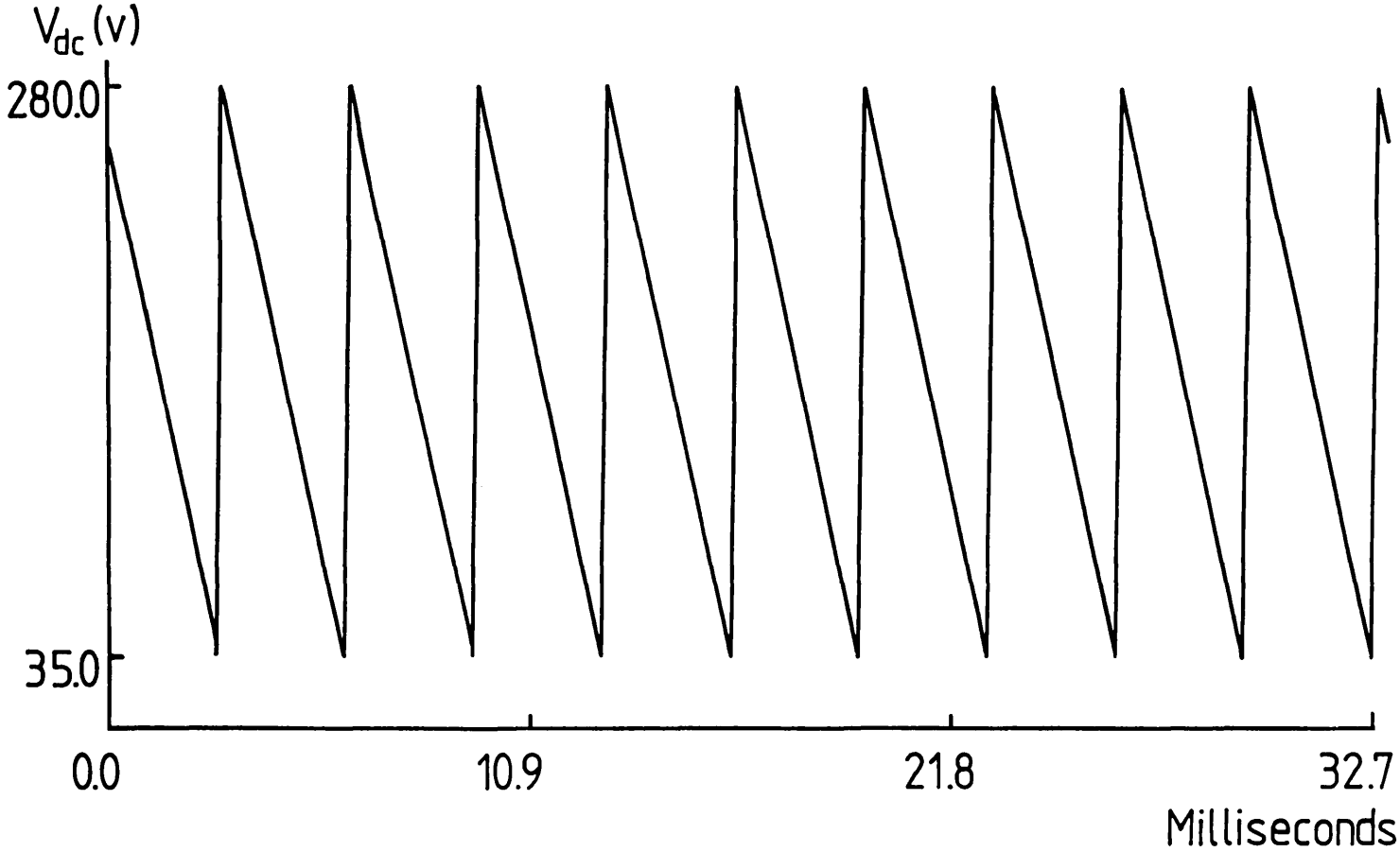


Fig.7.8. Computer Model Rectifier Voltage Corresponding to Fig.7.7.
Rectifier Firing Angle = 55°.

Reducing the stator slots and increasing the air gap by the amounts described previously, at the same time, markedly reduces the commutation time further to $\mu = 7^{o}$, fig 7.6. Again phase voltage is reduced compared to earlier simulations.

7.4 Reduction of Link Inductance

The link inductor L_{dc} is reduced to 0.03H from 0.7H for the experimental and actual curves shown in fig 7.7. The maximum link current possible on the experimental system is about 3A, above this level the link current began to oscillate. Oscillation of link current caused the motor speed to oscillate and increasing link current above 4A resulted in commutation failure. It can be seen from the experimental and simulated phase voltage waveforms that commutation time varies from zero to 3.2^{o}, and the interference caused by rectifier switching distorts current and voltage waveforms considerably.

Modelling of rectifier switching is accomplished by simply making V_{dc} vary as a function of time, as shown in fig 7.8. The voltage function values are calculated from the required rectifier firing angle to give the average V_{dc} to satisfy the value of link current. The falling slopes are approximated as a linear fall (in practice the falling slope has a sinusoidal function).

7.5 Conclusions

The alteration of magnetic circuit parameters is straightforward. It has been shown that the stator slot leakage paths contribute considerably to the value of commutating reactance. The motor's

relatively small air gap also adds to commutating reactance. However, the field excitation must be augmented if the air gap is increased.

Comparison between actual and computed results for the reduced link inductor case is very good considering the rectifier voltage is modelled with a degree of approximation.

CHAPTER EIGHT

CONCLUSIONS

8.1 General Conclusions

The performance prediction of a syncho-inverter system employing a solid salient rotor machine is not a straight forward task. The variation of the solid iron's parameters during a transient complicates a conventional analysis since the effects of eddy currents and flux distortion are considerable. It has been shown that the simple assumption of choosing a commutation reactance equal to the machine's substransient reactance although a good approximation for a laminated machine is an over-simplification for the solid rotor case. Subtransient reactances are normally found from machine tests and each test can yield a different value for the subtransient reactances.

The technique of choosing a reactance from the static frequency response method is used here. However, a frequency response technique tends to yield inductances that represent the stator winding's leakage paths, not giving the true inductance of the loaded flux pattern. Also, the method uses stator currents which are a fraction of actual loaded values so that the operating point on the B-H curve is very different to that of the actual situation. The success of frequency response tests is dubious and it is possible to speculate on the validity of computed as well as actual results.

Commutation reactance has been shown to not only depend upon the penetration depth of "commutating flux" but also upon the rotor's

position. The simplification of taking commutating reactance equal to the average of the subtransient reactances is invalidated if x_d'' is very different to x_q''. Any calculations should allow for these factors and so the adoption of a constant x_c is ruled out. Also, the motor's magnetic field pattern distorts due to commutation and probably never recovers before the next commutation takes place. A magnetic field solution has therefore been adopted.

The magnetic circuit technique's validity has been established by the successful simulation of simple models, machine tests, and a full synchro-inverter system model. The direct and complete coupling of magnetic and electric circuits facilitates the simulation of a machine transient without having to use complex referral techniques. In this manner static line-to-line short circuit tests are shown to improve upon conventional calculations of commutation time although the influence of rotor movement is neglected. A full synchro-inverter model comprising a machine magnetic circuit cross section and inverter has been shown to provide results comparable to laboratory tests and confirm speculation of the magnetic flux pattern behaviour.

In spite of the coarse discretization and lumping of eddy current paths the tests establish a technique which allows a full system to be modelled with the possibility of studying the influence of parameter changes (magnetic or electric). The preliminary testing of an actual machine to determine equivalent circuit parameters is erradicated since the magnetic circuit technique only requires a knowledge of the machine geometry and its materials.

The laboratory motor's stator is not of a typical design. Commutation reactance is enhanced by the small air gap and the virtually closed

stator slots although this provides a more rigorous test of the magnetic circuits accuracy. However, a larger air gap means the gap flux will not necessarilly be perpendicular to stator slot and rotor surfaces. Fringing and localized permeance variation due to differing ampere-turns of adjacent stator teeth may influence permeance values.

The laboratory system produces reliable, coherent results for comparison with computed waveforms. A bank of series inductors allows the influence of link inductance upon system operation to be studied and the inclusion of a large link inductance facilitated the measurement of waveform details. No problems were encountered in the operation of the test rig and the measures taken to reduce electromagnetic coupling and switching noise affecting the sensitive control circuitry were successful.

8.2 The Magnetic Circuit Method

The magnetic circuit technique has been introduced and applied to the solution of essentially a recurrent magnetic field transient problem allowing for interlude periods. The advantages of keeping electric and magnetic circuits separated but represented within a single computer model are apparent. Not only is a precise representation of the magnetic and electric circuits possible but the electric circuit is linked to the magnetic circuit in exactly the same way as the actual stator conductors link the core's magnetic flux paths. This is accomplished by the use of linkage devices, or gyrators.

Allowance is made for major leakage paths and flux fringing is taken into account. The solid rotor has been represented to allow for induced eddy currents and the associated skin effects. The grid of

flux paths formed assumes the existence of flux and rate of change of flux in horizontal and vertical paths only. The same is true of the eddy current representation where eddy currents are restricted to rectangular tubes of conducting material at right angles to the permeance grid. The assumption of commutation creating a wavefront of flux propagating down into the rotor pole is applied here. A similar argument is used by Bharali and Adkins [27]. The representation of eddy current paths or damping circuits therefore applies specifically to the problem encountered here and the representation may not be suitable for different kinds of machine transient simulations. It was found that considerable changes in the values of edddy current dampances had a marginal influence upon commutation times.

The variation of air gap permeances with rotor angle has been examined as a method of representing motion but abandoned due to its unsuitability for solution by the S.P.I.C.E. solver and the clumsy nature of the technique. The gyrator devices are conducive to the representation of rotation of the stator conductors around a stationary magnetic circuit. Application of the B.l.u. rule represents the actual rate of change of fluxes in the stator core which induce stator back e.m.f. due to motion. The method is simpler than the permeance variation technique and computationally more efficient.

Not only does motion allow for the generation of back e.m.f. and the coupling of a full inverter circuit, but allows for the change of reactance value due to relative rotor to stator position. More importantly the change of flux pattern in between commutations is taken into consideration. The motion is continuous and can be programmed to continue indefinitely. Slight tooth ripple is

experienced due to the nature of representing the rate of change of linkages. Good agreement is achieved using this method not only on open circuit but with the machine fully loaded. Also, second order effects are picked up by the computer simulation.

Notwithstanding the coarseness of discretization in the air gap and the solid rotor the results obtained are comparable to experimental waveforms, as shown in chapters five and six. It would be possible to increase discretization to a desired level, or conversely a very simple representation of a machine is possible perhaps where a detailed study of the power electronics is more important.

8.3 The Solving Routine - S.P.I.C.E.

The S.P.I.C.E. package is essentially an electronic circuit solver and not designed for the solution of machine magnetic circuit topologies. However, the discrete component form of a magnetic circuit and especially the specific form of the power electronic circuitry lends itself to solution with such a computer package. The input format is straight forward, sensible and the solver has a node connection checking routine which is very useful. Circuit components are represented as a list of elements which can be tedious to check if the listing is long. A visual display of the circuit is not, as yet, possible and would be of great benefit especially for displaying a complex machine magnetic circuit. A means of visual circuit assembly would be useful, as would an auto mesh generation program.

The insertion of dummy resistors lends itself to an automatic construction routine although the S.P.I.C.E. connection checking operation soon details any illegal connections and where they occur.

If the values of dummy resistors are too high the solution may not converge due to a numeric overflow caused by a large voltage drop across the offending dummy resistance. However, the reason for solution failure is speculative since the resulting warning and error messages do not reveal the cause(s) of errors. The S.P.I.C.E. manuals cast little light upon the causes of failure although a common error message, "Internal time-step too small in transient analysis...", points to an automatic time step control which with a high rate of change of voltage creates the necessity for an impossibly small time-step.

Obviously initial conditions must be precisely defined and the initital conditions at both nodes of a capacitor be specified. An incorrect setting usually led to solution failure although false solutions very often result.

Future development of this work should consider the possibility of improving upon S.P.I.C.E. or constructing a new solver. However, S.P.I.C.E. is ideally suited to the solution of electronic circuits whereas algorithms need to be written for the power electronics when, for example, finite element techniques are used.

8.4 Machine Design Changes and System Modifications

A system under consideration for future study uses two star-delta, delta-star transformers at the motor/converter and mains/converter interfaces. The representation of these transformers would be a straight forward task using techniques developed here. The magnetic circuit technique lends itself to problems which require the consideration of a detailed machine solution, the associated switching

of power electronics (which may be complex) and the influence of other specific electrical elements such as transformers.

The magnetic circuits' flexibility allows for the study of machine design changes, alteration of electronic component values and the study of operation under adverse conditions (which could possibly be disasterous for a laboratory model). For the motor considered here it is shown that slot leakage significantly adds to commutating reactance and the rotors close proximity to the stator also augments x_c. It is possible to improve machine designs with this technique and produce recommendations on machine design to limit x_c.

8.5 Further Work

Some possible improvements and further work have already been hinted at. Finally other more definite areas of future work are outlined.

The Laboratory Model

The method of load angle measurement needs to be investigated and improved upon. Also, the derivation of the inverter firing pulses relies on a crude method of phase voltage reduction leading to slight discrepancies between the firing points of each thyristor.

A Six Phase System

A three phase system has been considered here. The laboratory motor's stator is a double wound stator which can be connected in six phase configuration. Another inverter must be built but can be of exactly the same design as the three phase inverter. A study could then be

made to determine the benefits to be gained from such a scheme. Investigation into torque ripple and harmonics (which should be reduced) could be carried out upon the laboratory model and a magnetic circuit simulation.

Rectifier/Inverter Interaction

Rectifier and inverter interaction needs further investigation. It would be useful to set up rules or guidelines for choosing a minimum link inductance value at the same time satisfying system stability.

The Thyristor Model and Safety Angle

The S.P.I.C.E. thyristor model developed here is basically a switch and improvement upon this provides little benefit except for studying how safety angles can be reduced. The motor's power factor is compromised by the duration of safety angle and is therefore of concern.

Saturation of Iron

Saturation is allowed for by taking μ_r equal to 100, the influence of saturation has been regarded as a second order effect since the pole material is probably saturated before commutation anyway. It may be possible to represent saturation by the use of capacitors whose value is dependent upon the voltage across them (such devices exist in S.P.I.C.E.). It would then be possible to represent permeance as a function of Ampere-turns across the permeance element.

Torque Ripple

Motion is considered in the computer models although a constant speed is assumed. In reality torque ripple is present due to the repeated switching of the stator m.m.f. To allow for torque ripple in a computer model it is necessary to let the model's speed vary, requiring an algorithm to alter the rate of change of stator linkages.

Flux and Eddy Current Plots

A means of displaying flux plots and the eddy current pattern in a "user-friendly" manner would be useful and aid the analysis of machine behaviour. Not only could flux changes be studied during commutation but during interlude periods, thereby enablying an examination of critical areas of flux change and damping.

System Incorporating a Typical Motor

It is with great regret that an industrial synchro-inverter system was not available in time for test and analysis. As previously stated the motor used here was atypical and no data was available for the solid rotor.

Damper Circuit Representation

A proper damper circuit representation incorporating mutual damping effects should be investigated. The differences in a full representation and the approximate solution could then be assessed.

Solid Rotor Versus Laminated Rotor with Damper Cage

The solid rotor machine gives a reduced commutation time due to the eddy current skin effect. This cuts across previous expectations and it would be useful to carry out a more detailed appraisal of the advantages and drawbacks of the two rotor types.

REFERENCES

1. Meyer, A., Schweickhardt, H., Strazzi, P., "The converter fed synchronous motor as a variable-speed drive system", Baden, Brown Boveri Review, 4/5, 1982, pp. 151-156.

2. Davidson, D.F., Finney, D., "Supersynchronous electric motor drives", G.E.C. Journal for Industry, Vol. 8, No. 2, 1984, pp. 63-69.

3. Finney, D., "Synchdrive converters for high voltage motors", G.E.C. Journal for Industry, Vol. 7, No. 1, 1983, pp. 25-30.

4. Le Huy, H. et al "A self controlled synchronous motor drive using a terminal voltage system", Proc. IEEE (IA), Jan/Feb 1982, pp. 46-53.

5. Adkins, B., Harley, R.G., "The general theory of alternating current machines", 1975, Chapman and Hall, London.

6. Haydock L., "The systematic development of equivalent circuits for synchronous machines", Ph.D. thesis, University of London, 1986.

7. Carpenter, C.J., "Magnetic equivalent circuits", Proc. IEE, Vol. 115(10), 1968, pp. 1503-1511.

8. Pelly, B.R., "Thyristor phase controlled converters and cycloconverters", Wiley, 1971.

9. Bedford, B.D., Hoft, R.G., "Principles of inverter circuits", Wiley, 1964.

10. Millman, J., "Microelectronics: Digital and analog circuits and systems", McGraw-Hill, 1979.

11. Mawdsleys Limited, "operating and maintenance manual for the Mawdsley micro synchronous generator set", spec. no. 103/R13, Mawdsleys Limited, Dursley, Gloucestershire, 1980.

12. Coultes, M.E., "Standstill frequency response tests", Symposium on synchronous machine modelling for power system studies, IEEE winter power meeting, Feb. 1983.

13. Hurley, J.D., Schwenk, H.R., "Standstill frequency response modeling and evaluation by field tests on a 645 MVA turbo generator", Proc. IEEE (PAS), Vol. 100, 1981, pp. 828-836.

14. Coultes, M.E., Watson, W., "Synchronous machine models by standstill frequency response tests", Proc. IEEE (PAS), Vol. 100, 1981, pp. 1480-1489.

15. Diggle, R., Dineley, J.L., "Generator work testing. Sudden short circuit or standstill variable frequency response method", Proc. IEE, Vol. 128 (4c), 1981, pp. 177-182.

16. Hoeijmakers, M.J., "On the steady-state performance of a synchronous machine with converter", Ph.D. thesis, University of Eindhoven, 1984.

17. General Electric Company (USA), "Silicon controlled rectifier manual", Semiconductor products department, 6th Ed, Auburn, New York, General Electric Co, 1979.

18. Gayek, H.W., "Behaviour of brushless aircraft generating systems", IEEE transactions on aerospace-support conference procedures, Proc. 1963, pp. 594-621.

19. Sturgess, J.P., "Finite element electromagnetic analysis of generator transient performance", Ph.D. thesis, University of London, 1987.

20. Williamson, A.C., et al "Variable speed inverter fed synchronous motor employing natural commutation", Proc. IEEE, Vol. 125, No. 2, February 1978, pp. 113-120.

21. Takeda, T. et al "Generalised analysis for steady-state characteristics of D.C. commutatorless motors", Proc(B) IEE, Nov. 1983, Vol. 130, pp. 373-380.

22. Gopal-Reddy, I., et al "Line-to-Line short circuit of a synchronous machine: illustration of computer aided machine analysis", Proc. IEE, Vol. 118, January 1971, pp. 161-168.

23. Novotny, D.W., King, T.L., "Equivalent circuit representation of current inverter driven synchronous machines", Proc. IEEE, PAS-100, June 1981, pp. 2920-2926.

24. Rosa, J., "Utilization and rating of machine commutated inverter-synchronous motor drive", IEEE Trans., Vol IA-15, No. 2, March/April 1979, pp. 155-164.

25. Franklin, P.W., "Theory of three phase salient pole generator with bridge rectified output, parts 1 and 2", Proc. IEEE, PAS No. 5, 1972, pp. 1960-1975.

26. Widger, G.F.T., Adkins, B., "Starting performance of synchronous motors with solid salient poles", Proc. IEE, Vol. 115, No. 10, October 1968, pp. 1471-1484.

27. Bharali, P., Adkins, B., "Operational impedances of turbo generators with solid rotors", Proc. IEE, Vol. 110, No. 12, December 1963, pp. 2185-2199.

28. Heaviside, O., "Electromagnetic theory", Dover, 1950, Chapter two.

29. Gupta, S.C., Bayless, J.W., Peikari, B., "Circuit analysis with computer applications to problem solving", Matrix, 1977.

30. Draper, A., "Electrical machines", 2nd edition, Longmans Green and Co. Ltd., 1967, pp. 100-102.

31. Turner, P., "Finite element electromagnetic analysis of turbo generator performance", Ph.D. thesis, University of London, 1982.

32. Chenming, Hu, Waiman, F. Ki, "Toward a practical computer-aid for thyristor circuit design", Presented at IEEE Power Electronics Specialists Conference, 1980, pp. 174-179.

33. Barili, A., Cottafava, G., Dallago, E., "A S.P.I.C.E. 2 S.C.R. model for power circuit analysis", Computer Aided Design journal, Butterworth and Co. Ltd., 1984, pp. 279-284.

34. Avant, R.L., Lee, F.C., "A unified SCR model for continuous topology CADA", IEEE Trans. on industrial electronics, Vol. IE-31, No. 4, Nov. 1984, pp. 352-361.

35. Losic, N.A., Verbrugge, E.G., "A thyristor model for computer aided power electronic circuit design" IECON Proc., 1982, CH 1743, pp. 39-44.

36. Nagel, L.W., "S.P.I.C.E. 2: A computer program to simulate semiconductor circuits", Ph.D. thesis, Memorandum no. ERL-M520, Electronics Research Lab., College of Engineering, University of California, Berkeley, CA94720, 9th May 1975.

37. Vladimirescu, A. et al "S.P.I.C.E. version 2G.5 user's guide", Dept. of Elec. Eng. and Computer Science, University of California, Berkeley, CA94720, 10th August 1981.

38. Sutton, R., "A magnetic circuit model of an electrical machine", B.Sc. project report, 1982, Dept. of Elec. Eng., Trent Polytechnic.

39. Ostovic, "A method for evaluation of transient and steady-state performance in saturated squirrel cage induction machines", IEEE/PES 1985 Summer Meeting, Vancouver, B.C., Canada, July 14-19, 1985, 85 SM 343-9.

40. Ostovic, "Computation of saturated permanent magnet a.c. motor performance by means of magnetic circuits", IEEE Industry Applications Society Annual Meeting, IAS 86, Vol.1, pp 794-799.

41. Turner, P.J., "Finite element simulation of turbo generator faults and application to machine parameter prediction", IEEE Trans. on Energy Conversion, EC-2, No. 1, 1987, pp. 122-131.

42. Say, M.G., "Alternating Current Machines", Pitman Publishing Limited, 1983.

43. Kernigham, B.W., Ritchie, D.M., "The C programming Language", Prentice-Hall Inc., 1978.

44. Hughes, E., "Electrical technology", 5th edition, Longman, 1960, p. 189 and p. 457.

APPENDIX A: NONLINEAR DEPENDENT SOURCES

(Taken from reference 37)

S.P.I.C.E. allows circuits to contain dependent sources characterized by any of the four equations

i = f(v) v = f(v) i = f(i) v = f(i)

where the functions must be polynomials, and the arguments may be multidimensional. The polynomial functions are specified by a set of coefficients p0, p1, ..., pn. Both the number of dimensions and the number of coefficients are arbitrary. The meaning of the coefficients depends upon the dimension of the polynomial, as shown in the following examples:

Suppose that the function is one-dimensional (that is, a function of one argument). Then the function values fv is determined by the following expression in fa (the function argument):

```
fv = p0 + (p1*fa) + (p2*fa**2) + (p3*fa**3) + (p4*fa**4)
   + (p5*fa**5) + ...
```

Suppose now that the function is two-dimensional, with arguments fa and fb. Then the function values fv is determined by the following expression:

```
fv = p0 + (p1*fa) + (p2*fb) + (p3*fa**2) + (p4*fa*fb) +
     (p5*fb**2)

     + (p6*fa**3) + (p7*fa**2*fb) + (p8*fa*fb**2) +
     (p9*fb**3) + ...
```

Consider now the case of a three-dimensional polynomial function with arguments fa, fb and fc. Then the function value fv is determined by the following expression:

```
fv = p0 + (p1*fa) + (p2*fb) + (p3*fc) + (p4*fa**2) + (p5*fa*fb)

     + (p6*fa*fc) + (p7*fb**2) + (p8*fb*fc) + (p9*fc**2) +
     (p10*fa**3)

     + (p11*fa**2*fb) + (p12*fa**2*fc) + (p13*fa*fb**2)
     + (p14*fa*fb*fc)

     + (p15*fa*fc**2) + (p16*fb**3) + (p17*fb**2*fc) +
     (p18*fb*fc**2)

     + (p19*fc**3) + (p20*fa**4) + ...
```

Note: if the polynomial is one-dimensional and exactly one coefficient is specified, the S.P.I.C.E. assumes it to be p1 (and p0 = 0.0), in order to facilitate the input of linear controlled sources.

For all four of the dependent sources described below, the initial condition parameter is described as optional. If not specified, S.P.I.C.E. assumes 0 the initial condition for dependent sources is an initial 'guess' for the value of the controlling variable. The program uses this initial condition to obtain the dc operating point of the circuit. After convergence has been obtained, the program continues iterating to obtain the exact value for the controlling variable. Hence, to reduce the computational effort for the dc operating point (or if the polynomial specifies a strong nonlinearity), a value fairly

close to the actual controlling variable should be specified for the initial condition.

Voltage-Controlled Current Sources

General form:

GXXXXXXX N+ N- <POLY(ND)> NC1+ NC1- ... PO <P1 ...> <IC=...>

Examples:

G1 1 0 5 3 0 0. 1M

GR 17 3 17 3 0 1M 1.5M IC = 2V

GMLT 23 17 POLY(2) 3 5 1 2 0 1M 17M 3.5U IC = 2.5, 1.3

N+ and N- are the positive and negative nodes, respectively. Current flow is from the positive node, through the source, to the negative node. POLY (ND) only has to be specified if the source is multi-dimensional (one-dimensional is the default). If specified, ND is the number of dimensions, which must be postitive. NC1+, NC1-, ... Are the positive and negative controlling nodes, respectively. One pair of nodes must be specified for each dimension. PO, P1, P2, ..., Pn are the polynomial coefficients. The (optional) initial condition is the initial gues at the value(s) of the controlling voltage(s). If not specified, 0.0 is assumed. The polynomial specifies the source current as a function of the controlling voltage(s). The second example above describes a current source with value

I = 1E-3*V(17,3) + 1.5E-3*V(17,3)**2

note that since the source nodes are the same as the controlling nodes, this source actually models a nonlinear resistor.

Voltage-Controlled Voltage Sources

General Form:

EXXXXXXX N+ N- <POLY(ND)> NC1+ NC1- ... PO <P1 ...> <IC=...>

Examples:

```
E1 3 4 21 17 10.5 2.1 1.75
EX 17 0 POLY(3) 13 0 15 0 17 0 0 1 1 1 IC = 1.5, 2.0, 17.35
```

N+ and N- are the positive and negative nodes, respectively. POLY(ND) only has to be specified if the source is multi-dimensional (one-dimensional is the default). If specified, ND is the number of dimensions, which must be positive. NC1+, NC1-, ... are the positive and negative controlling nodes, respectively. One pair of nodes must be specified for each dimension. PO, P1, P2, ..., Pn are the polynomial coefficients. The (optional) initial condition is the initial guess at the value(s) of the controlling voltage(s). If not specified, 0.0 is assumed. The polynomial specifies the source voltage as a function of the controlling voltage(s). The second example above describes a voltage source with value

$$V = V(13,0) + V(15,0) + V(17,0)$$

(in other words, an ideal voltage summer).

Current-Controlled Current Sources

General form:

FXXXXXXX N+ N- <POLY(ND)> VN1 <VN2 ...> P0 <P1 ...> <IC=...>

Examples:

F1 12 10 VCC 1MA 1.3M

FXFER 13 20 VSENS 0 1

N+ and N- are the positive and negative nodes, respectively. Current flow is from the positive node, through the source, to the negative node. POLY(ND) only has to be specified if the source is multi-dimensional (one-dimensional is the default). If specified, ND is the number of dimensions, which must be positive. VN1, VN2, ... are the names of voltage sources through which the controlling current flows; one name must be specified for each dimension. The direction of positive controlling current flow is from the positive node, through the source, to the negative node of each voltage source. P0, P1, P2, ..., Pn are the polynomial coefficients. The (optional) initial condition is the initial guess at the value(s) of the controlling current(s) (in Amps). If not specified, 0.0 is assumed. The polynomial specifies the source current as a function of the controlling current(s). The first example above describes a current source with value

I = 1E-3 + 1.3E-3*I(VCC)

Current-Controlled Voltage Sources

General form:

HXXXXXXX N+ N- <POLY(ND)> VN1 <VN2 ...> P0 <P1 ...> <IC=...>

Examples:

```
HXX 13 20 POLY(2) VIN1 VIN2 0 0 0 0 1 IC = 0.5 1.3
HR 4 17 VX 0 0 1
```

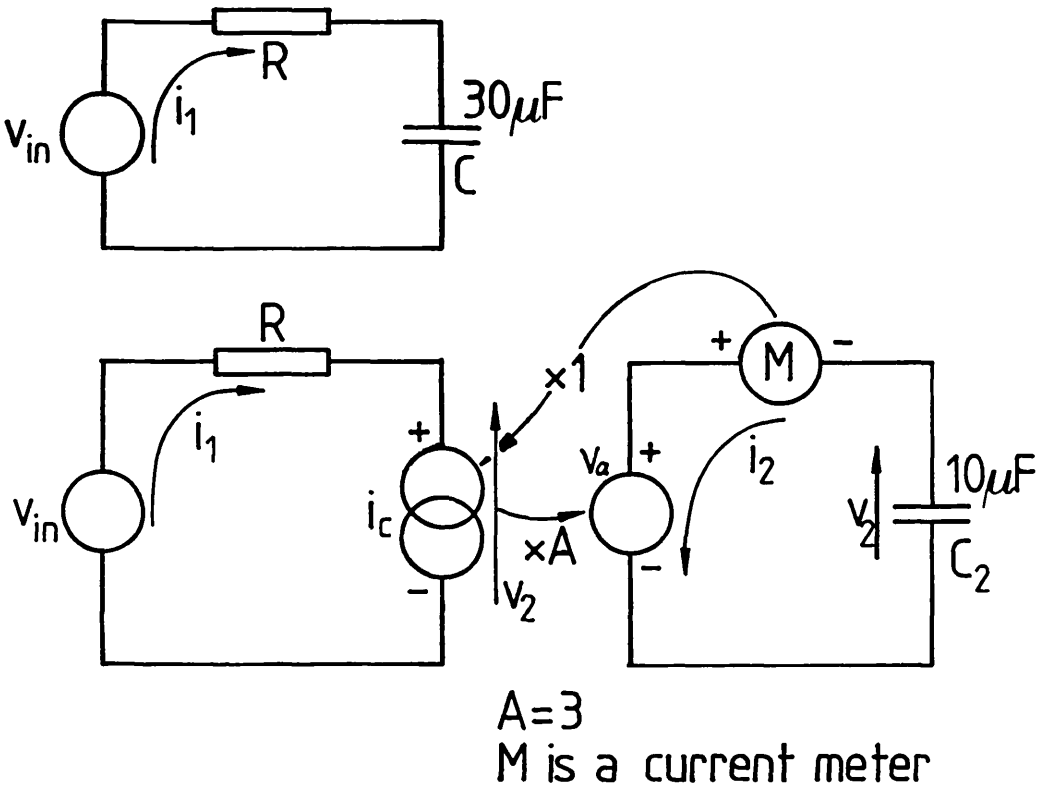
N+ and N- are the positive and negative nodes, respectively. POLY(ND) only has to be specified if the source is multi-dimensional (one-dimensional is the default). If specified, ND is the number of dimensions, which must be positive. VN1, VN2, ... are the names of voltage sources through which the controlling current flows; one name must be specified for each dimension. The direction of positive controlling current flow is from the positive node, through the source, to the negative node of each voltage source. P0, P1, P2, ..., Pn are the polynomial coefficients. The (optional) initial condition is the initial guess at the value(s) of the controlling current(s) (in Amps). If not specified, 0.0 is assumed. The polynomial specifies the source voltage as a function of the controlling current(s). The first example above describes a voltage source with value

V = I(VIN1)*I(VIN2)

APPENDIX B:

VARIATION OF CAPACITOR VALUE BY THE USE OF DEPENDENT SOURCES

The two circuits below are identical



A voltage controlled voltage source V_a, multiplied by constant A, sets the voltage V_2 across the auxiliary capacitor C_2. A current controlled current source i_c sets i_1. So

$$V_2 = A.v_1$$

$$i_2 = i_1$$

$$i = C \frac{dv}{dt} \qquad \text{(C constant)}$$

Therefore

$$i_2 = C. \frac{dv_2}{dt}$$

$$2 = A.v_1$$

Therefore

$$i_2 = C. \frac{d\ Av_1}{dt}$$

If A = constant then

$$i_2 = C.A. \frac{dv_1}{dt}$$

$$i_1 = i_2$$

then

$$i_1 = A.C. \frac{dv_1}{dt}$$

By adjusting A the value of C is effectively altered. For A non-constant

$$i_1 = A.C. \frac{dv_1}{dt} + v_1. \frac{d(A.C)}{dt}$$